2014-11

Optimised Integration of Grid-Connected Renewable Energy Technologies for Domestic Application in Ireland

Zhe Li
Technological University Dublin, zhe.li@tudublin.ie

Optimised Integration of Grid-Connected Renewable Energy Technologies for Domestic Application in Ireland

by

Zhe Li, B.Eng. (Hons)

A thesis submitted to the Dublin Institute of Technology in partial fulfilment of the requirements for the degree of

Doctor of Philosophy

Supervisors: Dr. Fergal J. Boyle and Dr. Anthony W. Reynolds

School of Mechanical & Design Engineering
Dublin Institute of Technology

Nov 2014

ABSTRACT

The utilisation of renewable energy resources for electricity and thermal generation is extremely important in Ireland due to the lack of indigenous fossil fuel resources and the high dependence on imported fossil fuels. The release of environmentally-damaging greenhouse gases in the combustion of fossil fuels in electricity and thermal generation is also a major issue. In Ireland, the domestic dwelling is recognised as one of the biggest energy consumers. The use of renewable energy technologies to provide electricity, heating and hotwater can effectively offset the usage of fossil fuels.

The aim of this research study was to develop a novel technique for the optimised integration of grid-connected renewable energy systems to satisfy the entire energy demand in a domestic dwelling. The development of the technique was carried out in a series of logical stages. In the first stage, a sub-technique for the optimised integration of grid-connected micro-renewable electricity generation systems was developed. In this sub-technique a detailed and accurate economic analysis of the investigated systems is performed. Net present value is the metric employed in the economic analysis and the system which achieves the highest net present value is deemed the optimal system. High-resolution measured electrical load data and a user-specified renewable energy requirement are employed in this sub-technique. The renewable energy requirement is the percentage of the household electricity demand that must be satisfied by the on-site grid-connected micro-renewable electricity generation system. In the second stage, a sub-technique for the optimised integration of grid-connected micro-renewable thermal generation systems was developed. In this sub-technique, following the completion of the life cycle cost (economic) analysis of the investigated systems, the system which achieves the lowest life cycle cost is deemed the optimal system. High-resolution measured thermal load data is utilised in this sub-technique. Finally, in the third stage, the overall integration technique was then developed by amalgamating these two sub-techniques. Life cycle cost analysis is again used to determine the optimal system.

In order to demonstrate their application, the two sub-techniques and overall technique were deployed with Irish conditions. The investigated systems were formed from commercially-available products; the products selected for this study were six micro wind turbines, three solar PV modules, three air source heat pumps and three solar thermal collectors. When the sub-technique for the optimised integration of grid-

connected micro renewable electricity generation systems was deployed under current Irish conditions, the optimal system, which meets the 50% renewable energy requirement, was a single micro wind turbine having a capacity of 2.4 kW. However, this optimal system is not economically viable as its net present value is negative. When the sub-technique for the optimised integration of grid-connected micro renewable thermal generation systems was deployed, the optimal system was a single air source heat pump having a thermal capacity of 14 kW. This optimal system is economically viable in comparison with an oil boiler system or an electrical heating system; however it is not economically viable compared with a gas boiler system. Finally, when the overall integration technique was deployed, the optimal system was a combination of an air source heat pump having a thermal capacity of 14 kW and grid supplied electricity; however this system is not economically viable in comparison with an economically-best-performing conventional combination of grid supplied electricity and a gas boiler system. The influence of several parameters on the economic performance of the investigated systems was also studied with the developed sub-techniques and overall technique.

Due to the wide range of micro-renewable energy generation systems available on the market and the broad range of existing capacities, the developed integration technique is extremely useful for performing an accurate economic analysis and determining a system that is most suitable for a domestic dwelling.

DECLARATION

I certify that this thesis, which I now submit for examination for the award of Doctor of Philosophy, is entirely my own work and has not been taken from the work of others, save and to the extent that such work has been cited and acknowledged within the text of my work.

This thesis was prepared according to the regulations for post-graduate study by research of the Dublin Institute of Technology and has not been submitted in whole or in part for another award in any institute.

The work reported in this thesis conforms to the principles and requirements of the Institute's guidelines for ethics in research.

The Institute has permission to keep, lend or copy this thesis in whole or in part, on condition that any such use of the material of the thesis is duly acknowledged.

Signature _____ Date _____

ACKNOWLEDGEMENTS

First and foremost, I would like to express my sincere thanks and gratitude to my supervisors, Dr. Fergal J. Boyle and Dr. Anthony W. Reynolds, for their continuous support of my PhD research. Their knowledge, understanding, motivation and enthusiasm were vital to my progression through this process. I would not have completed this thesis without the endless time and effort which they have invested in guiding this research over the years.

I would like to express a special thanks to Prof. David Kennedy for always making time for me and for his excellent advice and assistance. I would also like to thank the following people for their various contributions to this research over the years: Martin McCarthy and Mary Holland (Sustainable Energy Authority of Ireland) for providing important data and information that was used in the development of the research. Alan Brereton, Paul Stack, Ian Campbell, Simon Farrell and Michael Faherty for their technical assistance, and Bill Murphy and the rest of the DIT Bolton Street librarians for their continuous help.

I would like to thank all those post-graduate students, lecturers and technicians in Bolton Street for their help and friendship. In particular, I would like to thank Dr. David Martin, Eoin Murphy, Dr. Fergal O'Rourke, Mingzhu Chen, Dr. Dave Culliton, Dr. Lacour Ayompe, Arthur Henry, Dr. Michael Crowley and Dr. Michael Carr. I cannot thank you enough for all that you have done for me. I would also like to thank Kevin Byrne, Stephanie Alken, Simon Montgomery, Zhonghao Geng, Brian Higgins, Karel Pavka and the rest of the friends in Ireland and in China for their friendship and

constructive advice. I cannot imagine how hard the life would be without all of your support and help.

I am very thankful to my darling wife Xiaoyang Wang for her continued love and support throughout the course of this research. I understand this was a long and hard journey, but we walked through it together, and I am sure tomorrow will be much better. I am thankful to my daughter Zitong Li for all the joy she brings to me, and I cannot tell you how much I love you. I would also like to thank my parents-in-law and all my family members for their support and belief in me. Finally and most importantly, I would like to express my deepest thanks and gratitude to my parents, Xin Li and Yanping Wu, for their relentless support and encouragement. If it was not for you, I would not be where I am now.

NOMENCLATURE

Greek symbols

α	Temperature coefficient of power, Effect of unpredictable perturbations in the radiation attenuators
$\alpha(t)$	A first-order regression model
β	Solar absorptance of the PV array, Slope of the surface, Gaussian random variables
γ_s	Solar azimuth angle
γ	Azimuth angle of surface
Γ	Gamma function
δ	Diurnal pattern strength, Solar declination angle
δ_d	Standard deviation of the daily temperature about the monthly-average daily ambient temperature
$\delta_{d,max}$	Standard deviation of the daily-maximum temperature about the monthly-average daily-maximum temperature
δ_{yr}	Standard deviation of the monthly-average temperature about the yearly-average values
Δ	Number of hours goes into the time period
Δt	Time step
η_{STC}	PV module efficiency under standard test conditions
θ	Angle of incidence
θ_z	Solar zenith angle
λ, ε, κ	A function of daily clearness index k_d
ρ_{gr}	Ground reflectance
σ_w^2	Noise variance

σ_α	Standard deviation of uncorrelated random component
τ	Solar transmittance of any cover over the PV array
$(\tau\alpha)/(\tau\alpha)_n$	Incidence angle modifier
$(\tau\alpha)_b/(\tau\alpha)_n$	Incidence angle modifier for beam radiation
$(\tau\alpha)_d/(\tau\alpha)_n$	Incidence angle modifier for sky diffuse radiation
$(\tau\alpha)_{gr}/(\tau\alpha)_n$	Incidence angle modifier for ground-reflected diffuse radiation
$(\tau\alpha)_n$	Product of the cover transmittance and the absorber absorptance at the normal incidence
ϕ	Hour of peak windspeed, Latitude, Coefficient
ϕ_1	First-order autoregressive parameter
χ	Gaussian random variable
$\chi(n)$	Value of χ on day n
ω	Angular displacement of the sun
ω_s	Sunset hour angle
ω_1	Hour angle at the beginning of the hour
ω_2	Hour angle at the end of the hour

Non-Greek Symbols

a	Autoregressive parameter
c	Weibull scale parameter
c_{ave}	Average value of c over the time step
erf	Error function
f	Modulating factor, Annual inflation rate
f(t)	Random number drawn from a normal distribution having a mean of zero and a standard deviation of one
f_j	Unknown monthly transformation function

$f(v)$	Probability density function of a Weibull distribution
$g[\chi]$	Gaussian probability density function of χ
i	Real interest rate
k	Weibull k factor
k_d	Daily clearness index
k_{dl}	Lower bound of the range for k_d
k_{du}	Upper bound of the range for k_d
k_h	Hourly clearness index
k_{hbm}	Beam trend component
k_{hm}	Mean hourly clearness index
k_m	Monthly clearness index
$k_{m,ave}$	Monthly average clearness index
$\dot{m}$	Mass flow rate of fluid through the solar collector
$\dot{m}_{test}$	Mass flow rate of fluid under standard test conditions
n	Mean day of the month, Number of hour in a year
r_1	Autocorrelation factor
r_t	Ratio of hourly global solar radiation on a horizontal surface to daily global solar radiation on a horizontal surface
r^2	Coefficient of determination
t	Time
u	Cumulative probability of χ
$\bar{u}$	Mean of a random variable (u) within the range of between 0 and 1
σ_u	Standard deviation of a random variable (u) within the range of between 0 and 1
v	Cumulative probability of k_d
v_i	Wind speed at time step i

$\bar{v}$	Average wind speed value
$\bar{z}$	Yearly-average wind speed value
z_i	Hour i value
z_{i+1}	Value for the subsequent hour i+1
z_t	Hour t value
z_{t-1}	Value for the previous hour t-1
A	Total aperture area of a solar collector array, Peak-to-peak amplitude of the monthly-average diurnal variation of the ambient temperature
A_i	Anisotropy index
B	Amplitude for the particular portion of the day
C	Entire capital cost, Capacitance of the solar thermal collector
C_p	Specific heat of fluid
$C_{p,test}$	Specific heat of fluid under standard test conditions
CG	Capital grant
F'	Solar collector fin efficiency factor
$F[k_d, \bar{k}_d]$	Cumulative distribution function of k_d
$F[\alpha:k_d]$	Cumulative probability of α
F_{k_h}	Cumulative distribution function of k_h
F_{pv}	Derating factor
F_R	Heat removal factor
$F_R*(\tau\alpha)_n$	Intercept efficiency
F_R*U_L	First order efficiency (heat loss) coefficient
$F_R*U_{L/T}$	Second order efficiency (heat loss) coefficient
F(v)	Cumulative distribution function of a Weibull distribution
G_{sc}	Solar constant
G_t	Solar radiation incident on the PV modules in the current hour

$G_{t,NOCT}$	Solar radiation at which the NOCT is defined
$G_{t,STC}$	Incident radiation at standard test conditions
H	Hub height of the wind turbine
H_{ave}	Monthly-average daily solar radiation on a horizontal surface
$H_{o,ave}$	Monthly-average daily extraterrestrial solar radiation
H_o	Monthly-average daily extraterrestrial solar radiation on a horizontal surface, Anemometer height
I	Total solar radiation on a horizontal surface
I_b	Beam solar radiation on a horizontal surface
I_{bt}	Beam solar radiation on a tilted surface collector
I_d	Diffuse solar radiation on a horizontal surface
I_{dt}	Diffuse solar radiation on a tilted surface
I_{gr}	Ground reflected radiation on a tilted surface
I_o	Extraterrestrial solar radiation
I_T	Total solar radiation on a tilted surface
IAM	Ratio of the absorbed radiation at the current incidence angle to the absorbed radiation at the normal incidence
N	Number of days in the month, Number of power (energy) output for a year
P	Revenue generated
$P[k_d, \bar{k}_d]$	Generalised probability density function of k_d
R	Replacement cost, Number of hours in the appropriate time period
R_b	Ratio of beam solar radiation on a tilted surface to beam solar radiation on a horizontal surface
S	Savings made
SAL	Salvage value

T	Project lifespan, Temperature of the fluid in the collector at any point, Fluid temperature
T_a	Ambient air temperature
T_m	Monthly-average daily ambient temperature
$T_{m,max}$	Monthly-average daily-maximum ambient temperature
T_{ave}	Average temperature of a solar thermal collector, Median ambient temperature for the particular portion of the day
$T_{a,NOCT}$	Ambient temperature at which the NOCT is defined
T_c	PV cell temperature in the current hour
$T_{c,NOCT}$	Nominal operating cell temperature
$T_{c,STC}$	PV cell temperature under standard test conditions
T_{in}	Inlet temperature of a solar thermal collector
T_o	Outlet temperature of a solar thermal collector
T_R	Time of replacement occurring
$\bar{U}$	Overall mean wind speed
U_i	Mean wind speed in hour i
U_L	Overall thermal loss coefficient of the solar collector per unit area
V	Wind speed at the height H
V_0	Wind speed at the height H_0
$\overline{X}$	Mean of the hourly measured power (energy) outputs for a year
X_i	Hourly measured power (energy) output
$\overline{Y}$	Mean of the hourly predicted power (energy) outputs for a year
Y_i	Hourly predicted power (energy) output
Y_{pv}	Peak power output
Z_0	Surface roughness coefficient length

TABLE OF CONTENTS

LIST OF FIGURES

LIST OF TABLES

CHAPTER 1
INTRODUCTION

1.1. Background

The depletion of finite fossil fuel resources and the pollution of the environment are major problems worldwide. The first problem has even bigger impacts on Ireland as it has a very high dependency on imported fossil fuels. The use of fossil fuels accounted for 93.6% of all energy used in 2011. Ireland is heavily dependent on imported fossil fuels, oil and natural gas in particular. Imported oil and natural gas accounted for 79% of primary energy supply, and Ireland's overall import dependency was 88% in 2011 [1]. This extremely high imported-fuel dependency leaves Ireland very vulnerable to supply security and price volatility in addition to the environmental concerns raised through their consumption.

The increasing concentration level of greenhouse gases (GHGs) is believed to be a major cause of global warming. Carbon dioxide (CO_2) is a key component in GHGs, and burning fossil fuels to generate energy is one of the main sources of CO_2 emissions in Ireland. Ireland had committed in the Kyoto Protocol which was an international legally binding agreement to reduce GHG emissions. The target for Ireland was to limit GHG emissions to 13% above 1990 levels for the period of 2008 to 2012. According to the Environmental Protection Agency's (EPA) published projections for GHG emissions, Ireland had met its commitment under the Kyoto Protocol from 2009 onwards. However, the further reduction of CO_2 emission is required and targeted for delivering a 20% reduction relative to 2005 level by 2020 [2].

In contrast to Ireland's lack of fossil fuels, it has significant of renewable energy resources. Ireland has one of the best wind resources in Europe given its exposed location, and its solar resources are similar to what Germany has, where solar technology has been widely used. The biomass growth potential is also extremely high compared with other European countries because of the special climate here. Geothermal energy is also quite competitive in comparison with other European countries. The potential of renewable resources in Ireland has not gone unnoticed. There has been a significant increase in renewable energy generation in Ireland, mainly in large scale wind generation however. Renewable energy generation has more than tripled between 2003 and 2011, from 224 thousand toe (ktoe) to 782 ktoe in absolute terms. The Irish government has set its specific targets for energy supply from renewable resources and GHG emissions savings in the government white paper (published in 2007) "*Delivering a Sustainable Energy Future for Ireland"* [3]. The white paper projects energy consumption growth at a rate of 0.8% per annum from 2008 to 2020, although this is subject to change due to the economic recession. The increasing energy demand has to be met through consuming less fossil fuels, mitigating GHG emissions and through utilising renewable energy more extensively. The proposed European Union (EU) target of total final consumption (TFC) from renewable energy for Ireland in 2020 is 16%; however Ireland is currently aiming for 13%. The Irish government has also set individual targets which renewable energy is targeted to contribute to 33% of electricity consumption, 12% of thermal energy and 10% of non-aviation transport energy. The 2020 target in gross electricity consumption to come from renewable energy was extended to 40% in 2008.

Small-scale or micro-scale renewable energy generation have not yet made a major impact in Ireland. The Irish government has been trying to develop this potential

market. The direct renewable energy use decreased by 5.6% to 46 ktoe in the residential sector in 2011, even with the help of the Sustainable Energy Authority of Ireland (SEAI)'s *Greener Homes Scheme* implementation. The share of renewable energy use in households was only 1.6% up to that year.

The implementation of revised building regulations also helped to effectively reduce energy consumption in many new and existing houses. However, most domestic dwellings are still totally dependent on external energy supply. The vast renewable energy resources here are applicable and suitable for domestic dwellings. Local generation avoids a significant energy transmission loss in grid supply. In terms of electricity generation, only 35% of the energy input to power stations is delivered as electricity to the householder [4]. Local generation can improve the security of energy supply, minimise the impact of supply disruption and offset the impact of supply energy price fluctuation. For remote areas which have no electricity grid or natural gas connection, the micro-renewable energy generation system acts as a decentralised supply capable of providing partially or entirely the energy required. Once the cost of the installed renewable energy technology has been paid back, the householder can benefit from several years of free energy supply until the end of lifespan of the technology. This economic benefit for householders could be increased if the Irish government's carbon tax is added on. The use of micro renewable energy generation system to generate electricity, heating and hotwater in the domestic applications is an important part of renewable energy generation in Ireland.

1.2. Research Aim

The aim of this research is to develop a novel but generally-applicable technique for the optimised integration of grid-connected micro-renewable energy generation systems to provide the entire electricity, heating and hotwater demand for a domestic dwelling.

The technique employs economic analysis and can be used for specific case-by-case application depending on the weather conditions at the location of the domestic dwelling and the energy usage of the dwelling. The technique can be applied in the design of a new dwelling, but can also be used to improve the energy supply for an existing dwelling.

The proposed integration technique could be adopted by national energy authorities and energy research institutes, e.g. Sustainable Energy Authority of Ireland (SEAI), to identify optimal system combinations for domestic dwellings under various different scenarios, accounting for local weather conditions, household energy demands and the availability of various different renewable energy technologies.

The optimal system, obtained by applying the proposed integration technique, provides valuable information for the individual householder as it suggests the optimal micro-renewable energy generation system solution on a case-by-case basis.

1.3. Research Objectives

The specific objectives of this research are:

1) To develop a sub-technique for the optimised integration of grid-connected micro-renewable electricity generation systems.

2) To develop a sub-technique for the optimised integration of grid-connected micro-renewable thermal generation systems.

3) To develop an overall technique, through the combination of the two sub-techniques, for the optimised integration of grid-connected micro-renewable electricity and thermal generation systems.

4) To deploy the sub-techniques and overall technique to identify the optimal systems for an Irish domestic dwelling.

1.4. Structure of the Thesis

The thesis is divided into seven chapters and four additional appendices. In Chapter 2, the current energy situation in Ireland and the design of an energy efficient dwelling are described. In Chapter 3, the existing literature is reviewed and similar studies are demonstrated and explained. In Chapter 4, the details of the proposed integration sub-technique for grid-connected micro-renewable electricity generation systems are presented, and the results under current Irish conditions and with realistic parameter variations are demonstrated. In Chapter 5, the details of the proposed integration sub-technique for grid-connected micro-renewable thermal generation systems are presented, and the outcomes under current Irish conditions and with realistic parameter variations are given. In Chapter 6, the details of the proposed overall integration technique for grid-connected micro-renewable energy generation systems are presented, the results under current Irish conditions and with realistic parameter variations are shown. In Chapter 7, the conclusions are drawn from the results presented, the limitations of the proposed integration technique are then discussed and future work is recommended. In Appendix A, a detailed description of generating statistically-

reasonable hourly wind speed data from measured monthly wind speed data is given. In Appendix B, a detailed description of generating hourly solar radiation values for a tilted solar PV module from provided monthly solar radiation values is shown. In Appendix C, a detailed description of generating hourly solar radiation values for a tilted solar thermal collector from supplied monthly solar radiation values is presented. In Appendix D, a detailed description of generating hourly ambient air temperature values from provided monthly ambient air temperature values is given. Finally, in Appendix E, a detailed description of the MATLAB model developed and the sample codes is presented.

1.5. Novelty and Contribution

The work presented in this thesis contributes to the body of knowledge in the optimised integration of grid-connected micro-renewable energy generation area, and the novelty of this work arises from the facts as follows:

- The two sub-techniques and the overall integration technique are generally-applicable and robust to use for any location of interest.
- The integration technique is specifically designed to take into account the actual (measured) domestic hourly electrical load and domestic hourly heating load. This is different from other studies where artificial electrical and thermal load is used for integration.
- A renewable energy requirement concept is developed and implemented in this study in order to assure the percentage of the household electricity demand that must be satisfied by the on-site grid-connected micro-renewable electricity generation systems, and to eliminate systems that cannot meet this user-specified requirement.

- This is a very detailed and accurate economic analysis carried out for four of the most commonly utilised micro-renewable energy generation systems in Ireland to-date.

Due to the wide range of micro-renewable energy generation systems available on the market and the broad range of existing capacity, the developed integration technique is extremely useful for performing an accurate economic analysis and determining a system that is most suitable for a domestic dwelling.

1.6. Publications

The work presented in this thesis has led to the publication of three directly related and one relevant peer-reviewed journal papers in three international journals. Journal paper titled as follows:

- *Domestic application of micro wind turbines in Ireland: Investigation of their economic viability* was published in Renewable Energy in 2011.
- *Domestic application of solar PV systems in Ireland: The reality of their economic viability* was published in Energy in 2012.
- *Domestic integration of micro-renewable electricity generation in Ireland – the current status and economic reality* was published in Renewable Energy in 2014.
- *Rainwater harvesting and greywater treatment systems for domestic application in Ireland* was published in Desalination in 2010.

CHAPTER 2
ENERGY IN IRELAND AND THE DESIGN OF AN ENERGY EFFICIENT DOMESTIC DWELLING

2.1. Ireland's Current Energy Consumption

Ireland's energy consumption has increased significantly since the early 1990s. The total primary energy requirement was 14 million toe (Mtoe) in 2011. Ireland's TFC reached 11.154 Mtoe in 2011, a decrease of 6.7% compared in 2010, but still 54% above the 1990 level of 7.249 Mtoe. Oil (6,820 ktoe), natural gas (4,138 ktoe), coal (1,264 ktoe), peat (761 ktoe) and renewable energy (831 ktoe) were the dominant fuels and accounted for 49.2%, 29.8%, 9.1%, 5.5% and 6.0% of entire energy supply in Ireland in 2011 respectively. The share of total primary energy requirement by fuel type is shown in Figure 2.1. The energy was used for three modes of applications which were electricity generation, heat generation and transportation. The heat generation (4,550 ktoe) was slightly higher than electricity generation (4,506 ktoe) and transportation (4,448 ktoe). The share of primary energy used by each mode was 33%, 34% and 33% respectively.

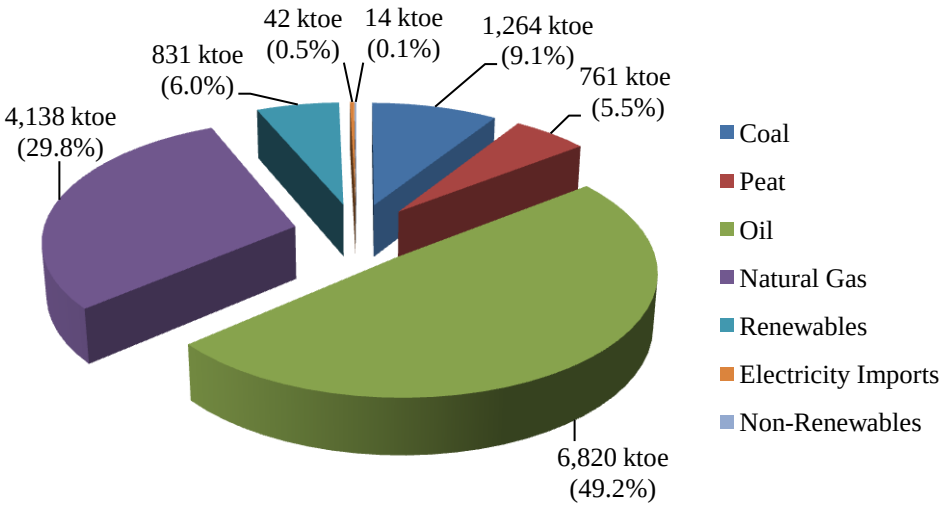

Figure 2.1. The share of total primary energy requirement by fuel in Ireland in 2011.

Ireland is one of the most imported fuels dependant countries in the EU. The overall energy import dependence decreased 2% points from a peak of 90% in 2006 to 88% in 2011 due to the greater utilisation of renewable energy, especially for wind energy deployment.

2.2. Ireland's Current Greenhouse Gas Emission Issues

Ireland is committed to the Kyoto Protocol (signed in 2007) which is an international legally-binding agreement to reduce GHG emissions. The target set for Ireland was to limit the annual GHG emissions to 13% above 1990 levels by the period 2008 to 2012. This target was achieved in 2009. The annual GHG emissions peaked at 27% above 1990 levels in 2001. The sources include energy, industrial processes, solvent and other product use, agriculture and waste. However, GHG emissions have fallen to 57.34 million tonnes (Mt) in 2011 which was below the Kyoto limit of 62.84 Mt CO_2 equivalent set for Ireland. The energy-related emissions were the most significant source of GHG emissions. The share of GHG emissions from energy-related activities

rose from 56% in 1990 to 64% in 2011. The GHG emissions by source in Ireland in 2011 are shown in Figure 2.2.

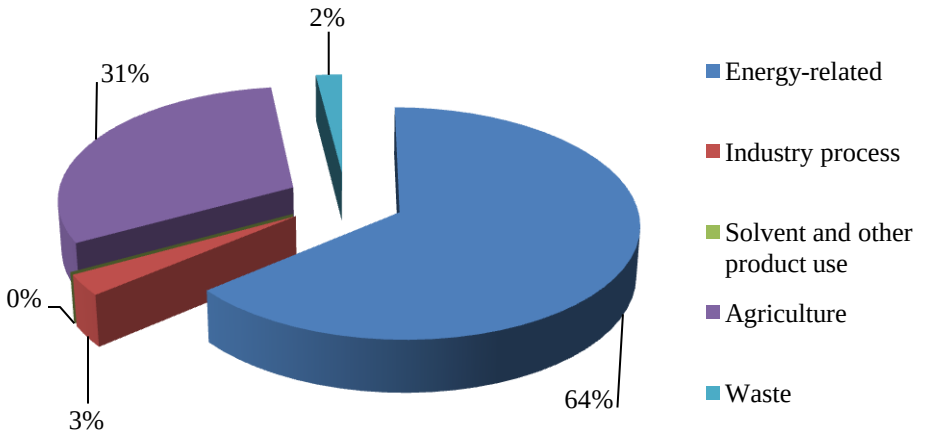

Figure 2.2. Greenhouse gas emissions by source in Ireland in 2011.

The energy-related emissions are also mainly obtained from three modes: electricity generation, transport and thermal generation. Electricity was the dominant mode in terms of emissions from 2000 to 2006. However transport surpassed electricity to become the largest mode from 2006 to 2010 at when thermal generation surpassed transport and became the largest mode in terms of GHG emissions. However transport overtook thermal generation in 2011 to become the largest emitter of GHGs in Ireland. The CO_2 emissions from transport were 13.1 Mt and at a rate of 117% higher than those in 1990. Even though emissions from both thermal and electricity generation had been decreasing since 2006, they still resulted in 12 Mt and 12.8 Mt CO_2 emissions in 2011 respectively.

2.3. Ireland's Residential Sector Energy Status

The average Irish house consumed 19,875 kilowatt hour (kWh) of energy in total based on climate corrected data in 2011. This was comprised of 14,858 kWh (about 79%) in the form of direct fossil fuels and the reminder (5,016 kWh) as electricity. The final energy use grew by 26% to 2,836 ktoe in the residential sector in 2011. This was taken without corrections for climate effects. Oil (1,035 ktoe) was the dominant fuel in the residential sector which had a share of 36% in 2011. Electricity (712 ktoe) and natural gas (569 ktoe) were the second and third most dominant energy form in this sector respectively. Houses built during the 1990s predominantly had oil or natural gas fired central heating; in some cases electric storage heating was in use. The household electricity usage had also risen from 356 ktoe in 1990 to 712 ktoe in 2011. This increase was likely to be the result of increased utilisation of electrical appliances such as washing machines, driers, dishwashers, computers and etc. The use of renewable energy in the residential sector reached 46 ktoe in 2011, but was still only 1.6% of the overall final energy use by fuel in households. The share of TFC by fuel in the residential sector in 2011 is shown in Figure 2.3.

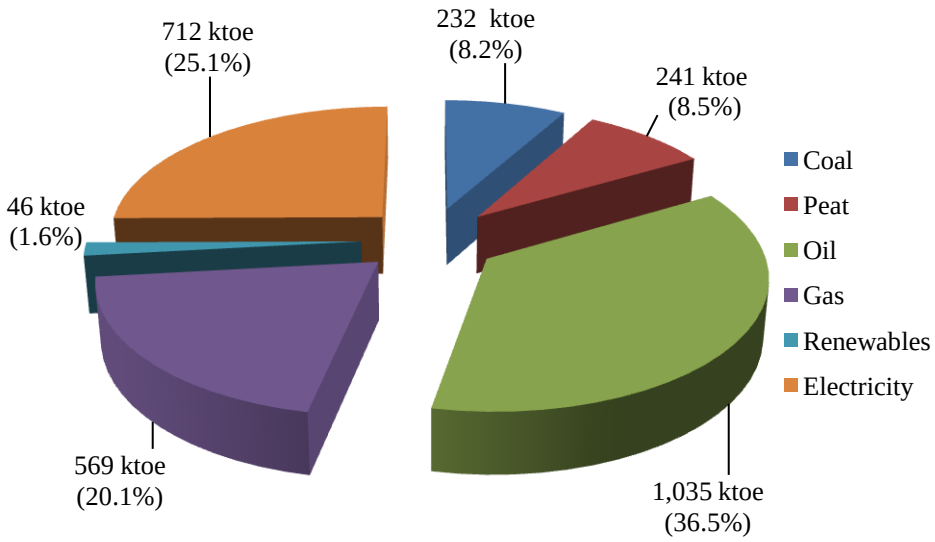

Figure 2.3. The share of total final consumption by fuel in the residential sector in Ireland in 2011.

In 2011, the total spend by the residential sector in Ireland on energy was approximately €3 billion. This high expenditure on energy may be attributed to the significant increase in the energy price in this sector. Based on the average household fuel mix in 2011, the energy price increased by 37% between 2006 and 2011. However, the average Irish household spend on energy fell by 2.3% in the same period and reduced to approximately €1,727 per annum. The reasons for this reduction were likely to include the economic recession forcing households to reduce their energy spend, energy efficiency improvements resulting in lower energy demand, and a greater effort made by householders to reduce their energy demand due to environmental concerns. The imported electricity price and natural gas price (including VAT at the rate of 13.5%) were €0.1928/kWh and €0.05894/kWh in January 2013 respectively. The electricity price (including all taxes) for residential householders in Ireland was 5.1% above the average of the EU-27 countries at the end of December 2011 and Ireland was ranked the eighth most expensive country. However, the natural gas price (including all taxes) for

domestic householders in Ireland were 3.9% below the average of EU-27 countries, and ranked the 11th most expensive country.

2.4. Ireland's Residential Greenhouse Gas Emissions Issues

The residential sector was the largest CO_2 emitting sector in 1990. Energy use in the residential sector accounted for more than 35% of overall energy-related CO_2 emissions. The residential sector started experiencing reductions in energy-related emissions in 2005. However, the residential sector was still the second largest energy-related CO_2 emitting sector following the transport sector in 2011. The residential sector energy-related CO_2 emissions were 10,479 thousand tonnes (kt) CO_2 and accounted for 27% of total energy-related CO_2 emissions in Ireland in 2007. The share of energy-related CO_2 emissions by sector in Ireland in 2007 is shown in Figure 2.4.

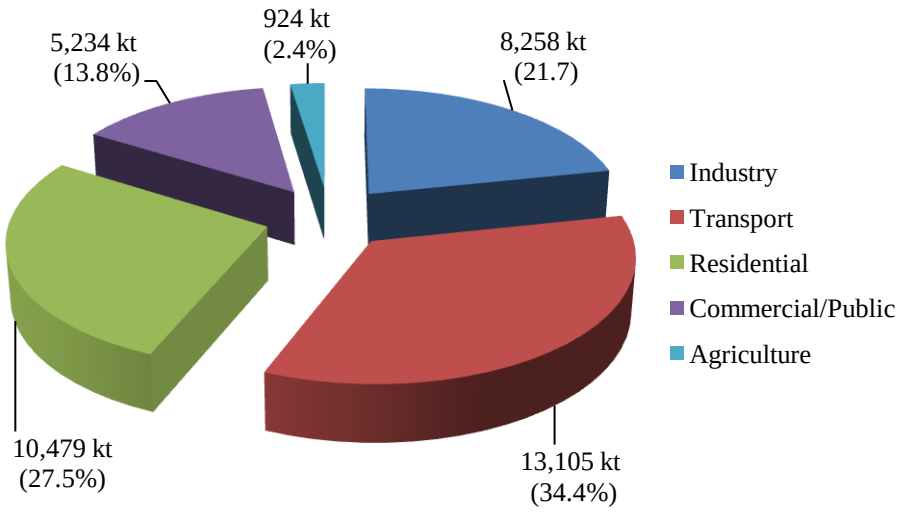

Figure 2.4. The share of energy-related CO_2 emissions by sector in Ireland in 2011.

The average domestic house was responsible for approximately 6.4 tonnes of energy related CO_2 emissions in 2011. This consisted of 3.9 tonnes CO_2 from direct fuel usage and the remainder indirectly from electricity utilisation. However, it should be noted

that the overall CO_2 emissions had reduced by 41% since 1990 and 24% since 2005 from per average domestic dwelling in Ireland.

2.5. Ireland's Domestic Dwelling Energy Consumption

The electricity consumption of an individual household accounts for approximately a quarter of overall energy use. Electricity is mainly used to run electrical appliances which can be separated into two categories: traditional appliances such as lighting, refrigerator with freezer, vacuum cleaner, washing machine, dishwasher, microwave, home computer, television etc and newer appliances such as electric blender, coffee machine, game console etc. Electricity may also provide other services to household such as hotwater generation and cooking. Electricity can be also utilised in electrical storage heaters and electrical instant heater to provide space heating, however this is mainly for apartments.

Domestic electricity demand has been increasing in recent years. One of the main reasons for this is the increasing electricity demand for various electrical appliances. The increase in electricity demand from digital appliances is the most significant due to largely increase in the number of digital appliances, e.g. multiple televisions, laptops, game consoles and etc. The increase can be also caused in some domestic dwellings due to the householders with higher incomes and those living in newer and larger homes who tend to have more electrical appliances and with larger capacities. However, some efficiency gains have been achieved through technical improvements and the labeling of appliances by energy usage, for example the introduction of mandatory labeling of traditional appliances such as refrigerators and freezers, influences the decision made for purchasing and helps reduce in energy demand.

The thermal generation in a domestic dwelling consumes roughly 75% of the total energy and therefore the method of space heating and hotwater generation is a significant factor in energy usage. Central heating systems are mostly utilised for providing space heating in Ireland. The proportion of domestic dwellings having central heating systems has increased from 52% in 1987 to 97% in 2010. Central heating systems are more efficient than individual room heating appliances and/or open fires, and therefore, less energy is required to provide the space heating for achieving the same level of comfort for householders. Gas or oil fired central heating systems are the most commonly installed. Automated control systems such as timers and thermostats are also regularly included into central heating systems for the improvement of convenience. However, energy usage can be increased through requirement of greater convenience and comfort levels in the form of higher temperatures and a move towards whole-house heating. Normally, the space heating raises the indoor temperature from approximately 8-10^{o}C to 18-21^{o}C in winter time [5].

A sharp increase in energy savings per dwelling was observed between 2005 and 2011. A number of standout reasons for this recent energy efficiency improvements were noted such as:

- the increased number of new houses built to achieve a higher energy efficiency standard and satisfy heating control requirements as specified in the building regulations.
- the existing housing stock were helped to make energy efficiency improvements by a number of national residential energy efficiency upgrade schemes offered, such as Greener Homes Scheme (ceased in 2011), Better Energy Homes scheme and Warmer Homes Scheme.

- the decrease in energy use per household included the increasing public awareness of the impacts of energy inefficiency on the environment and sustainability.
- the significantly increased energy price.

The method of hotwater generation is dependent on the central heating system type in each domestic dwelling, and the regularity of the use of the central heating system. Hotwater is generated regularly during the winter as the central heating system is regularly in use. In summer time, hotwater is usually generated from an electrical immersion since the central heating is rarely turned on.

2.6. Ireland's Renewable Energy Status

Renewable energy utilisation reached 747 ktoe in Ireland in 2011. Of this, most was contributed from wind energy (44%). The contribution of overall energy demand from renewable energy was 2.3% in 1990 rising to 6.5% in 2011. Renewable electricity contributed 3.7% to the overall energy demand. This was largely due to the continually increased contribution from wind energy. According to SEAI, the displacement of fossil fuel for electricity generation by renewable energy resulted in an avoidance of an estimated €300 million in natural gas imports. The installed generating capacity of wind power for electricity generation had reached 1,631 Mega Watts (MW) in 2011 and wind energy accounted for over 13% of all electricity generation in 2011. Heat generation from renewable energy accounted for 4.8% of all thermal energy demand in 2011. There was a growth in the contribution from renewable energy to thermal energy from 2.6% in 1990 in Ireland. This was mostly due to the increased use of biomass as an energy fuel mainly in the industrial sector. There was also an increase in biomass utilisation in the residential sector; the residential biomass energy use increased by 9.5%

between 1990 and 2011. However, it should be noted that there was also an increase in use of geothermal energy, air source energy, and solar thermal energy.

Ireland is targeted to meet 16% of its overall energy demand from the contribution of renewable energy by 2020 under EU Directive 2009/28/EC. In order to achieve this overall target, electricity generated from renewable energy will have to achieve 40% of gross electricity consumption; the use of biofuel or electricity generated from renewable energy will have to make up to 10% of road and rail transport energy usage, and 12% thermal (heating and cooling) demands must be generated from renewable energy.

Renewable energy utilisation can largely avoid CO_2 emissions and it was estimated that CO_2 emissions savings from renewable energy utilisation increased by 337% over the period from 1990 to 2011. The total CO_2 saving reached 3,640 kt in 2011. Of this 2,144 kt CO_2 was avoided by using wind energy, 633 kt CO_2 by using biomass and 346 kt CO_2 by using hydro energy.

2.7. Renewable Energy Situation for Domestic Application in Ireland

2.7.1. The Current Micro Wind Turbine and Solar PV System Market

Micro-renewable electricity generation has not been very popular in Ireland to-date. However, a micro wind turbine is by far the most popular type of system for micro-renewable electricity generation in Ireland. After a micro wind turbine, a solar PV system is the next most popular option. As shown in Figure 2.5, micro wind turbines and solar PV systems having total installed capacities of 2,227 kilowatts (kW) and 181 kilowatts peak (kW_p) respectively have been registered with Electric Ireland and connected to the Electricity Supply Board (ESB, the state owned utility) distribution system (electricity distribution system is referred to as “the grid” throughout this study)

in the period from January 2007 to November 2011. These accounted for 91% and 7.4% of the total installed capacity (kW) of grid-connected micro-renewable electricity generation systems in this period respectively [6]. However, the total capacity of installed micro wind turbines and solar PV systems is likely to be higher in this period, as a small number of micro wind turbines and solar PV systems are either connected with batteries or are waiting to connect to the grid.

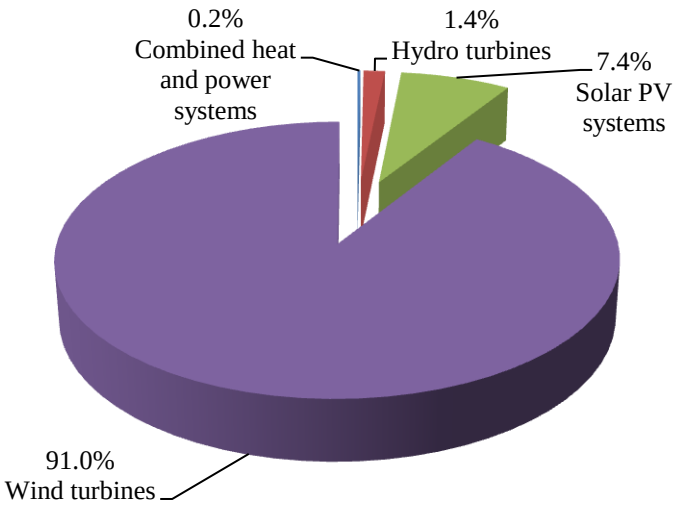

Figure 2.5. Breakdown of capacity (kW) of grid-connected micro-renewable electricity generation systems installed from January 2007 to November 2011 in Ireland. The total installed micro-renewable electricity-generation system capacity in this period was 2,448 kW.

Large capacity (>3 kW) micro wind turbines are the preferred option by householders in Ireland to-date. Of the 2,227 kW (428 turbines) of micro wind turbines installed, approximately 84% have a capacity greater than 3 kW, as shown in Figure 2.6.

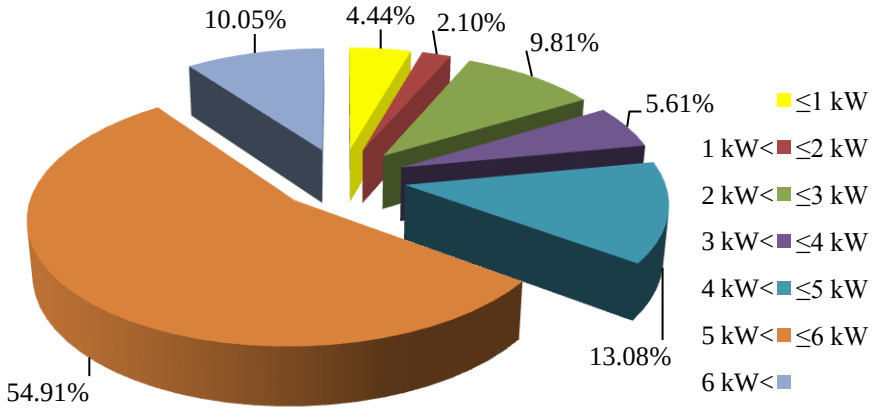

Figure 2.6. Breakdown of capacity of grid-connected micro wind turbines installed from January 2007 to November 2011 in Ireland. The total installed micro-wind-turbine capacity in this period was 2,227 kW.

In contrast to micro wind turbines, small capacity (≤3 kW_p) solar PV systems are preferred by householders to-date. Of the 181 kW_p (78 systems) of solar PV systems installed, approximately 81% have a capacity less than or equal to 3 kW_p, as shown in Figure 2.7.

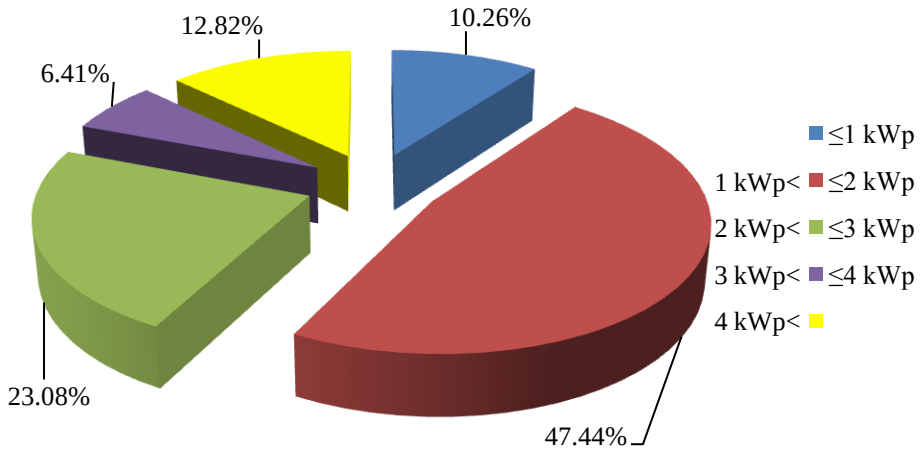

Figure 2.7. Breakdown of capacity of grid-connected solar PV systems installed from January 2007 to November 2011 in Ireland. The total installed solar-PV-system capacity in this period was 181 kW_p.

2.7.2. The Current Legislation and Regulations for Installing a Micro Wind Turbine and a Solar PV System in Ireland

Installing a micro wind turbine or a solar PV system in Ireland is usually subject to planning permission. However, the installation of these systems may be exempt from planning permission if installed under certain conditions. These exemption conditions are clearly stated in the Irish government report *Planning and Development Regulations 2007* produced by the Department of Environment, Heritage and Local Government in January 2007 [7-9]. The conditions for installing a micro wind turbine are:

- The turbine shall not be erected on, or attached to, the house or any building or other structure within its curtilage.
- The total height of the turbine shall not exceed 13 metres.
- The rotor diameter shall not exceed six metres.
- The minimum clearance between the lower tip of the rotor and ground level shall not be less than three metres.
- The supporting tower shall be a distance of not less than the total structure height (including the blade of the turbine at the highest point of its arc) plus one metre from any party boundary.
- Noise levels must not exceed 43 db(A) during normal operation, or in excess of 5 db(A) above the background noise, whichever is greater, as measured from the nearest neighbouring inhabited dwelling.
- No more than one turbine shall be erected within the curtilage of a house.
- No such structure shall be constructed, erected or placed forward of the front wall of a house.

- All turbine components shall have a matt non-reflective finish and the blade shall be made of material that does not deflect telecommunication signals.
- No sign, advertisement or object not required for the functioning or safety of the turbine shall be attached to, or exhibited on, the wind turbine.

The conditions for installing a solar PV system are:

- The total aperture area of any such panel, taken together with any other such module previously placed on, or within, the said curtilage, shall not exceed 12 m^2 or 50% of the total roof area, whichever is the lesser.
- The distance between the plane of the wall or a pitched roof and the module shall not exceed 15 cm.
- The distance between the plane of a flat roof and the module shall not exceed 50 cm.
- The solar module shall be a minimum of 50 cm from any edge of the wall or roof on which it is mounted.
- The height of a free-standing solar array shall not exceed 2 m, at its highest point, above ground level.
- A free-standing solar array shall not be placed on, or forward of, the front wall of a house.
- The erection of any free-standing solar array shall not reduce the area of private open space, reserved exclusively for the use of the occupants of the house, to the rear or to the side of the house to less than 25 m^2.

If the installation of a domestic micro wind turbine or a solar PV system does not satisfy these conditions, such as the turbine does not meet the height requirement or the total surface area of the solar PV panel is greater than the area stated, it must undergo the

planning process, and permission may still be given, However, a roof-top-mounted wind turbine does not qualify for exemption from planning permission; it must be considered on a case by case basis.

In order to protect the grid, the maximum export capacity from a grid-connected micro-renewable electricity generation system is subjected to a limit: 6 kW when the connection is single phase and 11 kW when the connection is three phase. However, a micro-renewable electricity generation system with a total capacity exceeding the above limits can still be connected to the grid once the maximum export capacity is limited to 6 kW single phase and 11 kW three phase. A micro-renewable electricity generation system having a total capacity of 50 kW or less is eligible for connection to the grid [10].

2.7.3. The Current Financial Support for Exporting Electricity Generated from a Grid-Connected Micro-Renewable Electricity Generation System

In general, €0.09 is paid by Electric Ireland to the householder for every kWh of electricity exported to the grid from a micro-renewable electricity generation system. This price is a standard payment tariff and there is no restriction on the amount of electricity exported. Previously there was an additional incentive payment of €0.10/kWh for the first 3000 kWh of exported electricity in a year. This payment applied for a maximum of five years and was supplied by Electric Ireland in order to encourage householders to utilise a micro-renewable electricity generation system [10]. This incentive payment was ceased on February 28th, 2012.

2.7.4 The Current Air Source Heat Pump and Solar Thermal System Market

A large number of micro-renewable thermal generation systems were installed in Ireland during the period when the Greener Homes Scheme grant was offered by SEAI. The solar thermal system is undoubtedly the most popular type of system for micro-renewable thermal generation in Ireland. Heat pumps and biomass-type systems are also popular options for households. As shown in Figure 2.8, solar thermal systems, heat pump systems and biomass systems having total installed numbers of 22,903, 6,029 and 6,113 respectively have obtained grants from the Greener Homes scheme for systems installation, and registered and stored in the Greener Homes scheme database in the period from March 2006 to May 2011. These accounted for 65%, 17.12% and 17.35% of the total number of installed micro-renewable thermal generation systems in this period respectively. However, the total number of installed solar thermal systems, heat pump systems and biomass systems is expected to be slightly higher than the number shown in this period, as a small number of solar thermal systems, heat pump systems and biomass systems did not apply for a grant, and therefore were not registered with SEAI. The number of solar thermal systems installed is continuously increasing with the help of Better Energy Homes scheme which is also provided by SEAI. The number of installed solar thermal system is 9,506 since the start of this scheme in March 2009 until December 2013. However, this scheme does not offer grants for other types of micro-renewable thermal generation systems. The number of these systems installed is expected to be small due to the lack of grant support and the adverse impact of the economic recession.

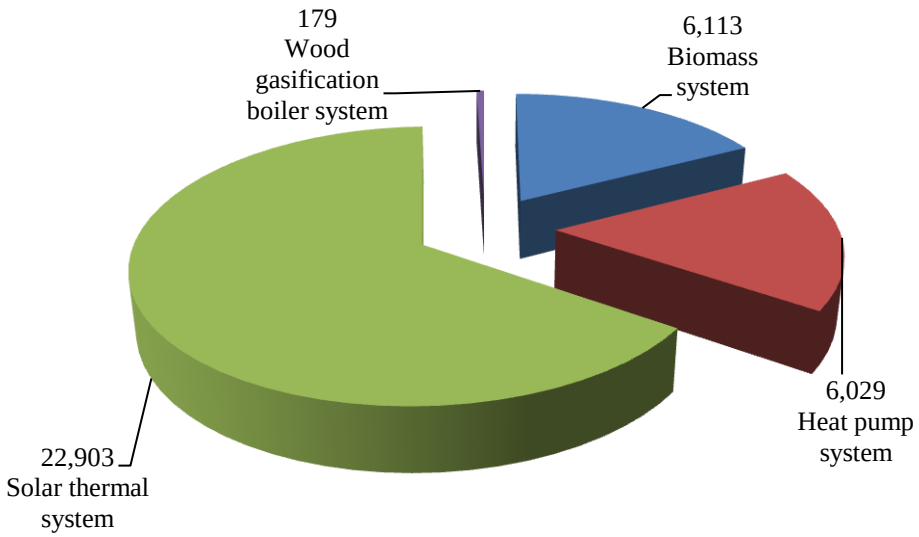

Figure 2.8. Breakdown of the number of micro-renewable thermal generation systems installed from March 2006 to May 2011 in Ireland. The total number of installed micro-renewable thermal-generation systems in this period was 35,224.

ASHPs are not the first choice for a domestic heat pump system installation to-date. The number of installed horizontal ground source heat pumps (GSHPs) was greater than the number of installed ASHPs during the period in which the Greener Homer Scheme was offered; however the number of installed ASHPs was not far from the number of installed vertical GSHPs, as shown in Figure 2.9.

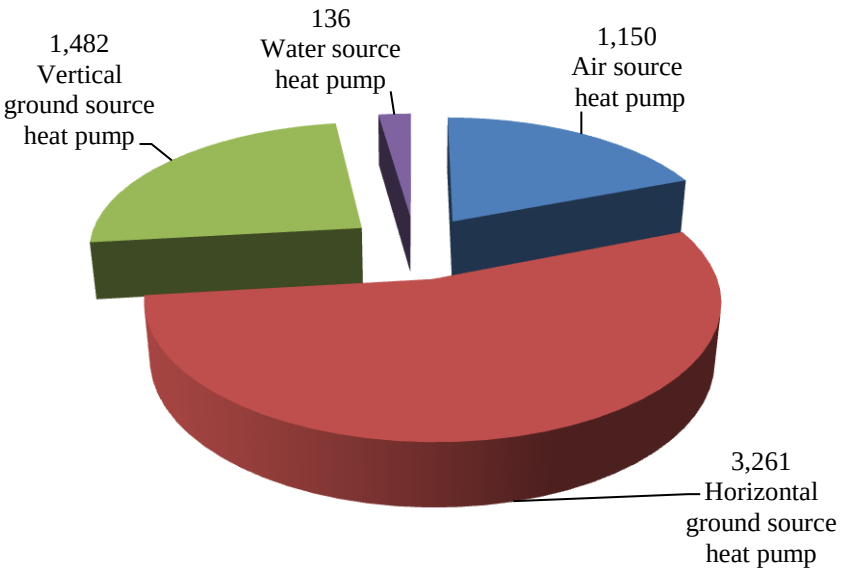

Figure 2.9. Breakdown of the number of heat pump type installed from March 2006 to May 2011 in Ireland. The total number of installed heat pumps in this period was 6,029.

During the period of Greener Homes Scheme application, the number of solar thermal system was recorded in two phases. In the first phase from March 2006 to July 2007, the number of installed solar thermal systems was recorded based on the application of the hotwater generated from the solar thermal system, as shown in Figure 2.10. This shows that the solar thermal system was mainly used for domestic hotwater application only; few systems were installed with the purpose of providing hotwater and heating.

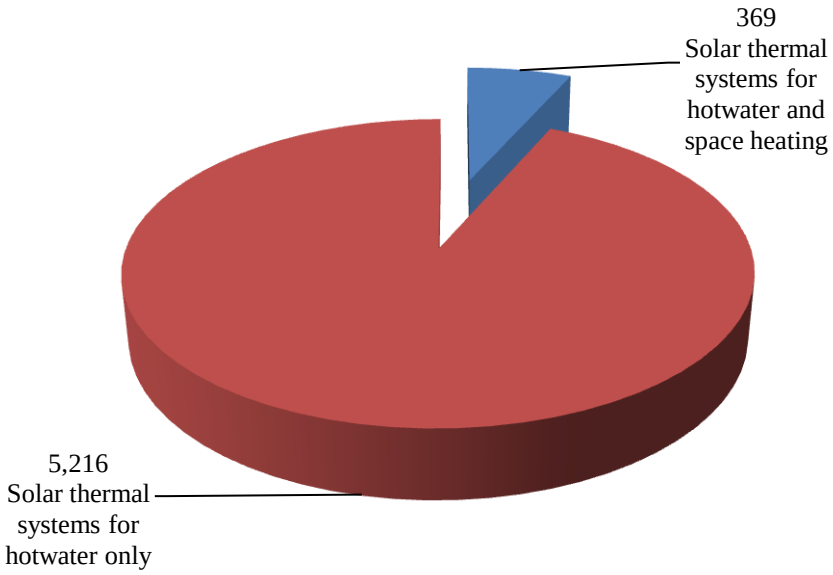

Figure 2.10. Breakdown of the number of solar thermal system installed by thermal application from March 2006 to July 2007 in Ireland. The total number of installed solar thermal system in this period was 5,585.

In the second phase from August 2007 to May 2011, the number of installed solar thermal systems was recorded based on the solar collector type. It can be noted that the number of solar flatplate collectors used was slightly greater than the number of solar evacuated tube collectors used for domestic application in Ireland, as shown in Figure 2.11.

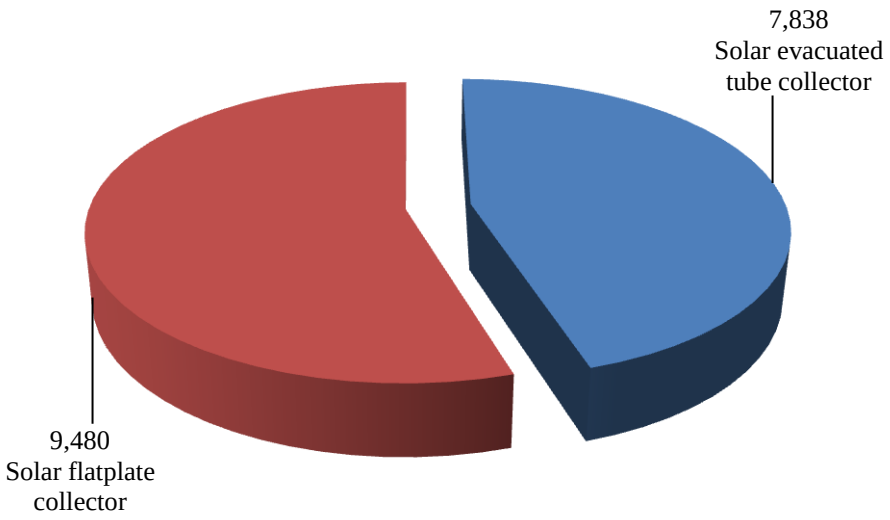

Figure 2.11. Breakdown of the number of solar thermal systems installed based on the type of solar thermal collector used from August 2007 to May 2011 in Ireland. The total number of installed solar thermal systems in this period was 17,318.

2.7.5. The Current Legislation for Installing an Air Source Heat Pump and a Solar Thermal System in Ireland

The installation of an ASHP or a solar thermal system in Ireland can be also exempt from planning permission if installed under certain conditions. These conditions for installing an ASHP are:

- The total area of an ASHP, taken together with any other pump previously erected, shall not exceed 2.5 m^2.
- The ASHP shall be a minimum of 50 cm from any edge of the wall or roof on which it is mounted.
- No such structure shall be erected on, or forward of, the front wall or roof of the house.
- Noise levels must not exceed 43 db(A) during normal operation, or in excess of 5 db(A) above the background noise, whichever is greater, as measured from the nearest neighbouring inhabited dwelling.

The exemption conditions for the installation of a solar thermal system are the same as for a solar PV system and stated above.

2.8. Energy Efficient Domestic Dwelling

Prior to the installation of any micro-renewable energy generation system, the domestic dwelling should improve its energy efficiency so that lower capacity electricity and space heating generation systems are required while maintain the same convenience and comfort for householders. Energy-saving electrical appliances and lighting devices should be used to lessen the electricity consumption in a domestic dwelling. Improvements in thermal insulation are the most important step towards reducing heating demand in a domestic dwelling. Wind is an excellent energy resource, but it also has a large influence on a dwelling's heat loss since heat can be quickly taken away from dwelling's surface by wind. Ireland is one of the windiest parts of Europe, resulting in a greater heating loss due to wind compared with other countries. The insulation thickness needed depends on the geometry of the house and the amount of the internal heating loads required. Thicker insulation implanted can result in less heating loss from the dwelling to the surroundings. The insulation materials chosen are also an important factor. Materials with a high thermal resistance can enhance the insulation performance. For a new dwelling, the insulation should be planned well before building. It is very costly to improve at a later stage compared to other components of the house. For an existing dwelling, insulation can be added to the walls or roof if none has been fitted, or, if insulation is already installed, it can be improved to help the dwelling become more energy efficient. The financial support for upgrading the domestic dwelling insulation is offered by SEAI through the Better Energy Homes scheme and Warmer Homes scheme. Well insulated doors and double or treble glazed windows can

also effectively lower the heating requirement in the dwelling. Therefore, a good insulation provides the advantage of having a need of a low temperature heating system. As a result, a reduction in supplying heat of $1^{o}C$ in internal air temperature may save up to 10% of energy consumption. The dampness can make people very uncomfortable, but this problem is occurred mainly in under-heated dwellings in winter and is rarely observed in well insulated dwellings. It is vital the occupants experience good thermal comfort in the dwelling.

Air leakage is also a major source of heating loss in the house. The abundant wind in Ireland has large impacts on houses having poor airtightness. The energy efficient dwelling envelope should be extremely air tight to avoid infiltration of cold air. This uncontrolled infiltration of air through cracks and gaps in the fabric of houses leads to an increase in energy demand for space heating and the cold draught also causes occupants' discomfort. Airtightness should be considered carefully at the design stage of a new dwelling construction or an existing dwelling renovation. The barriers employed to prevent air leakage should be identified and any gaps between the barriers should be sealed. This is of crucial importance to ensure that air leakage is avoided. It is equally important to carry them out in the construction phase. Even though good airtightness significantly reduces air leakage, the house should not be too airtight. The best airtightness level of an energy efficient house should be approximately 0.6 air changes per hour (ACH) by a pressurisation of 50 Pa, resulting in approximately 0.05 ACH infiltration rate under normal conditions [11]. Good ventilation ensures occupants live in a comfortable and healthy environment.

2.8.1. Passive Solar Features Applied in an Energy Efficient Dwelling

Solar energy is used indirectly to produce electricity and hotwater through solar PV systems and solar thermal systems respectively. These systems are defined as active energy generation systems. However, a passive solar system provides natural heating and cooling by using solar energy directly for the dwelling. Passive solar design involves the dwelling's location and orientation, windows' surface areas as well as the correct utilisation of energy efficient windows, shading and thermal mass. A passive solar system provides the interior thermal comfort for the occupants whilst reducing the requirement of active heating and cooling. It is one of the most cost-effective ways in improving the energy performance of a dwelling. Passive solar design also provides a better use of natural daylight for lighting purposes.

2.8.1.1. Passive Solar Heating for Domestic Dwellings

Passive solar heating as shown in Figure 2.12 presents the most cost-effective way of supplying heating to a dwelling. The two elements that are essential in all passive solar heating design are the:

- Selection of high-performance windows and the orientation of the windows area to face towards south.
- Use of high thermal mass materials to construct walls and floors. The heat is absorbed and stored in the walls and floors, and released by radiation, convection and conduction when the surrounding has cooled down.

According to research, a dwelling designed using passive solar principles can require less than half the heating energy of the same dwelling using conventional windows with random window orientation [12]. The standard space heating requirement is 15 kWh/m^2

annually in a well designed and constructed dwelling employing passive solar techniques in the Irish climate. The space heating demand can be reduced by up to 80% in comparison with a conventional dwelling in Ireland [13].

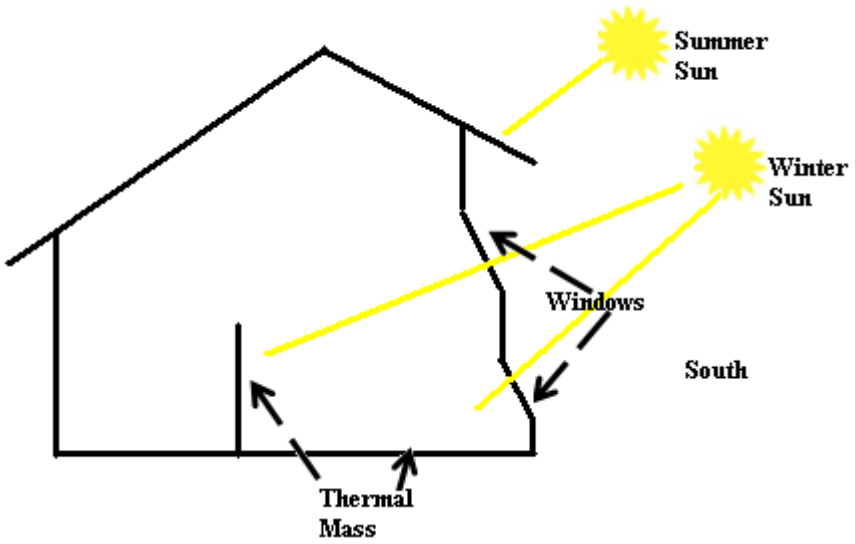

Figure 2.12. Passive solar heating for a domestic dwelling.

Passive solar heating systems can be separated into four types of system: direct gain, indirect gain, sunspace and rock bed.

- Direct gain - this is the simplest approach and it is the most common used in passive solar heating architecture. Sunlight is admitted to the interior space through south facing windows and skylights, and then stored as thermal energy. The roof, walls and floor are used for solar collection and heat storage by intercepting radiation directly and/or by absorbing reflected or reradiated energy. Once the temperature is high in the interior space, the thermal storage mass materials will conduct the heat to their cores. The stored heat is gradually released when the outside temperature drops and the interior space cools in order to reach equilibrium at night. Thermal mass plays the most important role in a direct solar gain house. A wide range of heavy materials like concrete, rocks, bricks all have high thermal mass. Water contained

within plastic or metal containers sometimes can take the place of heavy materials. Thermal mass not only causes delays in its response to heat sources such as solar gains (known as the thermal lag effect [14]) but also reduces the peaks of the temperature swings in the interior space. The effectiveness of thermal storage mass depends on its thickness, surface area and thermal properties. High density masonry performs well at a thickness of 10 cm to 20 cm, regardless of the location, configuration and mass surface area. The mass surface area should be relatively dark in colour and located in the dwelling zones which experience direct solar gain. The materials should possess high volumetric heat capacity and high thermal conductivity.

- Indirect gain - this design approach uses a mass wall placed between the interior space and the sun. There is no direct heating. A dark coloured thermal mass wall is usually placed just behind a south facing glazing. The heat is stored or conducted through the mass wall to the inside space. The sunlight enters through the glazing and is absorbed in the mass wall. The glazing functions to reduce the heat loss to the outside. This stored heat is emitted into the interior space when the temperature drops. There are three common types of thermal mass wall:
  - The masonry mass wall - this is the simplest mass wall. The wall absorbs sunlight radiation, stores the heat and reradiates it to the interior space when it cools down.
  - The Trombe-Michel wall - the Trombe-Michel mass wall cannot absorb solar energy as quickly as it enters the narrow space between the window area and the mass wall. Temperatures in this space can easily become very high. The Trombe-Michel mass wall has controllable vents at high and low levels to allow convective heat transfer. The heated air rises up due to less density. It flows into

the interior space from high level vent. Cool air is drawn into the heating space from the low level vent to replace outflow heated air. The air is continuously circulated as long as the air entering at the low level is cooler than the air at the high level. The vents can be also closed to keep cold air out, then the interior space is heated by the thermal mass wall.

- The water wall - this water wall can be used to replace the masonry wall as water has a greater unit heat capacity than masonry materials for a given volume. There are no vents at the high and low level of the water wall. Tall fibreglass tubes are often used in this application. The principle of operation is the same as the masonry wall. The water is heated, the convection process quickly distributes the heat throughout the mass, and the wall radiates heat to the interior space.

- Sunspace - a sunspace also known as solar greenhouse has become one of the most attractive passive solar features. A south facing sunspace is constructed in front of a thermal mass wall exposed to the direct sunlight. The wall is usually at the rear of the sunspace and at the front of the primary structure. The sunspace performs its passive solar heating function by transmitting solar radiation through its glazing and absorbing solar heat on its interior surfaces. Some of the heat is quickly transferred by natural convection to the sunspace air as the heat is directly used to maintain a suitable temperature in the sunspace. Some sunspaces are operated as a hybrid system. A fan is used to transfer heated air from sunspaces to other house spaces. A regulator is often used to control the sunspace and interior room temperature. It allows the heated air to flow into the interior rooms at appropriate temperatures from the sunspace. This is the primary purpose for many sunspace applications. The heat can also be absorbed and stored in the thermal mass walls. This is the same

principle as indirect gain. The heat stored in the thermal mass walls will be released when the interior space or sunspace temperatures drop. The Trombe-Michel wall and water wall are popular replacements to conventional masonry walls in this application.

- Rock bed - this is used as an effective and favourite hybrid application in a passive solar house. The rock bed is commonly located beneath the source of hot air. It absorbs the excess heat in the air in order to reduce the space temperature and improve thermal comfort. It is also possible to store heat in the rock bed for later use. Hot air flows through the rock bed by natural convection. A convenient approach is often used to place the rock bed underneath the floor in the house. The rock bed should spread across 75% to 100% of the floor area if the house is located in a cold climate, and 50% to 75% in the moderate climates [15]. The distribution of heat from the rock bed to the space is entirely passive. The floor temperature only needs to be a few degrees above the room temperature. The thermal comfort can be improved greatly by keeping the floor temperatures 3-6^{o}C above what they normally would be. A sunspace can work well with rock bed. The heated air from the direct gain is used to charge the rock bed. The heat is used by means of radiation and convection to the space from the heated rock bed surface. The rock bed also effectively reduces the large temperature swings in the house.

2.8.1.2. Passive Solar Cooling for Domestic Dwellings

Natural cooling can be as important as heating in a dwelling. Without a proper natural cooling system, a significant amount of energy may be required from air conditioning units to handle the peak heat gains and keep the rooms comfortable in the summer. However, active cooling is rarely required under the Irish climate since the internal

temperature of the dwelling seldom becomes too high to be of discomfort for householders. Very few dwellings have an air conditioning unit installed. Nevertheless, natural cooling using passive solar technique is still important for Irish applications especially for occasions when ambient temperature rises to an uncomfortable level.

The use of effective insulation and overhangs can reduce the heat gain. Movable, tightly sealed insulation always work well in the summer as the roof and glazing can be covered in order to reduce solar radiation entering the house during the day, thereby ensuring that less heat is received in the interior space. The moveable insulation is either manually operated or mechanically operated. An automatic timer, a thermostat or a light sensitive device is used to drive the motor in the mechanical system to open or close the insulation. South facing windows receive the best solar radiation in winter; however they also could be the potential source of overheating during summer months. The possibility of overheating can be significantly reduced by applying an overhang on the roof or on the glazing. The permanent overhang takes advantage of the fact that the sun is higher in the summer and lower in the winter. The length of an effective overhang should be roughly equal to half the height of the window opening [15]. The overhang usefulness can be increased if they are manually adjustable. The adjustable overhang can be rolled forwards or backwards to prevent or admit the sunlight entering into the house in different seasons. The thermal mass such as masonry walls, floor and water walls can act as heat sponges. They absorb heat and slow down internal temperature rise in hot days. The thermal mass can be cooled by night-time natural convective cooling and/or by using mechanical cooling during off-peak hours.

Heat can be removed by convective cooling methods in a dwelling. A fan assisted convective system is the most commonly used. The interior temperature is lowered by exhausting the warmer air through purposely installed high level openings and a fan is

used to draw in cooler, replacement air from low level openings. The interior space temperature can be also lowered by introducing air through a tube buried a couple of meters beneath the dwelling. A fan draws the outside air into the dwelling through the tube. This air cools down as it passes through the tube. The heat of entered air can be also reduced by a previously cooled rock bed. The rock bed is usually cooled from natural convective cooling at night or mechanical cooling at the off-peak time.

2.8.1.3. Passive Solar Lighting for Domestic Dwellings

The effective use of passive solar techniques for lighting can sufficiently reduce the time of having the electrical lighting turned on, thus decreasing the electricity consumption considerably. Sunlight provides natural lighting for daytime interior lighting. The general rule for a daylight room is that the glazing area is at least 5% of the room floor area. Good natural lighting in a dwelling can be accomplished by having high visible-light-transmittance (VT) glazing on the east, west and north façade, and large windows facing south. Low-emissivity coatings also help minimise glare while offering improved climatic heat gain or loss.

CHAPTER 3
LITERATURE REVIEW

3.1. Overview

In this chapter, the most recent literature on the integration of micro-renewable electricity and thermal generation systems is reviewed. The integration technique for each study is explicitly explained. The novelty of these integration techniques is presented. Common concepts employed in these integration techniques are identified. The most commonly employed/reputable software packages are described and a justification is presented for the selection of Hybrid Optimisation of Multiple Energy Resources (HOMER) and Transient System Simulation Tool (TRNSYS) as the most appropriate software packages for this research. The most recognised and employed optimisation approaches for integrating micro-renewable energy generation systems are also reviewed and a justification is given for the selection of the iterative approach as the most appropriate method for this research.

3.2. Literature review

McGowan et al. (2008) presented a study to investigate the feasibility of a renewable energy housing development in the United States using wind power and solar thermal systems to achieve a net-zero-energy consumption [16]. In this study, the problem, a lack of community-scale projects employing on-site renewable technologies (wind power and solar power technologies) and energy efficiency measures to successfully achieve the goal of net-zero-energy, had been identified. A tool was therefore developed

to analyse and compare various system designs for a net-zero-energy house. The energy performance and economics of the designs were compared for various sizes of housing development which itself depends on the number of houses available for the area considered. Seven wind turbine models having a capacity range from 10 kW to 1500 kW and various types of heating systems were selected for analysis. Hotwater was to be generated from a solar thermal system and an auxiliary electrical immersion; if possible, space heating was intended to be provided by a solar thermal system, with assistance from a single capacity ASHP or GSHP having a fixed coefficient of performance (COP), or from an electric resistance heater. Five U.S. cities, one in each of the five climate zones based on their wind power potential, were selected for this study. The optimal system integration for each city was determined based on economic benefit, taking into consideration the wind and solar energy availability, energy prices and state incentives. The primary conclusion drawn from this study was that there were cases for renewable, net-zero-energy housing development. However these cases were more expensive than the deployment of the natural gas heating systems. The key variables that affected the economics of net-zero-energy housing were the on-site load, in particular the heating load, and the price of energy. On final analysis, when net-metering programs were applied, the large-scale wind turbines presented greater economic advantage than small-scale and medium-scale wind turbines for community-scale projects. Figure 3.1 shows the prediction method used to obtain the total electrical load from a net-zero-energy house.

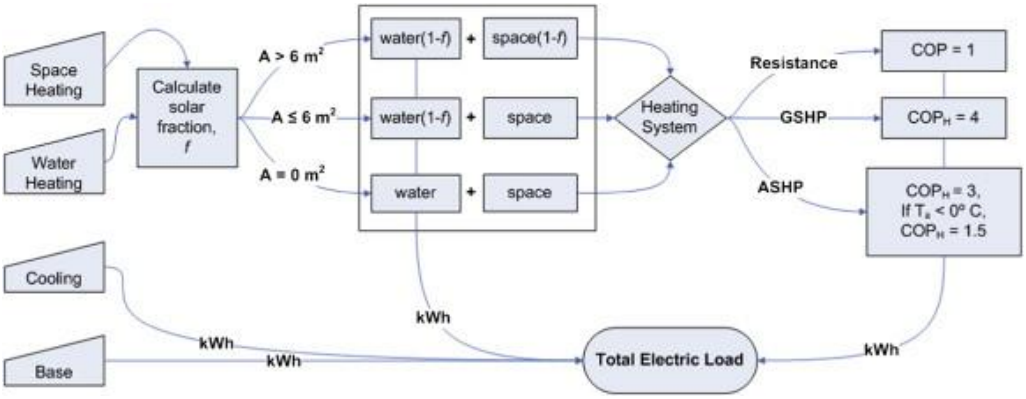

Figure 3.1. A prediction method used to obtain a total electrical load from a net-zero-energy house.

Wang et al. (2009) presented a study to investigate the feasibility of a net-zero-energy house design in the United Kingdom (UK), and also provide a specific method to achieve a net-zero-energy house design in the UK [17]. In this study, two simulation software packages (EnergyPlus and TRNSYS) were employed. EnergyPlus simulations were employed to perform a building envelope design of an energy efficient house, while considering building materials, window sizes and orientations. TRNSYS was employed to investigate the feasibility of a net-zero-energy house design objective through the integration of a renewable electricity generation system, a solar hotwater generation system and an energy efficient heating distribution system under Cardiff weather conditions. Prior to the deployment of renewable energy technologies, the prospective house design must have achieved the passive house standard. Following parametric studies, it was found by this study that the house should be south facing, have window to wall ratios of 0.4 at the south façade, 0.1 or less at other oriented facades, and have the U value of the external wall to be 0.1 W/m^{2}K. Furthermore, the U values of the glazing and the roof should be 1.367 W/m^{2}K and 0.2 W/m^{2}K respectively, and the air change rate should be 5 ACH. The solar thermal system was designed to provide domestic hotwater. Five varying solar collector areas and four varying mass

flow rates of fluid running in the solar circuit were investigated. Two factors were considered for selecting the optimal system: solar collector efficiency and solar fractional energy savings. A 5 m^2 solar collector area with a mass flow rate of 20 kg/h was selected. Underfloor heating had been demonstrated as the best space heating option due to its large heating area and lower temperature requirement. The ASHP and GSHP were considered for use with the underfloor heating; the energy consumed by the ASHP was 953.2 kWh with the assumption of a COP of 3.0 when providing water at 40^{o}C. The energy consumption would be further reduced if a GSHP was employed, as in general GSHP has a higher COP. Micro wind turbines and solar PV systems were studied to provide electricity for the net-zero-energy house. Two 2.5 kW wind turbines with the hub height of 15 m were selected for this study. A solar PV system with a total rated power of 1.32 kW_p was also employed. The total annual power output obtained from these two renewable electricity generation systems was 7,306 kWh which was sufficient to achieve the zero-net-energy house as the total electricity consumption of the house was 4,672 kWh. However it is noted that wind turbines generate a considerable amount of electricity during all four seasons, solar PV system can only produce comparable amount of electricity during the summer. Figure 3.2 shows a scheme diagram of a grid-connected renewable electricity generation system employed to achieve the net-zero-energy house.

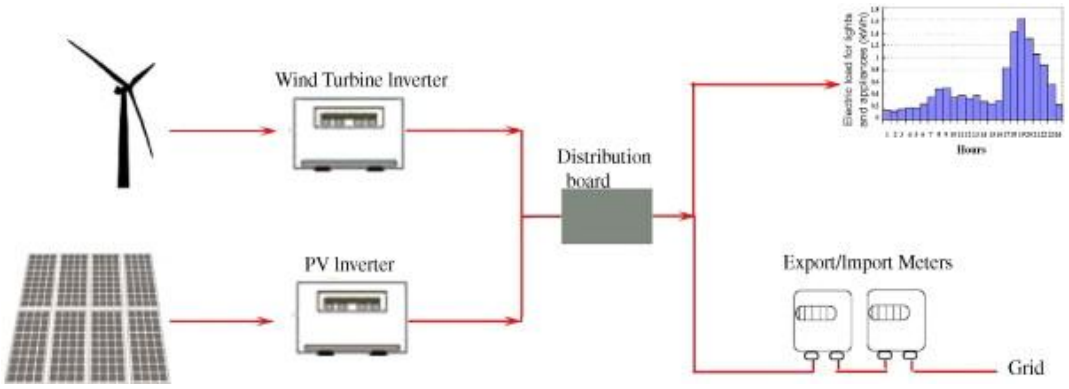

Figure 3.2. A scheme diagram of a grid-connected renewable electricity generation system.

Bojic et al. (2011) presented a study to report the investigation of a residential building energised by the electricity supplied from a solar PV system and the electricity grid in Serbia. In this study, the electricity generated from a solar PV system is either consumed by the building or fed to the electricity grid; the grid is used as a form of electricity storage. Electricity was utilised to run a GSHP for heating supply, to produce hotwater, and to operate lighting and electrical appliances. Three artificial residential buildings were investigated, each was designed to minimise the energy required for space heating during winter, and also to employ efficient lighting and electrical appliances. The first building was a net-negative-energy building where the solar PV system only produced sufficient electricity for the heating system. The second building was a net-zero-energy building where the solar PV system produced enough electricity to meet the entire electrical load. The third building was a net-positive-energy building where the south-facing roof of the building was entirely covered by solar PV panels. The solar PV system produced more electricity than the building required. The investigations were performed using EnergyPlus software package. The energy consumed from the building, energy generated from a solar PV system and energy purchased from the electricity grid were obtained. The study showed that it is critically

important to have a solar PV system connected with the electricity grid. The daily energy distribution clearly showed that the electricity grid was required to overcome periods of low energy production from the solar PV system. The findings also indicated that the quantity of electricity generated by a solar PV system during winter was almost one half the quantity produced during summer, on a monthly basis. The payback period method was used to make an economic comparison amongst the three buildings. The shorter payback was achieved by offering a higher feed-in tariff, charging a smaller unit price and installing a large size solar PV array. For better economy, it was also recommended that a net-zero-energy building should go forward to become a net-positive-energy building. Figure 3.3 shows a scheme consisting of the house, its heating system and the PV system employed in this investigation.

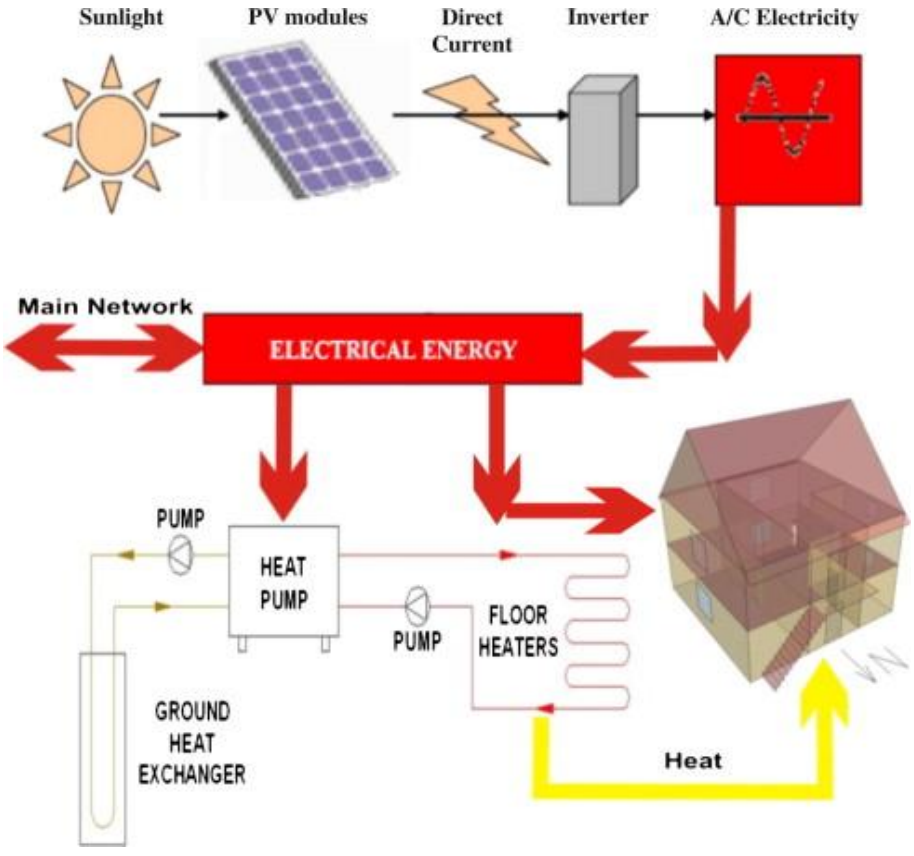

Figure 3.3. The house, its heating system, and a solar PV system under the investigation.

Marszal et al. (2011) presented a study in which the life cycle cost (LCC) analysis method was used to investigate the cost-optimal relationship between the implementation of energy efficient measures and the employment of renewable energy technologies [18]. In this study, the extent of energy efficient measures that should be taken before renewable energy technologies are applied for a net-zero-energy building design was considered. The economic analysis, applied into a multi-storey net-zero-energy building, was performed in order to identify the cost-effective relationship between energy efficiency measures and the implementation of renewable energy technologies. The energy demands were considered using the energy performance requirement as set by the Danish building regulations for 2010, 2015 and 2020. Three alternative energy supply systems were considered: a solar PV system with a solar PV/thermal (PV/T) system combined with an ambient air/solar source heat pump; a solar PV system with a ground source heat pump; and a solar PV system with district heating. Each of the alternative energy supply systems was employed to provide electricity, heating and hotwater for the three defined levels of energy demand in the building. The LCC (over the lifespan of a building) was evaluated considering the cost of investment, operation, maintenance, replacement and demolition. The results indicated that, with the intention of building a cost-effective net-zero-energy building, firstly the energy usage should be minimised, and thereafter the renewable energy generation systems should be employed to offset the remaining energy consumption. In this study, a combination of a solar PV system and a GSHP was found to be the cost-optimal system for the net-zero-energy building in a dense city area. If the cost was less important, the combination of a solar PV system, a solar PV/T system and an air/solar source heat pump was the most energy efficient solution, and this system also best suits cases where a limited area is available for renewable energy systems installation. It was

also found that the combination of a solar PV system with district heating was the most expensive and the least attractive option due to its high operation and maintenance cost. Several sensitivity analyses were also conducted to determine the influence of the price of solar PV and solar PV/T collectors, household electricity usage, primary energy factors for heating-electricity, real interest rate and lifespan of a building. Figure 3.4 shows the result of the differences in the LCC between reference case PV-PV/T-HP and other alternatives.

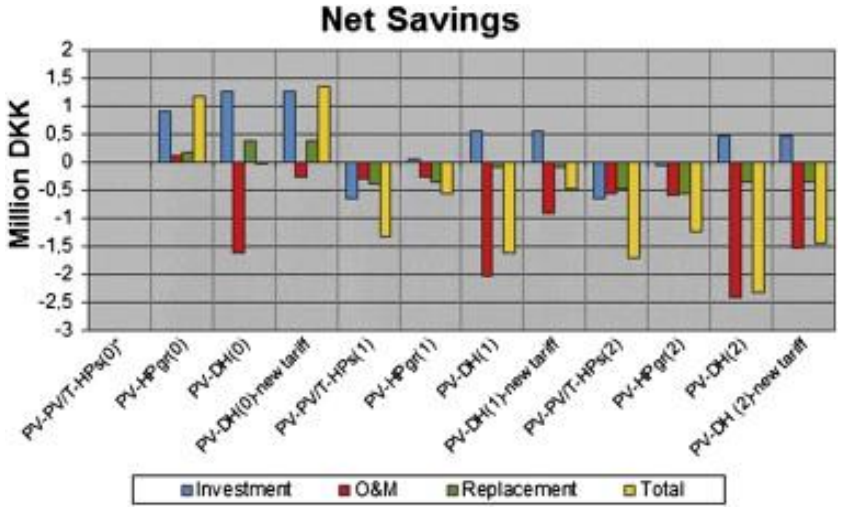

Figure 3.4. The differences in the present-value LCC between reference case – PV–PV/T–HPs and other alternatives. Positive values represent savings and negative values represent additional cost.

Graça et al. (2011) presented a study to explore the feasibility of solar net-zero-energy building systems for a typical single family home in the mild European climate zone [19]. The utilisation of solar energy, in the form of electricity and thermal generation, were the main focus of renewable energy systems proposed in this study. The impact of building envelope design, occupant behaviour and domestic appliance efficiency on the final energy demand for two representative house geometries was analysed. The energy demand profile of domestic heating and cooling, domestic hotwater and electricity were

predicted. Based on this prediction, combinations of renewable energy technologies were sized in order to meet all annual energy needs using a dynamic thermal simulation tool. The renewable energy technologies considered were a solar thermal system, a solar PV system and a heat pump. The solar thermal system was sized to meet the majority of the heating and hotwater demand. The heat pump, operated using electricity, was employed to provide the deficit heating that the solar thermal system could not supply. The design process began with sizing a solar thermal panel area and a storage tank volume, then sizing the capacity of a heat pump required for satisfying the deficit heating demand. The solar PV systems were then sized to supply the entire electricity requirement for the house, including that for the heat pump, on an annual basis. The optimal configuration was then identified by performing an economic and environmental analysis. From the results of economic analysis, all net-zero-energy building solutions were shown to have similar solar thermal systems, i.e. an area of 4 m^2 solar thermal collectors and a volume of 300 L thermal storage. However, the area of solar PV panels required to meet the demand of a net-zero-energy building can vary by a factor of three and a half, depending on the energy efficiency of the building and the electrical appliances used. From the results of this study shown, the initial costs of systems that were capable of achieving the net-zero-energy building target were significantly greater than the other systems that were unable to meet this target. The introduction of a micro-generation government incentive scheme made net-zero-energy buildings economically attractive, as the evidence showed that the payback period of renewable energy technologies was reduced as a result. Figure 3.5 shows a schematic of building energy systems employed in this study.

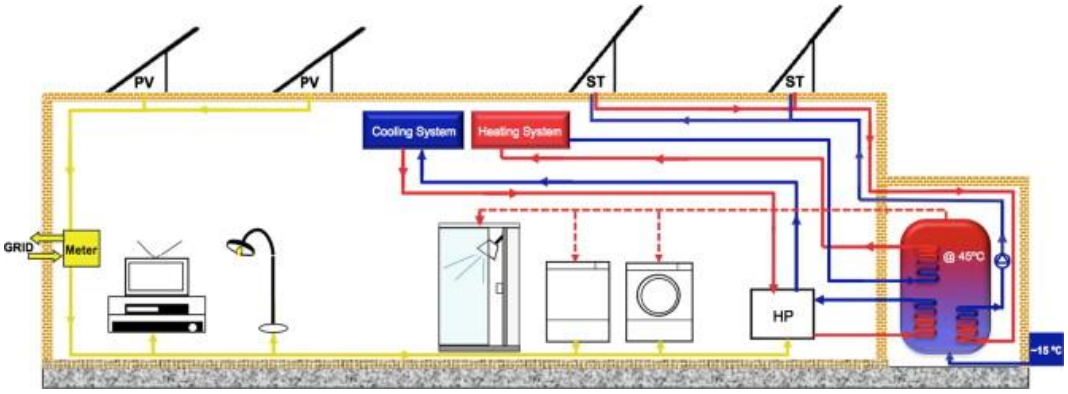

Figure 3.5. A schematic of building energy systems employed in the literature study.

Milan et al. (2012) presented a study to develop a simplified linear, ready-to-use design model for optimising a 100% renewable energy supply system for low energy buildings in terms of the overall costs [20]. In this study, the continuously increase in the use of on-site renewable energy resources in residential household had been noticed, and that many houses would be expected to depend solely on renewable sources of energy for electricity and thermal generation in the medium term future. Therefore computer models that can be used to assess and design energy supply systems for buildings were required. However, the current existing models mainly focussed on a national or a local scale. A technical engineering approach, based on real system efficiencies and the second law of thermodynamics, was applied to develop an optimisation model for sizing supply systems in terms of overall costs. In this optimisation approach, linear programming was adapted and three design variables (technologies) had been considered. These were a solar PV system, a GSHP and a solar thermal system. The mathematical representations of the modelling and optimisation were presented in the simplified form. Two constraints were applied into this study, they were the total electricity supplied from the grid had to be equal to or less than the electricity exported back to the grid, and the total surface area of solar PV panels and solar thermal

collectors had to be equal to or less than the available south facing roof space. A heat storage system had also been considered as part of the overall energy supply system. The backup system was strategically designed by adding a safety margin onto the supply system dimensions. This model was applied to a case study in Denmark. The results indicated that, under the chosen conditions, the optimal configuration was a solar PV system combined with a GSHP. This optimal system was around 180% more expensive than a conventional system consisting of grid supplied electricity and a gas boiler. The very high initial costs of renewable energy systems had been identified as one of the major barriers for these technologies to be broadly used. Figure 3.6 shows a principle diagram of the investigated energy supply systems.

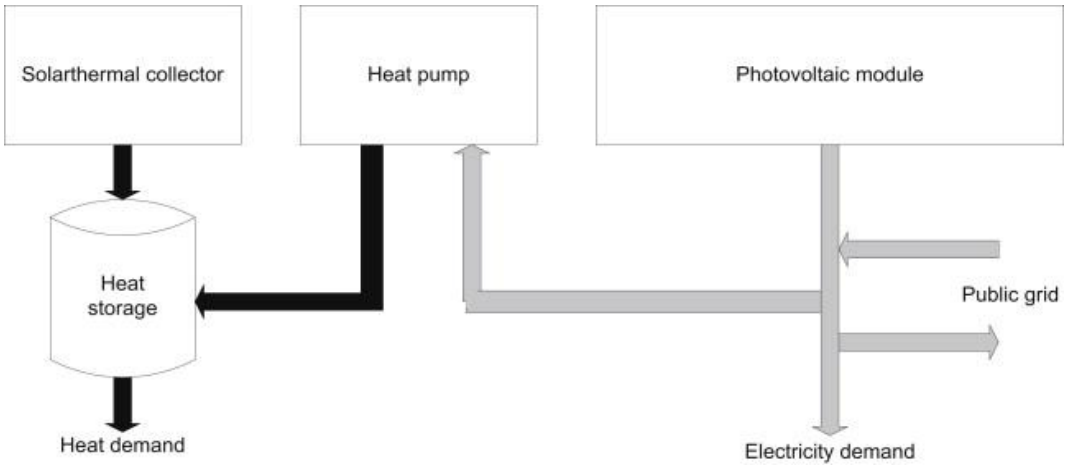

Figure 3.6. Principle diagram of the investigated energy supply systems.

Marszal et al. (2012) presented a study to investigate the LCC of different renewable energy supply options, and to identify the cost-optimal combination between energy efficiency and renewable energy generation [21]. In this study, the utilisation of renewable energy technologies to satisfy the energy demand of a net-zero-energy building was categorised as on-site options and off-site options. During the study period, the on-site option had been recognised as more popular than the off-site option.

However, with the number of wind turbine co-operatives, and the limited on-site renewable energy supply options available, the off-site renewable energy supply options could become a better solution for achieving the net-zero-energy goal. The analysis considered a total of seven technology types of which three are on-site options and four are off-site options. The three on-site options are: a solar PV system, a GSHP system and three micro combined heat and power (CHP) systems driven by three different fuel types. The four off-site options are: standalone wind turbine, shares in a wind turbine farm, the purchase of green energy from a 100% renewable utility grid, and a district heating grid. These renewable energy technologies were integrated into 10 systems in order to provide electricity, heat and hotwater for the net-zero-energy buildings. Firstly, the energy usage was calculated for a multi-storey residential building located in Denmark, which was used as the reference point for a net-zero-energy building. Secondly, the renewable energy system components were sized to generate enough electricity and thermal energy to offset demand and thus to meet the net-zero-energy objective on an annual basis. Finally, the LCC of all combinations were calculated based on the buildings' performance models. The energy efficiency should be prioritised for designing a cost-optimal net-zero-energy building if on-site renewable energy options were considered, however, it was more cost effective to invest in renewable energy technologies than in energy efficiency if off-site renewable energy options were considered. In addition, the off-site renewable energy options generally had lower LCC than the on-site options. The cost-optimal system selected from the on-site supply options was the solar PV-micro CHP (biomass) system. Two systems were selected from the off-site options since both had the same lowest cost. The two options were the share of a wind turbine farm and a GSHP, and the electricity grid and a GSHP. These two systems were also the most cost-effective amongst all of the 10 renewable

energy supply options considered. Several parameter studies were conducted to investigate their impacts on the determination of the cost-optimal combination, such as energy cost, PV price and real interest rate. Figure 3.7 shows the results of a total annual cost of net-zero-energy buildings for three levels of energy performance requirements and the renewable energy supply systems employed.

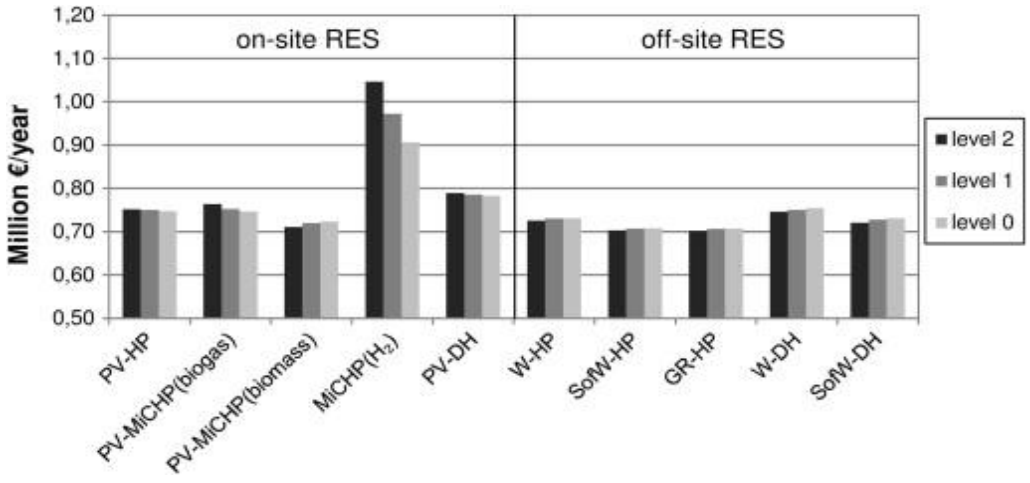

Figure 3.7. Total annual cost of net-zero-energy buildings for three levels of energy performance requirements and the renewable energy supply systems.

Kapsalaki et al. (2012) proposed a methodology and an associated calculation platform which was then used to identify the most economically efficient design solution for a residential net-zero-energy building, taking into account the influence of the local climate, the indigenous energy resources and the local economic conditions [22]. In this study, the economically efficient design, besides being technically effective, was recognised to be critically important. There was a need to continuously develop methodologies for identifying the best combinations of design variables. These methodologies ensure the pre-specified energy and environmental targets are met, while also accomplishing either a lowest LCC, a lowest initial cost, or a good compromise between the initial cost and the LCC. The analysis model was used to decide the most

adequate design solution that lead to a null annual energy balance. The energy demand of the dwelling was determined as a function of thermal insulation level, air leakage level, ventilation type, window and shading types, glazed area, orientation of the dwelling, lighting and electrical appliance usage, domestic hotwater usage and the number of occupants. The energy supply options included the heating and cooling generation systems, domestic hotwater generation systems, and electricity generation systems. These energy generation systems could be either conventional or renewable. Local climate data was pre-built in the design model for a number of locations. The economic evaluation was performed based on the selected energy demand and energy supply options, and the LCC of the design solution was then obtained. The developed methodology and model were deployed for a similar detached house, however three climates were considered: a cold winter, a mild winter, and a very mild winter but hot summer. From the results indicated, there was no trade-off between the LCC and the initial cost. A house which had a better economic performance over its life cycle generally had a higher initial cost. It was noted that if a greater investment was made on enhancing the energy efficiency of the dwelling, this would result in a smaller capacity heating and cooling generation system as well as a smaller capacity electricity generation system being required. Furthermore, the results also showed that the LCC of an economically efficient net-zero-energy building was up to one third less than the LCC of an economically inefficient net-zero-energy building. In addition, the results showed that the optimal economically efficient design of a net-zero-energy building in a mild winter climate can be significantly cheaper than in a climate with a cold winter. Figure 3.8 shows the interface of the developed software used to determine the most adequate design solution that achieves a null annual energy balance for a building.

Figure 3.8. Interface of the developed software used to determine the most adequate design solution that achieves a null annual energy balance for a building.

Walsh et al. (2012) presented a study in which they proposed a model that was capable of determining the most appropriate hybrid system for electricity and heating generation using indigenous, renewable energy resources in Ireland [23]. In this study, the over reliance on imported fossil fuels as the primary energy source for electricity and heating generation was identified as a major issue for Ireland. As a result, the nations' energy supply is at risk and the use of fossil fuels leads to climate damage due to the emissions of anthropogenic GHGs. A feasibility analysis to investigate the combination of available energy generation options was conducted using the HOMER software package. Ireland was divided into eight localised regions in order to assess the most suitable hybrid energy system for each region depending on the availability of renewable energy resources. For electricity and heating generation, the renewable energy options considered were wind, solar PV, biomass and hydroelectricity. The non-renewable energy options considered were diesel, electricity grid and natural gas. The total net present cost, cost of energy and the CO_2 emissions were the three parameters

used to determine the most suitable renewable and non-renewable hybrid system. The results indicated that wind energy had the greatest potential for renewable energy generation in Ireland since wind energy had been, based on economic investigation, selected as a component in the majority optimal hybrid systems. The utilisation of wind energy can also make a significant impact on the reduction of CO_2 emissions. More than half of the electricity generation systems analysed demanded the incorporation of wind energy to offset the CO_2 emitted from the non-renewable elements. However, due to the inherent variability of wind energy, the wind turbines were necessarily grid-connected in order to reliably satisfy the electricity and heating demand. The results also showed that hydropower generation has a good potential for electricity generation in Ireland. However, the employment of solar PV and biomass technologies had been restricted to a small number of regions and selected only for stand-alone systems. Figure 3.9 shows the results of the grid-connected optimal system determined for each region in Ireland.

Region	Energy demand	System components [a]	COE (€/kWh)	Renewable fraction (%)	CO_2 emissions (kg/yr)
NW rural	Electric + thermal		0.065	49	-33,208
NW rural	Electric		0.045	92	-218,070
W rural	Electric + thermal		0.106	33	135,313
W rural	Electric		0.092	83	-98,403
W urban	Electric + thermal		0.117	57	-18,071
W urban	Electric		0.133	0	169,165
SW rural	Electric + thermal		0.135	15	187,729
SW rural	Electric		0.094	73	-3,1895
S rural	Electric + thermal		0.137	23	106,382
S rural	Electric		0.105	67	27,554
S urban	Electric + thermal		0.129	35	89,252
S urban	Electric		0.084	77	-20,947
SE rural	Electric + thermal		0.131	24	104,053
SE rural	Electric		0.100	81	-79,190
E rural	Electric + thermal		0.150	19	111,891
E rural	Electric		0.120	60	57,843
E urban	Electric + thermal		0.106	47	59,143
E urban	Electric		0.127	30	118,301
Midlands N rural	Electric + thermal		0.160	0	137,324
Midlands N rural	Electric		0.140	0	212,735
Midlands S rural	Electric + thermal		0.160	0	219,534
Midlands S rural	Electric		0.140	0	212,735

[a] = grid; = wind; = hydro

Figure 3.9. Grid-connected optimal system determined for each region in Ireland.

Thygesen et al. (2013) presented a study to find the optimal system in terms of cost effectiveness while achieving the highest possible solar energy fraction [24]. In this study, three solar assisted heat pump systems, used to provide electricity, heating and domestic hotwater, were simulated in the programme TRNSYS. The three systems were: a GSHP in combination with a 5.19 kW_p solar PV system, a GSHP system in

combination with a solar flat plate collector system, and a GSHP system in combination with a solar flat plate collector system and a solar PV system. The heat pump was dimensioned for monovalent operation that was able to supply 100% of the building heating load. There were also three types of metering schemes introduced which were instantaneous metering, daily metering and monthly metering. For an instantaneous metering scheme, the electricity generated from a solar PV system had to be used at once in the building, otherwise the surplus electricity had to be exported to the grid and sold. However, for the daily metering and monthly metering scheme, the generated electricity from a solar PV system for a whole day or a month was settled against the building electricity demand at the end of the day or the month, therefore the occupants only pay for the net electricity purchased. In these cases, the electricity grid effectively acted as a storage device. The solar energy fraction and economic analysis of the considered systems were carried out based on the energy demand predicted for a building with four occupants and with the Swedish climate. The three main energy demands in the building were the household electricity, domestic hotwater and space heating, and heat recovery ventilation. The results showed that a GSHP in combination with a solar PV system was the most energy and cost effective solution when considered in conjunction with a monthly metering scheme. The system consisting of a GSHP and a solar thermal system was unprofitable, and also had a low solar electricity fraction (5.7%). The third combination consisting of all three technologies achieved a relatively high solar energy fraction, however was not profitable. Figure 3.10 shows the schematic of three alternative system combinations employed in this study.

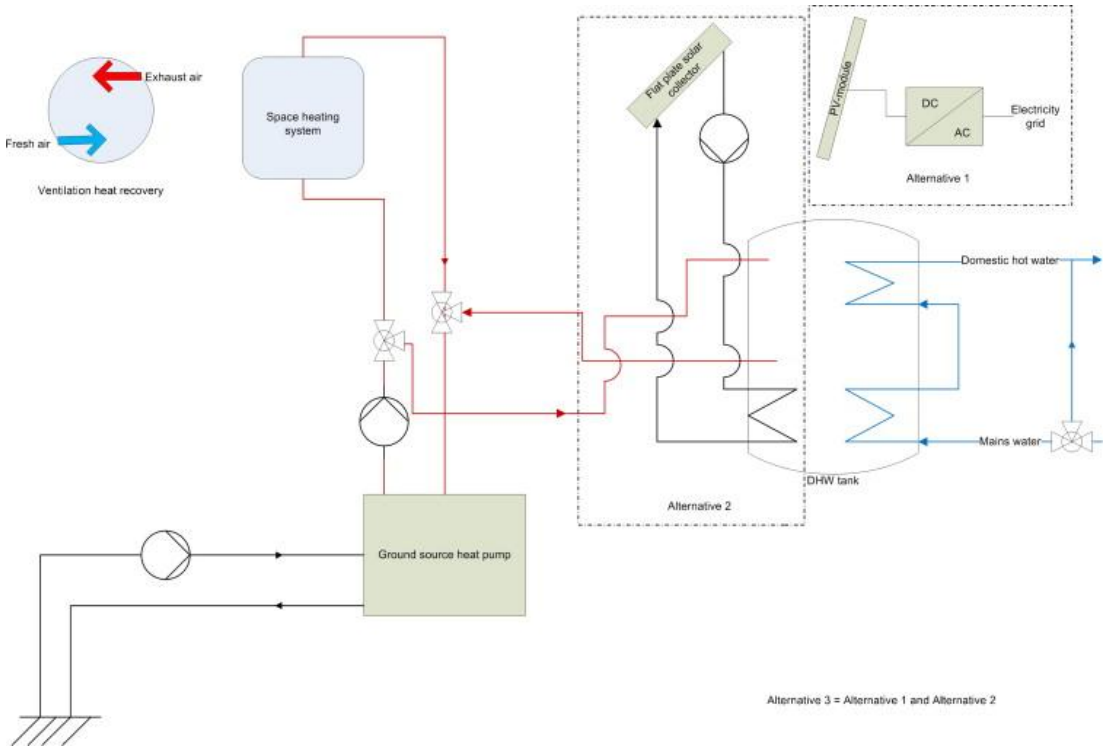

Figure 3.10. Main components of the systems considered. Alternative 1 was a GSHP and a solar PV system; alternative 2 was a GSHP and a solar thermal system and alternative 3 was a combination of alternatives 1 and 2.

3.3. Review of Software Packages for Conducting Energy Performance Simulation of Renewable Energy Systems

There are a number of software packages available for simulating the performance of renewable energy systems. A general review of these software packages was carried out. A comprehensive review was conducted of six of the most commonly employed/reputable packages. These software packages are as follows: RETScreen, Hybrid 2, EnergyPLAN, iHOGA, HOMER and TRNSYS. Following the completion of the review, HOMER and TRNSYS were chosen as the most appropriate packages for employment in this research. The software packages reviewed are as follows:

- RETScreen is developed by the Ministry of Natural Resources, Canada for evaluating the energy performance, financial and environmental costs, benefits

and risks of various renewable energy technologies for many locations around the world [25]. Fundamental to RETScreen is a comparison between a base case, typically a conventional technology, and a proposed case, typically a renewable energy technology. The costs of the proposed case that are in excess of those for the base case is the main concern for RETScreen rather than the absolute costs [13]. RETScreen has a global climate database of more than 6,000 ground stations (solar radiation and temperature data for a year) and energy maps (i.e. wind maps). It also has a product database which contains solar-photovoltaic-panel and wind-turbine details. RETScreen can be applied to any energy system ranging from an individual project to a global application. There are a number of worksheets for performing detailed project analysis including energy modelling, cost analysis, emission analysis, financial analysis, and sensitivity and risk analysis [26].

- Hybrid 2 is developed by the Renewable Energy Research Laboratory (RERL) at the University of Massachusetts, USA with support from the National Renewable Energy Laboratory (NREL) [25]. This software uses statistical methods to account for inter time step variations and can predict the performance of various renewable energy systems as well as performing detailed economic analysis. Hybrid 2 has four main components: the Graphical User Interface (GUI), the Simulation Module, the Economics Module and the Graphical Results Interface (GRI). Projects are constructed in four steps: an organised structure is maintained in the GUI; simulations are run and input errors are checked in the Simulation and Economics Modules; and detailed graphical output data is viewed in the GRI.

- EnergyPLAN is developed by Aalborg University, Denmark [27]. The main purpose of this tool is to assist in the design of national or regional energy planning strategies by performing energy-system simulations intended for heat and electricity supply from conventional and renewable energy generation [28]. EnergyPLAN is a deterministic input/output tool. The general inputs are demands, renewable energy sources, energy station capacities, costs, and regulation strategies for import/export and excess electricity production [29]. The outputs given are energy balances and resulting annual productions, fuel consumption, import/export of electricity, and total costs including income from the exchange of electricity. EnergyPLAN has been widely used to analyse large-scale renewable energy projects and small-scale combined heat and power plants, and has also been used to set up renewable energy strategies for sustainable development.

- iHOGA is developed by the University of Zaragoza, Spain. Multi or mono objective optimisation can be performed and a genetic algorithm is employed in iHOGA for optimum sizing of hybrid energy systems including solar PV, wind turbines, fuel cells, hydrogen tanks, storage systems and fossil-fuel-based generating systems. iHOGA is also able to perform sensitivity analyses with a relatively low computational time. The main functions of iHOGA are to optimise the slope of solar PV panels, calculate life cycle emissions, and also to allow the carrying out of probability analyses. iHOGA also provides the energy purchase and selling option, stores the component database and sets the parameter constraints.

- HOMER is developed by the NREL. HOMER has been downloaded by over 80,000 people in 193 countries to-date. HOMER may be adopted to analyse and optimise the performance of both stand-alone and grid-connected power generation systems with any combination of wind turbines, solar PV arrays, run-of-river hydro generators, biomass generators, internal-combustion-engine generators, fuel cells, batteries and hydrogen storage. The analysis and optimisation procedures take the component costs, resource availability and manufacturers' data into account to produce a list of feasible configurations which are sorted by net present cost. A variety of tables and graphs can also be generated to fully evaluate individual configurations based on both their technical and economic merits. These tables and graphs can also be employed to compare and contrast different configurations against one or another and can be exported from HOMER to allow external post-processing. Analyses are generally performed on an hourly basis for a year; however the simulation time step can be adjusted in HOMER to as short as one minute if required. HOMER can also incorporate input variables, such as resource availability and load size, to perform a sensitivity analysis.

- TRNSYS is developed by the Solar Energy Laboratory (SEL) in the University of Wisconsin, USA. The TRNSYS software package consists of many subroutines that model sub-system components. The mathematical models of the system components are given in terms of their ordinary differential or algebraic equations. TRNSYS is an extremely flexible, graphical-based package which also has the capability of interconnecting system components in any desired manner, solving the subsequent differential equations and facilitating

information output in various formats. The entire problem of system simulation reduces to a problem of identifying all of the individual components that comprise the particular system and then formulating a general mathematical description of each. Two parts, i.e. the kernel and the library, are then used to carry out the analysis. The kernel is used to process the input file and then solve the system based on the selected solution method and convergence criterion; the library is used to store the mathematical components, and these components can be updated or modified as required. TRNSYS is very popular for conducting analyses of solar thermal systems, low energy buildings, HVAC systems, renewable heating generation systems (i.e. ASHPs and GSHPs), cogeneration and fuel cells etc.

The reasons HOMER was chosen for predicting the performance of micro-renewable electricity generation systems over alternative software packages in this research are as follows:

- It has been used extensively in previous renewable-energy-system case studies, results from which have been widely published in international peer-reviewed journal articles [30-45].
- It has been tested by comparing generated results of case studies with results from alternative software packages [46-48].
- It works particularly well with small-scale, renewable-based energy generation systems [49].
- It provides a detailed explanation of the various input parameters that are required for carrying out a renewable energy system analysis.
- It can import weather and/or load data with various time steps.

- The developers offer both comprehensive training courses and long-term technical support.
- It is continuously updated with new features.

The reasons TRNSYS was chosen for predicting the performance of micro-renewable thermal generation systems over alternative software packages in this research are as follows:

- It has been used extensively in previous studies [15, 50-58].
- It has been validated against experimental measurements in previous studies [59-68].
- It can analyse single-project, local community or island energy systems.
- It is capable of simulating all thermal and renewable generation except nuclear, wave, tidal and hydro power.
- It is able to perform analyses with an extremely small time-step.
- It is possible to add user-specified mathematical tools and components.
- It has the ability to interface with other simulation programs, such as MATLAB and EXCEL.
- It provides a comprehensive mathematical description and explanation for each of the included components.
- It offers a number of component options for the same type of technology.
- The developers offer long-term technical support.
- It is continuously updated and improved upon with new features been added.

3.4. Review of the Optimisation Approaches for Integrating Micro-Renewable Energy Generation Systems

There are a number of optimisation approaches that could be adopted to perform the integration of grid-connected micro-renewable energy generation systems. A general review of these optimisation approaches was carried out. A comprehensive review was conducted of eight of the most commonly adopted/reputable approaches. These optimisation approaches are as follows: Artificial Neural Network, Simulated Annealing, Tabu Search, Evolutionary Algorithm, Genetic Algorithm, Swarm Intelligence, Particle Swarm Optimisation, and Iterative Optimisation. Following the completion of the review, Iterative Optimisation was chosen as the most appropriate approach for employment in this research. The optimisation approaches reviewed are as follows:

- An Artificial Neural Network (ANN) is inspired by biological neuron systems [69]. A ANN consists of units, called neurons, and interconnections among them. After specially training on some given data set, A ANN can make predictions for cases that are not in their training set, due to its pattern classification capability. The trained ANN provides extremely fast solutions, and it can accommodate new patterns or new operating conditions by generalising training data. Input and output data are fundamental in a ANN because they convey the necessary information to discover the optimal operation point. A target response to input data, set as the error information, must be fed back to the system, and then the system parameters can be adjusted. This process is repeated until the performance is considered acceptable. A ANN may not always work well because it may suffer from problems of underfitting or overfitting. These

problems are related to the accuracy of prediction. In fact, if a network is not complex enough, there may be a simplification of the rules to which that data obey, and this is called underfitting. On the other hand, the case of overfitting happens if a network is too complex; this may interfere with the process. The quality of prediction after training is deteriorated in both cases. The problem of premature convergence is also critical for a ANN, and another weak point of this approach is that the given data may not cover a significant portion of the operating conditions [70].

- A Simulated Annealing (SA) algorithm, developed based on the annealing process is to relax the system to a state with a minimum free energy, is used to solve complicated combinatorial optimisation [71]. The name is taken from the analogy with the optimisation process corresponding to the energy function and the state of statistical physics. In a large combinatorial optimisation problem, an appropriate perturbation mechanism, cost function, solution space and cooling schedule are required in order to find an optimal solution with a SA. The algorithm used in SA presents an approach similar to hill-climbing; however it occasionally accepts solutions that are worse than the current one. The probability of such acceptance decreases with time. The cost function with a smoothing strategy enables SA to escape more easily from local minima and to reach the optimal solution rapidly [72].

- A Tabu Search (TS) algorithm is basically a gradient-descent search with memory. The memory stores a number of previously visited states along with a number of states that might be considered unwanted. This information is placed in a tabu list. The definition of a state, the area around it and the length of the

tabu list are important design parameters. Aspiration and diversification are the two extra parameters often added into these tabu parameters. All of the neighbouring states to the current state may also be included in the tabu list; however this becomes an obstacle to the optimisation. In order to overcome this, aspiration is used and this means the selection of a new state; moreover diversification adds randomness to this search. If the TS is not converging, the search is reset randomly using diversification and to avoid local optima, and the repetition of recently made moves is not allowed [73].

- An Evolutionary Algorithm (EA) is a method that exploits ideas of biological evolution, such as reproduction, mutation and recombination to find the solution. An EA applies the principle of survival, as referring to a biological environment, on a set of potential solutions to produce gradual approximations to the optimum. The consequence of reproduction, mutation and crossover is the idea of evolution. A new set of approximations, often called the fitness function, is created by selecting individuals according to their objective function and breeding them together using operators inspired from genetic processes. This process leads to the evolution of populations of individuals that are better suited to their environment than their ancestors. The steps taken to perform the evolution are: initialise and evaluate the initial population, perform competitive selection, apply genetic operators to generate new solutions, evaluate solutions in the population, and then repeat the steps from "perform competitive selection" until some convergence criterion is satisfied. Evolutionary approaches can differ from one to another in the details of their implementation and the problems applied. Their main common traits are based in the survival set of potential

solutions and the evaluation of the goodness of a certain objective function. The fitness defines the improvement of the algorithm, as the fitness function is responsible for assigning quality measures and is the evaluation point of the process [74].

- A Genetic Algorithm (GA) is a search algorithm based on natural selection and genetics. The solution search is built in the form of number strings, usually binary. The features of a GA are different from other search techniques in several aspects. Firstly, the algorithm is a multi-path algorithm that searches for peaks in parallel and this reduces the possibility of local minima trapping. A GA works with a coding of parameters rather than the parameters themselves. The coding of a parameter will help the genetic operator to evolve from the current state to the next state with minimum computations. A GA also evaluates the fitness of each string to guide its search instead of the optimisation function. There is no need for the computation of derivatives or other auxiliary functions, as the GA only needs to evaluate objective function (fitness) to guide its search [74]. A GA is a very efficient technique to approximately solve many non-linear combinatorial optimisation problems having integer variables. Nevertheless, the main deficiency of a GA is the randomness involved in the search process [75].

- A Swarm Intelligence (SI) is an artificial intelligence approach based on the study of the behaviour of collective self-organised systems. An Ant Colonies Optimisation (ACO) is one of the main SI techniques applicable to power systems [76]. An ACO uses artificial ants to build solutions by moving on the problem graph, and changing it so that future ants are able to build better solutions. Artificial ants cooperate to find the solution of a combinatorial

optimisation problem by exchanging information via pheromone deposited on artificial paths. This algorithm counts on discrete time steps and memory allocation of the positions occupied by artificial ants. The solution quality is evaluated through artificial ants' trails and the shortest route determines the best solution [77].

- A Particle Swarm Optimisation (PSO) is for problems in which a best solution can be represented as a point or a surface in an n-dimensional space. A PSO establishes a system that is initialised with a population of random solutions. Unlike other algorithms, however, each potential solution (a particle) is also assigned a random velocity and then is flown through the problem hyperspace. The concept of individual learning and information transfer based on human characteristics is employed in a PSO algorithm. Each individual particle learns and transfers information by exchanging past experiences with other particles. A PSO has been found to be extremely effective in solving a wide range of engineering problems, since it can handle both discrete and continuous variables [78]. The main advantages of swarm intelligence techniques are that they are impressively resistant to the local optima problem, are simple to implement, and can solve problems in a short simulation time [79].

- An Iterative Optimisation approach compares the current solution with the previous optimal solution and, if the current solution is better than the previous optimal solution, it becomes the new temporary optimal solution. Alternatively, if the solution is worse than the previous optimal solution, it is simply discarded. This iterative process is repeated until the last solution is obtained and compared with the optimal solution. At this point, the overall optimal solution is

determined. Although the Iterative Optimisation approach requires more computational time than the more complex intelligent optimisation approaches, it is able to avoid common issues, such as the solution becoming stuck at the local minima/maxima, and is also guaranteed to identify the optimal solution. Furthermore, the Iterative Optimisation approach has been widely adopted in previous studies of renewable energy technologies, results from which have been presented in the literature [80-89].

3.5. Summary

The developed integration techniques, presented in various studies, for micro-renewable electricity and thermal generation systems are reviewed in this chapter. The explanation of each integration technique is given, and the novelty of it is stated. The identification of the general concept applied for these integration techniques is presented. The most recognised and utilised software packages are described and a justification is given for the selection of HOMER and TRNSYS as the most appropriate software packages for this research. The most recognised and employed optimisation approaches for integrating micro-renewable energy generation systems are also reviewed and a justification is given for the selection of the iterative approach as the most appropriate method for this research. In the next chapter, a novel sub-technique of grid-connected micro-renewable electricity generation integration is presented.

CHAPTER 4
OPTIMISED INTEGRATION OF GRID-CONNECTED MICRO-RENEWABLE ELECTRICITY GENERATION SYSTEMS

4.1. Overview

In this chapter, a sub-technique for the optimised integration of grid-connected micro-renewable electricity generation systems is presented. The chapter is split into five stages. In the first stage, the domestic household electrical load is accurately generated. In the second stage, the technology of micro wind turbine is reviewed, the methodology of statistically generating hourly wind speed values is presented, and the methodology of obtaining hourly power outputs of a micro wind turbine is then presented. In the third stage, the technology of a solar PV system is reviewed, the methodology of accurately generating hourly solar radiation values is described, and the methodology of obtaining hourly power outputs of a solar PV module is then given. In the fourth stage, a sub-technique is developed to optimised integrate the selected commercially-available micro wind turbines and solar PV systems. Finally, in the fifth stage, the results obtained from applying this technique for current Irish conditions and parameters studies are analysed and discussed.

4.2. Introduction

The rapid depletion of fossil fuel resources on a worldwide basis has necessitated the urgent employment of renewable energy to cater for future energy demand [90]. The utilisation of renewable energy is even more important for Ireland due to the lack of indigenous fossil fuel resources. Power generation in Ireland is mainly dependent upon imported fossil fuels. However Ireland has set the target of 40% electricity consumption from renewable energy by 2020 [91]. Ireland has a number of renewable energy resources available such as wind, solar, biomass, geothermal, hydropower, wave and tidal energy which can be exploited to meet the target set [23]. Wind and solar energy, which are clean, inexhaustible and environmental-friendly, are considered excellent power generating sources [92]. However, the disadvantages that prevent wind and solar energy been extensively used are their unpredictable nature and dependence on weather and climatic changes; solar also depends on rotation of earth (day/night). For domestic applications the variation of wind and solar energy may not match with the temporal distribution of the household electrical load. Fortunately, these problems can be partially or wholly overcome by integrating the two sources in a proper combination to form a hybrid system, using one source's strength to overcome the weakness of the other [93]. The utilisation of both wind and solar energy allows an improvement in the reliability of the energy supply and the economic viability by avoiding design over-sizing. However, the optimum design of a hybrid-energy system can be very complicated, with increased complexity in comparison with a mono-energy system.

In recent years, a number of different techniques for analysing the integration of hybrid wind and solar PV electricity systems have been presented in the literature. Hoicka et al. developed a technique to analyse the complementarity of integrated wind and solar PV

electricity generation from geographic dispersion and power reliability aspects for Ontario, Canada [94]. Essalaimeh et al. developed a technique to investigate the applicability of a combined wind and solar PV electricity generation system for heating and cooling in urban areas of Amman, Jordan [95]. Arribas et al. developed a procedure to evaluate the performance of a hybrid wind and solar PV electricity generation system and applied this procedure for a case study in Soria, Spain [96]. With the introduction of an exported electricity tariff in Ireland in 2009, the number of grid-connected micro-wind and solar PV electricity generation systems has increased significantly in recent years. Walsh et al. conducted a study to investigate the renewable energy options available on a regional scale in Ireland [23]. This study also presented an overview on the most suitable renewable and non-renewable hybrid energy systems for each region. However, an investigation of the economic viability of integrated micro-renewable electricity generation systems for domestic applications in Ireland has not been carried out to-date, something of critical important for the individual homeowner. It is very important for a homeowner to not only be aware of the different types of micro-renewable electricity generation systems but also of the optimal system for each individual case.

This chapter presents a sub-technique for the optimised integration of a grid-connected mono/hybrid micro-renewable electricity generation system consisting of a micro wind turbine and/or a solar PV system. A single micro wind turbine or a single solar PV system forms a mono system; a combination of both forms a hybrid system. The integration technique, generally applicable but deployed here for Ireland, takes into account technical and economical constraints (e.g. renewable energy requirement and maximum export capacity) and guidelines (e.g. exemption conditions for planning permission and exported electricity tariff). Net Present Value (NPV) is used to identify

the optimal system in this integration technique and is calculated from the hourly power outputs of the micro-renewable electricity generation system and high-resolution (hourly) household electrical load data. Realistic hourly power outputs for a year from the analysed micro wind turbines and the analysed solar PV systems are obtained from accurately predicted hourly wind speeds and hourly solar radiation values respectively by applying minimum weather data. The hourly household electrical loads for a complete year are calculated using an average annual household electrical load and an annualised electrical load profile. The predicted system performance and the obtained economic results are accurate and reflect the real-life situation of an actual installed system. The chapter also demonstrates the modification in the system configuration when realistic changes (economical, electricity consumption and weather conditions) are made.

4.3. The Generation of Hourly Household Electrical Load

In this integration technique, high-resolution (hourly) household electrical load data is required. However, the exact hourly household electrical load data is very seldom available. Therefore, a procedure is established to generate the hourly household electrical loads. This procedure, implemented in Microsoft Excel 2007, requires two items of information:

- An average annual household electrical load.
- An average annualised electrical load profile (ratio of hourly to yearly electricity consumption for a complete year). Generally, on average, electricity consumption is higher in winter than summer due to additional usage of electrical appliances and lighting devices in Ireland [97].

The 8,760 hourly household electricity load values, in kWh, can be obtained by multiplying the average annualised electrical load profile by the average annual household electrical load. Shown in Figure 4.1 are examples of generated daily household electricity load profiles for four days (one for each season) in the year using an annual electrical load of 5,016 kWh (value for an average house in Ireland in 2011 [98]) and an average annualised electrical load profile provided by ESB Networks for 2011.

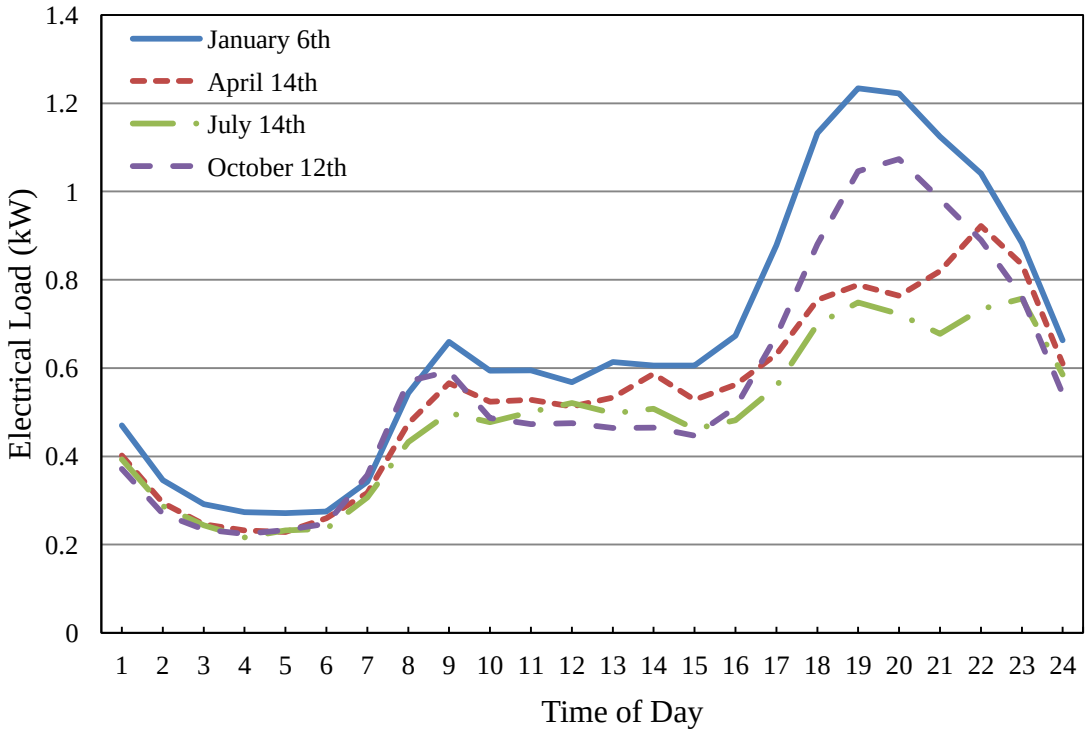

Figure 4.1. Example of generated hourly electrical loads for four days in Ireland.

Alternatively, hour-by-hour household electrical loads can be artificially generated by HOMER [9]. An hourly electrical load profile for one day (one set) in a year is the minimum requirement. Then, HOMER is capable of synthesising 8,760 hourly electrical load values for an entire year by using this hourly electrical load profile and adding random variability parameters (day-to-day, time-step to time-step). HOMER is able to take a maximum of 24 sets of hourly electrical load values consisting of two sets of

values for a weekday and a weekend for each month from January to December. In this case, the seasonal variation can be seen from the generated 8,760 hourly electrical load values. However, there is no recognition of any special events, e.g. holiday periods (Christmas, Easter), bank holidays and summer holidays.

4.4. Micro Wind Turbines

4.4.1. Technology Review of Micro Wind Turbine

The electricity produced from wind energy is one of the most cost effective from renewable energy. Ireland has an exceptional wind energy resource. Following the large wind generation development, connection to the ESB grid has become a major issue as the wind projects have to compete for access to the network. The capacity of the network is very limited in many places where the wind resources are the best. The employment of small-scale and micro-scale wind systems ensures best use of wind energy in the Irish windy climate.

Large-scale wind turbines are those rated above 100 kW. Small-scale wind turbines are those rated between 100 kW and 5 kW, and micro-scale wind turbines are those rated at less than 5 kW [99]. Turbines with ratings from 0.5 kW to 6 kW are the most suitable for domestic installation in Ireland. Typically, a 1 kW turbine has a rotor diameter of 1.75 m, a 2.5 kW turbine has a diameter of 3.4 m and a 6 kW turbine has a diameter of 5.6 m.

Wind energy conversion systems depend on either aerodynamic drag or aerodynamic lift; modern wind turbines are predominantly based on the aerodynamic lift [100]. These devices utilise rotor blades that interact with incoming wind. Therefore, the resulting force from the rotor blades intercepts the airflow and consists of a force component

which is perpendicular to the drag. As Figure 4.2 shown that, the lift force is a multiple of the drag force and it is perpendicular to the direction of the airflow that is intercepted by the rotor blade the leverage of the rotor, it causes the necessary driving torque.

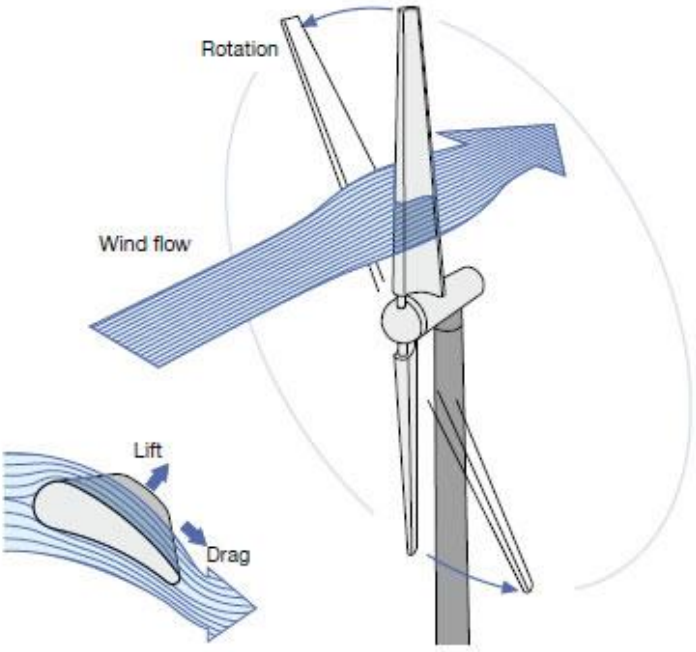

Figure 4.2. Aerodynamic principles of wind turbine capture wind energy [101].

Generally, a wind turbine comprises five main components which are [102]:

- rotor blades
- transmission including pitch control, hub, mounting, main shaft, bearings and gear box
- generator, electronic controls and cables
- tower including yaw
- foundation

However, there is an important difference between micro-scale and large-scale wind generators. The micro-scale wind systems as shown in Figure 4.3 are generally direct drive, the moving blades of the turbine turning the generator directly. Large-scale wind

turbines usually have a gearbox that matches the slowly turning rotor shaft to the generator. There are several existing mechanisms used to point the wind turbine towards the wind direction or to move away from the wind in case of strong wind speeds. For a micro-wind turbine, the rotor and the nacelle (containing the transmission system and generator) are oriented into the wind with a tail vane.

Figure 4.3. Domestic wind generation systems [103].

Like large-scale wind turbines, the micro-scale wind turbines fall into two categories: a horizontal axis wind turbine (HAWT) and a vertical axis wind turbine (VAWT). The HAWT, as shown in Figure 4.4, has its rotating shaft parallel to the ground. Two or three rotor blades are the most commonly used, as a wind turbine with only two or three blades has a high tip speed ratio with a low starting torque. Once the wind speed reaches the cut-in speed, these wind turbines could be started. The advantage of achieving a high tip speed ratio is that it allows the use of a smaller, lighter gearbox to attain the required high speed at the drive shaft of the power generator. Currently, the three-bladed wind turbine dominates the market. It has a lighter top compared with a VAWT. This results in a reduction in the weight of the hub, nacelle and tower structure, therefore the entire supporting structure has a lower cost. It is also attributed a better

visual aesthetics with lower noise level than a two-bladed wind turbine. There is a broad range of materials used for micro-wind turbine blade production, including aluminium, steel, wood epoxy and glass-reinforced plastic. The two last materials are the most commonly deployed as they have the best combination of strength, weight and cost. It is critically important to keep nacelle weights to the minimum, as the weight of a wind turbine has a strong influence on its overall cost. The HAWT is generally ground-based and mounted on a mast nearby the house. The energy captured by wind turbines is highly dependent on the local average wind speed. Most parts of Ireland have an annual average wind speed exceeds 5 m/s [104]. There may be an enhanced power output delivered from a wind turbine due to the increased wind speed at height, therefore a wind turbine mounted on a mast generally receive wind at the best possible mean speed. The wind turbine is also more likely to be above surrounding obstacles as turbulence around other dwellings or objects can have adverse effect on turbine output. Between 10 m and 15 m is the reasonable distance from the hub of the turbine to the ground. Nowadays, several newly-designed micro-wind turbines have a power output control mechanism built in for the rotor blades in order to improve the overall efficiency. For these micro-wind turbines, the angle of the rotor blades can be adjusted actively by the machine control system which is generally known as pitch control. This system has built-in braking, as the blades become stationary when they are fully feathered. Micro wind turbines normally reach the rated capacity which is the highest efficiency at the designed wind speed, usually, between 12 m/s and 16 m/s. If the wind speed exceeds the designed maximum wind speed, the power output can be limited to maintain the power output close to the rated capacity and thus reduce the driving forces on the individual rotor blade as well as the load on the whole wind turbine structure. The applied control mechanism can effectively increase the total amount of energy output,

and therefore improve the total efficiency. In traditional approaches, where either a brake is applied or where the micro wind turbine is turned away from the wind direction, the micro-wind turbine is brought to a standstill when the wind speed exceeds the maximum wind speed; however there is no energy output in this case. Rooftop wind turbines have become available recently. The turbine sizes are in the range of 400 W to 1.5 kW. The turbines have to be mounted on structurally sound gable end walls above the roofline. They are designed to be easily installed and can be also wired into a normal domestic ring main. This kind of system is quite economically attractive. The cost reduction in avoiding the use of a mast can make the system more affordable for householders. However the turbulence around dwellings effectively reduces local wind speed by at least 25% [105], hence power output is reduced considerably.

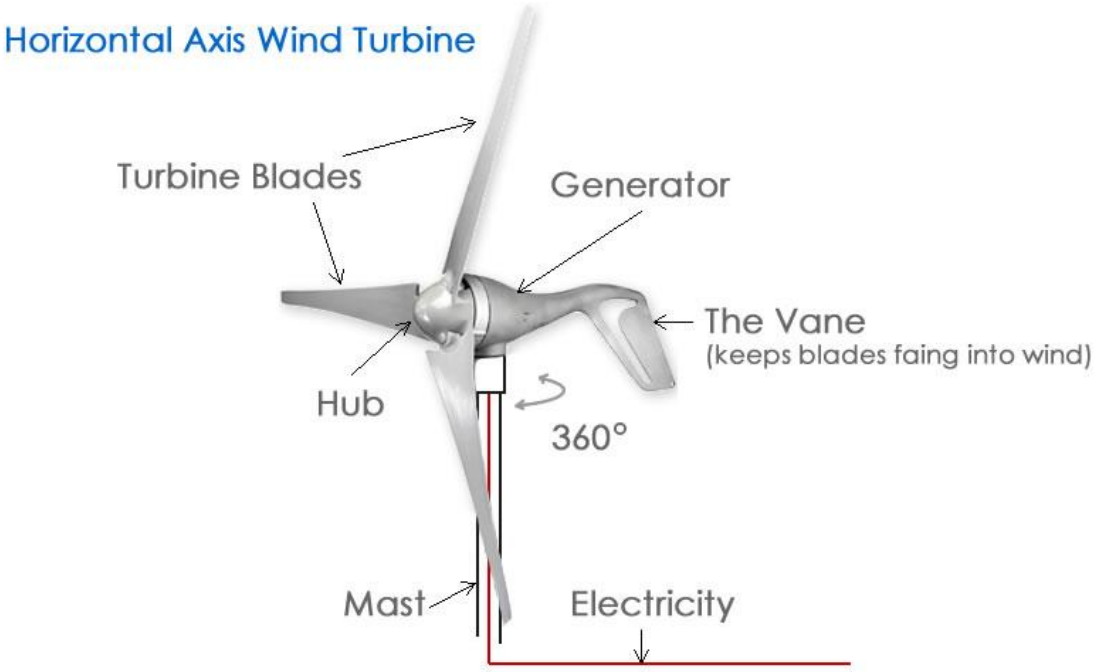

Figure 4.4. Schematic diagram of a horizontal axis wind turbine [106].

For a VAWT, as shown in Figure 4.5, the rotating shaft is perpendicular to the ground. Savonius and Darrieus are the two basic designs of VAWT. This type of wind turbine generally has a lower power output than the HAWT, but is virtually silent and less

affected by turbulence. These unique characteristics make VAWT more suitable for urban environment. The turbine can gather wind from all directions, even though more wind is needed to get it moving and higher wind speeds are also required to ensure it works well. Many manufacturing companies and organisations have shown their interests in VAWT for residential purpose. Research and development has been carried out to establish the best wind turbine design for domestic usage.

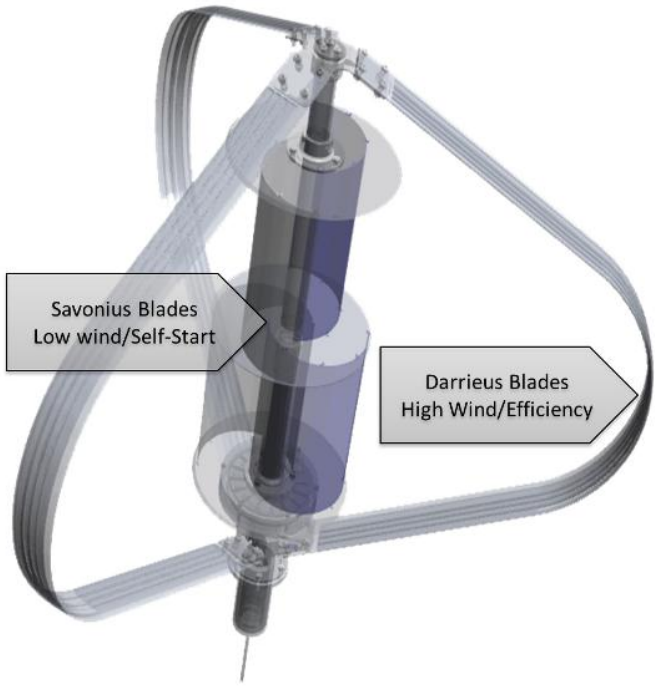

Figure 4.5. Schematic diagram of a vertical axis wind turbine [107].

The domestic wind turbine system can be categorised as either on-grid or off-grid:

- On-grid system - the wind turbine is connected to the grid. The power produced from the wind turbine is used to offset the cost of the grid supplied electricity. There is also a possibility of exporting electricity to the grid. The income obtained from selling electricity to the grid reduces the system payback period. Domestic electricity demand generally peaks twice a day, in the morning and evening. Daily,

stronger wind usually occurs from mid-afternoon onwards. Therefore, even though the wind intensity is relatively low in urban terrain, the wind resource is still well suited to match domestic electricity demand especially in the evening. If the wind turbine supplies insufficient electricity at the peak demand, it is possible to draw electricity back from the grid.

- Off-grid system - the wind turbine generates electricity at the point of use. The extra electricity produced is stored in batteries. This stored electricity is used when the turbine generates little power. This system is more expensive than an on-grid system (about 25%) because of the batteries required. The batteries usually last for 6-10 years, so extra costs will be needed to replace worn batteries.

It is very difficult to accurately predict the power output from a micro wind turbine. The power output varies significantly with local wind speed. It is generally worthwhile to gather information on local wind pattern before proceeding with design and purchase of an appropriate system. Extensive monitoring is not usually performed for a micro-scale wind turbine system as it may not justify the expense and time necessary to carry out such monitoring. However, generally, micro wind turbines are considered well suited to provide power during the evening period since the wind speeds are stronger from mid-afternoon onwards. A good match also occurs for seasonal variation, as wind is stronger during winter months and calmer during summer months. Furthermore, domestic electricity consumption follows a similar trend, with reduced lighting requirements in the summer coupled with lower usage of intense electrical appliances such as a clothes dryer.

There are many benefits that a micro-scale wind turbine system can offer; it can:

- generate clean green electricity.

- achieve significant CO_2 emissions reduction.
- help tackle fuel poverty.
- generate electricity at the point of use thus minimise transmission losses.
- reduce electricity bills greatly.
- lead to raised awareness of sustainability and renewable technologies in the highly populated urban environment.

However, there are also several downsides presented by installing a micro wind turbine for a domestic dwelling which may not be so important for other micro generation technologies. These drawbacks can be summarised as: mounting method, vibration, noise, colour and reflectivity, shadows and reflections, access for installation and maintenance, electromagnetic and electrical interference, physical damage, wake effect, driver distraction, and bird and animal (bat) strike. Of all of these the most significant aspects to be considered are noise, visual impact and animal strike [108]. For the micro wind turbine itself, the turbulent flow and lower wind speeds are common wind characteristics of the built environment which is possible to result in a lower utilisation and resultant energy yield. Moreover, the more random patterns of production are likely to increase wear and tear that could lead to shortened lifespan, safety concerns and deteriorated performance of the turbines.

4.4.2. The Generation of Hourly Wind Speed

The hourly wind speed data for an entire year at many locations are usually unavailable or too expensive to purchase. In order to achieve best accuracy, artificial but statistically reasonable hourly wind speed data can be generated using HOMER's synthetic wind speed data synthesis algorithm. This algorithm can produce data that mimic the

characteristics of real wind speed, including strong and sustained gusts, long lulls between windy periods, and seasonal and diurnal patterns [8].

In this technique, the monthly average wind speed at the turbine height for a year at the location where the turbine is installed is required. If the monthly average wind speed is not available, the annual average wind speed is used (for each month); the use of an annual average wind speed shows no realistic seasonal variation however. A logarithmic wind velocity profile, Equation 4.1, is used for calculating the wind speed at the micro wind turbine hub height if the turbine hub height differs from the height at which the measurements are taken. This accounts for the fact that wind speed tends to increase with height above ground, as the effect of obstacles (buildings and vegetation) decreases with height. A logarithmic wind velocity profile uses a surface roughness coefficient length in its calculation. The surface roughness coefficient length is to characterise the landscape condition; in this research a value 0.1 is used to represent a landscape condition of an open field [109].

$$\frac{V}{V_0} = \frac{\ln\left(H / Z_0\right)}{\ln\left(H_0 / Z_0\right)} \tag{4.1}$$

where V is the wind speed at the height H (m/s), V_0 is the wind speed at the height H_0 (m/s), H is the hub height of the wind turbine (m), H_0 is the anemometer height (m), Z_0 is the surface roughness coefficient length (m).

The hourly wind speed data is generated by performing complex statistical calculations; a detailed explanation is given in Appendix A. Figure 4.6 shows the HOMER display for generating the hourly wind speed data at Dublin. The calculation is based on the average monthly wind speed data at the measured height and adding four random

variability parameters. These four parameters can accurately reflect the wind condition for a particular location ensuring the most realistic hourly wind speed data are generated. The four parameters are: Weibull k factor, autocorrelation factor, diurnal pattern strength and hour of peak windspeed. These are described as follows:

- Weibull k factor reflects the breadth of a distribution of wind speeds in the Weibull distribution. The Weibull distribution is a two-parameter function that is commonly used to fit the wind speed frequency distribution [110]. A value of 2.12 was calculated in this research to represent Irish conditions.
- Autocorrelation factor is the degree of dependence on preceding values and is a measure of how strongly the wind speed in one hour depends on the wind speeds in previous hours. A value of 0.929 was calculated in this research to represent Irish conditions.
- Diurnal pattern strength reflects how strongly the wind speed depends on the time of a day. A value of 0.156 was calculated in this research to represent Irish conditions.
- Hour of peak wind speed is the hour of the day that tends to be the windiest, on average. The windiest time appears to be 14:00 in Ireland and this value is utilised in this study.

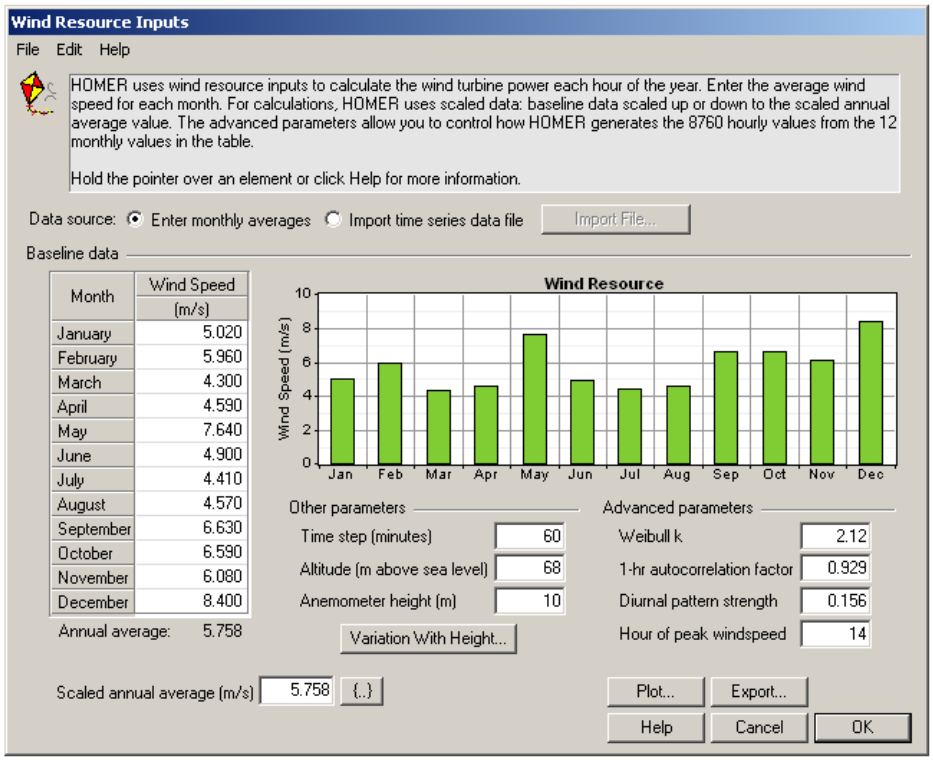

Figure 4.6. The HOMER display for generating the hourly wind speed data at Dublin.

4.4.3. The Generation of Hourly Power Output from a Micro Wind Turbine

A micro wind turbine is characterised by its power curve. The power curve gives the power output, in kilowatts (kW), for a given wind speed, in m/s, and takes into account all aspects including blade aerodynamics and auto-furling/stall effects, electrical generator, any gearing and the power electronics associated with turbine itself [97]. Figure 4.7 shows the power curves for the Skystream 3.7, the Evance R9000 and the CF6d micro wind turbines. Three wind speeds on the power curve are used to describe the operation of a particular turbine, and are:

- Cut-in wind speed. This is the minimum wind speed that a wind turbine can generate usable power. Typically the cut-in wind speed is around 3 m/s for micro wind turbines available in Ireland.

- Rated wind speed. This is the wind speed that a wind turbine can generate its rated power.
- Cut-out wind speed. This is the wind speed that a wind turbine ceases electricity generation and shuts down in order to prevent damage to itself. Typically the cut-out wind speed is 17 m/s for the micro wind turbines available in Ireland. Some micro wind turbines are designed to prevent the blades rotating when the wind speed exceeds the cut-out speed. However, newly-designed micro wind turbines like the CF6d and the Evance R9000 can regulate to their rated power and continuously generate power at high wind speeds.

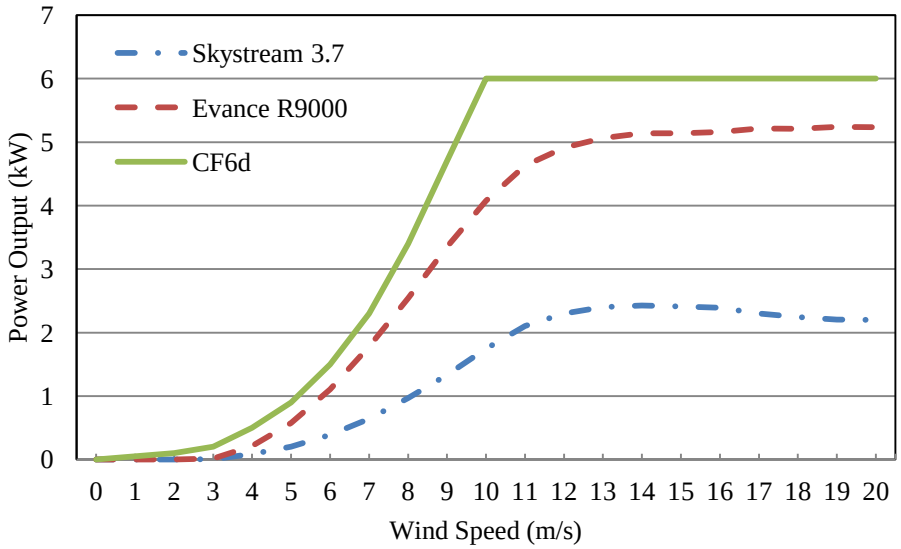

Figure 4.7. Power curves for three micro wind turbines available on the Irish market.

4.4.3.1. Validation of the Procedure to Predict the Power Output of a Micro Wind Turbine

The procedure to obtain the predicted power output of a micro wind turbine has to be validated in order to prove its accuracy. To do this the monthly power outputs from an Evance R9000 wind turbine are determined using both measured and predicted hourly

wind speeds at a hub height of 10 m and an annual average wind speed of 5.76 m/s. A Wilcoxon Rank-Sum Test, a non-parametric statistical hypothesis test, is employed to identify any statistically-significant difference between the two sets of power outputs. The measured hourly wind speeds are obtained directly from *Met Éireann,* the Irish national meteorological service and the leading provider of weather information and related services for Ireland. The predicted hourly wind speeds are obtained by applying monthly average wind speeds and all the parameters stated previously. The monthly power outputs, using measured and predicted hourly wind speeds, from the Evance R9000 wind turbine are obtained as described above. The two sets of power outputs are subjected to the Wilcoxon Rank-Sum Test. The sum of the ranks of the monthly power outputs using measured hourly wind speeds and predicted hourly wind speed are compared with a critical value (5% two-tail) for the Wilcoxon Rank-Sum Test corresponding to sample sizes of 12 and 12. The results, given in Table 4.1, show that neither rank sum is less than or equal to the critical value. The conclusion can be made, based on the available evidence, that the hourly wind speeds predicted by HOMER are accurate and realistic, and that they are appropriate for use in this study [111].

Monthly power output (kWh) using:			Ranking of monthly power outputs			
	Measured hourly wind speeds	Predicted hourly wind speeds				
Jan	741	698	1	445	13	966
Feb	966	975	2	480	14	975
Mar	545	445	3	510	15	1082
Apr	599	525	4	525	16	1091
May	1709	1730	5	536	17	1231
Jun	582	636	6	545	18	1305
Jul	510	480	7	560	19	1329
Aug	560	536	8	582	20	1348
Sep	1231	1305	9	599	21	1709
Oct	1348	1329	10	636	22	1730
Nov	1082	1091	11	698	23	1984
Dec	2066	1984	12	741	24	2066
Sum of the ranks of monthly power outputs using: measured hourly wind speeds = 155 predicted hourly wind speeds = 145						
Critical value for the Wilcoxon Rank-Sum Test (5% two-tail values) corresponding to samples sizes of 12 and 12 = 115						
Neither rank sum is less than or equal to the critical value. There is no statistically-significant difference between the two sets of power outputs.						

Table 4.1. Validation of the wind speed algorithm using the Wilcoxon Rank-Sum Test.

4.5. Domestic Solar PV System

4.5.1. Technology Review of a Solar PV System

A solar PV system, as shown in Figure 4.8, has the merit of converting solar radiation directly into electricity by semi-conductor cells (PV cell) without the intermediate stage of heat conversion. A PV module consists of a number of semi-conductor cells. A complete installed solar PV system includes an array of PV modules (PV panel), an inverter, interconnection wiring and batteries if necessary. The PV cell consists of a junction between two thin layers of dissimilar semiconducting materials. An electric field is formed in the region of the junction when sun light strikes the cell, causing negatively charged particles (electrons) to move in one direction and positively charged particles to move in the opposite direct. The flow of electrons is defined as electric current. The more intense the light becomes, the more electricity is produced. Therefore, a PV system does not only generate electricity from beam (direct) radiation but also from diffuse radiation which is likely to happen in cloudy days. Due to the reflection of sunlight, slightly cloudy days may even result in a greater amount of electricity generated than days having a complete cloudless sky [66]. The PV cell produces direct current (DC) electricity that can be directly used for powering DC electrical appliances or stored in batteries. This DC electricity can be also converted to alternating current (AC) electricity via an inverter for AC electrical appliances [112].

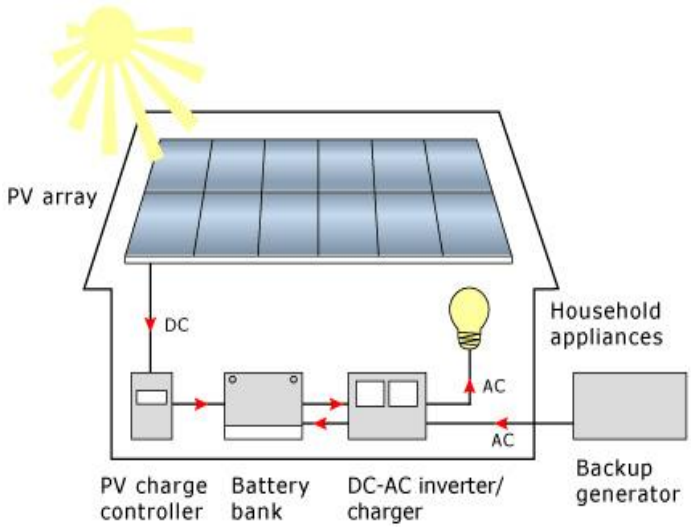

Figure 4.8. The illustration of a domestic solar PV system [58].

Silicon, the second most abundant material in the earth's mass and most commonly found in sand, is the most commonly utilised semiconductor material in PV technology. Monocrystalline, polycrystalline, amorphous silicon (thin film) and hybrid silicon are the most generally used silicon materials in a PV cell [113]. Monocrystalline silicon cell is the most conversion efficient cell. It has a conversion efficiency up to 20% but it is also the most expensive cell in use. A polycrystalline silicon cell is the second most efficient with up to 12% conversion efficiency; however the cost of manufacturing is lower. An amorphous silicon cell is the least efficient with a conversion efficiency between 6% and 10% but it is one of the most important materials in PV generation. The low cost of amorphous silicon makes it already very attractive in the market compared with other silicon materials. Amorphous silicon is the main material employed in thin film technology. Cadmium telluride, copper indium diselenide and copper indium gallium diselenide are the other materials employed. Thin film has many advantages over the conventional silicon technology. It is very light weight, relatively simple to produce and flexible and easy to place. Most important of all it has the potential to produce power significantly cheaper than current standard silicon

technology. Hybrid material has been developed to take advantage of the characteristics of both monocrystalline silicon and amorphous silicon in order to increase power generation and reduce the costs.

Solar PV panels can generate sufficient power to meet all or part of the electricity demand for a dwelling even in cloudy days or located in northern latitudes. The PV panel is commonly situated on the roof as well as integrated into a roof, but the later is more costly. The flexibility of PV panels also enables their use in many housing products such as solar roof tiles, curtain walls and decorative screens. The solar PV panels can directly replace conventional materials in the house fabrics. They serve the same structural and weather protection principle as well as offering the additional benefit in providing power to run the dwelling. PV panels can be also mounted on sun shadings or built into a double-glazed sealed sunspace to generate the most possible power for the dwelling.

A solar PV system can be operated as a stand-alone or a grid-connected system. Batteries are needed in a stand-alone system to store the extra electricity generated when there is no demand. The cost of batteries needs to be considered when designing a stand-alone PV system. Batteries usually have a life of about 6-10 years, but the PV panels have an expected life of around 25 years if they are properly maintained. Thus the batteries have to be replaced a few times before the PV panels are exhausted [105]. A back-up system is often needed in case of there is not sufficient sunlight for a period of time to generate enough electricity for the dwelling. The grid-connected system is the most commonly used; over 99.7% of the installed PV systems were grid-connected in Europe up to 2012 [67]. An inverter is required in the grid-connected PV system to convert DC from the PV to AC of desired voltage and frequency in order to send back the extra electricity to the grid. No back-up system is needed as the electricity can be

drawn back from the grid. Therefore, the elimination of the need for batteries can result a considerable reduction in the initial and replacement costs [114]. However, it should be noted that the inverter is an expensive component in the system and it is not 100% efficient. There is a considerable amount of electricity loss after conversion. It is very important to consider which type of the system suits the dwelling best at the design stage.

Solar PV systems with sizes of 1.0-3.0 kW are the most commonly used in domestic applications in Ireland. The power rating given by manufacturers is the peak power output that the PV system produces under the standard test conditions. However, the actual continuing power output can rarely achieve this as the real solar radiation levels are not always as high as under standard test conditions.

Solar PV electricity generation is broadly considered as one of the most promising renewable energy technologies. There are several main advantages associated with solar PV electricity generation such as:

- no moving parts operate.
- no emissions or noise generated.
- the fuel (sunlight) is abundant.
- safe and reliable.
- almost maintenance free and easy to install.
- easy to match load requirement by scaling up or down the size of panel once surface area is permitted.
- reduce reliance on imported electricity.

The main factor limiting the widespread use of solar PV electricity generation is its high costs associated with the manufacturing of PV modules; however the cost should reduce

significantly as a result of continuous advancements in technology and massive scale in production. For example, Germany is the leading country in PV electricity generation in Europe. PV panels integrated into roofs are commonly used in domestic houses and are generally grid connected. Ireland has a similar latitude as many parts of Germany with an average annual solar radiation of about 950 kWh/m^2 [115]. It is expected that PV systems will become one of the most important renewable technologies used in Irish dwellings in the 21st century.

4.5.2. The Generation of Hourly Solar Radiation on Solar PV Modules

The hourly solar radiation data for an entire year at many locations are usually unavailable or too expensive to purchase. In order to achieve best accuracy, artificial but statistically reasonable hourly solar radiation data can be generated using the *Graham Algorithm* employed by HOMER [116]. The synthetic solar radiation data display realistic day-to-day and hour-to-hour patterns. If one day is cloudy, the next day is likely to be cloudy; also, if one hour is cloudy, there is a relatively high possibility that the next hour will be cloudy. The hourly effective solar radiation incident on the tilted PV modules is generated by performing complex statistical calculations. The calculations are based on the latitude and longitude of the location where the PV modules are installed, the direction of the PV modules, the slope of the PV modules relative to the horizontal, ground reflectance (the fraction of solar radiation incident on the ground that is reflected), and 12 monthly-average daily solar radiation values for this location, one for each month. Daily solar radiation values are worked out from measured monthly solar radiation values obtained from *Met* Éireann. The detailed description of hourly solar radiation generated from monthly solar radiation is given in

Appendix B. Figure 4.9 shows the HOMER display for generating the hourly solar radiation data at Dublin.

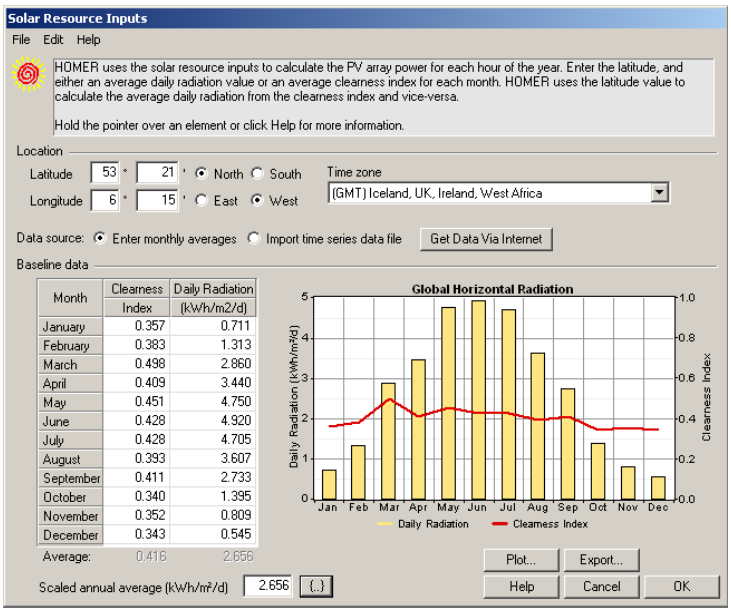

Figure 4.9. The HOMER display for generating the hourly solar radiation data at Dublin.

4.5.3. The Generation of Hourly Power Output from a Solar PV System

The power output from a domestic solar PV system (a solar PV array and an inverter) for a specific hour can be obtained by applying the artificial solar radiation generated by HOMER for this hour. The same procedure is applied for each corresponding hourly solar radiation for a year. Hence, there are a total of 8,760 hourly power outputs generated for a domestic solar PV system.

4.5.3.1. Power Output from a Domestic Solar PV Array

The power produced by a domestic solar PV array is calculated using the following equation:

$$P_{pv} = Y_{pv} F_{pv} \left[\frac{G_t}{G_{t,STC}} \right] (1 + \alpha (T_c - T_{c,STC})) \quad (4.2)$$

where Y_{pv} is the peak power output (kW), F_{pv} is the derating factor, G_t is the solar radiation incident on the PV modules in the current hour (kW/m^2), $G_{t,STC}$ is the incident radiation at standard test conditions (1 kW/m^2), α is the temperature coefficient of power (%/^{o}C), T_c is the PV cell temperature in the current hour (^{o}C), and $T_{c,STC}$ is the PV cell temperature under standard test conditions (25 ^{o}C). Each term is described as follows.

Peak power output (Y_{pv}) - the peak power output is the power output under standard test conditions.

Derating factor (F_{pv}) - the derating factor accounts for factors such as soiling of the modules, wiring losses, shading, snow cover and aging, and is used to account for the reduction in efficiency because of real world conditions being less favourable than standard testing conditions.

Solar radiation incident on the PV modules (G_t) – the total solar radiation received on the tilted PV modules. This includes beam (direct) radiation, diffuse radiation and ground reflected radiation strike on the tilted solar PV modules. The hourly solar radiation data is synthesised from widely-available coarse data (monthly-average daily global solar radiation) sources since the high-resolution measured data is rarely available for the location of interest.

Temperature coefficient of power (α) - the calculation of the power output specifically takes the effect of temperature on a solar PV module into account, since a solar PV module becomes less efficient as its temperature increases. A solar module is dark coloured, and tends to heat up significantly (as hot as 80^{o}C when there is no wind

blowing) when it is exposed to sunlight [37]. The power produced by a PV module is roughly nonlinear in the temperature range under which it is exposed. This characteristic is accounted for by manufacturers through a parameter called the temperature coefficient of power, usually expressed as a percentage change of the total power per ^{o}C. For example, a module produces 0.3% less power for every 1^{o}C increase in temperature above the cell temperature under standard test conditions (25^{o}C) if it has a temperature coefficient of power of -0.3%/^{o}C.

PV cell temperature in the current hour (T_c) - the PV cell temperature, the temperature of the surface of the PV module, is approximately the same as the ambient temperature at night; however it can exceed the ambient temperature by 30^{o}C or more at noon. In reality, PV cell temperature is very difficult to measure since the cells are tightly encapsulated for moisture protection [117]; however this is one of the most important variables to affect the performance of PV system and their electrical power production. The temperature variation is depended on parameters such as the thermal properties of materials utilised in PV module encapsulation, types of PV cells and weather conditions at the location of interest [118]. For example, crystalline silicon modules have a better performance in winter than in summer, however amorphous silicon modules perform seasonal reversely to crystalline silicon [119]. The PV cell temperature, T_c, is calculated from the ambient temperature and the radiation striking the array using the following formula (the temperatures in Equation 4.3 must be in degrees Kelvin):

$$T_c = \frac{T_a + (T_{c,NOCT} - T_{a,NOCT})\left\{\frac{G_t}{G_{t,NOCT}}\right\}\left[1 - \frac{\eta_{STC}\ 1 - \alpha T_{c,STC}}{\tau\beta}\right]}{1 + (T_{c,NOCT} - T_{a,NOCT})\left\{\frac{G_t}{G_{t,NOCT}}\right\}\left[\frac{\alpha\eta_{STC}}{\tau\beta}\right]} \qquad (4.3)$$

where T_a is the ambient temperature (K), $T_{c,NOCT}$ is the nominal operating cell temperature, $T_{a,NOCT}$ is the ambient temperature at which the NOCT is defined (293K), G_t is the solar radiation incident on the PV modules in the current hour (kW/m^2), $G_{t,NOCT}$ is the solar radiation at which the NOCT is defined (0.8 kW/m^2), η_{STC} is the PV module efficiency under standard test conditions, α is the temperature coefficient of power (%/K), $T_{c,STC}$ is the PV cell temperature under standard test conditions (298K), τ is the solar transmittance of any cover over the PV array (%), and β is the solar absorptance of the PV array (%). The monthly-average ambient temperature values are also obtained from *Met* Éireann, and each is used as the hourly ambient temperature in that month.

4.5.3.2. Validation of the Procedure to Predict the Power Output of a Solar PV System

The procedure to obtain the predicted power output of a solar PV system has to be validated in order to prove its accuracy and to employ it in the integration technique. This validation is carried out by comparing the measured power output with the predicted power output for a 1.72 kW$_p$ solar PV system, assembled from eight Sanyo 215 W solar PV modules and a Sunny Boy 1700 inverter. This solar PV system, as shown in Figure 4.10, was built and installed at a site in Dublin, and monitored by the Dublin Institute of Technology (DIT) [63]. The modules were mounted south facing and had a 53^o slope relative to the horizontal. The solar PV modules were left uncleaned throughout the monitoring period in order to mimic the realistic operation in a domestic dwelling [114]. The single phase Sunny Boy 1700 inverter, with a rated maximum efficiency of 93.5% and a maximum AC power output of 1700 W, was used to convert the power output from DC to AC. The power output was measured for a 12-month

period, between November 2008 and October 2009. The data acquisition system consisted of the Sunny Boy 1700 inverter, a Sunny SensorBox and a Sunny WebBox. The inverter and the Sunny SensorBox, used to measure in-plane global solar radiation on the solar PV modules, were connected to the Sunny WebBox. The data was extracted and recorded at five-minute intervals, and read directly into a computer. The data collection was in line with IEC 61724 standards [120]. The five-minute-interval data was aggregated by summing the power output over one-hour intervals and then employed in this validation study. The HOMER simulation inputs are taken the same as the experimental conditions; the solar radiation data used are for the period November 2008 to October 2009 in Dublin. The PV module specifications are shown in Table 4.2.

Figure 4.10. The actual solar PV system built and installed at a site in Dublin [121].

PV module - Sanyo 215 W	Specification
Material	Monocrystalline silicon
Maximum power (W)	215
Maximum power voltage (V)	42
Maximum power current (A)	5.13
Module efficiency (%)	17.2
Nominal operating cell temperature (^{o}C)	45
Temperature coefficient of power (%/ ^{o}C)	-0.3

Table 4.2. Relevant information for the Sanyo 215 W solar PV module.

The measured and predicted annual total power outputs are 885.1 kWh/kW_p and 865.1 kWh/kW_p respectively, a difference of 2.26%. This shows that the predicted power output from the solar PV system, as calculated by HOMER, agrees closely with the measured output on a yearly basis. The coefficient of determination is employed to detect the coincidence between the measured and predicted hourly power outputs. The coefficient of determination (r^2), the square of the Pearson (product moment) correlation coefficient (r) as shown in Equation 4.4, is defined as the proportion of the variance 'explained' by the model, which makes it useful as a measure of the success in predicting the dependent variable from the independent variables [122].

$$r^2 = \left[\frac{\sum_{i=1}^{N} (X_i - \overline{X}) * (Y_i - \overline{Y})}{\sqrt{\sum_{i=1}^{N} (X_i - \overline{X})^2} \sqrt{\sum_{i=1}^{N} (Y_i - \overline{Y})^2}} \right]^2 \tag{4.4}$$

where

$$\overline{X} = \frac{1}{N} \sum_{i=1}^{N} X_i$$

$$\overline{Y} = \frac{1}{N} \sum_{i=1}^{N} Y_i$$

where r^2 is the coefficient of determination, r is the correlation coefficient, X_i is the measured hourly power output, Y_i is the predicted hourly power output, $\overline{X}$ is the mean of the hourly measured power outputs for a year, $\overline{Y}$ is the mean of the hourly predicted power outputs for a year, and N is the number of power outputs for a year.

A coefficient of determination of 0.36 is obtained. This means that 36% of the variance in the measured hourly power outputs is predicted by the model; however 64% of the variance is not explained by the model. Figure 4.11 shows the scatter diagram of predicted hourly power outputs versus measured hourly power outputs for the 1.72 kW_p

solar PV system. There are a number of possible reasons why this coefficient of determination value is not higher:

- The monthly solar radiation data used for predicting the hourly solar radiation values was obtained from the national weather station (Dublin airport) closest to the location where the solar PV system was installed. However, there is quite a distance (approximately 10 km) between these locations, and the monthly solar radiation applied in the model was not the same as the solar radiation received by the installed solar PV system [123].
- The effect of clouds on the output of solar PV modules has been taken into account in the solar radiation prediction; however it is not possible to mimic the realistic circumstance i.e. clouds travel fast with a strong wind [124].
- The inverter is assumed to have a constant efficiency; however the efficiency of the inverter used in the actual solar PV system varies with time.

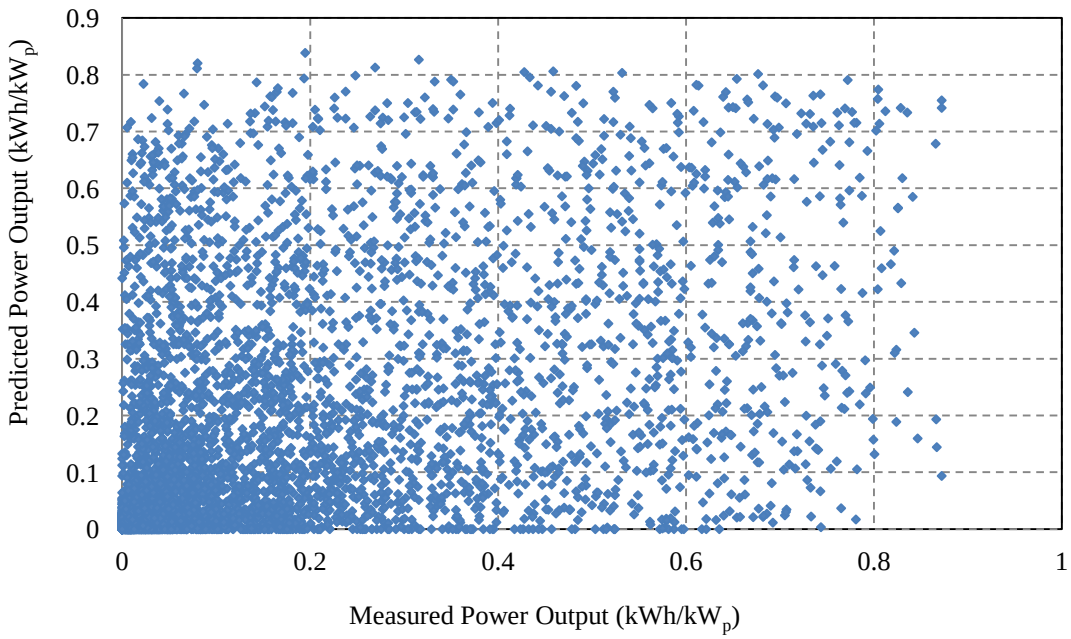

Figure 4.11. Scatter diagram of predicted hourly power outputs versus measured hourly power outputs for the 1.72 kW_p solar PV system.

To the best of the author's knowledge, this is the first time an attempt has been made to validate the predicted hourly power outputs of a modelled solar PV system for an entire year. There is no comparable value that can indicate the accuracy of the obtained coefficient of determination value since no other validations have been carried out to this degree previously. In 52 international peer-reviewed journal articles reviewed by the author [27, 32, 125-174] in which solar PV systems were modelled, only 22 articles included a validation of their model [27, 125-145]. However, in these articles no attempt has been made to validate models by comparing the predicted power output with the measured power output on an hourly basis for a complete year. Therefore, based on the comparison of annual measured and predicted power outputs, the procedure used to predict the power output for a solar PV module is considered appropriate for use in this study.

4.6. Economic Comparison Parameter – Net Present Value

NPV is the method most recommended for making investment decisions and calculates the net amount that the discounted cash flows of a project exceed the initial investment. All costs and revenues of the project are discounted as present value to a specified date, the base year [175]. The NPV calculates the exact monetary amount that a project exceeds or fails to meet [176]. If a project provides a rate of return exactly equal to the opportunity cost of capital, then the NPV of this project is zero as the discounted future cash flows equal the initial capital costs. Thus, the NPV provides a good decision criterion for the economic viability of a project. A project with a positive NPV should be deemed acceptable since it is economically viable; the project with a negative NPV should be considered unacceptable since it is not economically viable. In this study, NPV is the parameter used to perform a cost/benefit comparison and to identify the

optimal system in the micro-renewable electricity generation system [177]. NPV is calculated as follows:

$$NPV = \sum_{t=1}^{T} \frac{CF}{(1+i)^t} + \frac{SAL}{(1+i)^T} - C \tag{4.5}$$

where

- T is the project lifespan.
- C is the entire capital cost of the micro wind turbine and/or the solar PV system including the cost of installation and an inverter.
- SAL is the salvage value.
- i is the real interest rate, calculated as:

$$i = \frac{L - f}{1 + f} \tag{4.6}$$

  where L is the loan rate offered from a lending institution and f is the annual inflation rate.

- CF is the annual net cash flow calculated as follows:

$$CF = S + P - M \tag{4.7}$$

  where S is the savings made by replacing the imported electricity, P is the revenue generated from the exported electricity to the grid, and M is the annual maintenance cost.

4.7. Integration of a Micro Wind Turbine and a Solar PV System

4.7.1. The Integration Technique

The micro wind turbine and solar PV system integration technique, a flowchart for which is shown in Figure 4.12, obtains the optimal configuration of a grid-connected micro-renewable electricity generation system consisting of a micro wind turbine and/or

a solar PV system (formed from sole capacity solar PV modules). The integration technique is implemented in MATLAB. The integration begins with the selection of a number of micro wind turbines and solar PV modules for analysis. The height of the micro wind turbine and the orientation of the solar PV modules are then set. The realistic hourly power outputs of the selected micro wind turbines and the selected solar PV modules (at the optimal slope), and the hourly household electrical loads for a year are obtained from HOMER and Microsoft Excel respectively using the procedures described previously. A database containing the selected micro wind turbines and their hourly power outputs, the selected solar PV modules and their hourly power outputs, and hourly household electrical loads are stored in MATLAB. All possible systems, both mono and hybrid, that can be formed from the selected micro wind turbines and the selected solar PV modules are then analysed. For each system a renewable energy value is calculated and compared with the renewable energy requirement. The renewable energy requirement, a constraint in the integration, is the percentage of the annual household electrical load that must be satisfied from the micro-renewable electricity generation system. The renewable energy value is calculated using the hourly system power outputs and household electrical loads. The hourly power output is counted in the calculation of the renewable energy value if the power output is partially satisfying the household electrical load; the portion of hourly power output, equal to hourly household electrical load, is counted in the calculation if the power output is wholly satisfying the household electrical load. For a year, the renewable energy value is calculated using the sum of these counted hourly power outputs divided by the annual household electrical load. If a system cannot satisfy the user-specified renewable energy requirement it is eliminated. For those systems that do satisfy the user-specified renewable energy requirement the NPV is then calculated based on the capital costs of

the system, the savings made from replacement of the imported electricity, the revenue generated from the exported electricity to the grid, the costs of replacement of inverters, maintenance costs and the salvage value. The salvage value is the value left in a device (exclusive of installation cost) if the lifespan of a device is longer than the desired project lifespan. In this integration technique, the major assumption is made that the entire capital cost of the micro-renewable electricity generation system is funded from a loan. A capital grant option is also built into this integration technique. Once all possible system configurations have been analysed, the system having the highest NPV is deemed the optimal one and the system configuration is thus obtained.

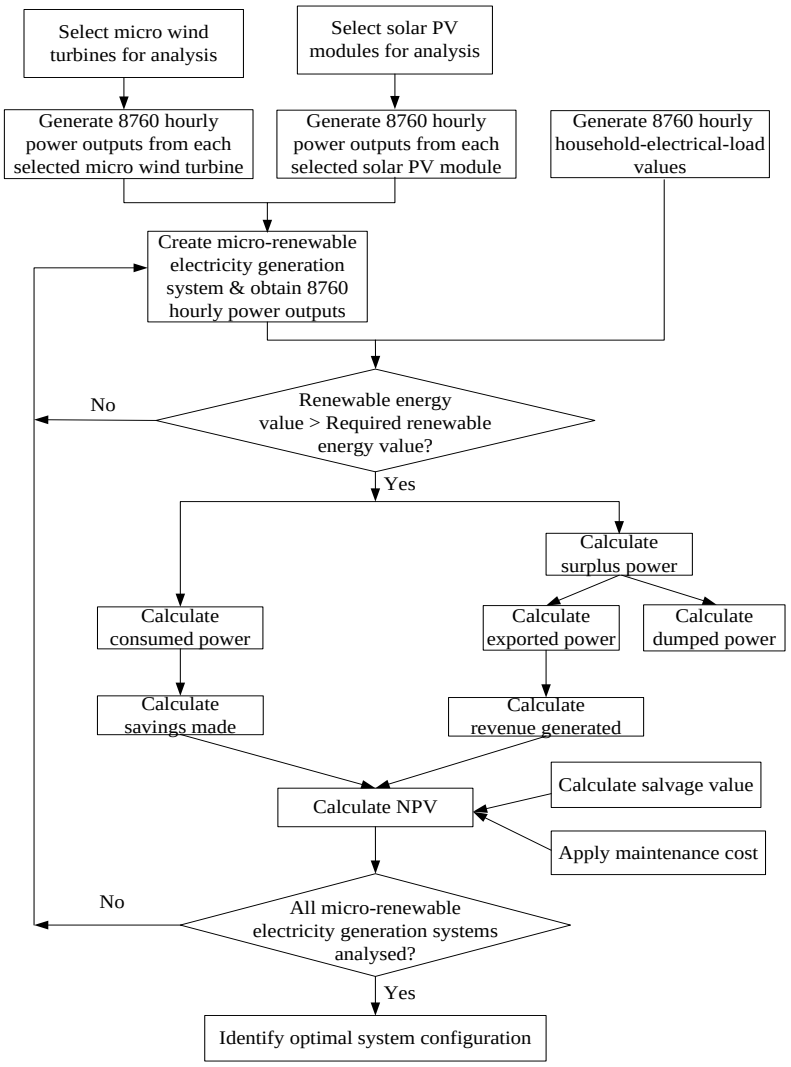

Figure 4.12. Micro wind turbine and solar PV system optimised integration technique [111].

4.7.2. Determination of the Optimal Slope Used for a Solar PV Module

Solar PV modules/panel generate the maximum power, for a fixed orientation, when installed at the optimal slope. The maximum power output of a solar PV module should only be obtained once the optimal slope is determined first. Three solar PV systems were utilised to determine the optimal slope for each represented solar PV module. These solar PV systems have capacities of 1.62 kW_p, 1.665 kW_p and 1.645 kW_p (in the capacity range of most installed solar PV systems in Ireland) and are assembled from the three capacities of solar PV modules employed in the study respectively.

The slopes analysed were from 0^o to 90^o at 5^o intervals. The slope of 40^o was identified as the optimal slopes for all three analysed solar PV systems. The power outputs obtained at this slope are greater than power outputs obtained at the other slopes investigated. Table 4.3-4.5 show the power outputs obtained from the analysed solar PV systems at the different slopes. This optimal slope is determined and used for acquiring power output for the three solar PV modules and also applied in the overall integration studies.

Slope (^{o})	0	5	10	15	20	25	30	35	40	45	50	55	60	65	70	75	80	85	90
Power Output (kWh)	1,285	1,342	1,393	1,437	1,473	1,502	1,523	1,536	1,542	1,539	1,529	1,513	1,490	1,460	1,424	1,381	1,332	1,276	1,216

Table 4.3. Power outputs obtained from a 1.62 kW_p solar PV system assembled from 135 W_p solar PV modules.

Slope (^{o})	0	5	10	15	20	25	30	35	40	45	50	55	60	65	70	75	80	85	90
Power Output (kWh)	1,318	1,375	1,427	1,472	1,508	1,538	1,559	1,572	1,577	1,575	1,565	1,548	1,524	1,494	1,458	1,414	1,364	1,308	1,246

Table 4.4. Power outputs obtained from a 1.665 kW_p solar PV system assembled from 185 W_p solar PV modules.

Slope (^{o})	0	5	10	15	20	25	30	35	40	45	50	55	60	65	70	75	80	85	90
Power Output (kWh)	1,300	1,357	1,409	1,452	1,488	1,517	1,538	1,551	1,556	1,554	1,544	1,527	1,504	1,475	1,438	1,395	1,346	1,290	1,230

Table 4.5. Power outputs obtained from a 1.645 kW_p solar PV system assembled from 235 W_p solar PV modules.

4.8. Results and Discussion

The optimised integration sub-technique is applied to determine the optimal system for Ireland. The selected micro wind turbines and solar PV modules for analysis represent other similar micro wind turbines and solar PV modules and include a range of suppliers and rated powers. The selected micro wind turbines and the solar PV systems (formed from selected solar PV modules) adhere to the conditions for exemption from planning permission. The maximum micro-wind-turbine capacity is set at 6 kW, and the minimum and maximum solar-PV-system capacities are set at 0.5 kW_p and 3 kW_p respectively. The selected micro wind turbines are the Ampair 600-230, the Swift 1.5 kW, the Skystream 3.7, the Siliken 3.4, the Evance R9000 and the CF6d; the selected solar PV modules are the Sharp 235 W, the CareyGlass Solar 185 W and the Kyocera 135 W. Tables 4.6-4.8 give relevant information for the selected micro wind turbines, the selected solar PV modules and the inverters employed respectively. This indicative information was obtained from either official websites or from personal communications. The system integration is carried out assuming the micro-renewable electricity generation system is installed in Dublin and with the following conditions and assumptions:

- An annual average wind speed of 5.76 m/s and an average annual solar radiation value of 970 kWh/m^2.
- An average annual household electrical load of 5,016 kWh.
- The Weibull k factor is 2.12, autocorrelation factor is 0.929, diurnal pattern strength is 0.156 and hour of peak wind speed is 14:00.
- The installed solar PV system is south facing.
- The ground reflectance is 0.2.

- The efficiency of a solar-PV-system inverter is taken as 95%.
- An imported electricity price of €0.1928/kWh.
- An exported electricity tariff of €0.09/kWh.
- The maximum rate of electricity export is capped at 6 kW.
- A green loan having a loan rate of 4.5%.
- An annual inflation rate of 2.26%. This was the average annual inflation rate for Ireland for the period January 2001 to December 2010 [178].
- No capital grant available.
- A 50% renewable energy requirement.
- The project lifespan is 20 years.

Wind Turbine	Rated Power (kW)	Cut-in Wind Speed (m/s)	Cut-out Wind Speed (m/s)	Hub Height (m)	Capital Cost inc VAT (2012 €)	O&M* Costs inc VAT (€/year)	Lifespan (years)
Ampair 600-230 [36]	0.6	3	none	10	4800	50	15
Swift 1.5 kW [179]	1.5	3.5	22	10	7000	50	20
Skystream 3.7 [180]	2.4	3.5	25	10	14000	125	20
Siliken 3.4 [181]	3.8	3.5	17	10	25000	125	20
Evance R9000 [182]	5	3	none	10	35000	200	20
CF6d [183]	6	1.2	none	10	45000	200	25

*O&M- Operation and Maintenance

Table 4.6. Relevant information for six micro wind turbines available on the Irish market in 2012 and selected for the system integration study.

Solar PV Module	Sharp 235 W	CareyGlass Solar 185 W	Kyocera 135 W
Material	Monocrystalline silicon	Monocrystalline silicon	Polycrystalline cell
Maximum power (W)	235	185	135
Module efficiency (%)	14.4	14.5	13.5
Maximum power voltage (V)	30.0	36.2	16.0
Maximum power current (A)	7.84	5.12	6.10
Lifespan (years)	25	25	25
Capital cost inc VAT (2012 €)	650	500	400
Installation cost per kW_p inc VAT (€)	1400	2050	2550
O&M costs inc VAT (€/year)	50	50	50

Table 4.7. Relevant information for three solar PV modules available on the Irish market in 2012 and selected for the system integration study.

Inverter	Sunny Boy 1200	Sunny Boy 2500	Sunny Boy 3000	Windy Boy 1200	Windy Boy 1700	Windy Boy 3000	Windy Boy 3800	Windy Boy 5000	Windy Boy 6000
Peak capacity (kW_p)	1.32	2.70	3.2	1.2	1.7	2.5	3.8	5	6
Capital cost inc VAT (2012 €)	1150	1700	1900	1100	1400	1800	2250	3200	3250
Lifespan (years)	15	15	15	15	15	15	15	15	15

Table 4.8. Relevant information for nine inverters available on the Irish market in 2012 and selected for the system integration study.

4.8.1. Economic Discussion and Identification of the Optimal System Based on Current Irish Conditions

The NPV of a mono micro-renewable electricity generation system consisting of a single micro wind turbine or a single solar PV system, and a hybrid system consisting of a micro wind turbine/solar PV system, has been calculated with the conditions given previously and represents a best case scenario. For example, in this study, the orientation of the installed solar PV module is assumed to be south-facing and therefore ensures that the maximum power output can be generated. However, this best case scenario does not always occur as the roof of the dwelling may not face directly south. However, the total annual power output is of the order of 95% of the maximum over a wide range of orientations, i.e. from 30^{o} south-east to 30^{o} south-west, once the PV module is installed at the optimum or near optimum slope, i.e. from 30^{o} to 45^{o} [184, 185]. The system with the highest NPV after the project lifespan is deemed the optimal system. The NPV (-€5,622) of the optimal system, which meets the 50% renewable energy requirement, is achieved by a single micro wind turbine having a capacity of 2.4 kW; the negative NPV however implies that the optimal system is not economically viable under these conditions. Figure 4.13 is an integration map for all the analysed systems in this study. The systems on and within the black frame meet the 50% renewable energy requirement and are eligible for optimal system determination.

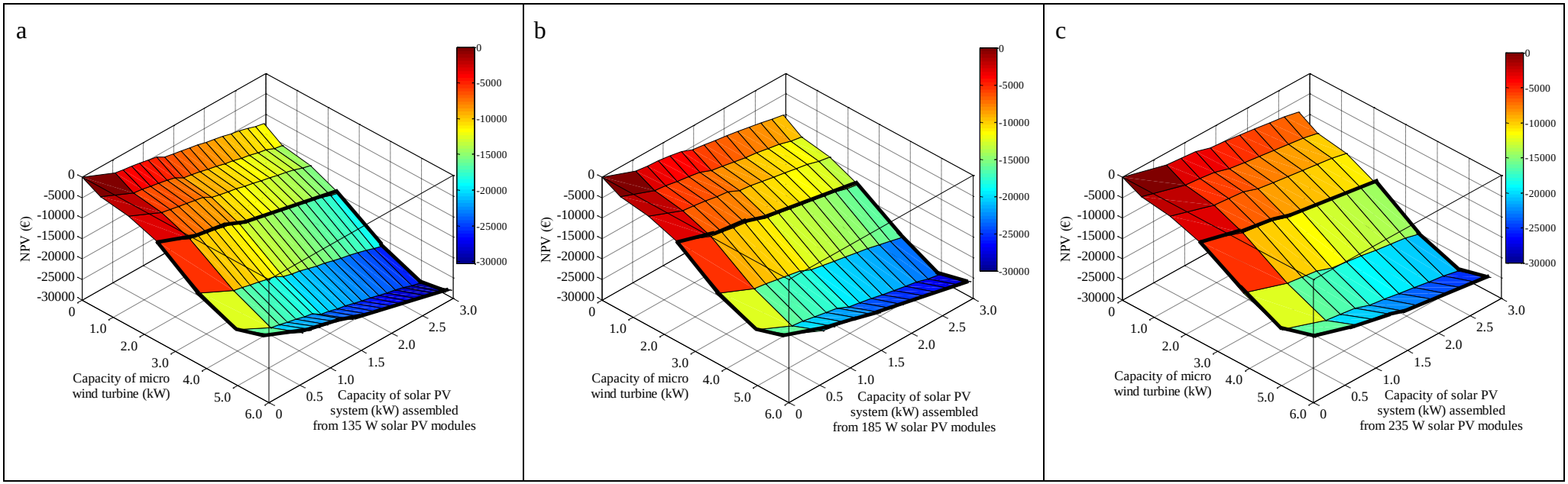

Figure 4.13. Integration map of all the analysed systems under current Irish conditions. Imported electricity price is €0.1928/kWh, exported electricity tariff is €0.09/kWh and the loan rate is 4.5%. The systems on and within the black frame meet the 50% renewable energy requirement.

4.8.2. Economic Discussion and Identification of the Optimal System Based on the Parameter Studies

4.8.2.1. Effect of Household Electrical Load on the Optimal System

The annual household electrical load depends on the number of occupants and the usage of electrical appliances. The electricity generated from a micro-renewable electricity generation system is more likely to be utilised entirely for the dwelling if the household electrical load is high, with very little generated electricity left to export to the grid. In contrast, there can be quite a lot of generated electricity to export if the household electrical load is low.

Figure 4.14 (NPV vs. household electrical load) shows that the NPV of the optimal system, which meets the 50% renewable energy requirement, varies moderately with increasing household electrical load. It is seen that the optimal system is not economically viable under the current conditions whether the household electrical load is high or low.

Figure 4.15 (integration map of NPV vs. sample mono/hybrid micro-renewable electricity generation systems) shows that a system assembled from the same capacity micro wind turbine and the same number of solar PV modules will suffer less economic loss over the project lifespan as the household electrical load increases. This is due to the difference between imported electricity price (€0.1928/kWh) and exported electricity tariff (€0.09/kWh), as the majority of generated electricity is utilised in the dwelling rather than exported to the grid. Figure 4.14 also shows that fewer systems are eligible for consideration as the household electrical load increases due to the 50% renewable energy requirement constraint.

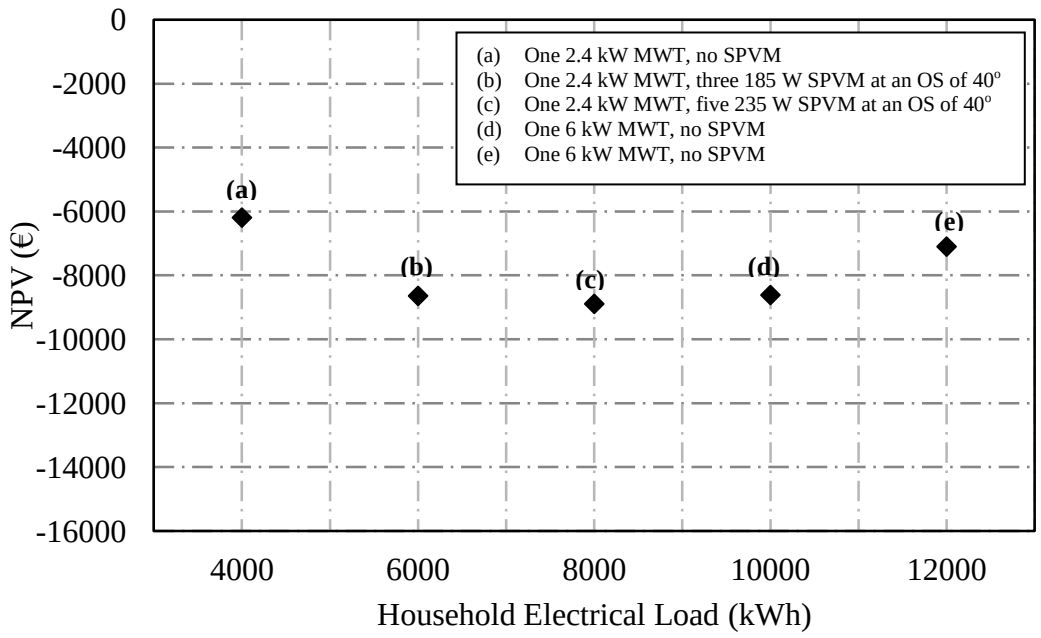

Figure 4.14. NPV of the optimal system versus household electrical load. Imported electricity price is €0.1928/kWh, exported electricity tariff is €0.09/kWh, the loan rate is 4.5% and the renewable energy requirement is 50%. MWT = Micro Wind Turbine, SPVM = Solar PV Modules, OS = Optimal Slope.

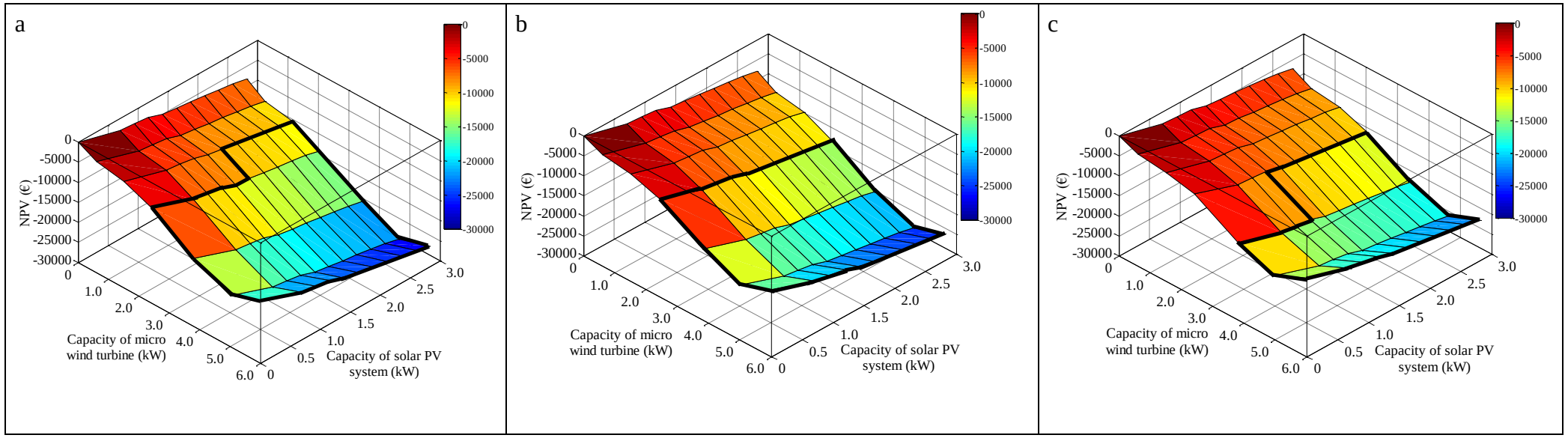

Figure 4.15. Integration map of selected micro wind turbines and solar PV systems assembled from 235 W modules for three household electrical loads. Imported electricity price is €0.1928/kWh, exported electricity tariff is €0.09/kWh and the loan rate is 4.5%. The electrical load is (a) 4,000 kWh, (b) 5,016 kWh and (c) 8,000 kWh. The systems on and within the black frame meet the 50% renewable energy requirement.

4.8.2.2. Effect of Imported Electricity Price on the Optimal System

The imported electricity price is another factor that can influence the optimal system. Electricity generation is mainly dependent on imported fossil fuels in Ireland. Fossil fuel prices are expected to rise in the coming years mainly due to greater global demand, and not any particular decline in supply. Also the recent unrest in many fossil-fuel-exporting countries may cause prices to rise significantly. For householders, there could also be other reasons for electricity price increases, including an increase in the VAT rate, a levy charge and/or an introduced carbon tax on the usage of electricity.

Figure 4.16 (NPV vs. imported electricity price) shows that the NPV of the optimal system improves considerably as the imported electricity price increases. If the imported electricity price rises to €0.298/kWh [186], the highest imported electricity price charged in the EU-27 in 2011 (Denmark), the optimal system will nearly be economically viable. Figure 4.17 (integration map of NPV vs. sample mono/hybrid micro-renewable electricity generation systems) shows that a system assembled from the same capacity micro wind turbine and the same capacity solar PV system will suffer less economic loss as the imported electricity price increases. Also it can be seen that large capacity systems are more affected by increasing imported electricity price since the NPV becomes significantly less negative.

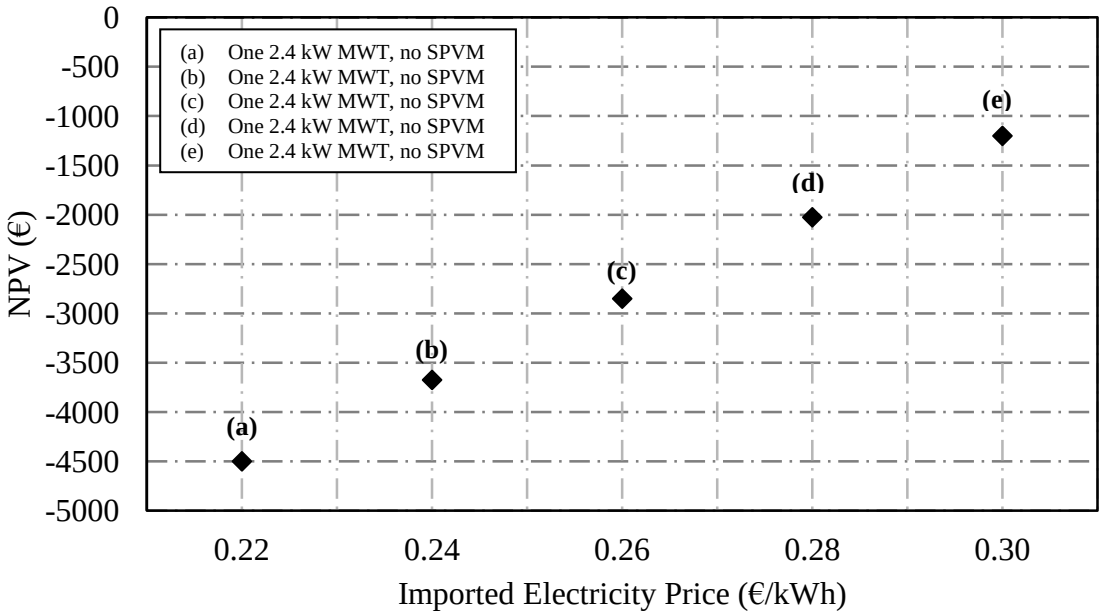

Figure 4.16. NPV of the optimal system versus imported electricity price. Exported electricity tariff is €0.09/kWh, the loan rate is 4.5% and the renewable energy requirement is 50%. MWT = Micro Wind Turbine, SPVM = Solar PV Modules.

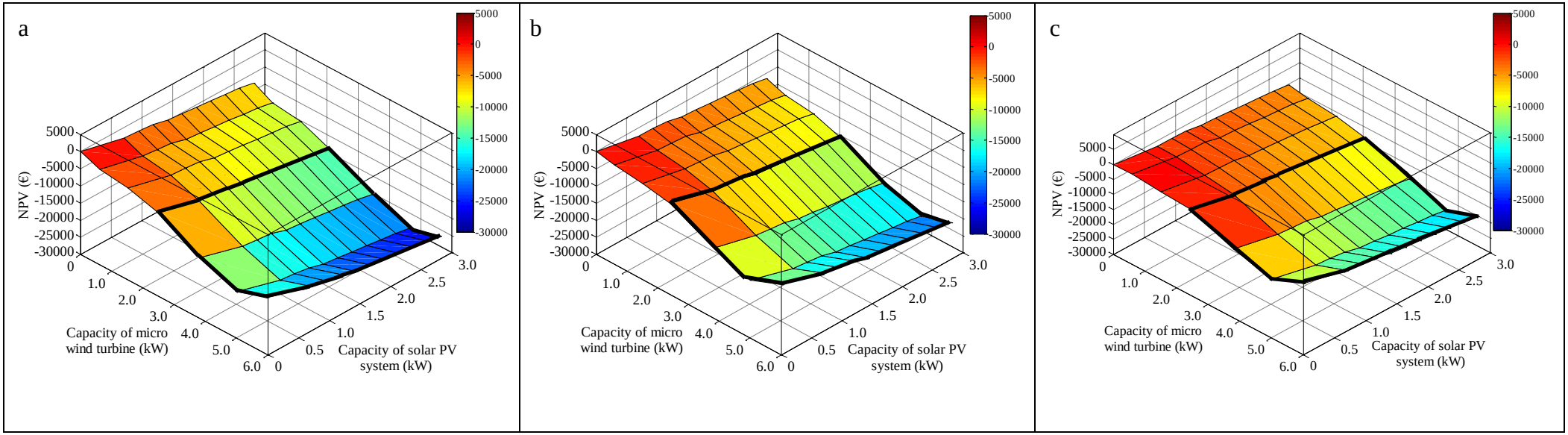

Figure 4.17. Integration map of selected micro wind turbine and solar PV system assembled from 235 W modules for three imported electricity prices. Exported electricity tariff is €0.09/kWh and the loan rate is 4.5%. The imported electricity price is (a) €0.1928/kWh, (b) €0.25/kWh and (c) €0.30/kWh. The systems on and within the black frame meet the 50% renewable energy requirement.

4.8.2.3. Effect of Exported Electricity Tariff on the Optimal System

The electricity generated by a micro-renewable electricity generation system may exceed the household electrical load. Before February 2009 there was no feed-in tariff in Ireland. The introduced exported electricity tariff has been the most direct incentive for householders having a micro-renewable electricity generation system. However, the uniform exported electricity tariff (€0.09/kWh) currently offered in Ireland for both a micro wind turbine and a solar PV system is too low to help these systems become economically viable. The United Kingdom, for example, offers a very attractive exported electricity tariff to householders with these systems. A householder with a micro wind turbine having a capacity less than or equal to 1.5 kW and greater than 1.5 kW and less than 15 kW can receive an exported electricity tariff of £0.362(€0.43)/kWh and £0.28(€0.33)/kWh respectively. A householder with a solar PV system having a capacity less than or equal to 4 kW_p can receive an exported electricity tariff of £0.433(€0.51)/kWh if applied for before December 12th, 2011; otherwise the householder can receive an exported electricity tariff of £0.21(€0.25)/kWh [187].

Figure 4.18 (NPV vs. exported electricity tariff) shows that NPV of the optimal system improves significantly with increasing exported electricity tariff. If an exported electricity tariff of €0.25/kWh was offered, the current exported electricity tariff offered for a solar PV system in the UK in 2012, the optimal system, which meets the 50% renewable energy requirement, is economically viable. Figure 4.19 (integration map of NPV vs. sample mono/hybrid micro-renewable electricity generation systems) shows that a system assembled from the same capacity micro wind turbine and the same capacity solar PV system will experience more economic

gain over the project lifespan as the exported electricity tariff increases. The exported electricity tariff is seen as the most effective way in making a micro wind turbine and a solar PV system turn into a good investment, e.g. based on our calculations, a single CF6d 6 kW micro wind turbine, manufactured in Ireland, can achieve an impressive NPV of €33,467 (16,087 kWh of electricity produced per annum) for 2011 weather, for a 20-year project lifespan, and assuming an exported electricity tariff of €0.33/kWh (the UK exported electricity tariff for a micro wind turbine of this size in 2012). However, it should be noted that the high exported electricity tariffs offered in the UK are based on expected generation costs which take into consideration the renewable resource availability. Ireland, in general, has a superior wind resource to that in the UK. Therefore, even if a higher exported electricity tariff was offered, it is still likely to be lower than those on offer in the UK. Figure 4.18 also shows, due to the larger amount of electricity produced, that a rising exported electricity tariff has a greater impact on large capacity systems than on small ones.

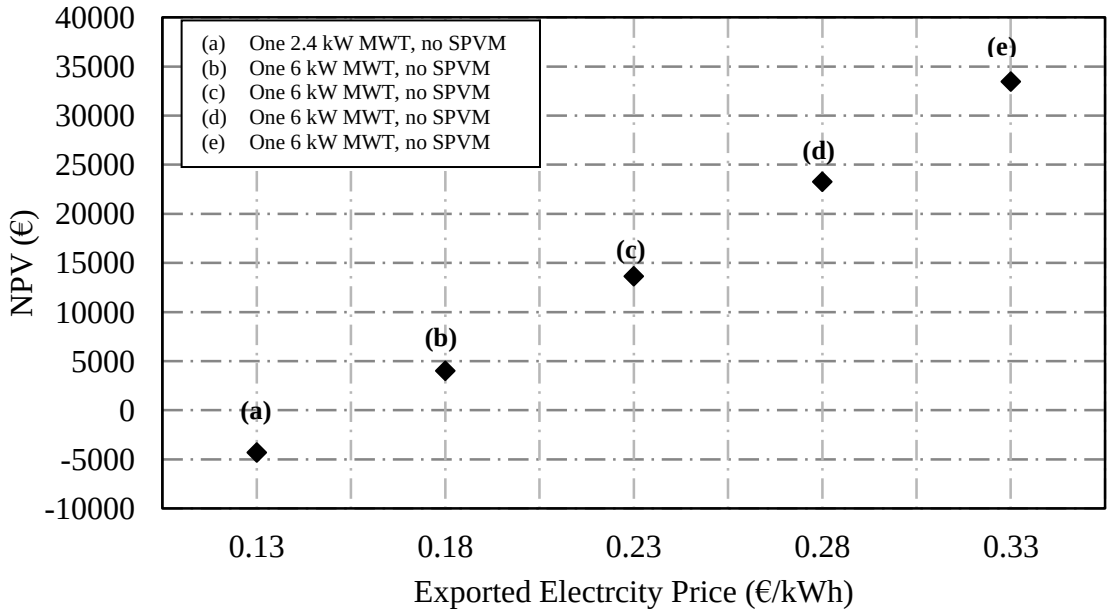

Figure 4.18. NPV of the optimal system versus exported electricity tariff. Imported electricity price is €0.1928/kWh, the loan rate is 4.5% and the renewable energy requirement is 50%. MWT = Micro Wind Turbine, SPVM = Solar PV Modules.

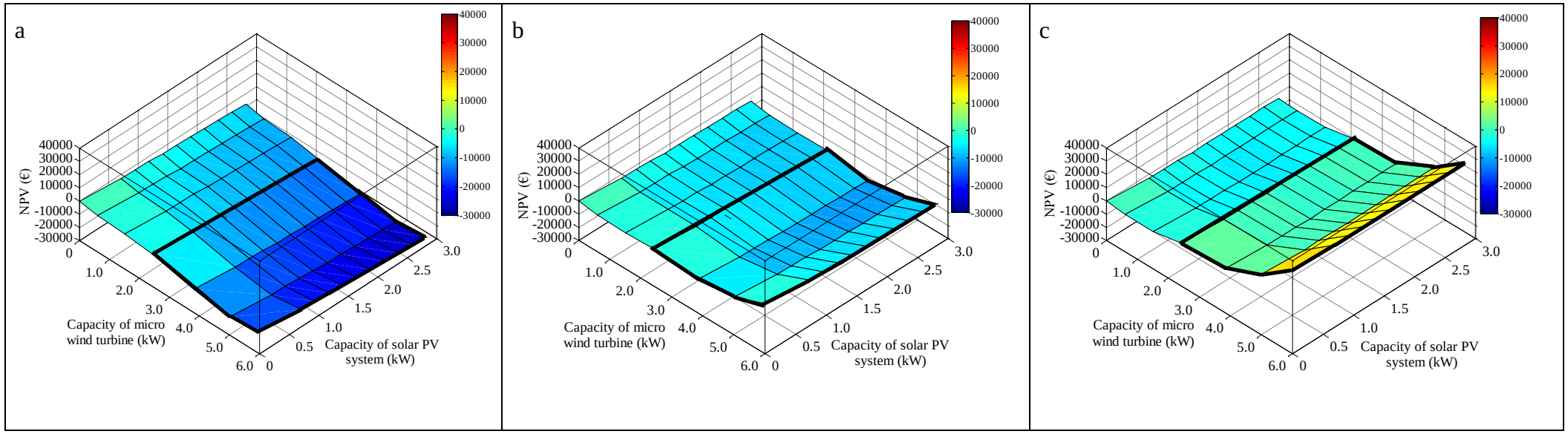

Figure 4.19. Integration map of selected micro wind turbines and solar PV systems assembled from 235 W modules for three exported electricity tariffs. Imported electricity price is €0.1928/kWh and the loan rate is 4.5%. The exported electricity tariff is (a) €0.09/kWh, (b) €0.20/kWh and (c) €0.33/kWh. The systems on and within the black frame meet the 50% renewable energy requirement.

4.8.2.4. Effect of Wind Speed on the Optimal System

The solar radiation received is almost the same throughout Ireland; hence the amount of electricity generated from a solar PV system is nearly independent of where it is located. However, Ireland has an excellent wind-energy resource which is four times that of the European average [188]. In general, the annual average wind speed is around 5 m/s in the midlands in Ireland; however, the annual average wind speed can reach 7 m/s for many parts of the country, especially along the coast.

Figure 4.20 (NPV vs. wind speed) shows the optimal system, which meets the 50% renewable energy requirement, is nearly economically viable with an annual average wind speed of 7 m/s. Figure 4.20 (integration map of NPV vs. sample mono/hybrid micro-renewable electricity generation systems) shows that a system assembled from the same capacity micro wind turbine and the same capacity solar PV system will suffer a modest economic loss or will even become economically viable once the system is installed in a location having a good wind resource. Figure 4.21 also shows that an increasing annual average wind speed has a greater economic impact on large capacity micro wind turbines than on small and medium capacity turbines. Hence, the wind speed at a location can be a decisive factor to determine the components of an optimal system.

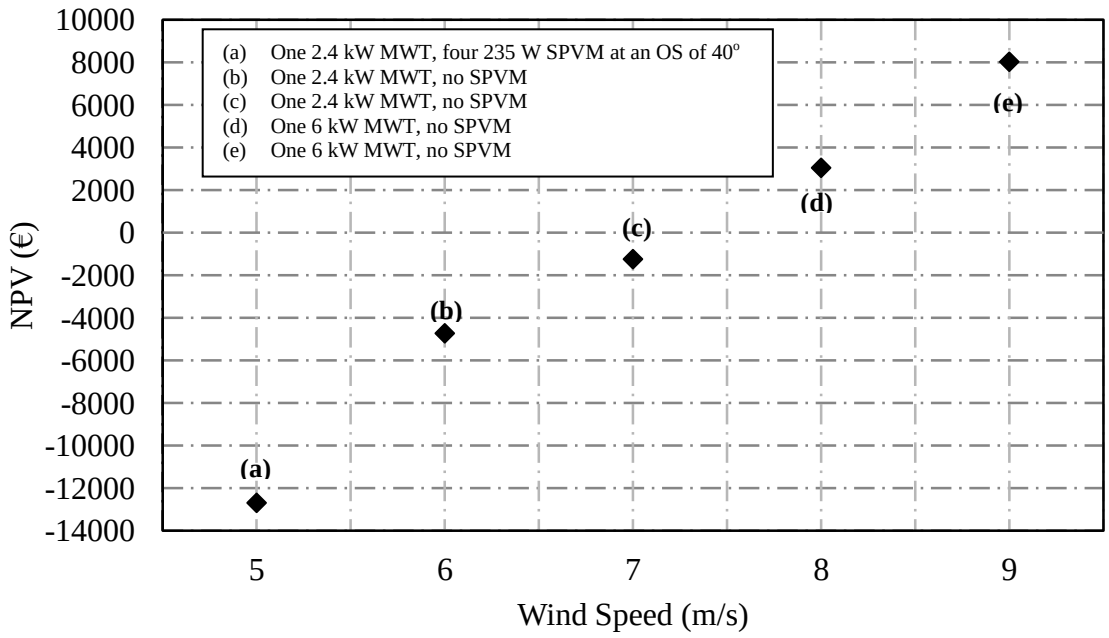

Figure 4.20. NPV of the optimal system versus wind speed. Imported electricity price is €0.1928/kWh, exported electricity tariff is €0.09/kWh, the loan rate is 4.5% and the renewable energy requirement is 50%. MWT = Micro Wind Turbine, SPVM = Solar PV Modules, OS = Optimal Slope.

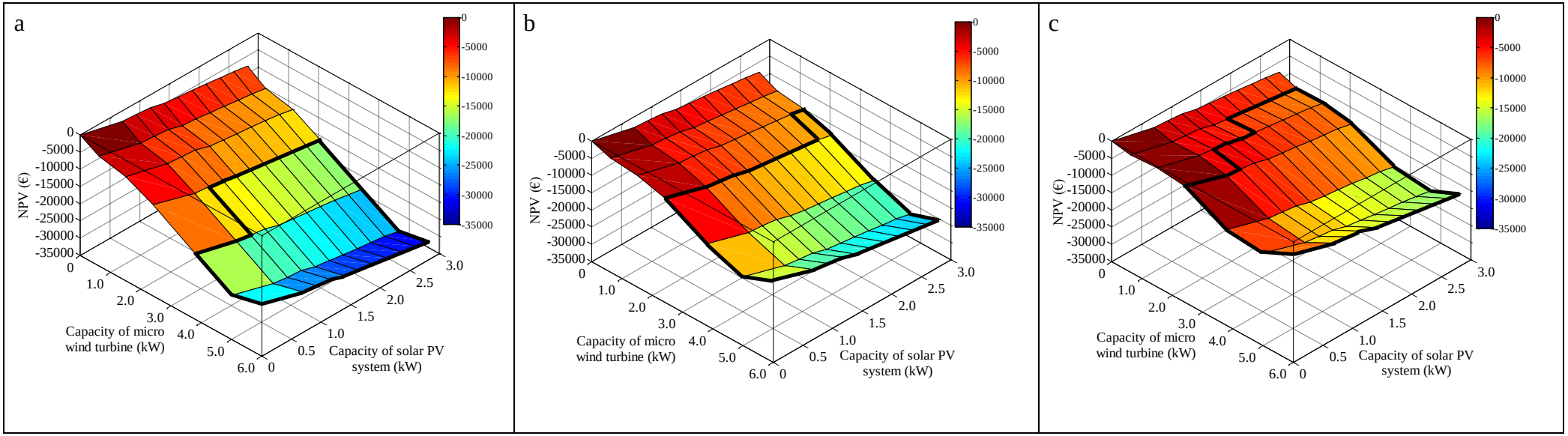

Figure 4.21. Integration map of selected micro wind turbines and solar PV systems assembled from 235 W modules for three wind speeds. Imported electricity price is €0.1928/kWh, exported electricity tariff is €0.09/kWh and the loan rate is 4.5%. The wind speed is (a) 5 m/s, (b) 6 m/s and (c) 7 m/s. The systems on and within the black frame meet the 50% renewable energy requirement.

4.9. Conclusion

In this chapter a sub-technique is presented for the optimised integration of a grid-connected mono/hybrid micro-renewable electricity generation system which employs a renewable energy constraint and the NPV concept. A mono micro-renewable electricity generation system is formed from a single micro wind turbine or a single solar PV system; a hybrid micro-renewable electricity generation system is formed from a combination of both. Six micro wind turbines and three solar PV modules (used to form the solar PV systems for analysis), which are commercially-available and industry-representative, are employed in this study. However, additional micro wind turbines and solar PV modules can be added to the existing database if a wider range of micro-renewable electricity systems is required for analysis. Using the developed integration technique, the system with the highest NPV after the project lifespan is deemed the optimal system. Under current Irish conditions, the optimal system, which meets the 50% renewable energy requirement is a mono system consisting of a 2.4 kW micro wind turbine. However, the system is not economically viable as the NPV is negative over the project lifespan. The large capital cost of micro wind turbines and solar PV systems and the lack of financial support in terms of both the low exported electricity tariff offered and the non-existent capital grant are the main reasons for the poor economic-viability of wind, solar and hybrid wind/solar systems in Ireland. Nevertheless, these systems should become economically viable in the future with reductions in the capital cost of these systems and increases in the cost of imported electricity. For example, the price of solar PV modules per kW_p in Europe in 2012 was less than half of the price in 2001 [189] and the imported electricity price has increased by 20.58% from the end of 2007 to the end of 2011 in Ireland [190, 191]. Four parameter studies to assess the effect of household electrical load, imported electricity

price, exported electricity tariff and wind speed have also been carried out. From the results presented, offering a greater exported electricity tariff is seen as the most effective support for a mono/hybrid system. Therefore, in order to make micro-renewable electricity generation systems economically attractive and to promote their widespread installation, the current financial support provided under Irish renewable energy policies must be improved. One possible strategy is to reinstate the ceased exported electricity additional payment of €0.10 for every kWh of electricity exported. This tariff would help some micro-renewable electricity generation systems become economically viable, and in particular the optimal system as this study shows. Moreover, this tariff would encourage householders to satisfy their own demand at the location of production first since it is still slightly lower than the current imported electricity price applied in Ireland. Another possible strategy could be to provide a scheme that offers a financial reward to householders who meet the majority of their electricity demand from installed renewable energy systems.

The weather conditions at a specific location where wind and solar systems are installed can also play a major part in determining their economic viability. The excellent wind resource available in Ireland is more likely to help micro wind turbines become economically viable before solar PV systems. Ultimately, each householder should always make a decision based on his/her individual case as to whether a micro wind turbine, a solar PV system or a hybrid wind-solar system is worthwhile to be installed or which system can achieve the most economic benefit. The renewable energy system market is dynamic, continuously influenced by improvements in micro-wind-turbine and solar-PV technologies, the economy of scale in production and changes in Irish government policies towards micro renewable energy technologies.

4.10. Summary

A sub-technique for the optimised integration of grid-connected micro-renewable electricity generation systems is presented in this chapter. The reviews of micro wind turbine and solar PV system are presented. The methodology of generating hourly wind speed values and hourly solar radiation values is described; subsequently the methodology of predicting hourly power output from a micro wind turbine and a solar PV system is presented. The developed integration technique for selected micro wind turbines and solar PV systems is explained in detail. The results are then analysed and discussed. In the next chapter, the optimised integration sub-technique for grid-connected micro-renewable thermal generation systems is presented.

CHAPTER 5
OPTIMISED INTEGRATION OF GRID-CONNECTED MICRO-RENEWABLE THERMAL GENERATION SYSTEMS

5.1. Overview

In this chapter, a sub-technique for the optimised integration of grid-connected micro-renewable thermal generation systems is presented. The chapter is split into six stages. In the first stage, the realistic hourly domestic heating demand and profile is obtained. In the second stage, the practical daily domestic hotwater demand and profile is acquired. In the third stage, the technology of domestic solar thermal system is reviewed, the methodology of statistically generating hourly solar radiation values is presented, and the methodology of obtaining hourly energy outputs of a solar thermal system is then presented. In the fourth stage, the technology of an ASHP is reviewed, the methodology of accurately generating hourly ambient air temperature values is described, and the methodology of obtaining hourly energy outputs of an ASHP is then given. In the fifth stage, a sub-technique is developed to integrate the selected commercially-available solar thermal systems and ASHPs. Finally, in the sixth stage, the results obtained from applying this sub-technique for current Irish conditions and parameters studies are analysed and discussed.

5.2. Introduction

The rapid growth of the global economy has resulted in an exponential increase in energy requirements worldwide. The fossil fuel resources required for the generation of energy are becoming increasingly scarce and climate changes related to excessive carbon emissions has increased interest in both energy saving and environmental protection [192]. In recent years, the use of renewable energy technologies has been identified as the most effective solution to these problems. The deployment of renewable energy technologies is crucial in Ireland given that there are very few indigenous fossil fuel resources available. For domestic dwellings, the largest source of energy consumption is space heating which accounts for approximately 60% of the total domestic energy consumption. Hotwater generation was the second largest source and accounts for 18% of the total domestic energy consumption. In Ireland, heat generation is dependent on the importation of fossil fuels. Ireland has set a target of 12% of heat generation to be met by renewable energy by 2020. Ireland has numerous accessible renewable energy resources, such as solar, biomass and geothermal energy, which are suitable for domestic heating and hotwater generation. Geothermal heat pumps for domestic dwellings have existed for many years. Unfortunately, these devices are often extremely expensive, require a large ground area and are primarily applicable to new dwellings. ASHPs, which use air as a heat source, are an alternative and relatively newer technology which are less expensive, require a smaller amount of space and are fit for both new and existing dwellings. As the air temperature tends to fluctuate throughout the year whilst the ground temperature remains practically stable, the COP achieved by ASHPs is not always comparable to that achieved by geothermal heat pumps. However, the temperate climate in Ireland is suitable for ASHP operation since the winters rarely become too cold. Solar thermal systems, which are typically used for

hotwater generation (and in rare cases for domestic space heating) have been extensively and successfully adopted worldwide. However, in most cases, these solar thermal systems are operated in combination with a conventional heating system such as a gas boiler, an oil boiler or an electric immersion to satisfy the hotwater requirement and to manage the intermittent nature of solar radiation. The use of ASHPs in combination with solar thermal systems is becoming popular due to the promise of reduced energy consumption and cost savings. In this study, the ASHP is analysed for the provision of domestic space heating and for the preheating of supply water within a hotwater storage cylinder. A solar thermal system is also adopted to raise the temperature of the supply water within the hotwater storage cylinder to a desired value. The use of both an ASHP and a solar thermal system ensures the maximum use of renewable energy for thermal generation. Additionally, the interaction between the ASHP and the solar thermal system improves both their economic viability and the effectiveness of the energy supply.

In Ireland, grants provided under the former Greener Homes Scheme resulted in a large increase in the number of ASHPs and solar thermal systems installed between March 2006 and May 2011. However, subsequent grants provided under the Better Energy Homes Scheme are limited to solar thermal systems only. These schemes were/are designed to stimulate householder interest in the installation of micro-renewable thermal generation systems. To date however, a detailed investigation of the economic viability of typical domestic integrated micro-renewable thermal generation systems, which is of critical importance to individual householders, has not been carried out. As well as knowing the various types of micro-renewable thermal generation system that are currently available, it is also important to determine the optimal system for each scenario.

This chapter presents a novel sub-technique for the optimised integration of a mono/hybrid micro-renewable thermal generation system consisting of an ASHP and/or a solar thermal system. A single ASHP or a single solar thermal system forms a mono system whilst a combination of an ASHP and a solar thermal system forms a hybrid system. The integration technique is generally applicable but is deployed here for Ireland, takes into account technical constraints (e.g. exemption conditions for planning permission) and economic supports (e.g. grants available for solar thermal systems). LCC is used to identify the optimal system in this integration technique; the heating demand and hotwater requirement have to be satisfied from the mono/hybrid micro-renewable thermal system (a primary and/or an auxiliary heater may be required). Realistic hourly thermal (heating and hotwater) outputs for a year from the analysed ASHPs and the analysed solar thermal systems are obtained from accurately predicted hourly ambient air temperature values and hourly solar radiation values respectively by applying monthly weather data. The hourly household thermal loads for a complete year are obtained from smart meter trials carried out by the Commission for Energy Regulation (CER). The predicted system performance and the obtained economic results are accurate and reflect the real-life situation of an actual installed system. The chapter also demonstrates the modification in the system configuration when realistic changes (economical and heating consumption) are made.

5.3. Hourly Heating Demand and Profile

The hourly thermal loads (demand) and profiles employed in this study were obtained by multiplying the typical efficiency of a conventional gas boiler with gas consumption data obtained from the Smart Metering Gas Customer Behaviours Trials initiated by CER [193]. Almost 2,000 Irish homes took part in these trials between December 2009

and January 2011. During the trial, a gas smart meter was installed in each individual household, and realistic gas consumption behavioural and usage patterns were then recorded. Following the completion of the trial, the data was reported in an anonymous format and no personal and confidential information were revealed. Five domestic hourly gas consumption behavioural and usage patterns in 2010 were selected based on the limited information available. The gas consumed is only used for providing heating in these five houses; therefore no gas is utilised for water heating and cooking purposes. The hourly gas consumption data having a total usage value of 16,536 kWh, the closest value obtained when referencing the average energy consumed of 16,232 kWh in the form of fossil fuels in 2010, is employed as the base data in this study. These selection processes are critically important in determining the hourly thermal heating loads and profile. The efficiency of a conventional gas boiler is assumed to be 85%. Although the current range of gas boilers have efficiencies of greater than 90%, gas boilers over 15 years old tend to have efficiencies of less than 80%. Due to the fact that the age of the gas boilers which were involved in the trial was not revealed, an average efficiency of 85% was adopted in this study. Figure 5.1 demonstrates examples of the generated hourly household thermal load profiles for four days (one for each season) from the base data throughout the year.

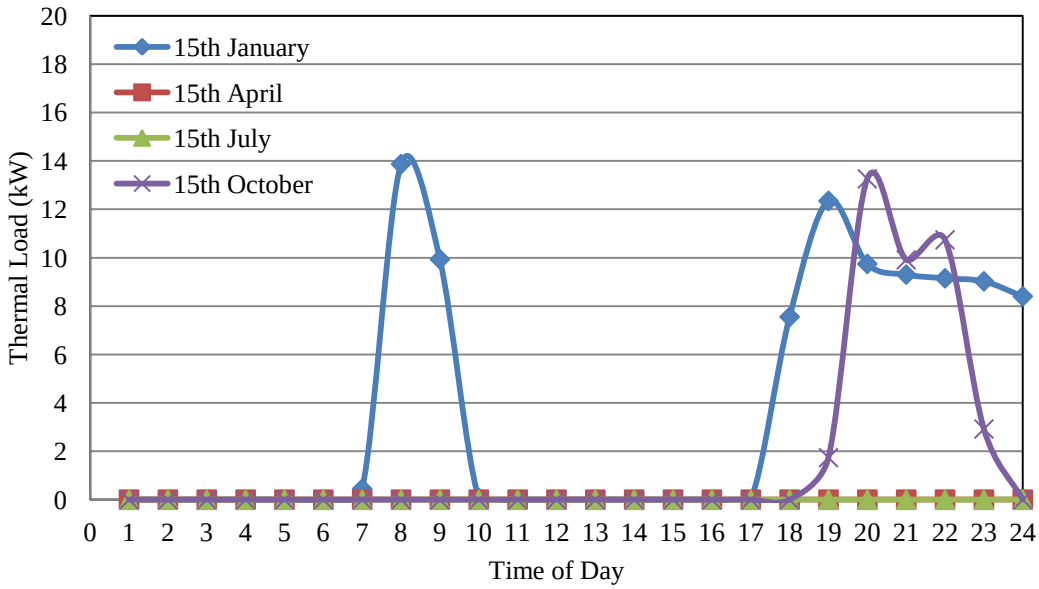

Figure 5.1. Examples of generated hourly thermal loads for four days from the base domestic thermal load.

Five domestic hourly thermal loads, employed in the parameter study of the effect of domestic thermal load on the optimal system, are examined in order to assess if their mean values are statistically different. This examination is performed using Tukey's test which is one of the multiple comparison tests of one-way analysis of variance (ANOVA). One way ANOVA enables the comparison of several means of populations simultaneously. Using ANOVA, it can be determined whether there is any statistical difference between the population means. Tukey's test may then be employed to compare the difference between each pair of means with appropriate adjustment for the multiple tests. The results are presented in a matrix that shows the result for each pair, either as a P-value or as a confidence interval. Tukey's test assumes that the data from the different groups come from populations where the observations have a normal distribution and the standard deviation is the same for each group [194]. This nonparametric test is robust and works best if sample sizes are equal.

In this analysis of the five domestic thermal loads using Tukey's test, the simultaneous confidence interval utilised is 95% and the sample size of each domestic hourly thermal load is 8,760. The results, given in Table 5.1, show that these five sets of hourly domestic thermal load have significantly different means since they do not share a letter in the grouping obtained from Tukey's test.

	Size of Sample	Mean	Grouping
Household 1	8,760	2.90	A
Household 2	8,760	2.31	B
Household 3	8,760	1.96	C
Household 4	8,760	1.60	D
Household 5	8,760	1.24	E

Table 5.1. The result of Tukey's test showing that the five selected household thermal loads are statistically different.

The statistical maximum, minimum, mean and variance of each the domestic hourly thermal loads are demonstrated in Table 5.2. Also, the examples of domestic hourly thermal load profiles for four days (one for each season) in the year are shown in Figure 5.2; these figures represent the annual thermal load of 10,890 kWh, 17,172 kWh, 20,235 kWh and 25,425 kWh respectively. As shown in these figures, very little thermal load is observed during the summer months. Winter and spring generally require the most domestic heating since the thermal loads are very active in these periods. Furthermore, the domestic thermal profiles with a high thermal load are a lot "busier" (more heating is required) than those profiles with a low thermal load.

	Maximum (kWh)	Minimum (kWh)	Mean (kWh)	Variance
House 1	13.35	0.00	1.24	9.55
House 2	18.44	0.00	1.60	14.76
House 3	13.20	0.00	1.96	9.69
House 4	17.59	0.00	2.31	12.63
House 5	19.83	0.00	2.90	20.84

Table 5.2. The statistical maximum, minimum, mean and variance of the five selected domestic hourly thermal loads.

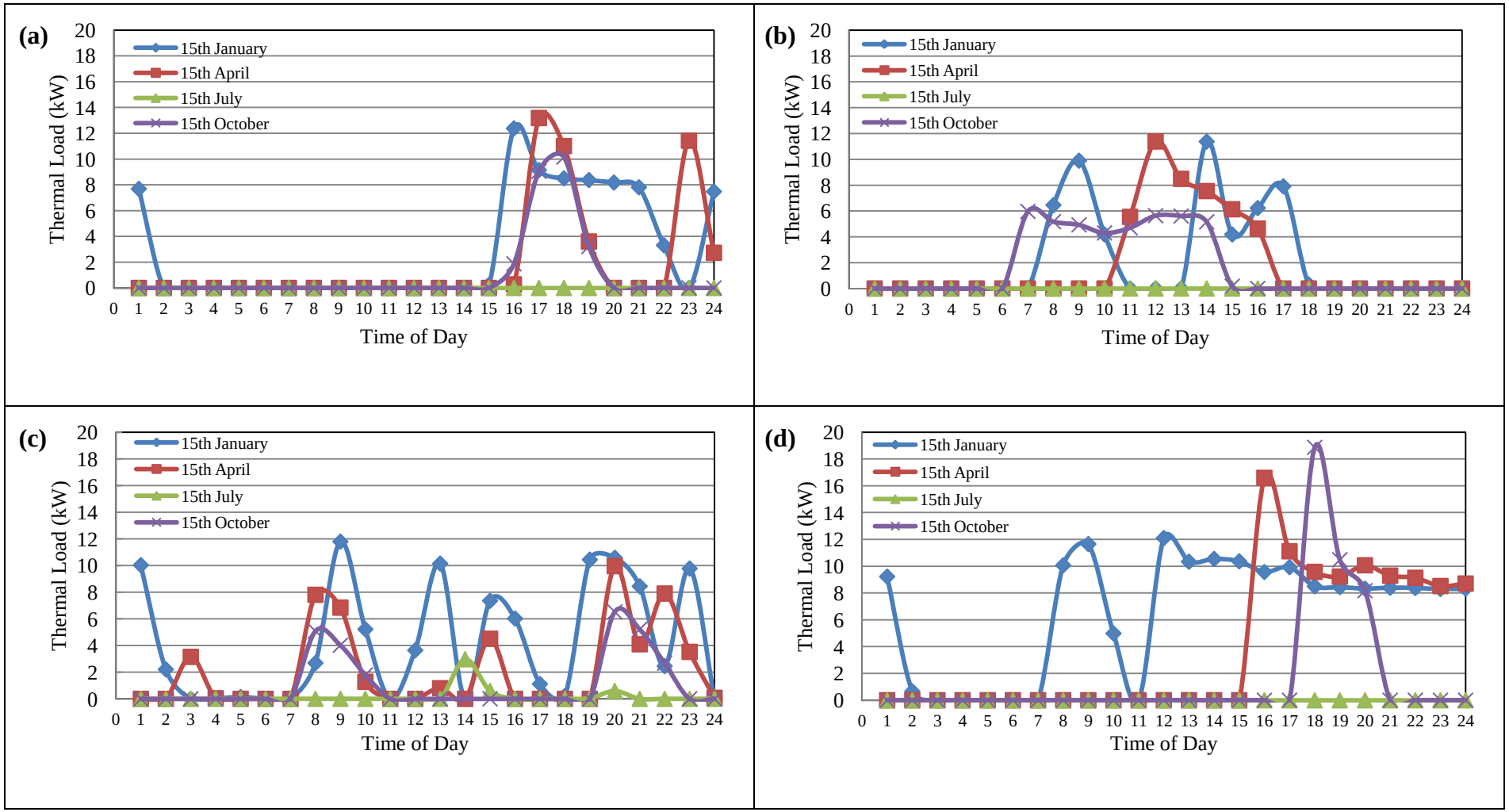

Figure 5.2. Examples of generated hourly domestic thermal loads for four days (a) 10,890 kWh, (b) 17,172 kWh, (c) 20,235 kWh and (d) 25,425 kWh.

5.4. Daily Hotwater Demand and Profile

The daily hotwater demand and profile was employed from the EU reference tapping cycle number 3. The energy output of 11.7 kWh for each day is equivalent to a total volume of 199.8 L at 60^{o}C. This is based on the EU mandate for the elaboration and adoption of measurement standards for household appliances EU M324EN [63]. This hotwater demand profile consists of 24 draw-offs, and is presented in Figure 5.3. The large quantity of hotwater usage is possibly due to the following: showering, bathing, dish-washing and etc. Although the daily hotwater demand and profile may vary significantly from both day to day and from resident to resident, it is impractical to use anything but a repetitive load profile. This is not quite correct for the summer period where the hotwater consumption pattern is slightly higher due to frequent showering and bathing. However, the temperature requirement for hot water during this period is not as high as during winter period. Consequently, the total thermal energy requirement is reasonably constant throughout the year.

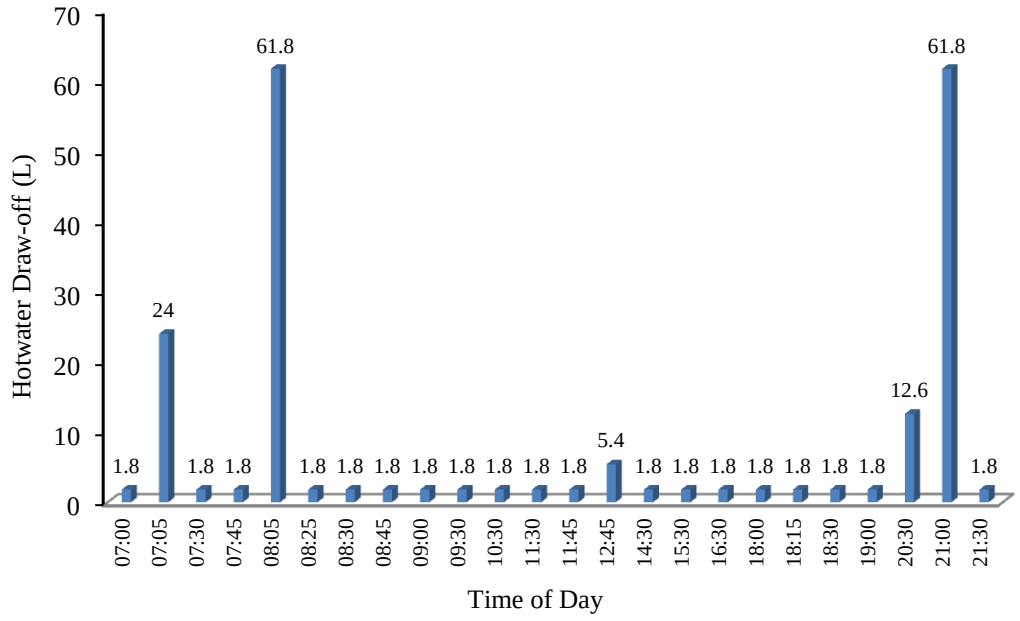

Figure 5.3. Volume of hotwater draw-off at various time of the day.

5.5. Domestic Solar Thermal System

5.5.1. Technology Review of Solar Thermal System

The solar water heating system, as shown in Figure 5.4, collects solar thermal energy. This solar heat is primarily employed for heating water and the heated water is then used for the domestic hotwater supply. The heated water may also be employed for space heating if a larger solar collector area, a larger hot water storage cylinder and more complex control systems are implemented. A solar water heating system can typically meet between 30% and 70% of the total annual hot water demand. Ideally, a solar water heating system should provide close to 100% of the hot water demand during the summer months and a portion of the hot water demand during the winter months when there is less solar thermal energy available.

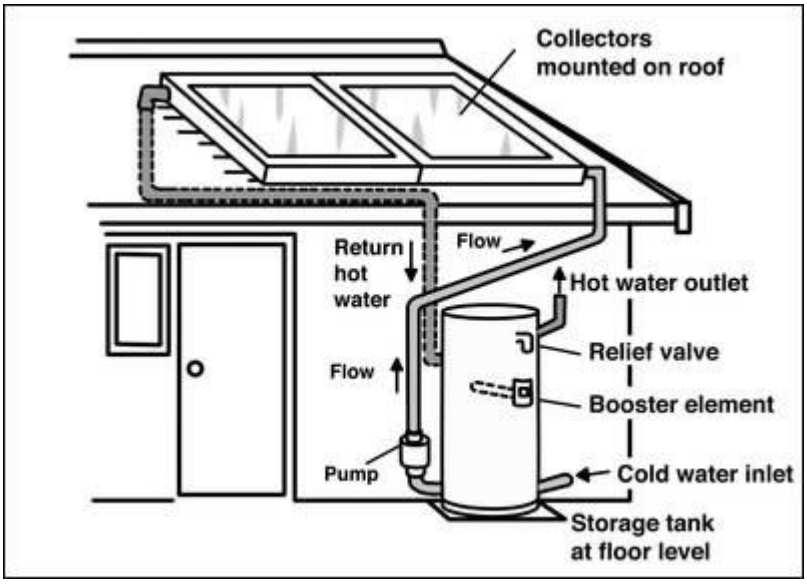

Figure 5.4. Schematic diagram of a domestic solar thermal system [195].

The power output of the solar collector is dependent upon its location, orientation, slope and its efficiency. The maximum annual energy output is obtained from a solar collector in Ireland when the collector is oriented due south at a slope angle of 30-45^{o} to the

horizontal. However, a solar thermal collector is capable of achieving close to 95% of the maximum output when it is orientated within 45^{o} of south and with tilt angles from $10\text{-}50^{o}$ [196].

There are two dominant types of solar collector which are employed for domestic water heating applications: a flat plate collector and an evacuated tube collector as shown in Figure 5.5. These two types of solar collector are both of interest to this research since they are both commonly used in Ireland. The flat plate collector has a flat plate absorber which is typically coated with a special absorptive layer which maximises solar radiation capture. The heat transfer fluid is circulated through channels in the plate or pipes bonded to the back. There are headers at each end of the plate for connecting to the heat transfer circuit. A translucent glass or a plastic screen (single or double glazed) covers the plate. It functions to reduce the heat loss to the surroundings when the fluid in the collector is heated to a high temperature. The back and sides of the collector are always well insulated. The evacuated tube collector has a long and narrow collector plate enclosed in an evacuated tube. The plate is either a pipe containing a heat transfer fluid or a metal rod that is heated and transfers the heat via conduction. The vacuum can greatly reduce heat loss because there is no air to conduct the heat away. The evacuated tube collector generally delivers a higher power output per unit area than a flat plate collector. The translucent cover of the flat plate collector reflects some of the solar radiation away, especially when the sunshine level is low. Also the plates can be rotated to face the sun in the evacuated tube collector. Even though the evacuated tube collector generally achieves better efficiency, it is usually more expensive due to the increased complexity of its manufacturing process. Solar collectors can be set in a stationary (fixed permanent position) or in motion (adjust the position to face the sun) via a single or dual axis sun tracking device. The sun tracking device ensures the solar collector

receives maximum solar irradiation at all times [197]. The use of this device can improve the efficiency of the solar collector, in particular for flat plate solar collectors since it produces maximum energy when it is directly facing the sun. However, due to the mechanical complexity and the additional cost for installation and operation, the sun tracking device has not been widely adopted in Ireland. As such, the stationary solar collector is evaluated in this research.

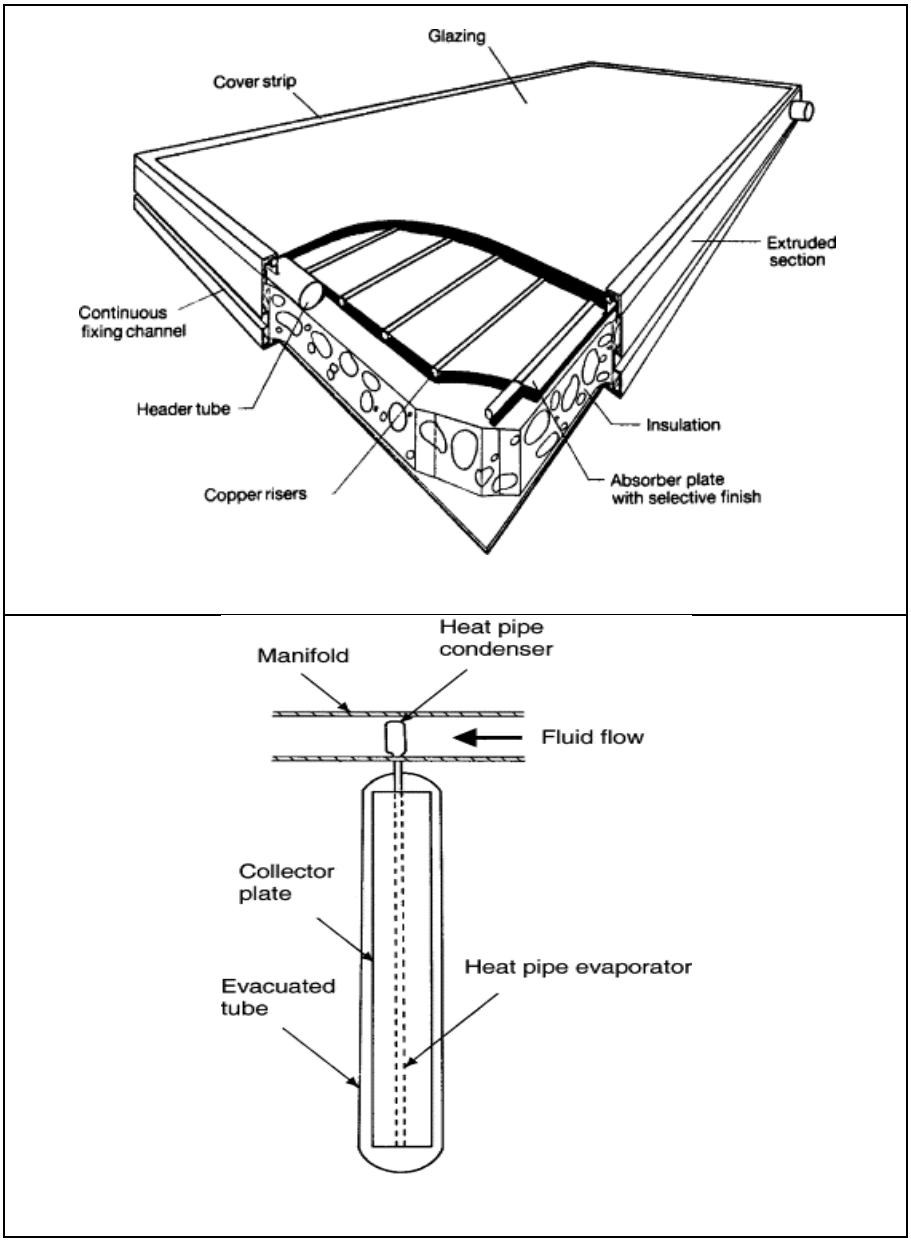

Figure 5.5. Schematic diagram of (a) a flat plate solar collector and (b) an evacuated tube solar collector [198].

Heat is removed from a solar collector using either an indirect system or a direct system. Most of the solar collectors deliver heat using an indirect system. In an indirect system, a solar fluid circuit is employed to transfer heat from the solar collectors to the hotwater storage cylinder. This solar fluid circuit consists of the solar collectors, the connecting pipeworks, the electrical pump and a heat exchanger. A fluid that consists of water, anti-freeze and anti-corrosion inhibitor is commonly used in the solar fluid circuit. A domestic hotwater circuit consists of the hotwater storage cylinder, the cold water supply, the hotwater taps and shower, and connecting pipeworks. The flat plate collector can work also as a direct system in which household water is circulated directly through the solar collector, then stored in the hotwater storage cylinder and supplied to the house. The direct system only works well in climates where the water rarely freezes [199] and, as such, it is seldom employed in Ireland.

There are two main circulation methods: natural thermosyphon systems and pumped systems. A natural thermosyphon system uses the temperature difference generated from the collector to drive the water flow around the heat transfer circuit. The hotwater storage cylinder should always be located at least 0.5 m above the collector. The heated water naturally rises above the cooler water to create a thermosyphon pressure. This pressure drives the water up through the distribution pipes into the storage cylinder. Cold water is drawn into the bottom of the collector from the base of the storage cylinder by gravity. This system is simple and low-cost, but performs poorly in the Irish interim weather conditions. A pumped system uses an electrical pump operates by a controller to move the solar fluid between the collector and hotwater storage cylinder via a heat exchanger. The electrical pump operated when there is a sufficient difference between the inlet and outlet solar fluid temperature in the solar collector. No controller is required in the thermosyphon system as the circuit only operates when a positive

temperature gradient exists. However, a non-return valve is often required to ensure the heat is not transferred reversely from the hotwater storage cylinder to the collector. The pumped system can reduce heat loss through pipes effectively and also removes the heat from the collector at the optimum rate. However its operation cost is higher than that of a thermosyphon system as more electricity and maintenance is required. The pumped system is predominantly used in Ireland due to the temperate climate, but also works well in central and northern Europe.

The hotwater storage cylinder is a key component in the solar heating system and is used to store thermal energy in the form of hotwater [200]. The solar energy availability varies with time (day and night) and season. The solar water heating system should be prepared for operation whenever solar energy is available. The surplus heat is stored and ready for use when required. A duel coil or a multiple coil cylinder (a cylinder with two or more heat exchangers) is always used for domestic applications in Ireland. The solar fluid circuit should be connected to the heat exchanger located at the bottom of the hotwater storage cylinder and the electrical auxiliary immersion should be connected to the heat exchanger located at the top of the cylinder [35]. The hotwater storage cylinder should be optimally sized. This ensures that full use is made of the energy available in the collectors. An under-sized hotwater storage cylinder could lead to frequent overheating in the solar fluid circuit and hotwater storage cylinder. The controller, used to control the circulating pump, also monitors this excess temperature and may shut down the entire system for safety concerns. An over-sized hotwater storage cylinder could result in extensive use of the electrical auxiliary immersion which may increase both the capital and running costs of the cylinder. The average hotwater consumption rate per person is between 40 L and 50 L in Ireland. In general, the hotwater storage cylinder should be sized to accommodate between one and two days usage [37]. The

hotwater storage cylinder should always be well-insulated using either an insulation jacket or a semi-rigid foam coating. These insulation materials can help hotwater storage cylinders to retain heat in an effective manner. Precautions have to be taken in order to prevent the system from freeze damage. The system can be effectively protected using appropriate anti-freeze fluids and insulation. In some cases it may be necessary to drain fluid from the collector.

In recent years, solar thermal systems have seen significant advances in technological development, increases in production volumes and reductions in installed costs. For example, the use of surfaces with increased absorptive and lower emissivity can enhance the thermal performance of solar collectors [201]. Research and development has been conducted on the use of PV/T collectors instead of conventional solar thermal collectors [182]. Improved pump designs have been implemented to suit different flow systems. New hotwater storage cylinders with enhanced stratification mechanisms have also been developed and employed, thus reducing system heat loss.

5.5.2. The Generation of Hourly Solar Radiation on Solar Thermal Collectors

The hourly solar radiation data for a whole year is very rarely available at a lot of sites. In order to accomplish the most accurate analysis, artificial but statistically reasonable hourly solar radiation data can be generated using a combination of Degelman's, Graham's, Erb's and Redinll's algorithm [202]. These data are generated in a manner such that their associated statistics are approximately equal to the long term solar radiation data statistics at the specified location. The hourly solar radiation values on the tilted solar thermal collector can be calculated by performing sophisticated statistical calculations. These calculations are carried out in four steps and require 12 monthly-

average daily solar radiations for the location, i.e. one for each month, the latitude of the location where the solar thermal collector is installed, the shift angle in solar time, i.e. the angle difference between the standard meridian for the local time zone and the longitude of the location where the solar thermal collectors are installed, the solar azimuth angle, i.e. the angle between the local meridian and the projection of the line of sight of the sun on to horizontal plane, the slope of the solar thermal collector relative to the horizontal, and ground reflectance, i.e. the fraction of solar radiation incidence on the ground is reflected.

The input monthly-average daily solar radiation values are converted into a dimensionless form called the clearness index which is the ratio of the total solar radiation on a horizontal surface to the extraterrestrial solar radiation on a horizontal surface. The daily clearness index values for each month are calculated using Degelman's algorithm. The values of daily clearness index are obtained from a cumulative distribution function (with 1 corresponding to the smallest daily clearness index value and 31 to the largest value for a 31-day month) and then ordered in a predetermined sequence. The same sequence of the numbers 1 to 31 is always used for ordering the daily clearness index values. The starting position within the sequence however is determined randomly at the beginning of each generation process.

Once the daily clearness index values for each month are generated, the hourly clearness index for each day can be calculated using Graham's algorithm. The hourly clearness index values are transformed into a sequence of normally distributed values which are generated from a first-order autoregressive model. The parameter of this first-order autoregressive model is a function of the daily clearness index and the use of this first order autoregressive model introduces a variable whose probability structure changes

for each hour. The generated hourly clearness index values can also be converted back to the hourly solar radiation value.

The diffuse solar radiation on a horizontal surface for each hour is deterministically calculated using the hourly diffuse fraction correlation developed by Erbs. The ratio of the hourly diffuse solar radiation on a horizontal surface to the hourly global solar radiation on a horizontal surface can be determined based on the generated hourly clearness index value. The hourly beam solar radiation on a horizontal surface can be computed by subtracting the calculated hourly diffuse solar radiation from the hourly global solar radiation.

The beam, diffuse and ground-reflected solar radiation on a tilted surface can then be estimated based on the calculated hourly beam and diffuse solar radiation values and the slope provided for the solar thermal collector relative to the horizontal using Reindl's algorithm. A detailed description of the procedure employed to generate hourly solar radiation data for a solar thermal collector is given in Appendix C.

5.5.3. The Generation of Hourly Energy Output from a Solar Thermal System

The general first-order differential equation for the fluid temperature change with respect to time in a solar thermal collector is given in Equation 5.1 [203].

$$C * \frac{dT}{dt} = F' * \left[S - A * U_L * (T - T_a) \right] - \dot{m} * C_p * (T - T_{in}) \qquad (5.1)$$

where

$$S = (\tau\alpha)_n * IAM * A * I_T \qquad (5.2)$$

and where C is the capacitance of the solar thermal collector including the fluid, F' is the solar collector fin efficiency factor, A is the total aperture area of a solar collector array, U_L is the overall thermal loss coefficient of the solar collector per unit area, T is the temperature of the fluid in the collector at any point, T_a is the ambient air temperature, $\dot{m}$ is the mass flow rate of fluid through the solar collector, C_p is the specific heat of fluid in the solar collector, T_{in} is the inlet temperature of fluid to the solar collector, $(\tau\alpha)_n$ is the product of the cover transmittance and the absorber absorptance at the normal incidence, IAM (Incidence Angle Multiplier) is the ratio of the absorbed radiation at the current incidence angle to the absorbed radiation at normal incidence, and I_T is the total radiation on a tilted solar collector.

Equation 5.2 assumes that the heat loss to the ambient environment varies linearly with respect to the temperature difference between the fluid and the ambient air. However, a more accurate expression containing the quadratic loss coefficient, $U_{L/T}$, should be employed. The $U_{L/T}$ is multiplied by both the temperature difference between the fluid and the ambient temperature and the absolute temperature difference between the fluid and the ambient temperature. This quadratic equation is as follows [203]:

$$C*\frac{dT}{dt} = F^{'}*\left\{\begin{array}{c} S - A*U_L*(T-T_a) - \\ A*U_{L/T}*(T-T_a)*\left|(T-T_a)\right| \end{array}\right\} - \dot{m}*C_p*(T-T_{in}) \qquad (5.3)$$

The collector is discretised into several isothermal temperature nodes and the main differential equation for node i is expressed using Equation 5.4:

$$C_i*\frac{dT_i}{dt} = F^{'}*\left\{\begin{array}{c} S_i - A_i*U_L*(T_i-T_a) \\ -A_i*U_{L/T}*(T_i-T_a)*\left|(T_i-T_a)\right| \end{array}\right\} - \dot{m}*C_p*(T_i-T_{in,i}) \qquad (5.4)$$

where

$$C_i = \frac{C}{Number - of - Nodes} \tag{5.5}$$

$$A_i = \frac{A}{Number - of - Nodes} \tag{5.6}$$

$$S_i = \frac{S}{Number - of - Nodes} \tag{5.7}$$

$$T_{in,i} = T_{i-1} \tag{5.8}$$

In order to analytically solve this differential equation, the Equation 5.4 is placed into the form as Equation 5.9.

$$\frac{dT_i}{dt} = a * T_i^2 + b * T_i + c \tag{5.9}$$

For $T>T_a$	$a = \frac{-F' * A_i * U_{L/T}}{C_i}$ $b = \frac{-F' * A_i * U_L}{C_i} + \frac{2 * F' * A_i * U_{L/T} * T_a}{C_i} - \frac{\dot{m} * C_p}{C_i}$ $c = \frac{F' * S}{C_i} + \frac{F' * A_i * U_L * T_a}{C_i} - \frac{F' * A_i * U_{L/T} * T_a^2}{C_i} + \frac{\dot{m} * C_p * T_{in,i}}{C_i}$
For $T<T_a$	$a = \frac{F' * A_i * U_{L/T}}{C_i}$ $b = \frac{-F' * A_i * U_L}{C_i} - \frac{2 * F' * A_i * U_{L/T} * T_a}{C_i} - \frac{\dot{m} * C_p}{C_i}$ $c = \frac{F' * S}{C_i} + \frac{F' * A_i * U_L * T_a}{C_i} - \frac{F' * A_i * U_{L/T} * T_a^2}{C_i} + \frac{\dot{m} * C_p * T_{in,i}}{C_i}$

where T is the fluid temperature and is the dependent variable, t is the time, a and b are constants; c however can be either a function of time or a function of the dependent variable. If c is a constant with respect to time, then the differential equation can be readily solved. If c is not a constant and is a function of the previous node fluid temperature, then a reasonable assumption has to be made in which c is constant and is equal to its average value (c_{ave}) over the time step. If a is equal to zero in Equation 5.9, then the outlet temperature, $T_{o,i}$ and the average temperature, $T_{ave,i}$ can be calculated from Equation 5.10 and 5.11 respectively.

$$T_{o,i} = (T_{in,i} + \frac{c_{ave}}{b}) * e^{b\Delta t} - \frac{c_{ave}}{b} \tag{5.10}$$

$$T_{ave,i} = \frac{1}{b * \Delta t} * (T_{in,i} + \frac{c_{ave}}{b}) * (e^{b\Delta t} - 1) - \frac{c_{ave}}{b} \tag{5.11}$$

where Δt is the time step.

If a is not equal to zero in Equation 5.9, the outlet temperature and average temperature are calculated using formulae presented in Table 5.3 which depends on the value of the determinant q as follows:

$$q = 4 * a * c_{ave} - b^2 \tag{5.12}$$

For $q < 0$	For $q = 0$	For $q > 0$
$T_{o,i} = \dfrac{\dfrac{\sqrt{-q} * \tanh(-\sqrt{-q} * \frac{\Delta t}{2}) + 2*a*T_{in,i} + b}{1 + \tanh(-\sqrt{-q} * \frac{\Delta t}{2}) * \frac{2*a*T_{in,i} + b}{\sqrt{-q}}} - b}{2*a}$	$T_{o,i} = \dfrac{1}{\dfrac{1}{\frac{b}{2*a} + T_{in,i}} - a*\Delta t} - \dfrac{b}{2*a}$	$T_{o,i} = \dfrac{\dfrac{\sqrt{q} * \tanh(\sqrt{q} * \frac{\Delta t}{2}) + 2*a*T_{in,i} + b}{1 - \tanh(\sqrt{q} * \frac{\Delta t}{2}) * \frac{2*a*T_{in,i} + b}{\sqrt{q}}} - b}{2*a}$
$T_{ave,i} = \dfrac{\dfrac{-2*\ln\left[\begin{matrix}\sqrt{-q}*\cosh(\sqrt{-q}*\frac{\Delta t}{2}) - (2*a \\ *T_{in,i} + b)*\sinh(\sqrt{-q}*\frac{\Delta t}{2})\end{matrix}\right] - b*\Delta t}{2*a} + \dfrac{\ln\sqrt{-q}}{a}}{\Delta t}$	$T_{ave,i} = \dfrac{\dfrac{-\ln\left[\dfrac{1}{\frac{b}{2*a} + T_{in,i}} - a*T_{in,i}\right] - \frac{b*\Delta t}{2*a}}{2*a} + \dfrac{\ln\left[\dfrac{1}{\frac{b}{2*a} + T_{in,i}}\right]}{a}}{\Delta t}$	$T_{ave,i} = \dfrac{\dfrac{-2*\ln\left[\begin{matrix}\sqrt{q}*\cosh(\sqrt{q}*\frac{\Delta t}{2}) - (2*a \\ *T_{in,i} + b)*\sinh(\sqrt{q}*\frac{\Delta t}{2})\end{matrix}\right] - b*\Delta t}{2*a} + \dfrac{\ln\sqrt{q}}{a}}{\Delta t}$

Table 5.3. Formulae employed to calculate $T_{o,i}$ and $T_{ave,i}$ values [203].

In the case that multiple solar thermal collectors are connected in series, this process is repeated for each individual collector. The inlet temperature of the n^{th} solar collector is set equal to the outlet temperature of the $(n-1)^{st}$ solar collector. The solar thermal collector efficiency can be calculated using Equation 5.13 based on the collector thermal efficiency parameters provided under standard test conditions: $F_R*(\tau\alpha)_n$, F_R*U_L and $F_R*U_{L/T}$. F_R is the heat removal factor and F_{ave} represents F_R at the average temperature condition.

$$\eta = \frac{Q_u}{A*I_T} = \frac{\dot{m}*C_{p*}(T_{ave}-T_a)}{A*I_T}$$
$$= F_{ave}*(\tau\alpha)_n - F_{ave}*U_L*\frac{(T_{ave}-T_a)}{I_T} - F_{ave}*U_{L/T}*\frac{(T_{ave}-T_a)*|(T_{ave}-T_a)|}{I_T} \quad (5.13)$$

The collector thermal efficiency parameters $F_R*(\tau\alpha)_n$, F_R*U_L and $F_R*U_{L/T,}$ which are generally represented as a_0, a_1 and a_2, are referred to as the intercept efficiency, first-order efficiency (heat loss) coefficient and second-order efficiency (heat loss) coefficient respectively. The standard operating conditions for obtaining these parameters are [51]:

- The total solar radiation incidence on the tilted solar thermal collector is 900 W/m^2.
- The temperature difference between the average temperature of the solar thermal collector and the ambient temperature is 50^oC.

Since these parameters are provided, a methodology is required to convert $F_R*(\tau\alpha)_n$, F_R*U_L and $F_R*U_{L/T}$ into $F'*(\tau\alpha)_n$, $F'*U_L$ and $F'*U_{L/T}$ in order to use Equation 5.3. If the heat removal factor F_R is given and the solar thermal collectors have a linear efficiency curve ($U_{L/T}$=0), as shown in Figure 5.6, $(\tau\alpha)_n$ and U_L can be obtained by dividing $F_R*(\tau\alpha)_n$, F_R*U_L and $F_R*U_{L/T}$ by F_R.

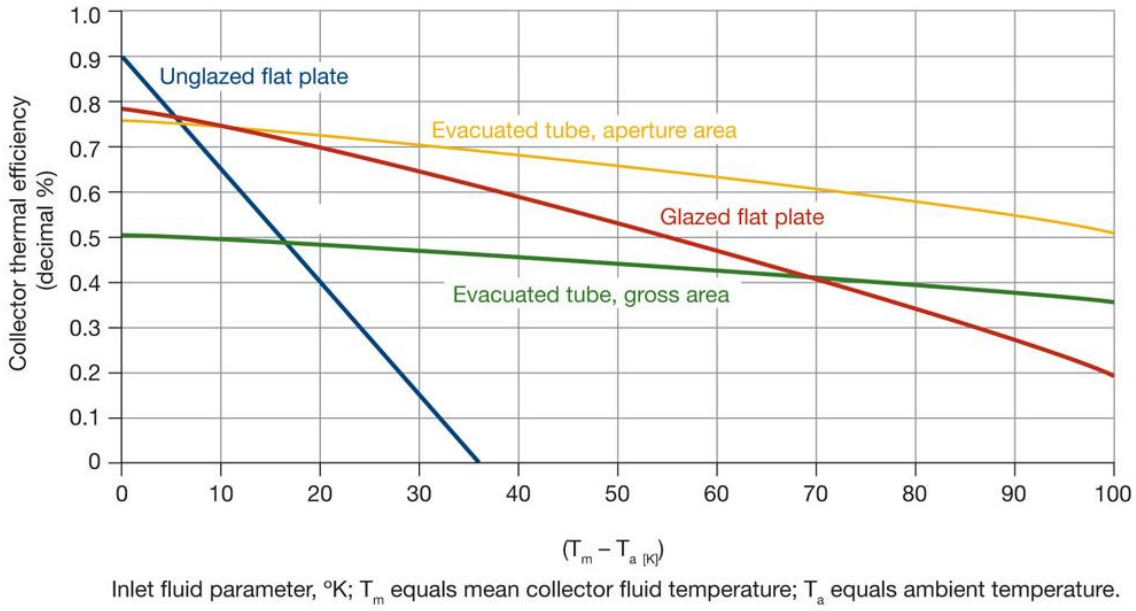

Figure 5.6. A typical efficiency curve of a solar thermal collector [204].

F' is the function of these variables ($(\tau\alpha)_n$ and U_L), and can be solved using Equation 5.14 . $F'*(\tau\alpha)_n$ and $F'*U_L$ can be obtained by multiplying $(\tau\alpha)_n$ and U_L by F'.

$$F' = -\frac{\dot{m}_{test} * C_{p,test}}{A * U_L} * LOG\left[1 - \frac{F_R * A * U_L}{\dot{m}_{test} * C_p}\right] \qquad (5.14)$$

where $\dot{m}_{test}$ is the mass flow rate of fluid under standard test conditions and $C_{p,test}$ is the specific heat of fluid under standard test conditions.

However, for collectors that have a nonlinear efficiency curve ($U_{L/T}$<>0), also shown in Figure 5.6, F's varies based on the variables ($(\tau\alpha)_n$, U_L and $U_{L/T}$) in the efficiency equation; also the heat removal factor F_R is not commonly provided. As a result, direct calculation of the variables $(\tau\alpha)_n$, U_L and $U_{L/T}$ is not possible. Nevertheless, due to the interrelated nature of the variables, the values of $F'*(\tau\alpha)_n$, $F'*U_L$ and $F'*U_{L/T}$ can be solved by arbitrarily choosing a value for F_R, dividing the efficiency parameters by F_R to obtain $(\tau\alpha)_n$, U_L and $U_{L/T}$, and then calculating F' as a function of these variables. The

resulting products of $F'*(\tau\alpha)_n$, $F'*U_L$ and $F'*U_{L/T}$ will be the same regardless of the value chosen for F_R. Equations for F' as a function of F_{ave} are given in Tables 5.4-5.8. θ is the angle of incidence.

For $S > 0,\ U_L > 0, U_{L/T} <> 0, T_{ave} > T_a$

$$F' = \frac{\ln\left[\left\{\frac{-2*\sqrt{q}}{\frac{4}{k}*\left(\frac{k*m}{2}+1-\sqrt{(\frac{-k*m}{2}-1)^2+k^2*U_{L/T}*(S-\frac{U_L*\theta}{2}-\frac{U_{L/T}*\theta^2}{4}+\frac{\theta}{k})}\right)-U_L+\sqrt{q}}+1\right\}*\left(\frac{2*U_{L/T}*\theta+U_L-\sqrt{q}}{2*U_{L/T}*\theta+U_L+\sqrt{q}}\right)\right]}{\frac{A*\sqrt{q}}{\dot{m}*C_p}}$$

where $k = \frac{A*F_{ave}}{(\dot{m}*C_p)}$, $q = 4*U_{L/T}*S+U_L{}^2$, $m = U_L + U_{L/T}*\theta$

Table 5.4. Equations employed to calculate F' as a function of F_{ave} [205].

For $S>0,\ U_L>0,\ U_{L/T}<>0,\ T_{ave}<T_a$	
$U_L{}^2>4*U_{L/T}*S$	$F'=\dfrac{\ln\left[\left\{\dfrac{-2*\sqrt{q}}{\frac{4}{k}*\left(\frac{k*m}{2}+1-\sqrt{(\frac{-k*m}{2}-1)^2-k^2*U_{L/T}*(S-\frac{U_L*\theta}{2}-\frac{U_{L/T}*\theta^2}{4}+\frac{\theta}{k})}\right)-U_L+\sqrt{q}}+1\right\}*\left(\dfrac{-2*U_{L/T}*\theta+U_L-\sqrt{q}}{-2*U_{L/T}*\theta+U_L+\sqrt{q}}\right)\right]}{\frac{A*\sqrt{q}}{\dot{m}*C_p}}$
where $k=\dfrac{A*F_{ave}}{(\dot{m}*C_p)},\ q=4*U_{L/T}*S+U_L{}^2,\ m=U_L+U_{L/T}*\theta$	
$U_L{}^2<4*U_{L/T}*S$	$F'=\dfrac{\tan^{-1}\left[\dfrac{\frac{4}{k}*\left(\frac{k*m}{2}+1-\sqrt{(\frac{-k*m}{2}-1)-k^2*U_{L/T}*(S-\frac{U_L*\theta}{2}-\frac{U_{L/T}*\theta^2}{4}+\frac{\theta}{k})}\right)-U_L}{\sqrt{4*U_{L/T}*S-U_L{}^2}}\right]-\tan^{-1}\left[\dfrac{2*U_{L/T}*\theta-U_L}{\sqrt{4*U_{L/T}*S-U_L{}^2}}\right]}{\frac{A*\sqrt{4*U_{L/T}*S-U_L{}^2}}{2*\dot{m}*C_p}}$
where $k=\dfrac{A*F_{ave}}{(\dot{m}*C_p)},\ q=4*U_{L/T}*S+U_L{}^2,\ m=U_L-U_{L/T}*\theta$	

Table 5.5. Equations employed to calculate F' as a function of F_{ave} [205].

For $S=0,\ U_L=0,\ U_{L/T}<>0,$	
$T_{ave} > T_a$	$$F' = \frac{\left[\frac{-2}{A*F_{ave}*U_{U/L}}*\left\{\frac{A*F_{ave}*U_{U/L}*\theta}{2*\dot{m}*C_p}+1-\sqrt{\left(\frac{A*F_{ave}*U_{U/L}*\theta}{2*\dot{m}*C_p}+1\right)^2+\frac{A*F_{ave}*U_{U/L}}{\dot{m}*C_p}*\left(\frac{-A*F_{ave}*U_{U/L}*\theta^2}{4*\dot{m}*C_p}+\theta\right)}\right\}\right]^{-1}-\frac{\dot{m}*C_p}{\theta}}{A*U_{L/T}}$$
$T_{ave} < T_a$	$$F' = \frac{\left[\frac{2}{A*F_{ave}*U_{U/L}}*\left\{\frac{-A*F_{ave}*U_{U/L}*\theta}{2*\dot{m}*C_p}+1-\sqrt{\left(\frac{A*F_{ave}*U_{U/L}*\theta}{2*\dot{m}*C_p}-1\right)^2-\frac{A*F_{ave}*U_{U/L}}{\dot{m}*C_p}*\left(\frac{A*F_{ave}*U_{U/L}*\theta^2}{4*\dot{m}*C_p}+\theta\right)}\right\}\right]^{-1}-\frac{\dot{m}*C_p}{\theta}}{-A*U_{L/T}}$$

Table 5.6. Equations employed to calculate F' as a function of F_{ave} [205].

For $S > 0,\ U_L = 0,\ U_{L/T} <> 0$

$T_{ave} > T_a$

$$F' = \frac{\ln\left[\left\{\left(\frac{\dot{m} * C_p * \left(\frac{k * U_{L/T} * \theta}{2} + 1 - \sqrt{\left(\frac{-k * U_{L/T} * \theta}{2} - 1\right)^2 + k^2 * U_{L/T} * \left(S - \frac{U_{L/T} * \theta^2}{4} + \frac{\theta}{k}\right)}\right)}{F_{ave} * A * \sqrt{U_{L/T} * S}} + \frac{1}{2}\right)^{-1} - 1\right\} * \left(\frac{S - \theta * \sqrt{U_{L/T} * S}}{S + \theta * \sqrt{U_{L/T} * S}}\right)\right]}{\frac{2 * A * \sqrt{U_{L/T} * S}}{\dot{m} * C_p}}$$

$T_{ave} < T_a$

$$F' = \frac{\tan^{-1}\left[\frac{\sqrt{U_{L/T} * S}}{S} * \frac{2}{k * U_{L/T}} * \left(\frac{k * U_{L/T} * \theta}{2} + 1 - \sqrt{\left(\frac{k * U_{L/T} * \theta}{2} - 1\right)^2 + k^2 * U_{L/T} * \left(S + \frac{U_{L/T} * \theta^2}{4} + \frac{\theta}{k}\right)}\right)\right] - \tan^{-1}\left(\theta * \frac{\sqrt{U_{L/T} * S}}{S}\right)}{\frac{A * \sqrt{U_{L/T} * S}}{\dot{m} * C_p}}$$

Table 5.7. Equations employed to calculate F' as a function of F_{ave} [205].

For $S = 0,\ U_L > 0,\ U_{L/T} <> 0$

$T_{ave} > T_a$

$$F' = \frac{\ln\left[\left\{\frac{\frac{k * U_{L/T} * U_L}{2}}{\frac{k*(U_L + U_{L/T}*\theta)}{2} + 1 - \sqrt{\left(\frac{-k*(U_L + U_{L/T}*\theta)}{2} - 1\right)^2 + k^2 * U_{L/T} * \left(-\frac{U_L*\theta}{2} - \frac{U_{L/T}*\theta^2}{4} + \frac{\theta}{k}\right)}} - U_{L/T}\right\} * \left(\frac{\theta}{-U_L - U_{L/T}*\theta}\right)\right]}{\frac{A * U_L}{\dot{m} * C_p}}$$

$T_{ave} < T_a$

$$F' = \frac{\ln\left[\left\{\frac{\frac{-k * U_{L/T} * U_L}{2}}{\frac{k*(U_L - U_{L/T}*\theta)}{2} + 1 - \sqrt{\left(\frac{-k*(U_L - U_{L/T}*\theta)}{2} - 1\right)^2 - k^2 * U_{L/T} * \left(-\frac{U_L*\theta}{2} - \frac{U_{L/T}*\theta^2}{4} + \frac{\theta}{k}\right)}} + U_{L/T}\right\} * \left(\frac{\theta}{-U_L + U_{L/T}*\theta}\right)\right]}{\frac{A * U_L}{\dot{m} * C_p}}$$

Table 5.8. Equations employed to calculate F' as a function of F_{ave} [205].

The solar thermal collector tests are generally performed on clear days at normal incidence so that the transmittance-absorption product is nearly the same as the normal incidence of beam radiation. However, it is important to determine the effects of angle of incidence of the incident radiation on solar thermal collectors. The intercept efficiency is corrected for non-normal solar radiation incidence by the incidence angle modifiers $(\tau\alpha)/(\tau\alpha)_n$. The IAM is calculated from Equation 5.15 [203]:

$$\mathrm{IAM} = \frac{(\tau\alpha)}{(\tau\alpha)_n} = \frac{I_{bt} * \frac{(\tau\alpha)_b}{(\tau\alpha)_n} + I_{dt} * \frac{(\tau\alpha)_d}{(\tau\alpha)_n} + I_{gr} * \frac{(\tau\alpha)_{gr}}{(\tau\alpha)_n}}{I_T} \tag{5.15}$$

For a flat plate solar thermal collector, the incidence angle modifier for beam radiation, $(\tau\alpha)_b/(\tau\alpha)_n$, can be approximated from Equation 5.16:

$$\frac{(\tau\alpha)_b}{(\tau\alpha)_n} = 1 - b_0 * \left(\frac{1}{\cos\theta} - 1\right) - b_1 * \left(\frac{1}{\cos\theta} - 1\right)^2 \tag{5.16}$$

where b_0 is the first-order incidence angle modifier coefficient and b_1 is the second-order incidence angle modifier coefficient. The incidence angle modifier for both sky diffuse, $(\tau\alpha)_d/(\tau\alpha)_n$, and ground-reflected diffuse, $(\tau\alpha)_{gr}/(\tau\alpha)_n$, are determined by integrating the ratio of the absorbed diffuse radiation to the incident diffuse radiation over the sky dome and ground dome respectively. The evaluation of the sky diffuse radiation modifier $(\tau\alpha)_d/(\tau\alpha)_n$ and the ground-reflected diffuse modifier $(\tau\alpha)_{gr}/(\tau\alpha)_n$ are presented as follows respectively [203]:

$$\frac{(\tau\alpha)_d}{(\tau\alpha)_n} = \frac{\int_{\frac{\pi}{2}-\beta}^{\frac{\pi}{2}} \int_{-\frac{\pi}{2}}^{\frac{\pi}{2}} \frac{(\tau\alpha)_b}{(\tau\alpha)_n} * \theta * \cos\theta * \sin\theta d\gamma_s d\theta + \int_{\frac{\pi}{2}-\beta}^{\frac{\pi}{2}} \int_{-\frac{\pi}{2}}^{\sin^{-1}(\frac{\cot\beta}{\tan\theta})} \frac{(\tau\alpha)_b}{(\tau\alpha)_n} * \theta * \cos\theta * \sin\theta d\gamma_s d\theta}{\int_0^{\frac{\pi}{2}} \int_{-\frac{\pi}{2}}^{\frac{\pi}{2}} \cos\theta * \sin\theta d\gamma_s d\theta + \int_{\frac{\pi}{2}-\beta}^{\frac{\pi}{2}} \int_{-\frac{\pi}{2}}^{\sin^{-1}(\frac{\cot\beta}{\tan\theta})} \cos\theta * \sin\theta d\gamma_s d\theta} \tag{5.17}$$

$$\frac{(\tau\alpha)_{gr}}{(\tau\alpha)_n} = \frac{\int_{\frac{\pi}{2}-\beta}^{\frac{\pi}{2}} \int_{\sin^{-1}(\frac{\cot\beta}{\tan\theta})}^{\frac{\pi}{2}} \frac{(\tau\alpha)_b}{(\tau\alpha)_n} * \theta * \cos\theta * \sin\theta d\gamma_s d\theta}{\int_{\frac{\pi}{2}-\beta}^{\frac{\pi}{2}} \int_{\sin^{-1}(\frac{\cot\beta}{\tan\theta})}^{\frac{\pi}{2}} \cos\theta * \sin\theta d\gamma_s d\theta} \quad (5.18)$$

The solar azimuth angle, γ_s, is the angular displacement from south of the projection of beam radiation on the horizontal plane and shown in Figure 5.7. The angle of incidence, θ, is the angle between the beam radiation on a surface and the normal to that surface and shown in Figure 5.8.

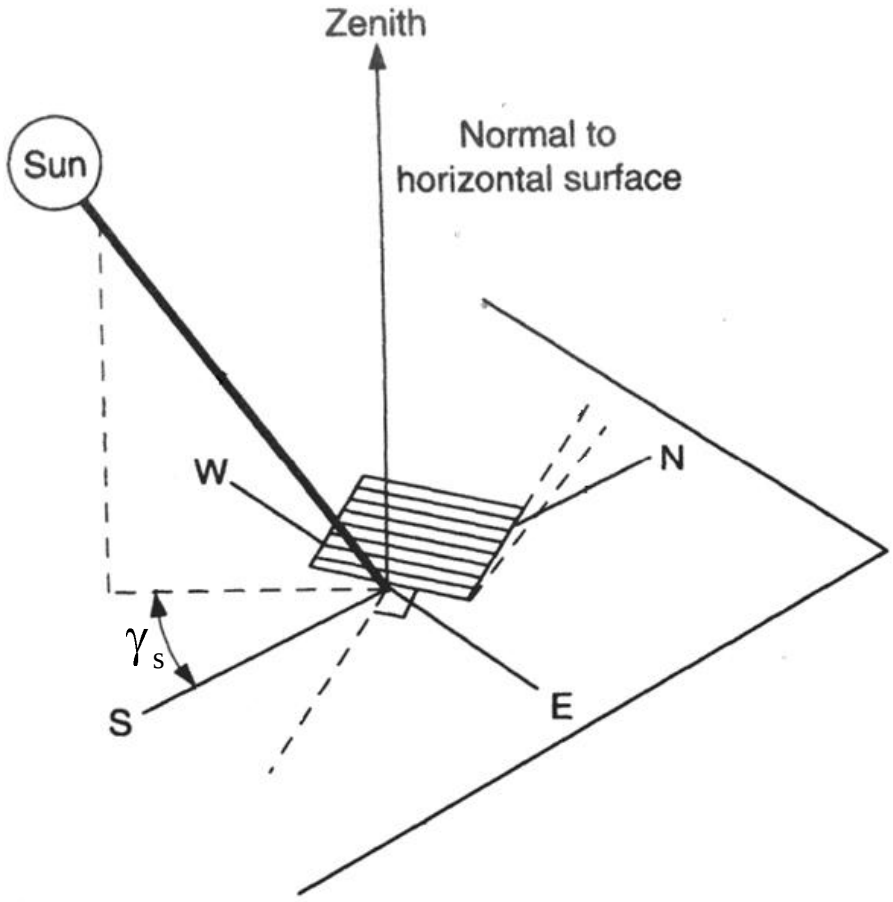

Figure 5.7. An illustration of solar azimuth angle for a tilted surface [206].

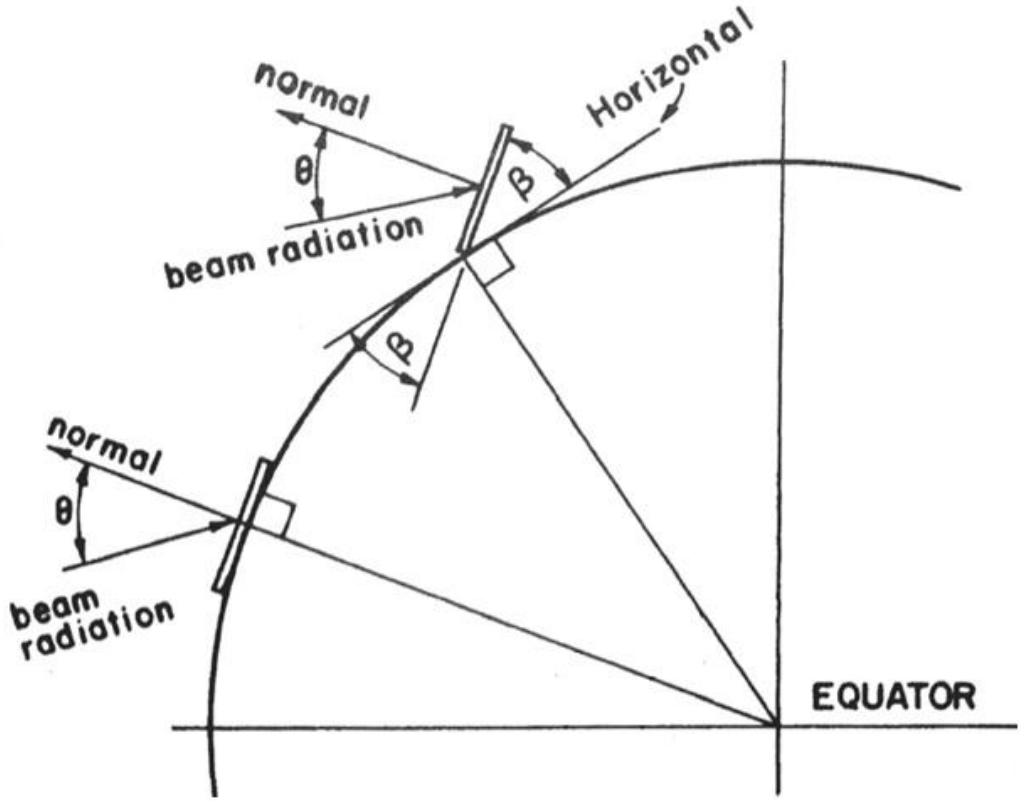

Figure 5.8. An illustration of angle of incidence (θ) and slope (β) for a south-facing surface [206].

For evacuated tube collectors, $(\tau\alpha)_b/(\tau\alpha)_n$ is the product of the longitudinal incidence angle value and the transversal incidence angle value [207]. The values of different longitudinal incidence angles are obtained in a plane that is perpendicular to the collector plane and contains the collector azimuth (transversal angle =0); the values of different transversal incidence angles are obtained in a plane that is perpendicular to both the collector aperture plane and the longitudinal plane (longitudinal angle = 0). The graphical representation of the longitudinal and transversal incidence directions are shown in Figure 5.9.

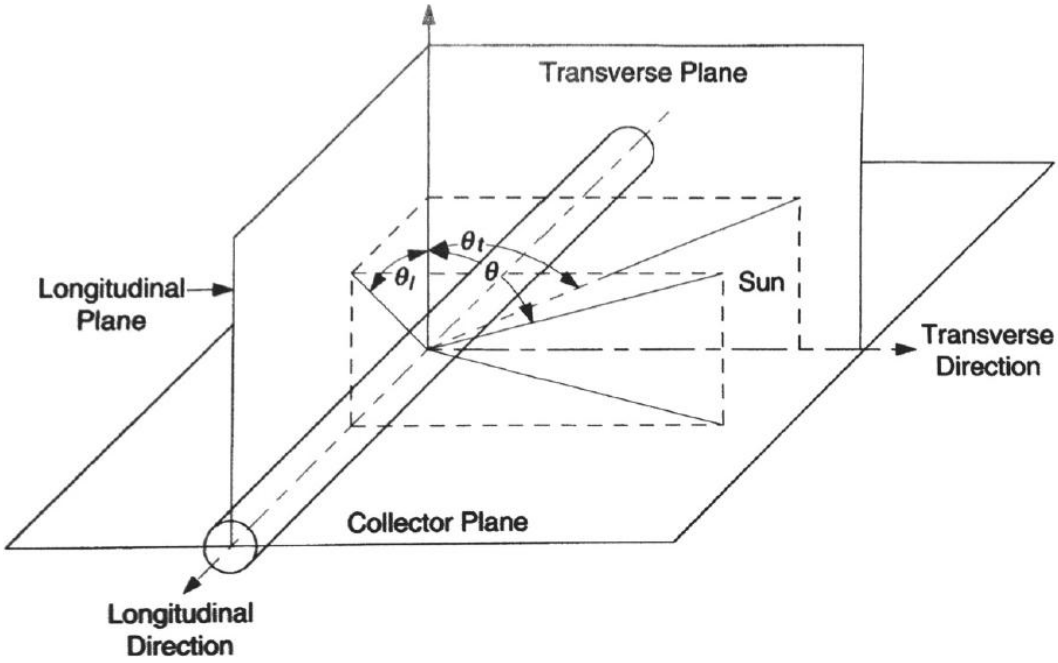

Figure 5.9. Graphical representation of the longitudinal (θ_l) and transversal (θ_t) incidence directions [206].

The $(\tau\alpha)_b/(\tau\alpha)_n$ of a solar thermal evacuated tube collector is characterised by its type; hence each collector has a unique $(\tau\alpha)_b/(\tau\alpha)_n$. The values of the longitudinal incidence angle and the transversal incidence angle are available from test report and are required for this calculation. If the incidence angle is not identical as the angles provided in the test data, an interpolation has to be performed in order to obtain the accurate $(\tau\alpha)_b/(\tau\alpha)_n$ value. The Table 5.9 shows the transversal and longitudinal angle values obtained for Kingspan HP400 and HP450 solar evacuated tube collectors under standard test conditions.

	0^o	10^o	20^o	30^o	40^o	50^o	60^o
θ_t	1	1.01	1.02	1.04	1.04	0.99	0.9
θ_l	1	1	0.99	0.97	0.95	0.91	0.83

Table 5.9. Transversal and longitudinal angle values obtained for Kingspan HP400 and HP450 solar evacuated tube collectors under standard test conditions [208].

5.5.3.1. Validation of the Procedure to Calculate the Energy Outputs of a Solar Thermal Flat Plate Collector System and a Solar Thermal Evacuated Tube Collector System

The simulation models set up to predict the energy output of solar thermal systems have to be validated in order to prove their accuracy. The validations are carried out by comparing the predicted energy outputs with the measured energy outputs for two installed solar thermal systems. The first system was assembled from two solar flat plate collectors having a total aperture area of 3.95 m^2 and the second system was assembled from one solar evacuated tube collector having a total aperture area of 3.021 m^2. These solar thermal systems, shown in Figure 5.10, were both built and installed at a site in Dublin and then monitored by DIT. The solar thermal collectors were positioned south facing and had a 53^o slope relative to the horizontal. An automated hot water dispensing unit was used to extract water from the hot water cylinder in order to mimic the real life operation in a domestic application [114]. A RESOL DeltaSol M solar controller was used to control the operation of the solar pump station for each of the solar thermal systems. Eight temperature sensors were employed to measure the water and the solar fluid temperatures. The volumetric flow rate of the solar fluid was measured using RESOL V40-06 impulse flow meters which react at 10 litres per pulse. RESOL DL2 data loggers were used to record data at one-minute intervals. The one-minute-interval

data was used to calculate the useful energy gain by the solar thermal collector. The calculated useful energy gain was aggregated by summing them over one-hour intervals and then employed in this validation study. The energy outputs were obtained for a 12-month period, between June 2009 and May 2010. The parameters used in simulation models were then set identical to the test conditions; the solar radiation and ambient temperature data used were for the period June 2009 to May 2010 in Dublin and were also obtained from *Met* Éireann. The specifications of the solar thermal collectors are shown in Table 5.10.

Figure 5.10. The solar thermal systems built and installed at a site in Dublin [63].

Parameter	Flat Plate Collector	Evacuated Tube Collector
Number in series	2	1
Collector aperture area (m^2)	3.95	3.021
Fluid specific heat ($kJkg^{-1}K$)	3.708	3.708
Tested flow rate ($kghr^{-1}m^{-2}$)	/	80
Intercept efficiency	0.776	0.778
First order efficiency coefficient ($kJhr^{-1}m^{-2}K^{-1}$)	14.22	3.276
Second order efficiency coefficient ($kJhr^{-1}m^{-2}K^{-2}$)	0.0594	0.036
Maximum flow rate ($kghr^{-1}$)	212	330
Collector slope (Degrees)	53	53

Table 5.10. Specifications of the solar thermal collectors [63].

The measured annual total energy outputs generated from the flat plate and evacuated tube solar collectors were 1,984 kWh and 2,056 kWh respectively [209]. The predicted annual total energy outputs were 1,824 kWh and 2,075 kWh for the flat plate and evacuated tube solar collectors respectively. The percentage difference between the measured and predicted annual energy outputs are 8.06% and 0.09% for the flat plate and evacuated tube solar collectors respectively. This shows a good agreement between the predicted energy outputs and the measured data on a yearly basis. The coefficient of determination is also employed to detect the coincidence between the measured and predicted hourly energy outputs of the solar flat plate collector system and the solar evacuated tube collector system for a whole year. A coefficient of determination value of 0.34 is obtained for the solar flat plate system. This means that 34% of the variance in the measured hourly energy outputs is predicted by the model; however 66% of the

variance is not explained by the model. Figure 5.11 shows a scatter diagram of predicted hourly energy outputs versus measured hourly energy outputs for the solar flat plate collector system. A coefficient of determination value of 0.4 is obtained for the solar evacuated tube system. This demonstrates that 40% of the variance in the measured hourly energy outputs is predicted by the model and 60% of the variance remains unexplained by the model. Figure 5.12 shows a scatter diagram of predicted hourly energy outputs versus measured hourly energy outputs for the solar evacuated tube collector system. There are a number of possible reasons why these coefficient of determination values are not higher:

- The monthly solar radiation data used for predicting the hourly solar radiation values was obtained from the national weather station (Dublin airport) closest to the location where the two solar thermal systems were installed. However, there is quite a distance (approximately 10 km) between these locations, and the monthly solar radiation applied in the model was not the same as the solar radiation received by the installed solar thermal collector systems [7].
- The temperature difference set to remove hotwater from the solar thermal collectors is not revealed for the installed solar thermal systems. As such, the temperature difference set in the solar thermal system models possibly differs from the value used in the experiment.

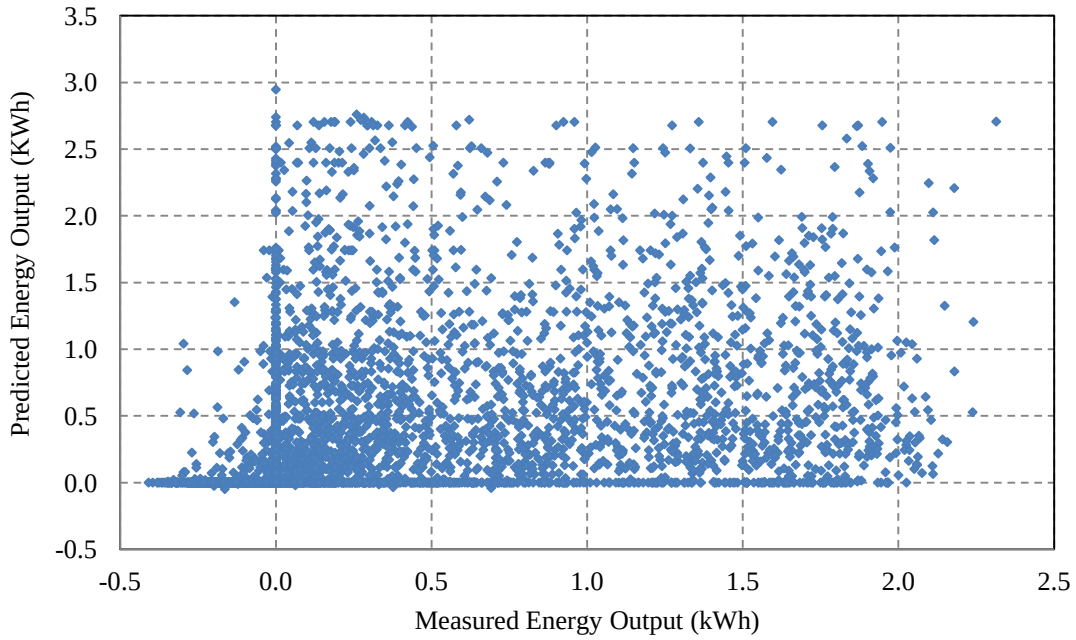

Figure 5.11. Scatter diagram of predicted hourly energy outputs versus measured hourly energy outputs for the solar flat plate collector system.

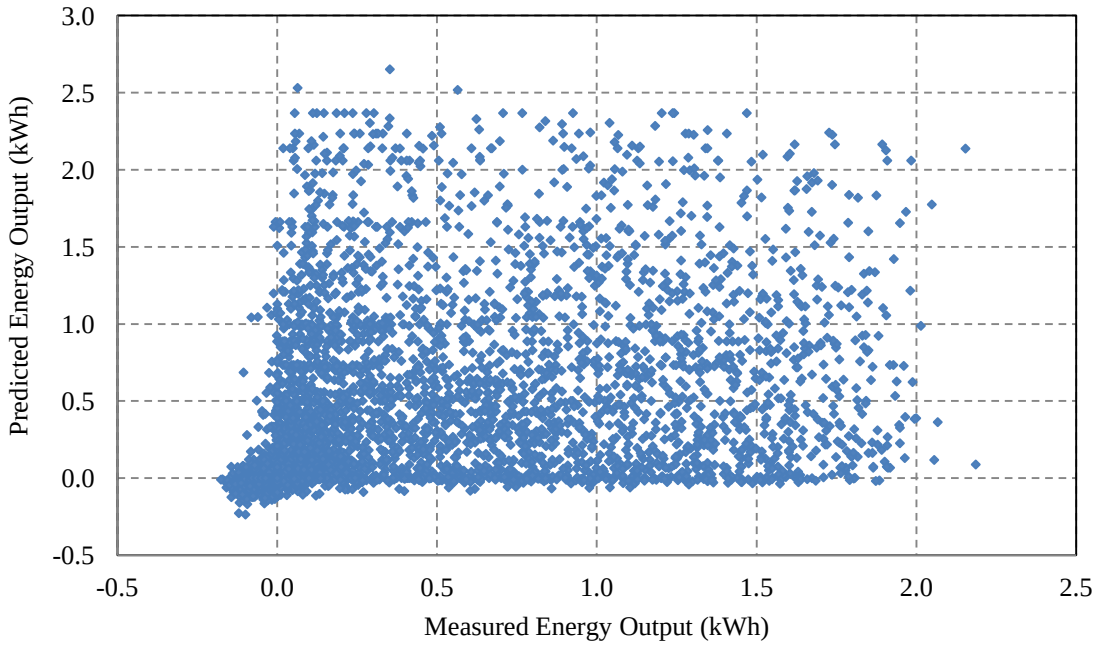

Figure 5.12. Scatter diagram of predicted hourly energy outputs versus measured hourly energy outputs for the solar evacuated tube collector system.

To the best of the author's knowledge, this is the first time an attempt has been made to validate the predicted hourly energy outputs of solar thermal system models for a complete year. There is no comparable value that can indicate the precision of the

obtained coefficient of determination value since no other validations have been carried out to this degree previously. In 55 international peer-reviewed journal articles reviewed by the author [63, 65, 133, 135, 136, 210-259] in which solar thermal systems were modelled, only 25 articles included a validation of their model [63, 65, 133, 135, 136, 210-229]. However, in these articles no attempt has been made to validate models by comparing the predicted energy output with the measured energy output on an hourly basis for a complete year. Nonetheless, based on the comparison of annual measured and predicted energy outputs, the procedure used to predict the energy output for solar thermal systems is considered appropriate for use in this study.

5.6. Domestic Air Source Heat Pump

5.6.1. Technology Review of an Air Source Heat Pump

Heat pumps, as shown in Figure 5.13, are a promising technology and use the same mechanical principles as refrigerators and air conditioners [260]. A refrigerator removes heat from an interior section and discharges it to the ambient environment, whereas heat pump extracts heat from the ambient environment and uses it to provide heating and hotwater for domestic dwellings. A heat pump can be also operated in reverse, whereby it extracts heat from the interior of a dwelling and releases it to the environment. The electric compressor built into a heat pump is used to move a refrigerant around in a closed refrigerant circuit. The refrigerant, known as the working fluid, absorbs the heat from the surroundings through the external heat exchanger and is vaporised. The evaporated refrigerant is transferred to and compressed in the compressor. The compressor pressurises the evaporated refrigerant which significantly raises its temperature. The high-temperature and pressurised evaporated refrigerant then passes through an internal heat exchanger where heat is transferred to the heating systems (e.g.

underfloor heating, radiators and hotwater cylinder) and such that the refrigerant condenses. The refrigerant then passes through an expansion valve where it is de-pressurised and returns to a low-pressure liquid/vapour mixture and the cycle is subsequently repeated.

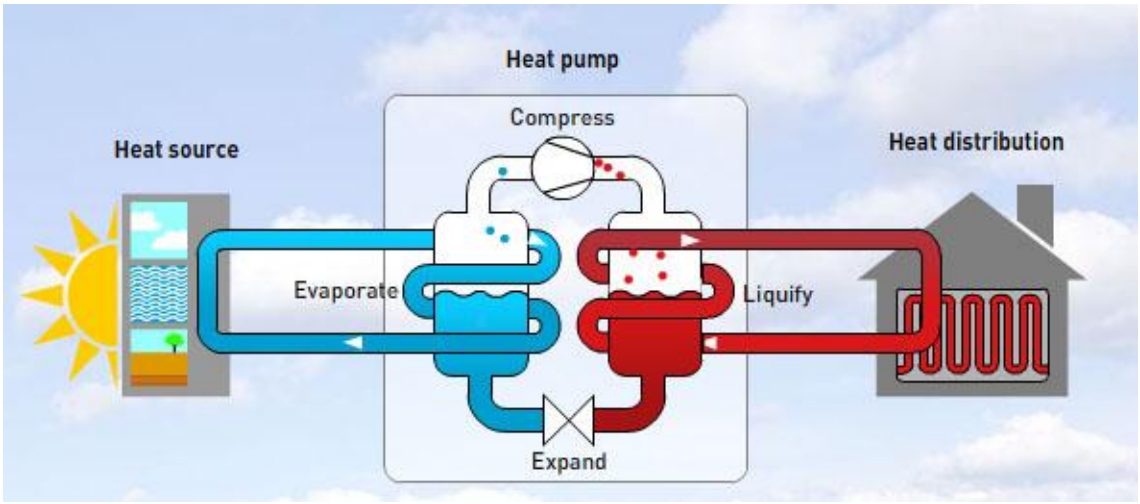

Figure 5.13. A schematic diagram of demonstrating how a heat pump functions [261].

A basic factor of great importance for the successful operation of a heat pump is the availability of an abundant and dependable heat source for the evaporator preferably one at a relatively high temperature. The COP of a heat pump system is the ratio of heat energy output to electrical power input, and generally lies between two and five depending on the heat pump type, the temperature of the heat source, the temperature requirement of the heating distribution system, the type of refrigerant and the specific components of the heat pump system. The COP will decrease when the difference in temperature between the heat source and the heating distribution system increases, as shown in Figure 5.14. This can occur in response to a drop in heat source temperature, an increase in the temperature required for the heating distribution system, or a combination of both.

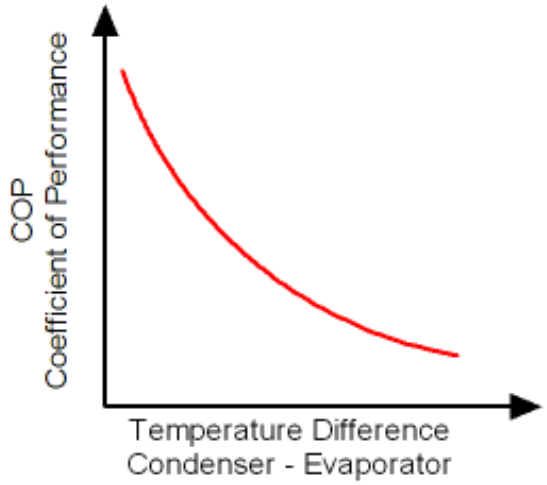

Figure 5.14. An illustration of COP of a heat pump varies with temperature difference [262].

A heat pump is the most suitable system for low-temperature heating distribution systems such as underfloor heating systems, which require temperatures of 30-45^{o}C [263]. This temperature requirement is the lowest compared with other domestic distribution systems such as low-temperature radiators and conventional radiators. The underfloor heating system is the most preferable as a higher COP is achieved when the heat pump produces low-temperature heat. In an underfloor heating system, the floor slab acts as a thermal storage facility which is very important for two reasons:

- It minimises the on/off frequency of the heat pump
- The area of heat release is very large and the required temperature of the water flowing through the pipes is significantly lower than that required by conventional radiator systems.

The highest reasonable temperature which the heat pump can supply is about 50-55^{o}C. This temperature is sufficient for low-temperature radiators (45-50^{o}C). Increased radiator surface areas are required to maintain the same heat output when this type of radiator is in use. However, low-temperature radiators are generally operated in

conjunction with a buffer tank to achieve an alternative design solution for a heat pump. A buffer tank is used to serve a similar purpose like the storage effect of underfloor heating and is incorporated into systems using radiators to provide the required thermal storage. However, a buffer tank is not always required if the heat pump can vary its heat output to match the heat requirement of the dwelling. Higher temperature heat from other sources must be obtained to reach the temperature requirement for the conventional radiators (60-90^{o}C).

Domestic hotwater can also be preheated by heat pump systems. The heat pump raises the incoming water from a water supply temperature to around 35-40^{o}C, and other sources are then used to heat the water to the desired storage temperature of 60^{o}C.

R22 (a single hydrochlorofluorocarbon (HCFC) compound) refrigerant has been widely adopted in heat pump systems for many decades due to its excellent safety, energy efficiency and operating characteristics [264]. However, R22 is considered to be harmful to the environment due to its ozone depleting potential and its manufacture by-product contributes significantly to global warming [265]. R22 is now a controlled substance by the Montreal Protocol and will be phased out by 2020 in developed countries and by 2030 in developing countries [266]. R410, a blend of hydrofluorocarbons (HFCs) was developed as a substitute to R22, is an environmentally friendlier refrigerant and does not contribute to ozone depletion. This refrigerant has been employed for newly-designed heat pump systems such as the Aeromax (Kingspan) and Ecodan (Mitsubishi) heat pumps. There are other substitutes to R22 used in heat pumps depending on the application and system design. These include R134, which is a low pressure refrigerant, and R407, which is a look-alike zeotropic mixture [264]. There are three main types of heat pumps utilised for domestic dwellings: GSHP, water source heat pump (WSHP) and ASHP.

5.6.1.1. Ground Source Heat Pump

The heat energy in the soil is used as a heat source for a GSHP. The soil generally provides a stable temperature throughout the year with minor fluctuations at depths of 1 m or more; at a distance of 2 m or 3 m below the ground, the soil temperature remains between 11^{o}C to 13^{o}C in Ireland [263]. The majority of the energy available in the soil at shallow depths is solar heat; however, the energy available at greater depths is generally referred to as geothermal energy. GSHP systems, as shown in Figure 5.15, are often characterised by the method used to enable access to the ground: open loop or closed loop. In an open loop system, ground water is extracted via a borehole. This water is used as a heat source for the heat pump, and then it is returned to the ground. Several boreholes can be linked to increase the capacity of the system. This is the most widely used and cost effective type of system where there is a good source of ground water available. However, ground water availability is limited, and both fouling and corrosion may also cause problems depending on water quality. Most importantly, environmental regulations are becoming increasingly restrictive on the use of ground water. In a closed loop system, a fluid, usually water or water with anti-freeze, is used to transfer heat. The fluid absorbs heat as it flows in a closed loop of high-density polyethylene pipe that is in contact with the ground. There are two main ways in which the closed loop is installed: vertical and horizontal loop configurations. A vertical loop system has the sealed loop of pipes inserted into pre-drilled boreholes. The pipes are buried at the depth between 15 m and 120 m into the earth [267]. Its main advantage over the horizontal loop system is that it is less affected by the fluctuation of temperatures in the soil or rock and it requires less pipes and pumping power. However it is more expensive. A horizontal loop system has the sealed loop of pipes buried in a horizontal trench about 1.5-3 m deep [268]. In general, the area of the buried pipes is

more or less equivalent to the floor area of the house. It is cheaper than the vertical loop type, but it requires a large land area. Temperature fluctuations within the soil can also have a large impact on the system's performance. The GSHP systems have a typical COP of around 3.5-4 [196].

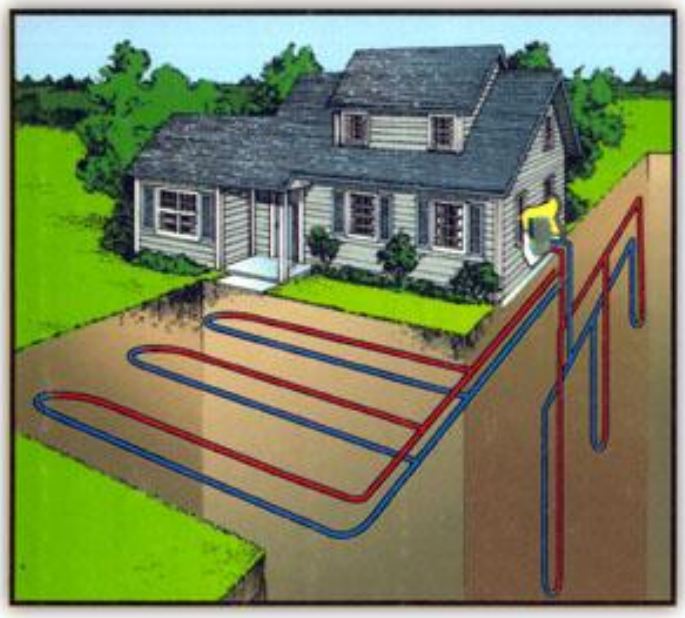

Figure 5.15. A schematic diagram of a GSHP system [269].

5.6.1.2. Water Source Heat Pump

The heat energy available in water is used as a heat source for a WSHP. A WSHP system, as shown in Figure 5.16, can be classified as either an open loop or a closed loop system. For an open loop system, water from a water source, usually a well, is passed directly through the heat pump. The heat is removed and then the water is discharged to the water source. For a closed loop system, a series of pipes are used to extract heat from a water source such as a local lake, river or stream. A mixture of anti-freeze and water in the closed pipe loop is then used to extract the heat. Water is considered as an ideal heat source for a heat pump, and the COP of WSHP systems can

reach values as high as 5. However, water must be present in sufficient quantity such that drinking water resources are not affected. The water quality, i.e. hardness, corrosivity etc, is an important consideration for an open loop system. The environmental issues associated with the discharge of the working fluid back into the water source have also caused concern.

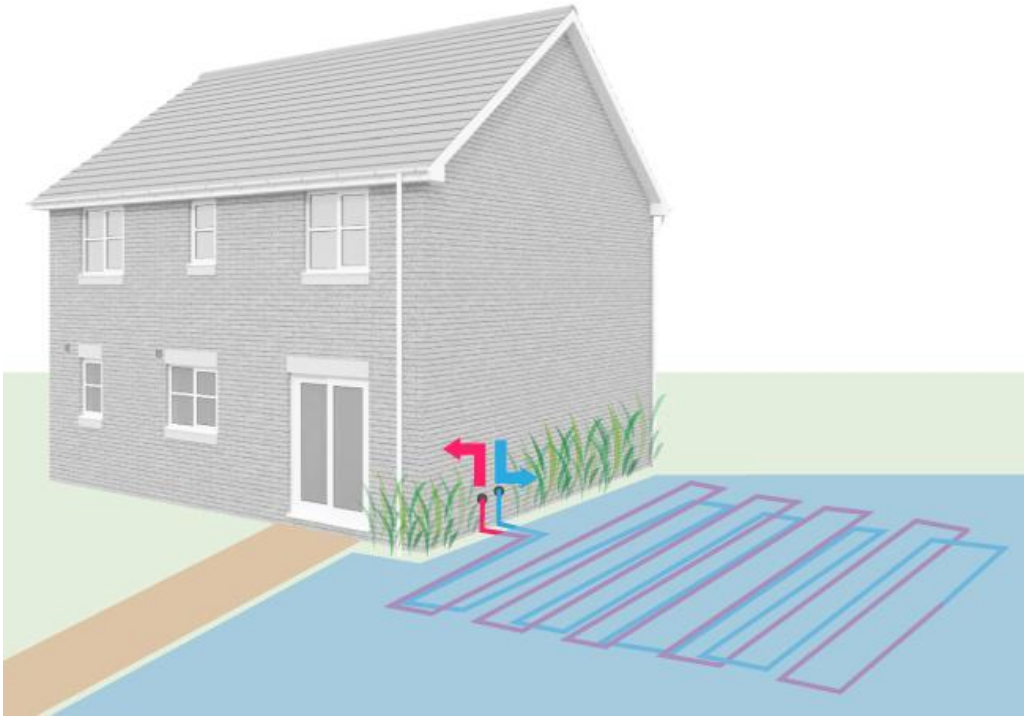

Figure 5.16. A schematic diagram of a WSHP system [270].

5.6.1.3. Air Source Heat Pump

The external air is used as a heat source for an ASHP. The most common type of ASHP used in a dwelling is an air-to-water heat pump as shown in Figure 5.17, where the water is referred to as the working fluid of the heat distribution system, e.g. underfloor heating, radiators etc. Another type of ASHP is an air-to-air heat pump which is mainly fitted to ventilation systems to provide hot air for a dwelling. The seasonally variation of air temperature is the key factor that decides the performance of an ASHP. The

maritime climate in Ireland, and the moderating influence of the sea in winter lead to relatively few days having an air temperature below 0^oC and as a consequence, ASHPs are very applicable for Irish dwellings [271]. A built-in electrical immersion heater is available in some ASHPs. The electrical immersion heater is used to make up the shortfall in temperature if the heat pump cannot satisfy the heating requirement in the dwelling. An ASHP is very unlikely to generate hotwater at a temperature of 60^oC which is recommended for storage. An electrical immersion heater is generally utilised to boost up the hotwater temperature as required. ASHPs have slightly lower COPs than GSHPs and WSHPs and, according to manufacturers' data, have a COP of between 1.5 and 5. However this slight reduction in COP can be reflected in costs since it is typically less expensive and easier to install than other types of heat pump. The utilisation of an ASHP is much less restricted than either a GSHP or a WSHP. The GSHP requires a large space for the collector which is rarely available in urban areas; the extra costs added for drilling can be very significant, and the access for drilling and excavating machinery can also be restricted. WSHPs require a water source at a nearby location which very seldom exists; there is a concern about using water from a well as the discharged water may affect the quality of drinking water. ASHPs are not only suitable for newly-built dwellings, but also for retrofit dwellings which make it extensively applicable. Therefore, the ASHP is investigated in this study.

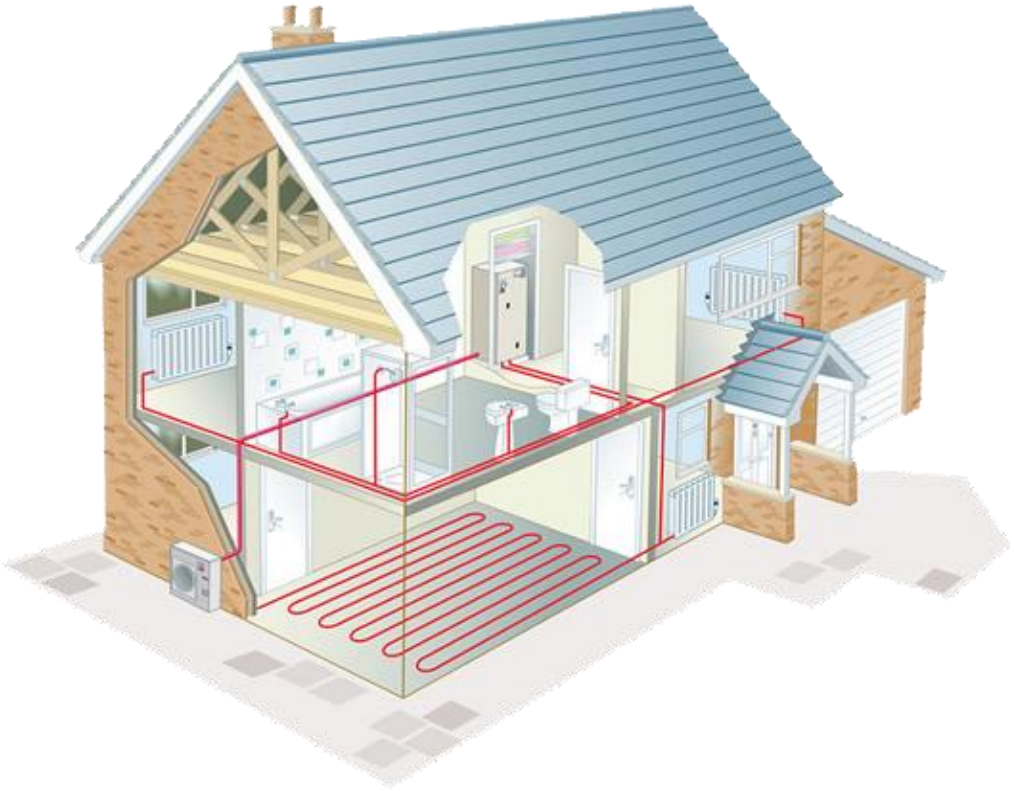

Figure 5.17. A schematic diagram of an ASHP system [272].

5.6.2. The Integration of an Air Source Heat Pump and a Solar Thermal System

There are a number of ways to integrate an ASHP and a solar thermal system to provide both heating and hotwater for a dwelling. The most conventional, and also the most commonly used method, is to directly connect the ASHP with the heating distribution system to provide the entire heating load. The ASHP is also connected to a heat exchanger in the hotwater storage cylinder to preheat the water. The solar thermal system is connected with another heat exchanger to heat water to the required temperature (60^{o}C). Electrical immersion heaters are also used when heating or hotwater requirements cannot be met. A schematic diagram of the integrated system is shown in Figure 5.18.

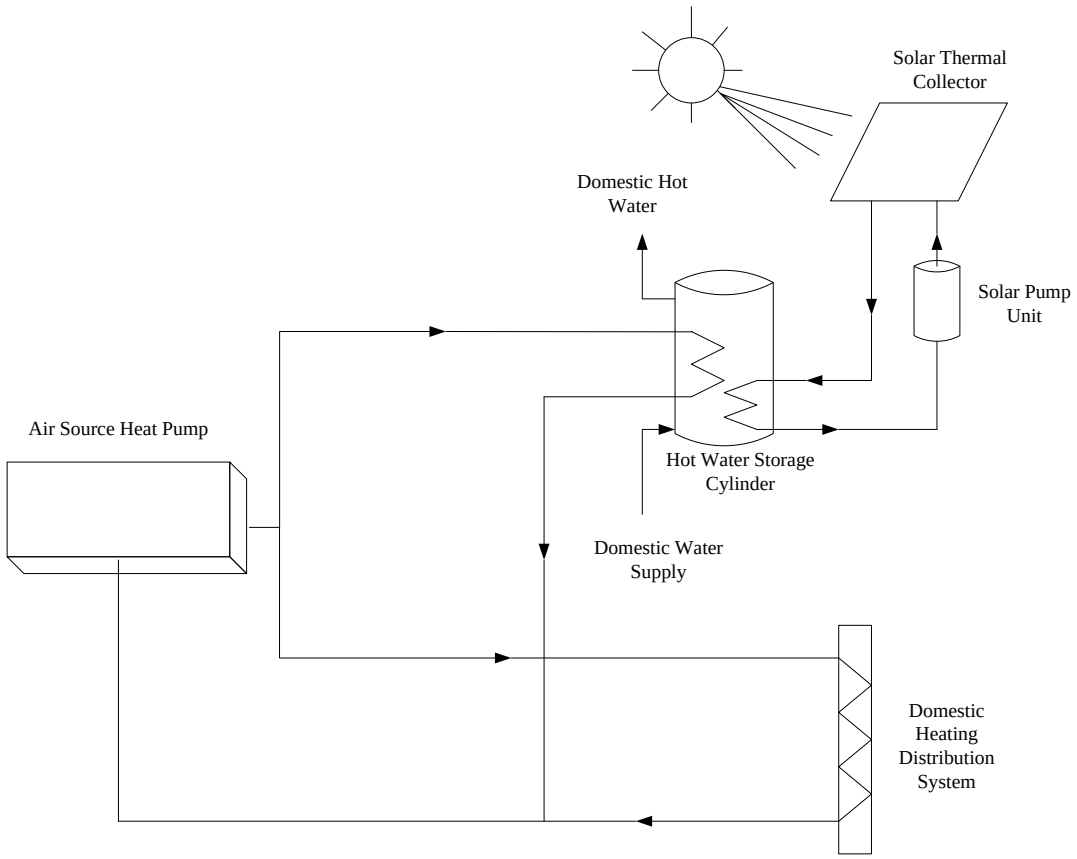

Figure 5.18. Domestic integrated micro-renewable thermal generation system for a dwelling.

The second way is to have the ASHP and the solar thermal system both connected with a buffer tank. The buffer tank is connected with the heating distribution system to provide heating for the dwelling. The hotwater is also drawn from the top of the buffer tank to satisfy the domestic hotwater requirement. A schematic diagram of this system is shown in Figure 5.19.

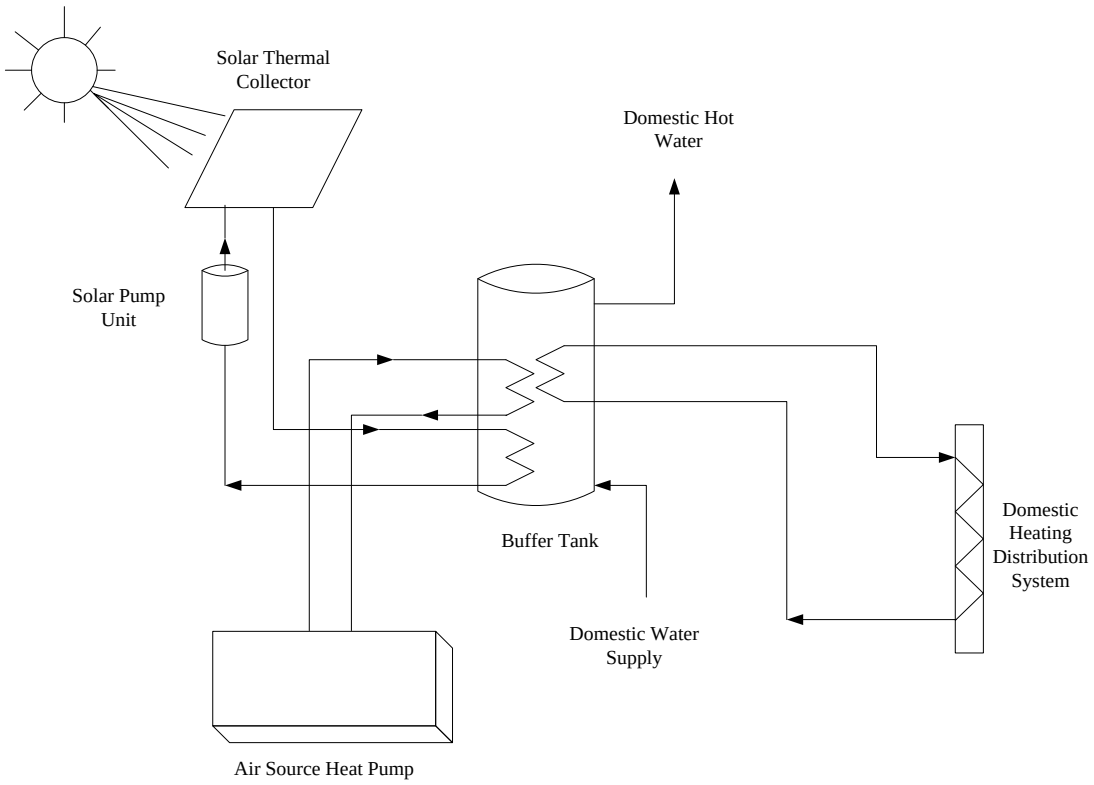

Figure 5.19. Domestic integrated micro-renewable thermal generation system with a buffer tank for a dwelling.

Many different and more complex combinations of an ASHP and a solar thermal system have been proposed by researchers in recent years and certain combinations have even been evaluated in experimental tests. As these more complex configurations have not yet been widely adopted however, they are not considered appropriate for system integration in this study. Nonetheless, these combinations are still worth mentioning as some may become popular in the future. Xu et al. presented a study on the operating performance of a solar-assisted ASHP for hot water heating, as shown in Figure 5.20 [273]. A specially designed flat plate collector/evaporator with spiral-finned tubes was used to absorb both energy from solar radiation and ambient air in both a simultaneous and independent manner. Depending on the weather conditions, the overall COP of the system can be improved if this solar-assisted ASHP is operated in different modes. When there is sufficient solar energy, such as sunny days in the summer, solar energy is

the dominant heat source for hotwater heating. When there is not sufficient solar energy, such as sunny days in winter, overcast or rainy days, both solar energy and ambient air are the heat source. Finally, when there is no solar energy, such as at night, ambient air is the only heat source.

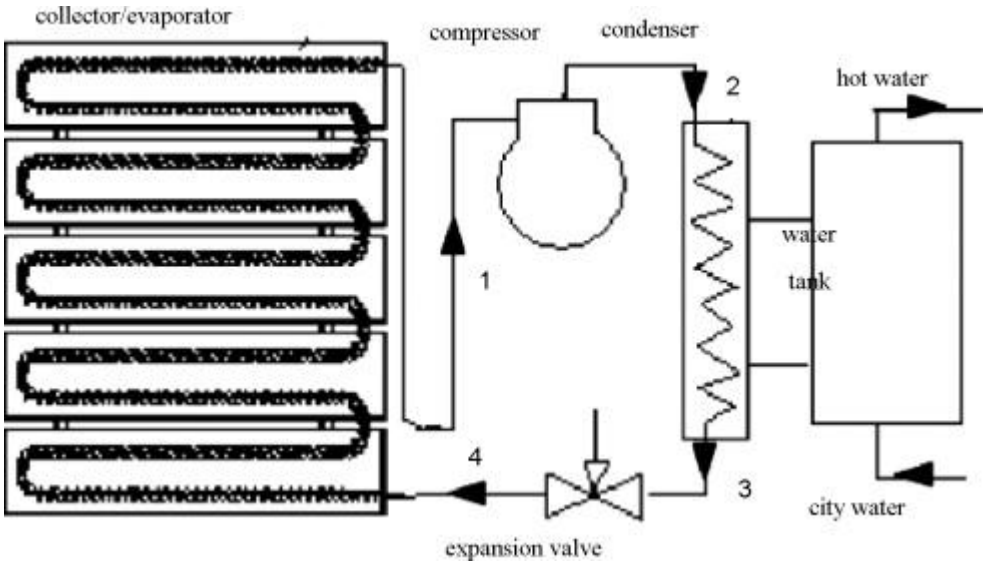

Figure 5.20. Schematic diagram of a solar-assisted ASHP [273].

A number of similar studies have also been carried out in order to investigate the possibility of improving the COP of an ASHP by incorporating a solar thermal collector as an evaporator. Analytical and experimental studies were performed by Kuang et al [274] using a solar-assisted ASHP with a 2 m^2 flat collector that acted as a heat source and also as an evaporator for the refrigerant. The long term thermal performance of the system was predicted and the monthly COP was found to vary between 4 and 6. Another study was conducted and an experimental set-up was introduced and analysed by Li et al [275] on solar-assisted ASHP. The experimental results showed that the seasonal average COP of system was 5.25, and could even reach 6.61 when the system was operating at the optimal condition. In another case, a solar heat pipe collector enhanced solar-assisted ASHP was studied by Huang et al [276]. This combined system, as shown in Figure 5.21, is operated in a heat pump mode similar to the

operation of a conventional electricity-driven heat pump system when solar radiation is low; however the combined system is operated in a heat pipe mode when solar radiation is high while the heat pump system is not operated and therefore no electricity is required. The system can thus achieve a high efficiency.

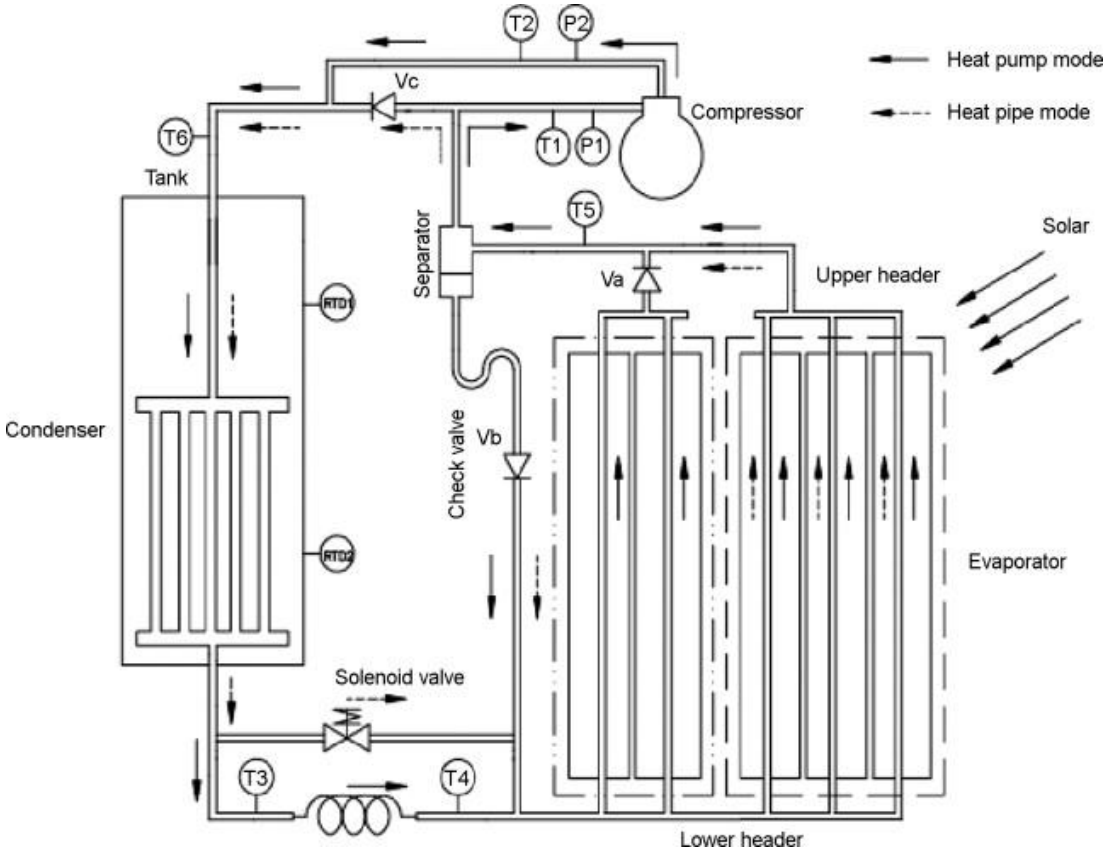

Figure 5.21. Schematic diagram of a solar-assisted ASHP [276].

5.6.3. The Generation of Hourly Ambient Air Temperature Values

The hourly ambient air temperature values are also very rarely available for a large number of locations. The hourly ambient air temperature values are generated using Degelman's algorithm and are based on the supplied 12 monthly-average daily ambient air temperature. The procedure adopted for the generation of the hourly ambient air temperature values is similar to the procedure used for generating the hourly solar radiation values. The daily-average ambient air temperature values and the daily-

maximum ambient air temperature values for each month are calculated from daily-average and daily-maximum cumulative distribution functions respectively. The monthly-average daily ambient temperature value and the standard deviation of the daily-average temperature about the monthly-average daily ambient air temperature, and the monthly-average daily-maximum ambient temperature value and the standard deviation of the daily-maximum temperature about the monthly-average daily-maximum temperature are used to establish the cumulative distribution functions. The calculated daily-average and daily-maximum ambient air temperature values are then ordered accordingly in a predetermined sequence. Two sequences are employed; one is utilised for the daily-average ambient air temperature whilst the other is utilised for the daily-maximum ambient air temperature. The daily-average ambient air temperature is considered to be both the mean value and the median value. Therefore the daily-minimum ambient air temperature can be determined from these daily-average temperatures and the daily-maximum ambient air temperatures. Sunrise and 3pm are taken as the time at which the minimum and maximum temperatures are observed, respectively. The hourly ambient air temperature values are calculated between the daily-maximum ambient air temperature values and daily-minimum ambient air temperature values using a cosine interpolation method. A detailed description of the procedure employed to generate the hourly ambient air temperature values is given in Appendix D.

5.6.4. The Generation of Hourly Energy Outputs from an Air Source Heat Pump

The investigated ASHP model is a single-stage heat pump and is intended for use in a domestic application. In the study, the hourly heating output generated from an ASHP is calculated based on the predicted hourly ambient air temperature, the supplied rated

ASHP capacity, the supplied fluid flow rate and an external heating performance file. This non-dimensional heating performance file contains catalogue data for the generic correction factors (capacity fraction and power fraction) for heating capacities and electrical powers. The hourly capacity and power of the ASHP can be calculated using Equation 5.19 and 5.20 respectively [277].

$$\text{Capacity} = \text{rated\_capacity} * \text{capacity\_fraction} \tag{5.19}$$

$$\text{Power} = \text{rated\_power} * \text{power\_fraction} \tag{5.20}$$

The correction factors for capacities and powers correspond to the ambient air temperature and the fluid temperature entering the ASHP. Table 5.11 and Table 5.12 show the generic correction factors for capacities and powers for an ASHP and these data are used for this study. A linear interpolation is accomplished between the heating performance data to calculate the capacity fraction and power fraction for a particular hour if the entering hourly ambient air temperature and the entering fluid temperature do not equal to the exact values reported in the data. However, the data cannot be extrapolated beyond the given range. If the entering conditions of the ASHP are below the range, the model will get the capacity fraction and power fraction of the closest point, i.e. the bottom of the range. The case is similar for the top of the range; the interpolation routine will find the closest available point. The ASHP hourly heating output temperature and COP are calculated from Equation 5.21 and 5.22 respectively [277]:

$$T_{out} = T_{in} + \frac{\text{Capacity}}{\dot{m} * C_p} \tag{5.21}$$

$$\text{COP} = \frac{\text{Capacity}}{\text{Power}} \tag{5.22}$$

Inlet Water Temperature (^{o}C) / Inlet Air Temperature (^{o}C)	25	30	35	40	45	50
2.2	0.759	0.737	0.714	0.692	0.67	0.648
7.2	1.08	1.048	1.017	0.986	0.955	0.923
12.2	1.137	1.106	1.075	1.043	1.012	0.981
15	1.233	1.199	1.165	1.131	1.097	1.062
20	1.403	1.359	1.314	1.269	1.224	1.18

Table 5.11. Correction factors for capacities for corresponding ambient inlet air temperature and inlet water temperature [278].

Inlet Water Temperature (^{o}C) / Inlet Air Temperature (^{o}C)	25	30	35	40	45	50
2.2	0.787	0.86	0.944	1.027	1.132	1.249
7.2	0.868	0.938	1.044	1.136	1.255	1.385
12.2	0.843	0.923	1.016	1.108	1.224	1.352
15	0.843	0.924	1.017	1.109	1.226	1.355
20	0.844	0.924	1.018	1.112	1.229	1.359

Table 5.12. Correction factors for powers for corresponding inlet ambient air temperature and inlet water temperature [278].

5.6.4.1. Validation of the Procedure to Calculate the Energy Output of a Domestic Air Source Heat Pump

The TRNSYS simulation model used to predict the energy output from an ASHP system must be validated in order to prove its accuracy. The validation is carried out by comparing the measured energy output with the predicted energy output for a Mitsubishi Ecodan 8.5 kW ASHP. This ASHP system was installed in a three-bedroom semi-detached house with four occupants in Hertfordshire, UK, and monitored by Mitsubishi Electric. A 180 L hotwater storage cylinder was connected, but was not used; hence the energy output from this hotwater storage cylinder was not measured and was neglected in the validation. An intelligent operating system was incorporated with a series of sensors to monitor the temperature inside and outside the house. These sensors constantly communicated with each other, and the output from the air source heat pump was then adjusted to respond to changes in the weather. The one-minute-interval data, i.e. inlet water temperatures, outlet water temperatures and mass flow rates, was recorded and used to calculate the energy output from the installed ASHP. The calculated energy output at one-minute-interval was aggregated by summing them over one-hour intervals and then employed in this validation study. The energy output was obtained for a 12-month period, between January 2011 and December 2011 [279]. The parameters used in the simulation model are set the same as the measured conditions. The ambient air temperature data used are for the period January 2011 to December 2011 in Hertfordshire, UK. This meteorological data was obtained from the Royston weather station in the UK [280]. The ASHP specification is shown in Table 5.13.

Parameter	Value
Heating capacity (kW)	8.50
Power input (kW)	2.88
Nominal water mass flow rate	1548
Fan air flow (m^3s^{-1})	0.916
Fan power (kW)	0.06

Table 5.13. The Mitsubishi Ecodan 8.5 kW air source heat pump specification.

The thermal load enforced for this simulation model was the same as the total thermal load delivered from the ASHP for the year. Low-temperature radiators are used in this house; the typical temperature required for these radiators is 45^{o}C. The TRNSYS simulation model is designed to supply circulating fluid temperature at 45^{o}C. The measured annual total energy output generated from the Mitsubishi Ecodan 8.5 kW ASHP was 15,466 kWh. The predicted annual total energy output was 15,696 kWh. The percentage difference between the measured and predicted energy output is 1.48% on a yearly basis. The coefficient of determination is utilised to determine the correlation between the measured and the predicted hourly energy outputs for a year. A coefficient of determination value of 0.88 is obtained and this means that 88% of the variance in the measured values is predicted by the model; however 12% of the variance is not explained by the model. A scatter diagram of predicted hourly energy outputs versus measured hourly energy outputs for the air source heat pump system is shown in Figure 5.22. This coefficient of determination value is considerably higher than the values obtained for the solar-type technologies. This can possibly be explained by the fact that the monthly ambient air temperatures applied in the ASHP model are approximately the same as the ambient air temperatures experienced by the installed ASHP system. The temperature variation between two sites located within a relatively short distance is small; the variation of solar radiation, however, can be significant. Nonetheless, there is

no comparable value available to show the accuracy of the obtained coefficient of determination value since no other validations have been carried out to this degree previously. In 45 international peer-reviewed journal articles reviewed by the author [60, 273, 281-323] in which ASHPs were modelled, only 15 articles included a validation of their model [60, 281-294]. However, in these articles no attempt has been made to validate models by comparing the predicted energy output with the measured energy output on an hourly basis for a complete year. Nonetheless, based on the very good agreement between the measured data and the predicted data on an annual basis, the simulation model is considered appropriate for this study.

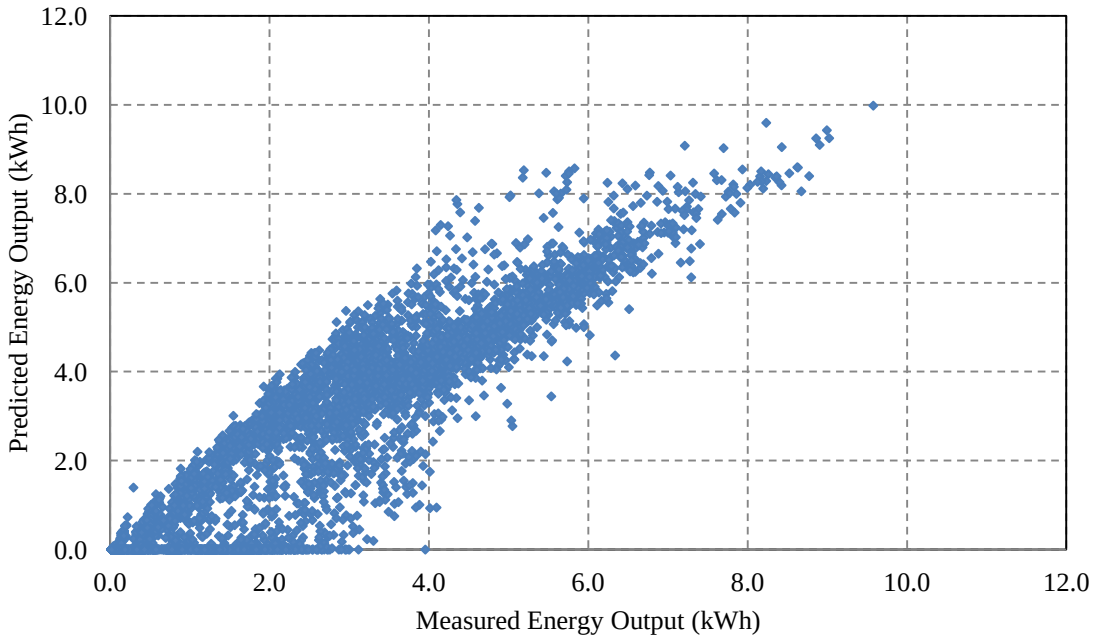

Figure 5.22. Scatter diagram of predicted hourly energy outputs versus measured hourly energy outputs for the air source heat pump system.

5.7. Life Cycle Cost Analysis

LCC offers a means of obtaining the true cost of an individual component, system, or an entire project by taking into account capital, energy, maintenance and other operational costs over the life of the facility [324]. The LCC always requires that all costs and

savings are evaluated over a long period of time and discounted to present value before they can be meaningfully compared. This presents an accurate comparison for a component, a system or a project, as all major costs associated with its parts as well as the capital cost and the installation cost are considered. From a decision-making point of view, the LCC of a project with its alternatives can only be meaningfully compared when they are all fulfilling the same basic performance requirements [325]. The cost effectiveness is the basic criterion for determining a component, a system or a project has an economic advantage over other components, systems or projects respectively. For an example, a system has an increased capital cost and a decreased operational cost which results in greater savings than additional capital costs, thus this system is deemed to be more cost effective. If several systems are being considered, the most cost effective system is the one with the lowest LCC. In this study, LCC is the parameter employed to perform a cost/benefit comparison and to identify the optimal system in the micro-renewable thermal generation system and the overall integration system [326]. LCC is calculated as follows:

$$LCC = C + \sum_{t=1}^{T} \frac{CF}{(1+i)^t} + \sum \frac{R}{(1+i)^{T_R}} - \frac{SAL}{(1+i)^T} - CG \qquad (5.23)$$

where

- C is the entire capital cost of the micro-renewable thermal generation system consisting of an ASHP and/or a solar thermal system in this chapter. However C represents the entire capital cost of the micro-renewable energy generation system in Chapter 6.
- T is the project lifespan.
- T_R is the time of replacement occurring.

- R is the replacement cost of components such as a solar pump unit and a domestic circulation pump, also includes the replacement of any micro-renewable thermal (current chapter) or energy (Chapter 6) generation device if the project lifespan is greater than the lifespan of the device itself.
- SAL is the salvage value.
- CG is the capital grant available for any of the system.
- i is the real interest rate.

5.8. Integration of Micro-Renewable Thermal Generation Systems

5.8.1. The Integration Technique

The ASHP and solar thermal system optimised integration sub-technique, a flowchart for which is shown in Figure 5.23, obtains the optimal configuration of a micro-renewable thermal generation system consisting of an ASHP and/or a solar thermal system (formed from either flat plate or evacuated tube solar thermal collector(s)). The integration technique is implemented in TRNSYS. The integration begins with the selection of a number of ASHPs, a flat plate solar thermal collector and two evacuated tube solar thermal collectors for analysis. The orientation of the solar thermal collectors is then set, i.e. facing south. The optimal slope of the flat plate solar thermal collector is determined based on the maximum annual total energy (hotwater generated equivalent) predicted from a solar thermal system assembled from solar flat plate collectors in TRNSYS. Subsequently all flat plate solar thermal collectors are set at this optimal slope respectively. The same procedure can be applied to determine the optimal slope for evacuated tube solar thermal collectors; hence all of these collectors are also set at this corresponding optimal slope. A detailed description of the procedure employed to calculate the optimal slope is presented in the following section. All possible systems,

both mono and hybrid (based on the number of renewable energy technologies used), that can be formed from the selected ASHPs and the solar thermal systems are analysed. A primary electrical heating system is employed to provide heating and preheat hotwater if an ASHP is not included in a formed mono or hybrid system. An electric boiler with a thermal capacity of 9 kW is employed for the primary electrical heating system in this study. An auxiliary electrical heater is a common electric element, similar to an immersion heater, which switches on to boost the output of a heating generation system. An auxiliary electrical heater with a thermal capacity of 3 kW is employed in this study. This auxiliary electrical heater is designed to turn on if the temperature of heating output from the ASHP or the primary heating system is less than or equal to 25^{o}C; and turn off when the temperature of heating output is greater than or equal to 35^{o}C. An electrical immersion is programmed to turn on between 5am-8am and 6pm-9pm daily (the peak hotwater usage periods). However, the immersion heater will be turned off if the temperature of water at the tank top exceeds 60^{o}C. The ASHP or the primary electrical heating system is not only used to provide heating for the dwelling but also to preheat water in the hotwater storage cylinder. Due to this interaction effect, six system combinations can be formed individually in this study:

- a combination of an ASHP and a solar thermal system assembled from a number of flat plate solar thermal collectors and is shown in Figure 5.24.
- a combination of an ASHP and a solar thermal system assembled from a number of evacuated tube collectors and is shown in Figure 5.25.
- a combination of an ASHP and an electrical immersion for hotwater heating and is shown in Figure 5.26.
- a combination of a primary electrical heating system and a solar thermal system assembled from a number of flat plate collectors and is shown in Figure 5.27.

- a combination of a primary electrical heating system and a solar thermal system assembled from a number of evacuated tube collectors is shown in Figure 5.28.
- a combination of a primary electrical heating system and an electrical immersion for hotwater heating is shown in Figure 5.29.

The hourly electricity consumption of operating an ASHP or a primary electrical heating system, running a solar pump unit and a domestic circulating pump, driving the auxiliary electrical heater, and functioning an electrical immersion in the hotwater storage cylinder for a year is collected and summed. The LCC is calculated based on the capital costs of the system, the cost of the imported electricity, the costs of replacing the circulating pump and/or solar pump unit, maintenance costs and the salvage value. The salvage value is the value left in a device (exclusive of installation costs) if the lifespan of a device is longer than the desired project lifespan. In this integration technique, the major assumption is made that the entire capital cost of the micro-renewable thermal generation system is funded from a loan. Capital grant options are also built into this integration technique. Once all possible system configurations have been analysed, the system having the lowest LCC is deemed optimal and the optimal system configuration is thus identified.

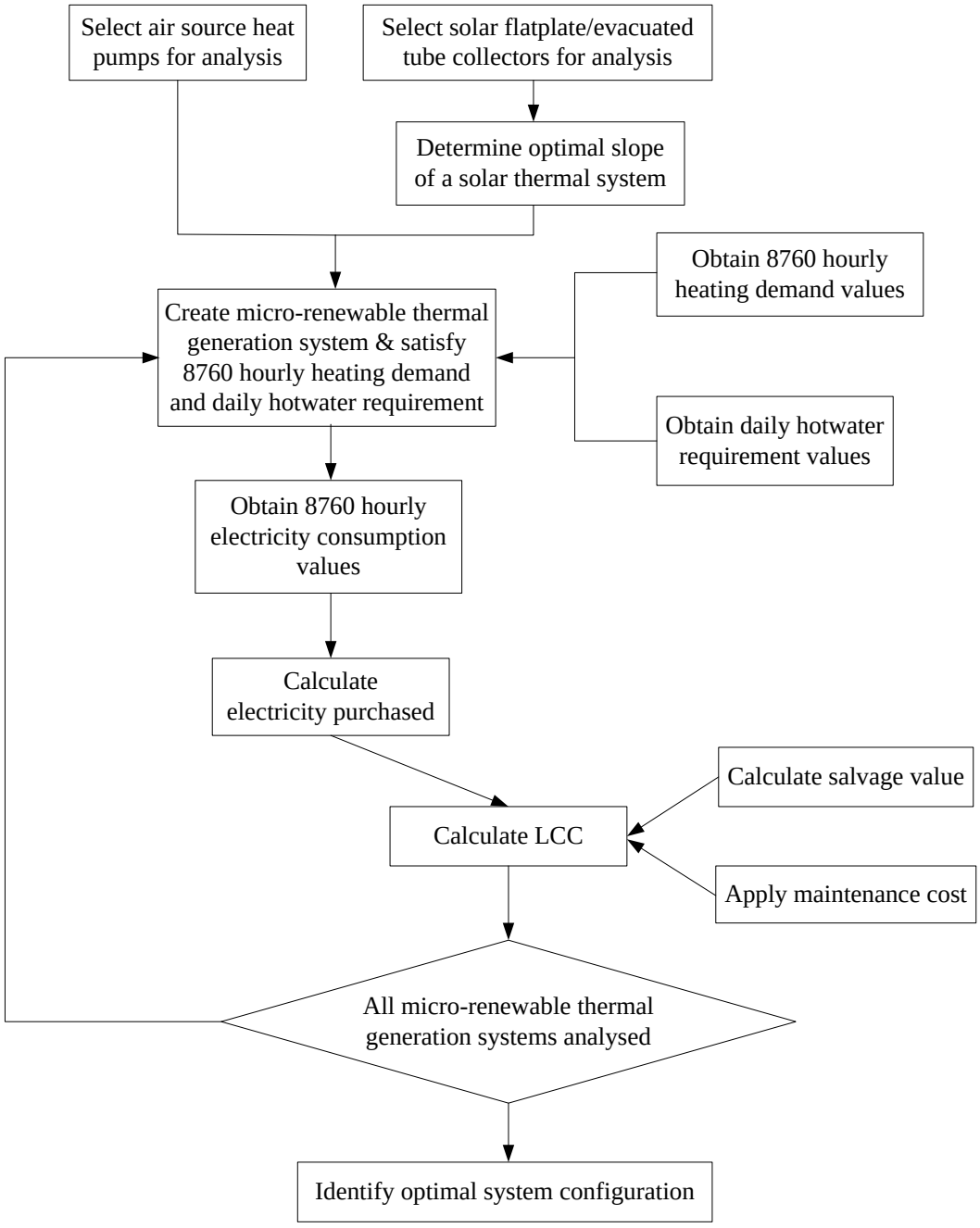

Figure 5.23. An air source heat pump and a solar thermal system integration technique.

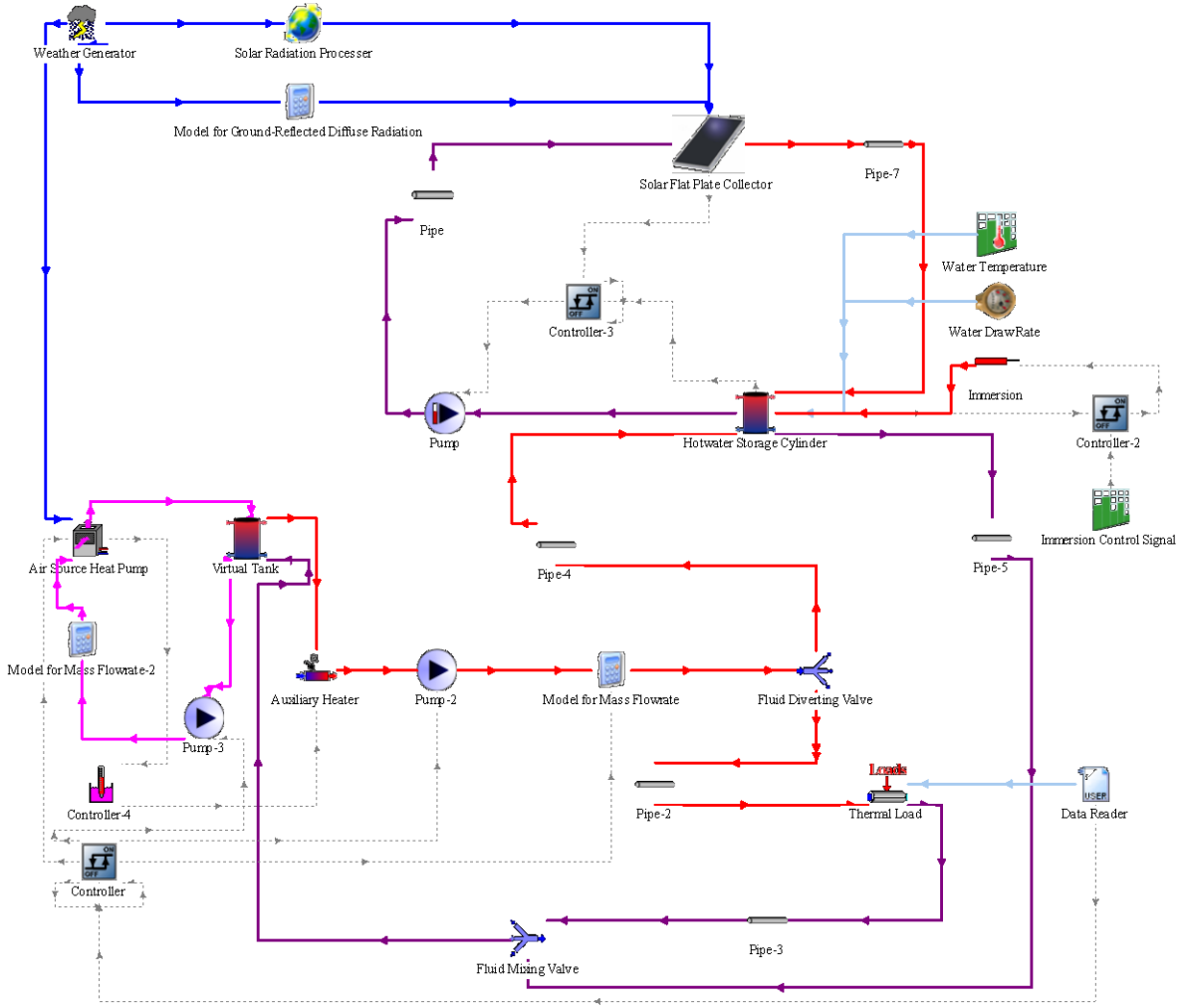

Figure 5.24. A domestic thermal generation system consisting of a combination of an air source heat pump and a solar thermal system assembled from a number of solar flat plate collectors.

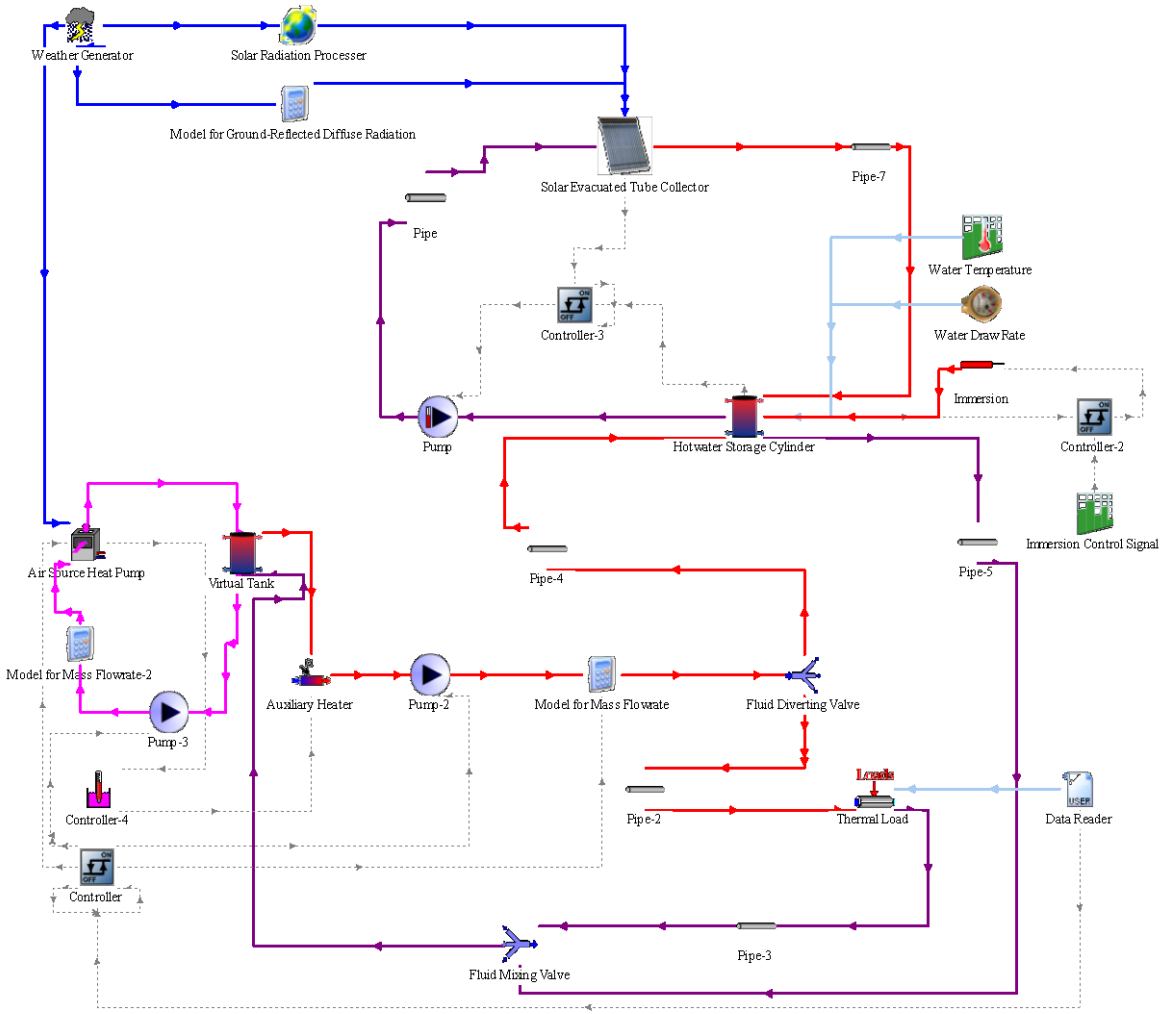

Figure 5.25. A domestic thermal generation system consisting of a combination of an air source heat pump and a solar thermal system assembled from a number of solar evacuated tube collectors.

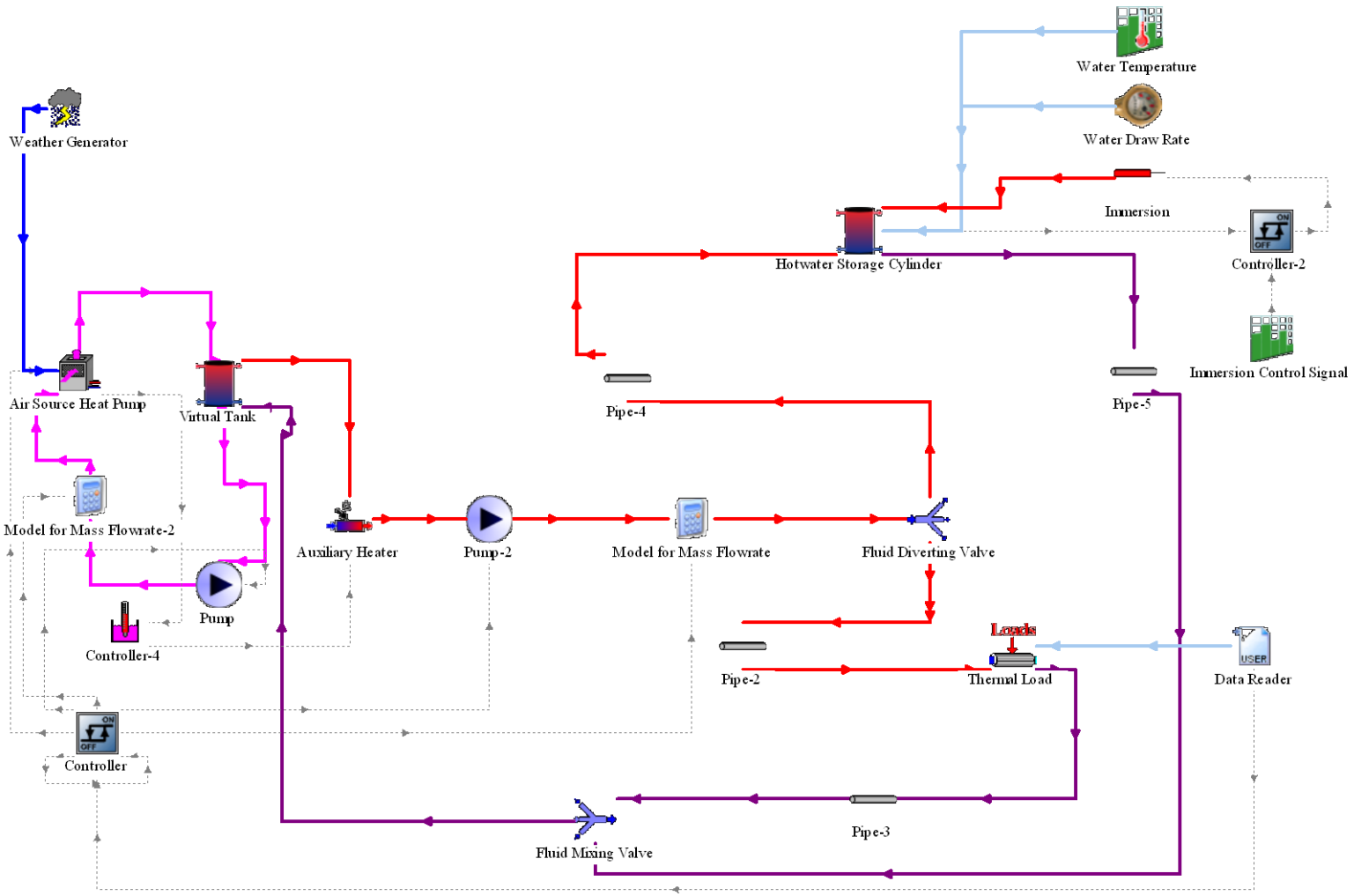

Figure 5.26. A domestic thermal generation system consisting of a combination of an air source heat pump and an electrical immersion for hotwater heating.

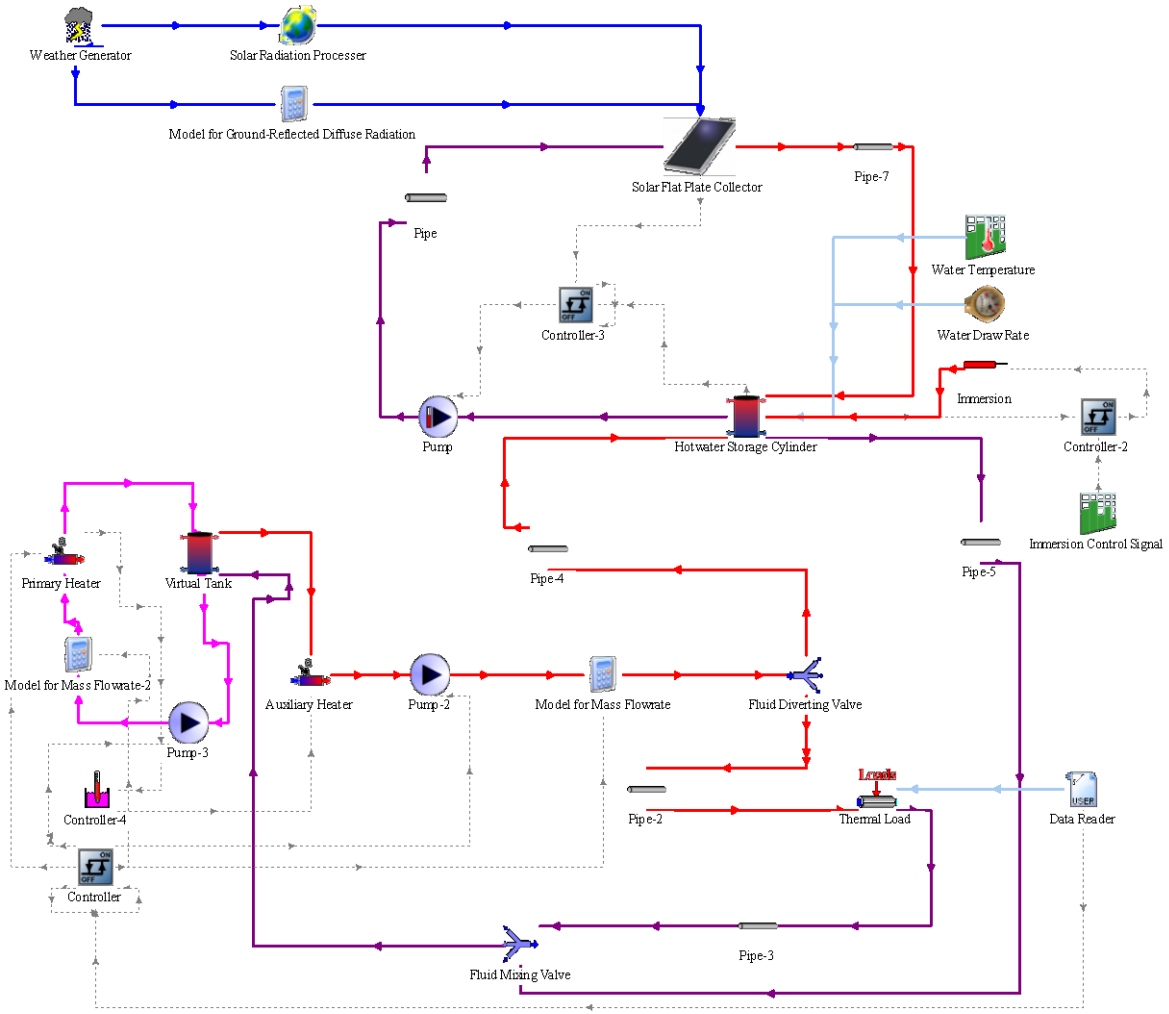

Figure 5.27. A domestic thermal generation system consisting of a combination of a primary electrical heating system and a solar thermal system assembled from a number of solar flat plate collectors.

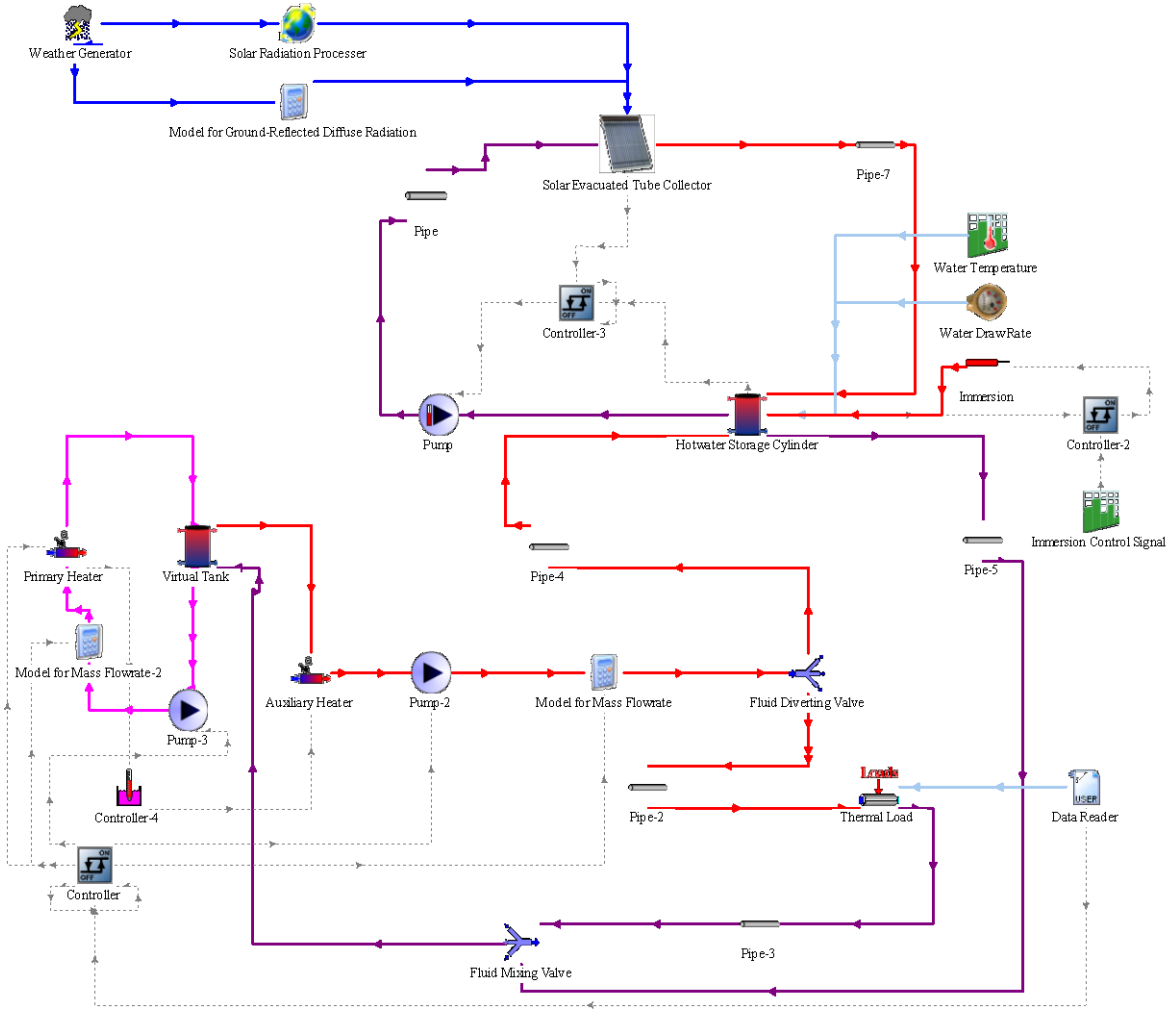

Figure 5.28. A domestic thermal generation system consisting of a combination of a primary electrical heating system and a solar thermal system assembled from a number of solar evacuated tube collectors.

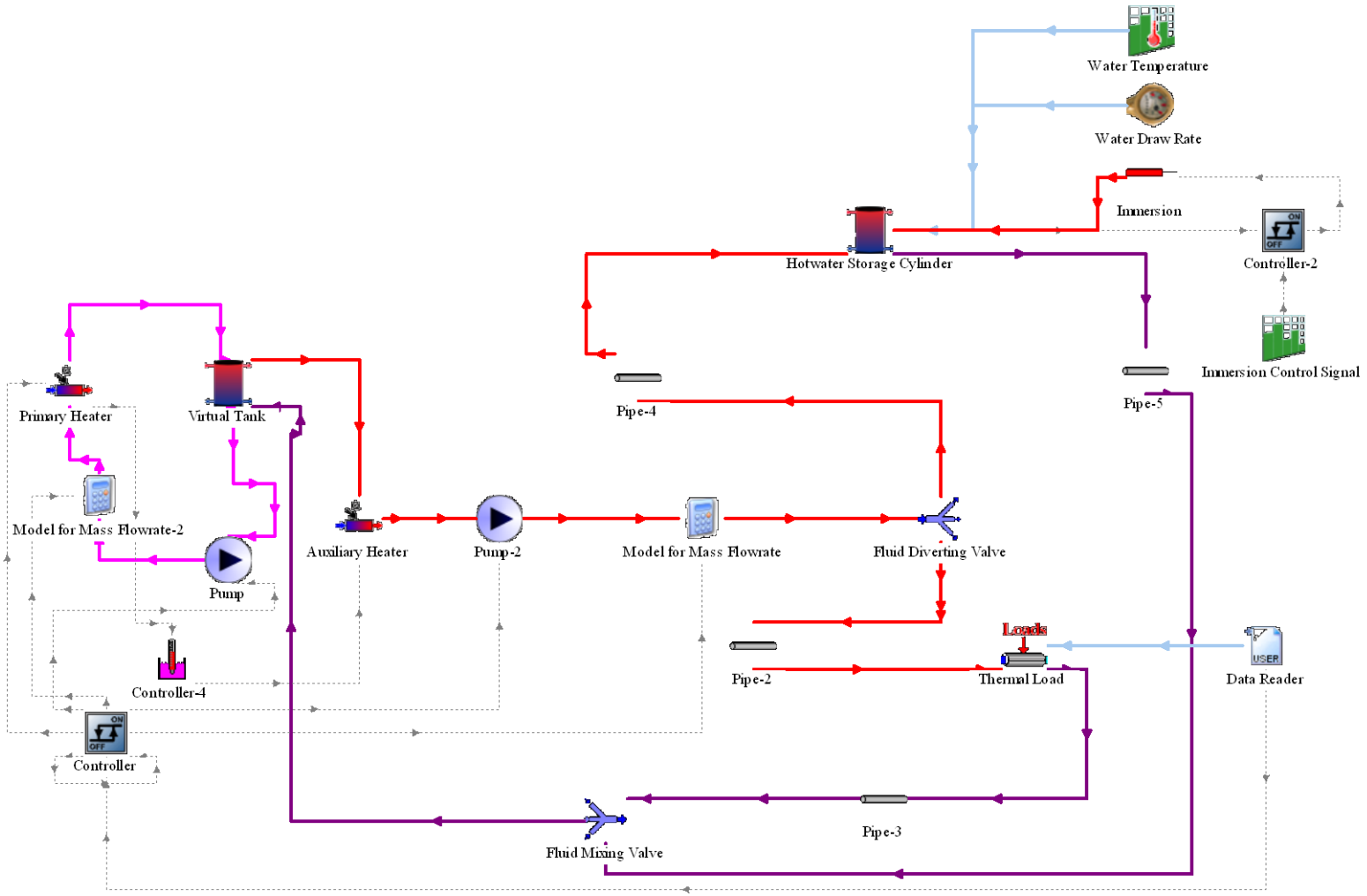

Figure 5.29. A domestic thermal generation system consisting of a combination of a primary electrical heating system and an electrical immersion for hotwater heating.

5.8.2. Determination of the Optimal Slope for Flat Plate and Evacuated Tube Solar Thermal Collectors

The flat plate and evacuated tube collectors produce their maximum energy output, at a fix orientation, when they are installed at the optimal slope. The optimal slope of solar thermal collectors should first be determined; the energy outputs then obtained are critically important for identifying the optimal system configuration from all possible combinations of micro-renewable thermal generation systems.

One solar thermal flat plate collector system with an aperture area of 3.95 m^2 and one solar thermal evacuated tube collector system with an aperture area of 3.23 m^2 system were used to determine the optimal slope in this study. They are the most commonly utilised collector aperture areas respectively for domestic applications in Ireland. The systems set up are similar to the solar hotwater generation portion of the micro-renewable thermal generation system; the two main differences are that water is not being preheated from a domestic heating generation system, and no immersion is used at the scheduled time. However, various conditions such as the weather data, hotwater draw-off rate and water entering temperatures are all identical. The solar thermal hotwater generation systems are shown in Figure 5.30 and Figure 5.31.

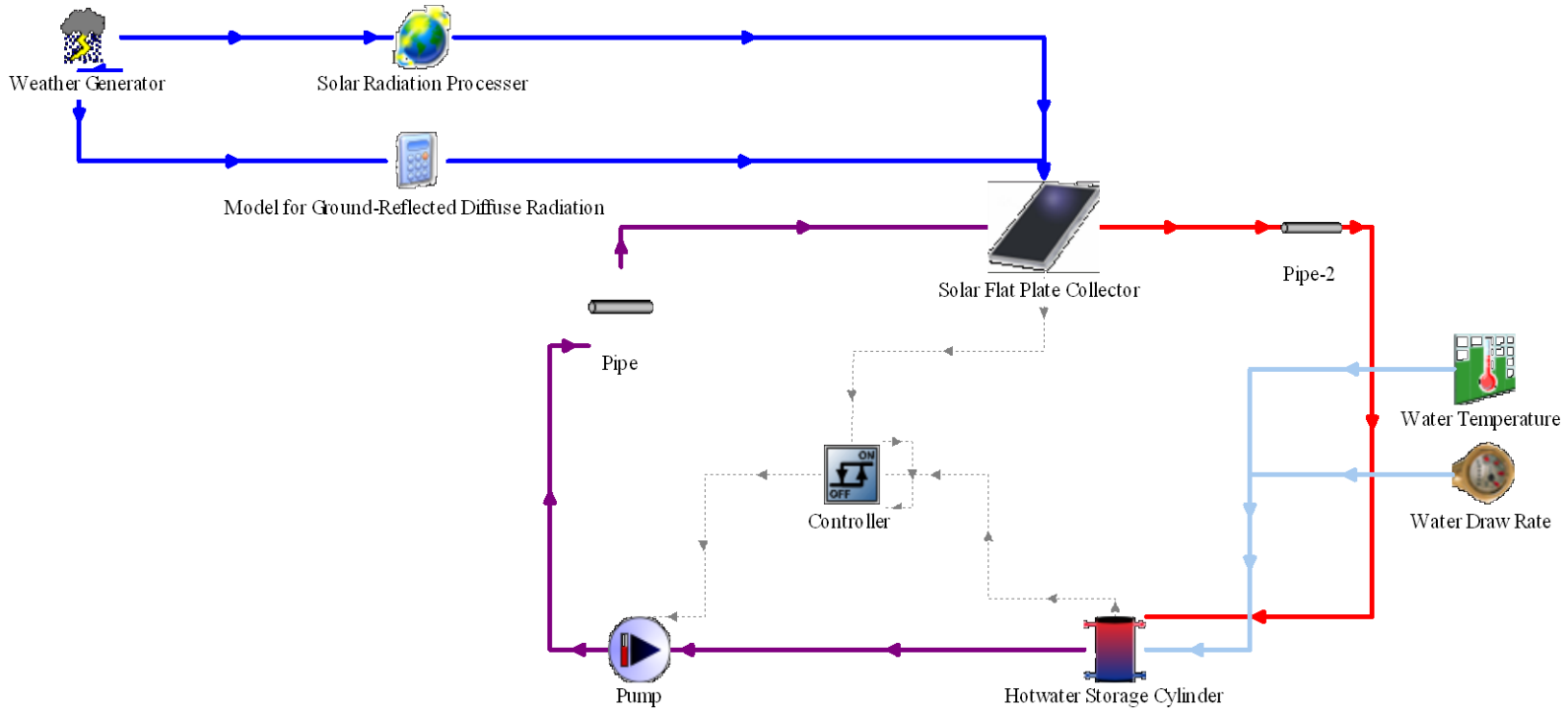

Figure 5.30. The solar thermal flat plate hotwater generation system.

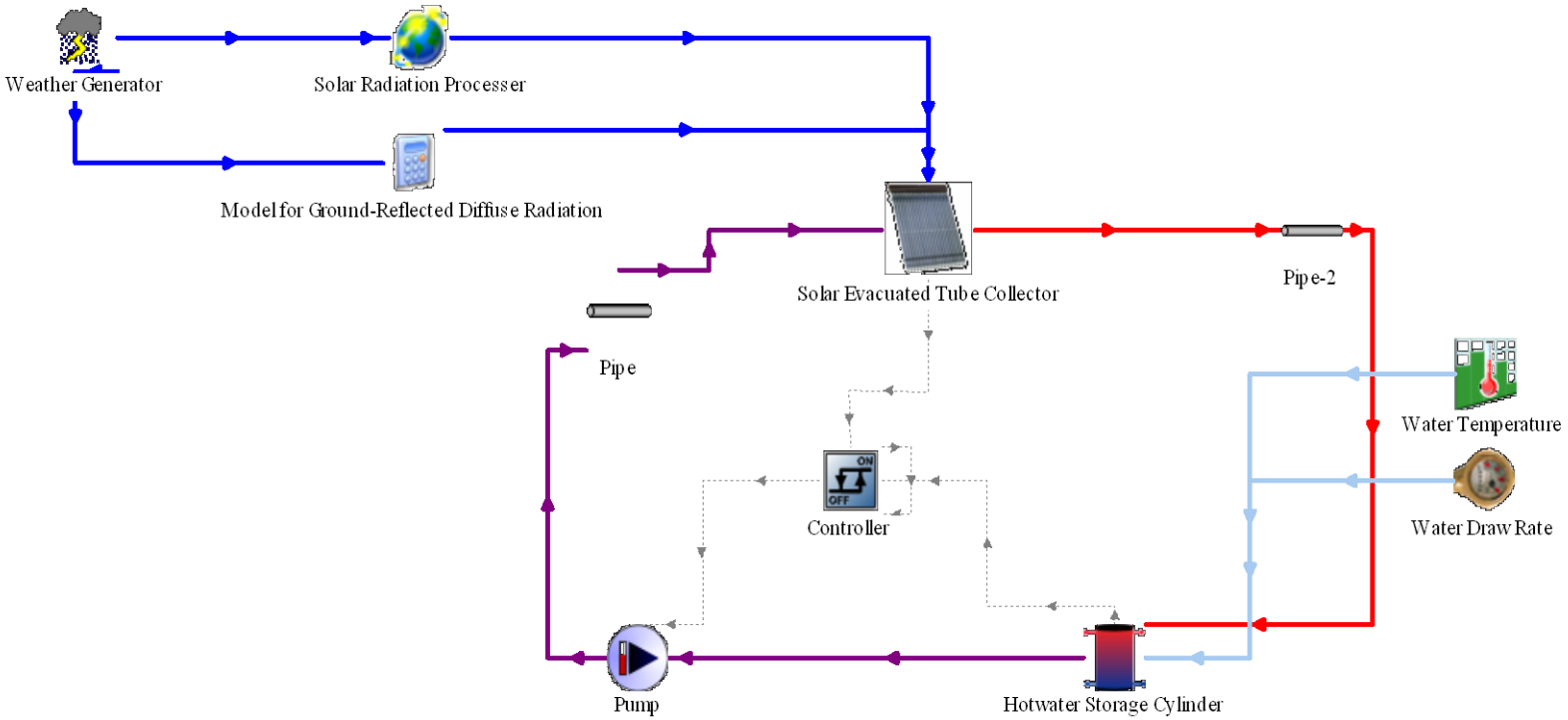

Figure 5.31. The solar thermal evacuated tube hotwater generation system.

The slopes specified in the analyses ranged from 30^o to 60^o with 5^o intervals. As shown in Tables 5.14 and 5.15, a value of 45^o was identified as the optimal slope angle for both the flat plate and evacuated tube collectors. Therefore, a value of 45^o is specified for the slope angle in the overall integration studies.

Slope (^{o})	30	35	40	45	50	55	60
Power output (kWh)	1,767	1,807	1,834	1,846	1,845	1,829	1,801

Table 5.14. Results of energy output achieved at various slopes from a solar flat plate collector having an aperture area of 3.95 m^2.

Slope (^{o})	30	35	40	45	50	55	60
Power output (kWh)	2,269	2,312	2,340	2,351	2,347	2,327	2,291

Table 5.15. Results of energy output achieved at various slopes from a solar evacuated tube collector having an aperture area of 3.23 m^2.

5.8.3. TRNSYS Simulation Model

The micro-renewable thermal generation system is developed and built using TRNSYS simulation software package. All appropriate components for constructing these micro-renewable thermal generation systems have been selected. Each component, based on specific mathematic descriptions, requires a number of constant parameters and time dependent inputs to produce a time dependent output. Once each component is characterised (parameters defined), it is then interconnected with other components to create the desired micro-renewable thermal generation system model.

The main components employed for this simulation model in this study are:

- ASHP (Type 941)
- solar thermal flat plate collector (Type 539)

- solar thermal evacuated tube collector (Type 538)
- hotwater storage cylinder (Type 534)
- weather generator (Type 54)
- solar radiation processor (Type 16)
- flow stream loads (Type 682) which was used as the compulsory hourly thermal load

The assistant components employed are:

- pumps (Type 3b)
- data reader (Type 9e) which was used to provide the existing thermal load
- fluid diverting valve (Type 647)
- fluid mixing valve (Type 649)
- differential temperature controller (Type 2b) which was used to control the pump in the solar collector loop. The pump would start operating signalled from the controller once the outlet temperature of the solar collector was $5^{o}C$ hotter than the temperature of the supplied water, and stop operating when the difference reduced to $2^{o}C$
- variable speed pump (Type 110)
- pipe duct (Type 31)
- water heater energy supply (Type 1226) which was used as an electrical immersion for hotwater storage cylinder
- forcing functions (Type14) that were used a number of times to input a control signal for the electrical immersion, hotwater demand profile and mains water supply temperature
- plotter and result summary (Type 65c)

Tables 5.16-5.18 show the values of parameters used for ASHPs, a solar thermal flat plate collector, two evacuated tube collectors and a hotwater storage cylinder.

Three additional components are used to complete the desired systems model, they are:

- the individual ground-reflected diffuse radiation on a tilted solar collector equation performa.
- virtual tank mode.
- mass flowrate equation performa.

Both individual beam solar radiation and sky diffuse solar radiation on the tilted solar collector, as well as the total solar radiation on the tilted solar collector consists of beam solar radiation, sky diffuse solar radiation and ground-reflected radiation can be calculated from the solar radiation processor. Although the individual ground-reflected diffuse radiation on the tilted solar thermal collector cannot be determined, it is required for both types of solar thermal collectors (Type 538 and Type 539). Therefore the ground-reflected diffuse radiation on the tilted solar thermal collector was estimated using Equation 5.24 [206] and is incorporated into the TRNSYS simulation model using the equation proforma as follows.

$$I_{gr} = I * \frac{1}{2} * \rho_{gr} * (1 - \cos\beta) \qquad (5.24)$$

where I_{gr} is the ground-reflected radiation received by the collector, I is the global solar radiation on a horizontal surface, ρ_{gr} is the ground reflectance and β is the slope of the collector relative to the horizontal.

A virtual tank (hotwater storage cylinder component with two inlets and two outlets) is used between the ASHP loop (or a primary electrical heating system) and the

domestic heating loop. The ASHP component (Type 941) available in TRNSYS is an on/off device which does not meet a set point temperature but simply puts its entire current capacity into heating up the domestic heating loop when the controller detects a heating load for any hour. Therefore the ASHP can dramatically overheat the domestic heating loop when under low heating load conditions. Since the newly-designed commercial ASHPs are commonly inverter-drive such that the power outputs can be modulated depending on the heating load requirement, the use of this virtual tank is the most effective approach to mimic a realistic ASHP system. However this virtual tank is not working as a buffer tank which is sometimes used in an (traditional) ASHP system.

The pump component (Type 3b) is used as the domestic circulating pump. This component is an on/off device which enforces the maximum flowrate when it is on, and a zero flowrate when it is off. However, this does not reflect the physical scenario whereby the domestic heating fluid is still circulating with a very low flowrate excepting the time that the maximum flowrate is enforced. This was observed from the Mitsubishi Ecodan W85 ASHP testing report [327]. The mass flowrate equation performa, incorporated into the TRNSYS simulation model, reflects a real-operation mass flowrate circumstance in the domestic heating loop and is expressed using Equation 5.25.

$$\dot{m} = 0.8 + a * (pump\_rated\_flowrate - 0.8) \tag{5.25}$$

where $\dot{m}$ is the mass flowrate in the thermal load loop (kg/min) and a is the control signal from the controller in the heating load loop.

5.9. Results and Discussion

The integration technique is applied to determine the optimal system for Ireland. The ASHPs and solar thermal collectors selected for analysis represent other similar thermal capacity ASHPs and types solar thermal collectors. The selected ASHPs and the solar thermal systems (formed from the selected solar thermal collectors) adhere to the conditions for exemption from planning permission. The maximum overall collector surface area of the solar thermal system is 12 m^2. The selected ASHPs are the Mitsubishi Ecodan W50 (rated thermal capacity of 5 kW), the Mitsubishi Ecodan W85 (rated thermal capacity of 9 kW), and the Mitsubishi Ecodan W140 (rated thermal capacity of 14 kW). The selected solar thermal collectors are the Kingspan flat plate collector and the Kingspan Evacuated tube collectors HP400 and HP450. Tables 5.16-5.18 give relevant information for the selected ASHPs and solar thermal collectors employed respectively. This indicative information was obtained from either official websites or from personal communications. The system integration is carried out assuming the micro-renewable thermal generation system is installed in Dublin and with the following conditions and assumptions:

- An annual average air temperature of 9.9^oC and an annual solar radiation value of 970 kWh/m^2.
- An average annual household thermal load of 16,536 kWh.
- The daily hotwater requirement of 199.8 L at 60^oC.
- The installed solar thermal system is south facing.
- A ground reflectance of 0.2.
- An imported electricity price of €0.1928/kWh.
- A green loan having a loan rate of 4.5%.

- An annual inflation rate of 2.26% (which was the average annual inflation rate for Ireland for the period January 2001 to December 2010 [178]).
- A solar thermal system capital grant of €800.
- The project lifespan is 20 years.

5.9.1. Economic Discussion and Identification of the Optimal System Based on Current Irish Conditions

The LCC of a mono micro-renewable thermal generation system consisting of a single ASHP or a single solar thermal system, and a hybrid system consisting of an ASHP/solar thermal system, has been calculated with the conditions given in the previous section. However, it should be noted that the cost of the heating distribution system is not included when comparing the micro-renewable thermal generation systems. The system with the lowest LCC after the project lifespan, that satisfies both the heating requirement and the hotwater demand, is deemed the optimal system. The LCC (€33,604) of the optimal system is achieved by a single ASHP having a thermal capacity of 14 kW. Figure 5.32 is an integration map for all the analysed systems in this study. The economic viability of the micro-renewable thermal generation system can be determined by comparing it with other conventional thermal (heating and hotwater) generation systems. Oil, natural gas and electricity are the most common fuels used for domestic heating and hotwater generation. The oil boiler system for providing heating and hotwater for domestic dwellings was the most popular in Ireland; 711,330 were installed by the end of 2011. The natural gas boiler system was the second most popular used, as there were 550,215 installed by the end of 2011. The electricity system was popular, however, it is mainly used for apartments; 140,419 was the total number installed by the end of

2011 in Ireland [328]. Therefore, the determination of economic viability of the micro-renewable thermal generation system has to be made in comparison with each individual conventional thermal generation system. However, the micro-renewable thermal generation system is designed to connect with an underfloor heating distribution system. Other conventional thermal generation systems are generally

Air Source Heat Pump	Thermal Capacity (kW)	Power Input (kW)	Air Flow Rate (m^3/min)	Fan Power (kW)	Compressor Power (kW)	Compressor Start Type	Nominal Water Flow Rate (L/min)	Refrigerant	Installed Cost inc VAT (€)
Ecodan W50	5	1.22	50	0.086	0.9	Inverter	14.3	R410A	8100
Ecodan W85	9	2.34	55	0.06	1.3	Inverter	25.8	R410A	9500
Ecodan W140	14	3.34	100	0.074*2	2.5	Inverter	40.1	R410A	12200

Table 5.16. Relevant information for three air source heat pumps available on the Irish market in 2013 and selected for the system integration study [329, 330].

Hotwater Storage Cylinder	Height (mm)	Width (mm)	Depth (mm)	Tank Volume (L)	Surface Area of Heat Pump Coil (m^2)	Surface Area of Solar Coil (m^2)	Backup Immersion Heater Rating (kW)	Standing Losses kWh/24 hours	Capital Cost Inc VAT (€)
Kingspan Aerocyl Plus-me Cylinder	2050	550	720	300	3	0.96	3	2.43	950

Table 5.17. Relevant information for hotwater storage cylinder available on the Irish market in 2013 and selected for the system integration study [331].

Solar Thermal Collector	Kingspan Solar Flat Plate Collector	Thermomax HP400	Thermomax HP450
Type	Flat plate	Evacuated tube	Evacuated tube
Aperture area (m^2)	1.93	2.16	3.23
Intercept efficiency	0.732	0.75	0.75
First order efficiency coefficient (W/m^2K)	3.472	1.18	1.18
Second order efficiency coefficient (W/m^2K^2)	0.008	0.0095	0.0095
Rated flow rate (L/hr)	96	160	240
Absorbance (%)	95	95	95
Emittance	3	5	5
Heat transfer fluid	Water/Glycol	Water/Glycol	Water/Glycol
Initial cost inc VAT (€)	2750	2700	2700
Installed cost inc VAT (€)	580/2m^2		500/10 tubes

Table 5.18. Relevant information for three solar thermal collectors available on the Irish market in 2013 and selected for the system integration study [332-335].

connected with traditional radiators. The underfloor distribution system is normally more expensive than the traditional radiator system. The cost difference between these two distribution systems has to be taken into consideration in order to accurately determine the economic viability of the micro-renewable thermal generation system. A difference of €1,100 is employed in this study for a typical 3-bedroom dwelling and is added to every optimal system when comparison is made with a conventional thermal generation system. The LCC of an oil boiler system, which satisfies both the heating requirement and the hotwater demand, is approximately €44,500 over a 20-year project lifespan. The optimal system, i.e. a single ASHP, is economically viable since its LCC (increased to €34,704 when the cost difference between the underfloor heating system employed for a micro-renewable thermal generation system and the radiators system employed for a conventional thermal generation system is taken into account) is less than the LCC of the oil boiler system. The LCC of a natural gas boiler system is approximately €25,670 for a 20-year project lifespan. In this case the optimal micro-renewable thermal generation system is not economically viable since its LCC is greater than the LCC of this natural gas boiler system. The electrical system is rarely used for domestic heating in dwellings in Ireland. The approximate cost of €58,370 for a 20-year lifespan, is considerably higher than the other two conventional heating and hotwater generation systems. As the LCC of the optimal micro-renewable thermal generation system is much less than the LCC of the electrical system, it is deemed economically viable. A detailed description of the three conventional thermal generation systems is displayed in the Table 5.19.

	Oil Boiler System	Natural Gas Boiler System	Electricity Heating System
Efficiency (%)	75	85	100
Installed cost (€)	4,000	2,500	1,800
Cost of hotwater storage cylinder (€)	500	500	500
Cost of fuel (€/kWh)	0.1013	0.05894*	0.1928
Maintenance cost (€)	85	85	0

* An annual standing charge of €89.93 is applied.

Table 5.19. A detailed description of three typical conventional thermal generation systems [336].

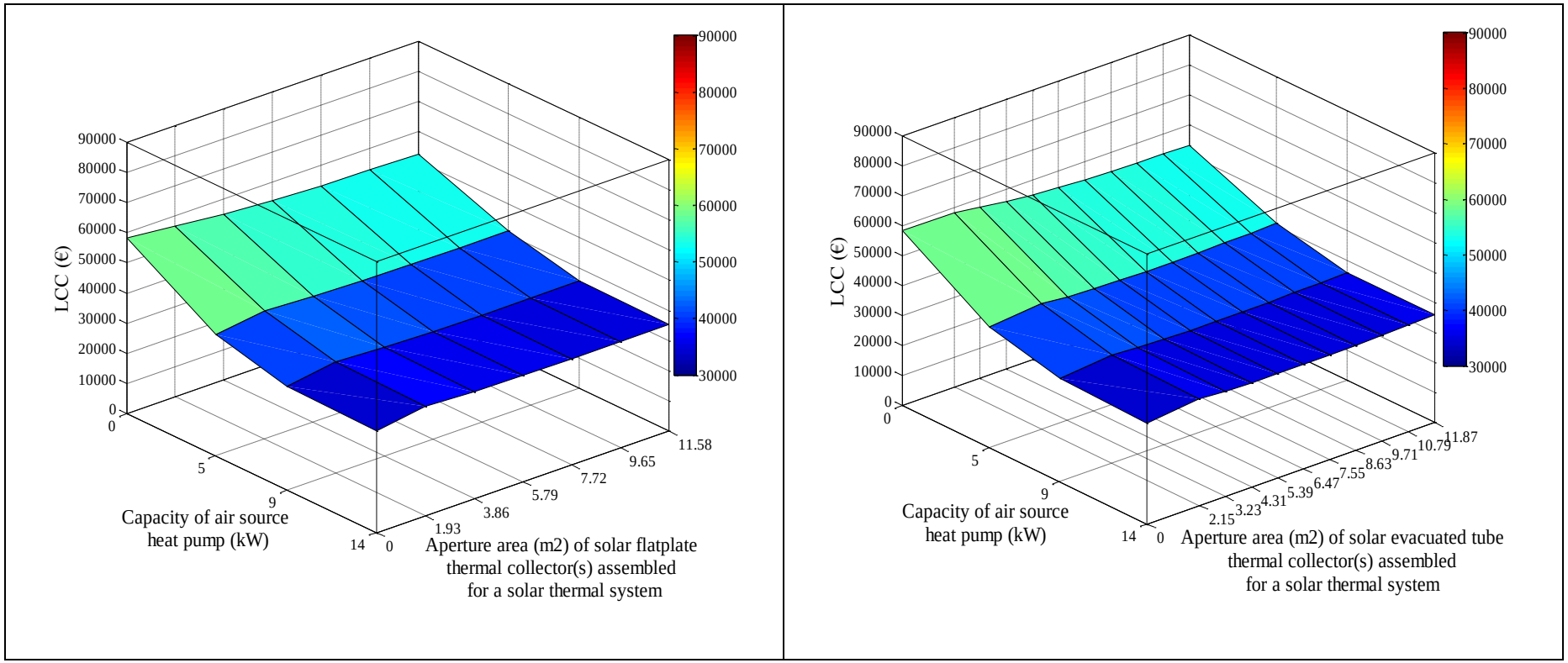

Figure 5.32. Integration map for all micro-renewable thermal system combinations; mono systems consist of a single ASHP or a single solar thermal system, which hybrid systems consist of an air source heat pump with a solar thermal system assembled from solar flat plate collectors (left) or an air source heat pump with a solar thermal system assembled from solar evacuated tube collectors (right).

5.9.2. Economic Discussion and Identification of the Optimal System Based on Parameter Studies

5.9.2.1 Effect of Household Thermal Load on the Optimal System

The annual household thermal load is divided into two parts: heating and hotwater. The domestic heating is seasonally dependent since heating is required more often in the winter than it is in the summer. The domestic heating is also affected by its distribution system installed in the dwelling. The low-temperature heating distribution systems, such as underfloor heating system, generally requires less energy input to satisfy the domestic heating requirement in comparison with the medium and high-temperature heating distribution systems such as low-temperature radiators or conventional radiators. The same level of comfort is experienced by occupants with a lower room temperature, i.e. at the low end of the comfort level room temperature range, when using an underfloor heating system as oppose to a radiator-based system. The domestic heating requirement also depends on the occupants' comfort expectations. Some occupants may have the desired room temperature greater or less than the comfortable temperature of 18^{o}C-21^{o}C. Other occupants may operate the heating generation system for an extensive period in order to ensure that the room temperature remains constant for a longer time. Therefore, the domestic heating is first varied significantly for each different scenario as the total heating load and the load profile will differ depending on the occupants' behaviour in each dwelling. The volume of hotwater consumption is mainly dependent on the number of occupants in the dwelling. Four occupants are assumed for a standard dwelling. The total volume of approximately 199.8 L of hotwater at 60^{o}C per day is a reasonable assumption made in this study. Various

domestic heating loads have been applied and the effect of these domestic heating loads has been investigated.

Figure 5.33 (LCC vs. household heating load) shows that the LCC of the optimal system, increases in an almost linear fashion as the household heating load is increased. However, it should be noted that a unique profile is obtained for each thermal load (statistically different as determined previously from Tukey's test) therefore the effect of the profile must be taken into consideration.

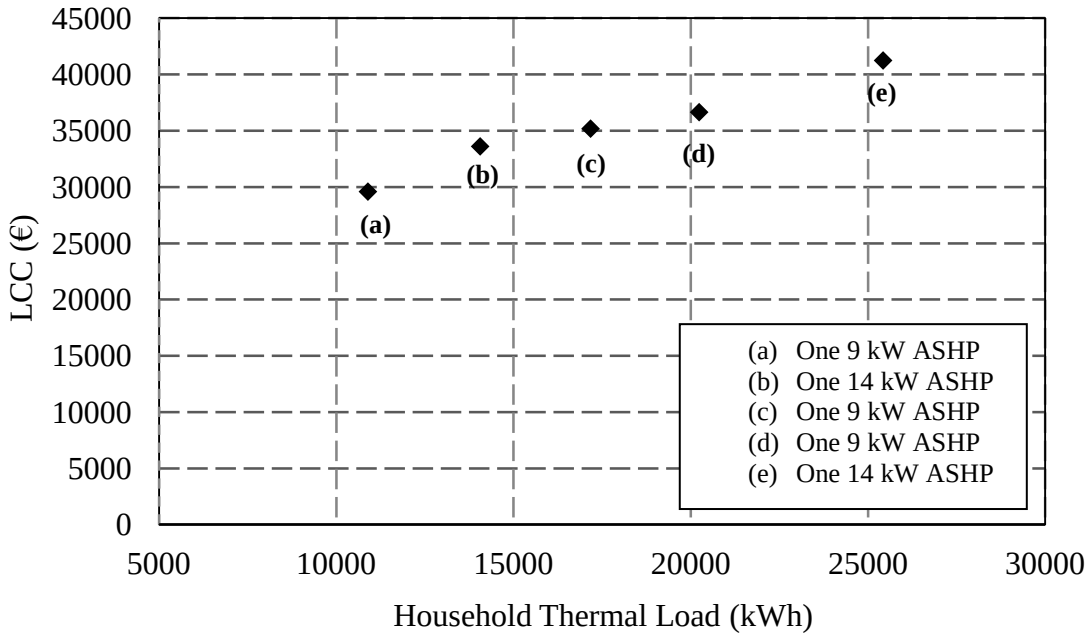

Figure 5.33. LCC of the optimal system versus household thermal load. Imported electricity price is €0.1928/kWh and the loan rate is 4.5%. ASHP = air source heat pump.

A study was carried out in order to investigate the LCC obtained from various profiles where the total thermal loads were statistically similar. The effect of different heating profiles having statistically the same heating load for a mono micro-renewable thermal generation system (an ASHP alone) is summarised in Table 5.20.

ASHP Thermal Capacity (kW)	Heating Load (kWh)	LCC (€)
5	15,016	39,213
	15,045	32,315
	15,147	36,157
9	15,016	32,987
	15,045	32,916
	15,147	32,654
14	15,016	34,426
	15,045	35,058
	15,147	34,298

Table 5.20. The power outputs obtained from various domestic heating profiles which having statistically the same heating load for an air source heat pump system.

From the result shown, different profiles make a significant impact on the calculated LCC of micro-renewable thermal generation systems having a small thermal capacity. For example, the LCCs obtained for satisfying a heating load of 15,016 kWh and 15,045 kWh from a 5 kW ASHP system is €39,213 and €32,315 respectively, a difference of 17.6%. However, it was found that different profiles have an insignificant influence on the calculated LCC of micro-renewable thermal generation systems having a medium (9 kW) and large (14 kW) thermal capacity, e.g. a difference of 0.02% and 1.8% are obtained for a heating load of 15,016 kWh and 15,045 kWh from these two ASHP systems respectively.

The investigation is extended to calculate and compare the LCCs of ASHP systems for two statistically different heating loads, with each having its unique profile. For a 9 kW ASHP system, the result shows that the LCC obtained is €34,564 for satisfying a heating load of 14,056 kWh; however the LCC of €32,987 is calculated for a heating

load of 15,016 kWh. In this case, it is actually more expensive to run this 9 kW ASHP system over a 20-year project lifespan for a lower total heating load (14,056 kWh) than a larger one (15,016 kWh) due to the fact that the different profile is applied. When the same profiles are applied to a 14 kW ASHP system, the calculated LCCs are €33,603 and €34,426 for heating loads of 14,056 kWh and 15,016 kWh, respectively. This is as expected since the cost of running the 14 kW ASHP system over a 20-year project lifespan is lower for a lower total heating load than for a larger one.

Figure 5.34 and Figure 5.35 (integration map of LCC vs. sample mono/hybrid micro-renewable thermal generation systems) shows that a system assembled from the same thermal capacity ASHP and the same size of solar thermal collectors will economically cost more over the project lifespan as the household thermal load increases. This is because the ASHP has to operate either continuously at its rated capacity or for longer periods in order to meet the increased domestic heating demand. Also the increased thermal load has a greater impact on the economic analysis for the small capacity ASHPs than for the large capacity ASHPs, as the auxiliary heater has to turn on frequently in order to assist the small capacity ASHP in satisfying the demand. However, the auxiliary heater is not often used since the heating demand can generally be met from the large capacity ASHP. The cost saving from operating the auxiliary heater can be significant.

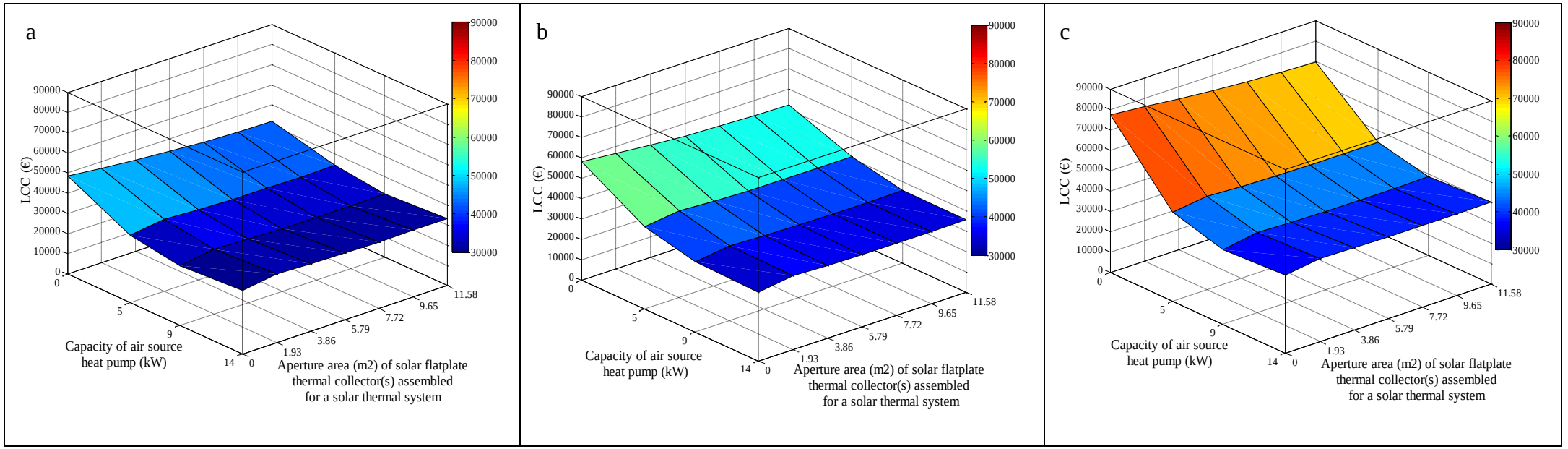

Figure 5.34. Integration map of selected air source heat pump and solar thermal system assembled from solar flat plate collector for three domestic thermal loads. The domestic thermal load is (a) 10,890 kWh, (b) 14,055 kWh and (c) 20,235 kWh.

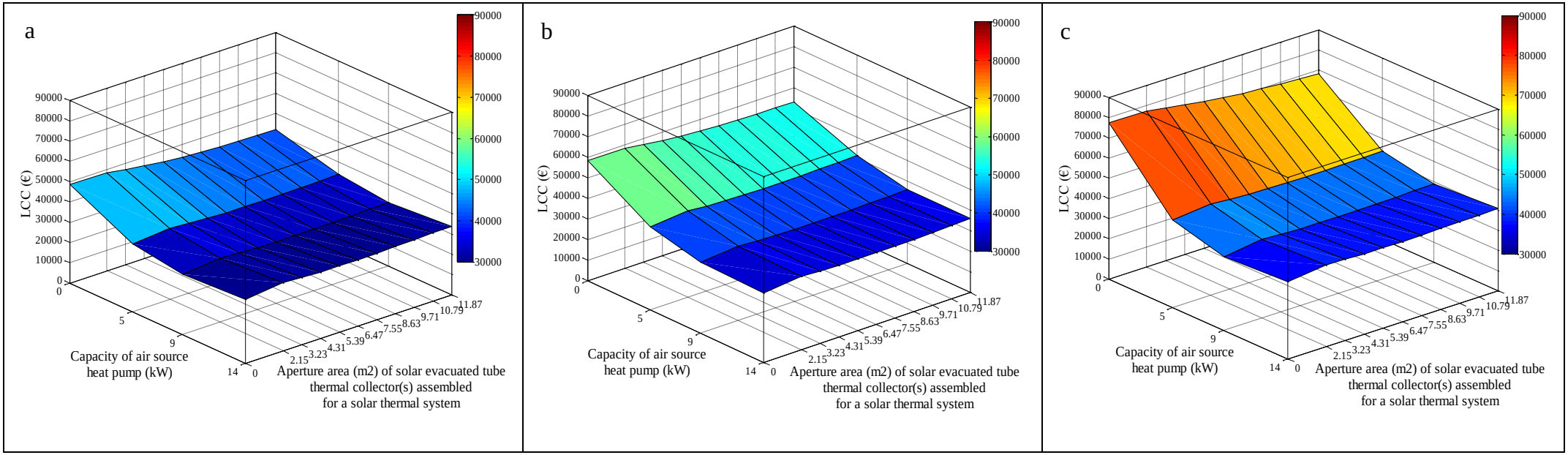

Figure 5.35. Integration map of selected air source heat pump and solar thermal system assembled from solar evacuated tube collector for three domestic thermal loads. The domestic thermal load is (a) 10,890 kWh, (b) 14,055 kWh and (c) 20,235 kWh.

5.9.2.2 Effect of Imported Electricity Price on the Optimal System

The imported electricity price is a significant factor that can impact the determination of the optimal system. The ASHP and solar thermal system are operated using electricity only. Hence, the imported electricity price is directly related to the operational cost of the micro-renewable thermal generation system. The imported electricity price is expected to rise in the coming years. This increased electricity price can be in the form of an actual price increases, and/or an increase in the VAT rate and a levy charge on the usage of electricity.

Figure 5.36 (LCC vs. imported electricity price) shows that the LCC of the optimal system increases moderately as the imported electricity price increases. This increase is due to the rising operational cost for every kWh electricity consumed from both the ASHP and solar thermal system. Figure 5.37 and Figure 5.38 (integration map of LCC vs. sample mono/hybrid micro-renewable thermal generation systems) shows that a system assembled from the same capacity ASHP and the same size solar thermal system will economically cost more to satisfy the entire heating requirement and hotwater demand as the imported electricity price increases. It can be also noted that small capacity ASHP systems are influenced more by an increase in the imported electricity price since the LCC becomes significantly larger.

For a hybrid system containing an ASHP and a solar thermal system, it was found that the lowest LCC of the system, for the same capacity ASHP, is achieved by employing an increasing size of solar thermal system as the imported electricity price increases. For example, a hybrid system consisting of a 9 kW ASHP, the smallest LCC of €35,519, €39,788, €45,083 are achieved by combining this capacity ASHP with a solar thermal system having flat plate collector areas of 7.72 m^2, 9.65 m^2 and 11.58 m^2, and the

lowest LCC of €35,016, €38,952, €43,942, are achieved by also combining this capacity ASHP with a solar thermal system having evacuated tube collector areas of 6.47 m^2, 7.55 m^2 and 7.55 m^2 when the imported electricity prices are €0.193, €0.24 and €0.30 per kWh respectively.

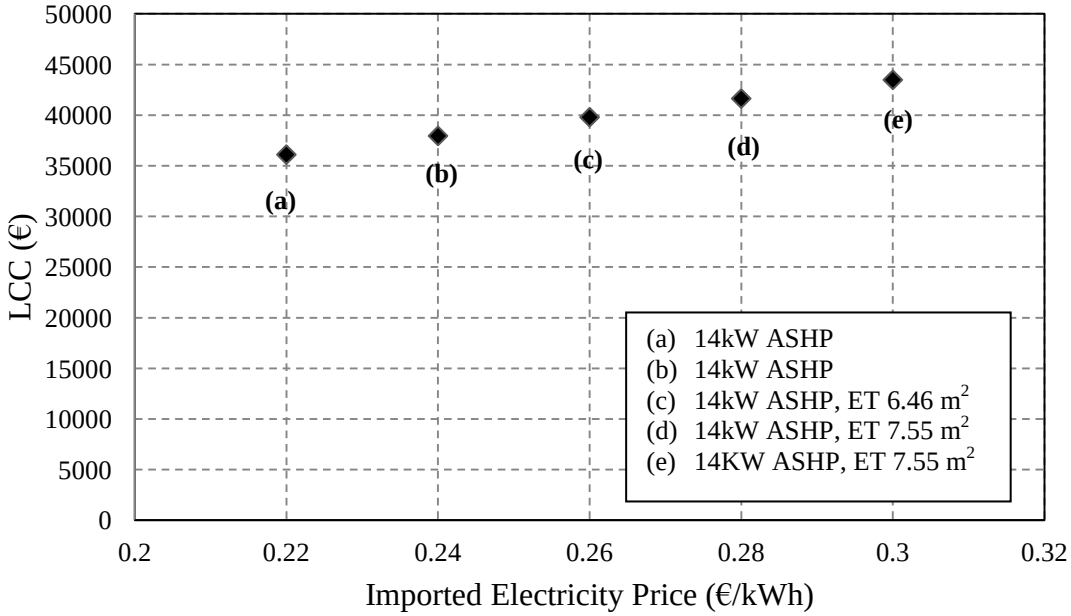

Figure 5.36. LCC of the optimal system versus imported electricity price. The loan rate is 4.5%. ASHP = air source heat pump, ET = solar thermal evacuated tube collector system.

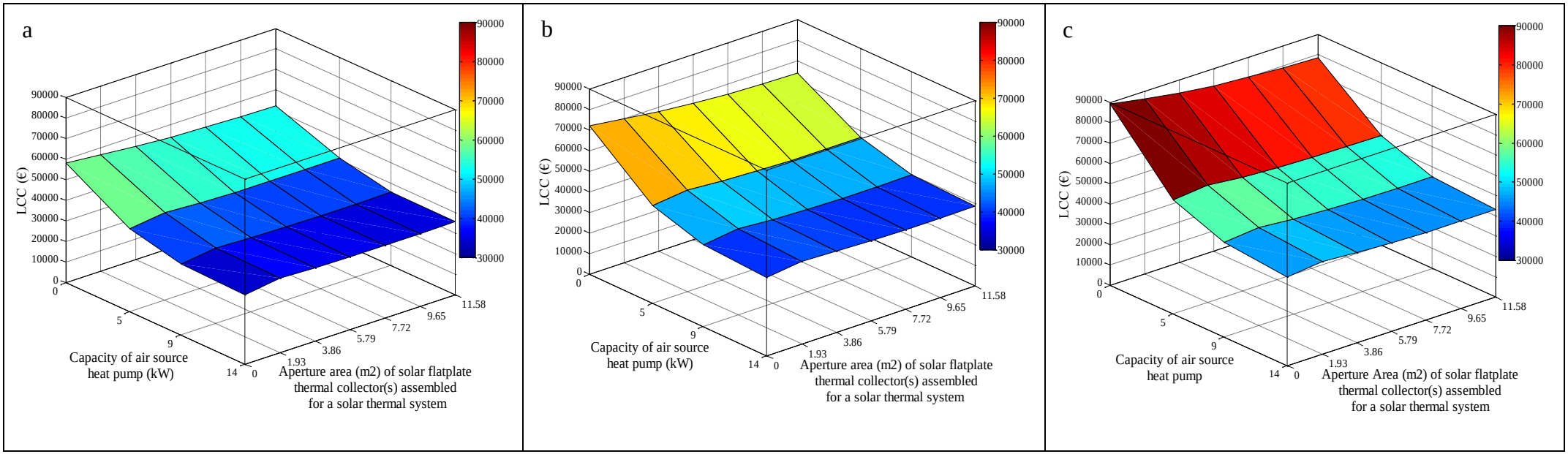

Figure 5.37. Integration map of selected air source heat pump and solar thermal system assembled from solar flat plate collectors for three imported electricity prices. The imported electricity price is (a) €0.1928/kWh, (b) €0.24/kWh and (c) €0.30/kWh.

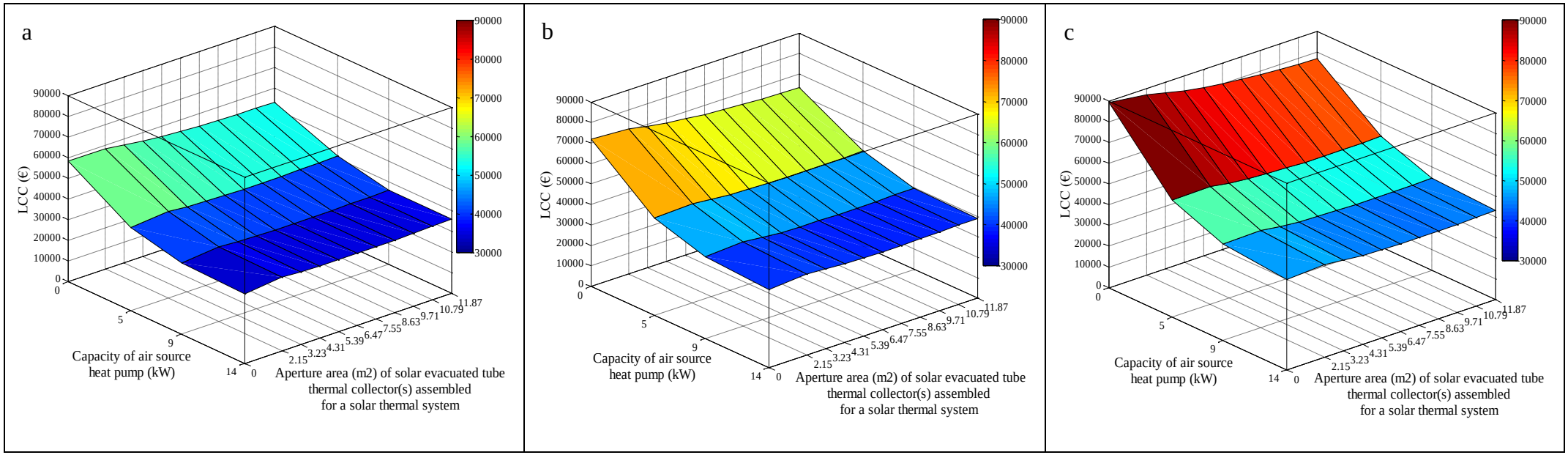

Figure 5.38. Integration map of selected air source heat pump and solar thermal system assembled from solar evacuated tube collectors for three imported electricity prices. The imported electricity price is (a) €0.1928/kWh, (b) €0.24/kWh and (c) €0.30/kWh.

5.10. Conclusion

In this chapter, a sub-technique is presented for the optimised integration of a mono/hybrid micro-renewable thermal generation system in order to satisfy the heating demand and hotwater requirements of a domestic dwelling. The mono micro-renewable thermal generation system is formed from a single ASHP or a single solar thermal system; the hybrid micro-renewable thermal generation system is formed from a combination of both. Three thermal capacity ASHPs, one flat plate solar collector and two evacuated tube solar thermal collectors (used to form the solar thermal systems for analysis) which are commercially-available and industry-representable are employed in this study. However, additional ASHPs and solar thermal collectors can be added to the existing database if a wider range of micro-renewable thermal generation systems is required for analysis. Using the developed integration technique, the system with the lowest LCC after the project lifespan is deemed the optimal system. Under current Irish conditions, the optimal system, is a mono system consisting of an ASHP having a thermal capacity of 14 kW. The system is not economically viable when compared with a domestic gas boiler system for generating the same amount of heating and hotwater since the LCC of this optimal system is greater than that of the gas boiler system. However, the LCC of this optimal system is lower than that LCC of a domestic oil boiler system or a domestic electrical system for generating the same amount of heating and hotwater and therefore it becomes economically viable. The large capital cost of ASHPs and solar thermal systems, and the current nonexistent /insufficient financial support (nonexistent capital grants for ASHPs and insufficient capital grants for solar thermal systems) are the main reasons for the micro-renewable thermal system not being able to compete with cheaper thermal generation systems (e.g. a domestic gas boiler system) in Ireland. Nevertheless, these systems should become economically

viable in the future with reductions in the capital cost of these systems and improved capital grant. The current capital grant is only offered to the solar thermal system with a flat rate of €800 per dwelling under the Better Energy Homes scheme by SEAI, and no grant is available for an ASHP. These have been reduced or terminated from previously available capital grants to householders from Greener Homes Scheme by SEAI. A grant of €2,000 was provided for an ASHP per dwelling; a grant was provided for €250/m^2 and €300/m^2 for a solar flat plate system and a solar evacuated tube system respectively subject to a maximum area of 6 m^2. Two parameter studies to assess the effect of household heating load and imported electricity price have also been carried out. From the results shown, the LCC of the micro-renewable thermal generation system increases moderately with an increased domestic heating load. However the LCC of the system can be also affected significantly by the heating load profile, even if the total heating load is almost identical. The increased imported electricity price can lead to a significant increase in the operational cost for a micro-renewable thermal generation system, particularly for the ASHP. Consequently, the LCC of the system over the project lifespan will also increase.

Finally, each householder should always make a decision based on his/her individual case as to whether an ASHP, a solar thermal system or a hybrid system is economically meaningful and should be installed. The renewable energy system market is dynamic, and is continuously influenced by improvements in ASHP and solar thermal collector technologies, the economy of scale in production and changes in Irish government policies towards micro-renewable energy technologies.

5.11. Summary

An optimised integration sub-technique for grid-connected micro-renewable thermal generation systems is presented in this chapter. The reviews of solar thermal system and ASHP are presented. The methodology of generating hourly solar radiation values and hourly ambient air temperature values is described; subsequently the methodology of predicting hourly energy output from a solar thermal system and an ASHP is presented. The developed integration sub-technique for selected solar thermal systems and ASHPs is explained in detail. The results are then analysed and discussed. In the next chapter, the novel optimised integration overall technique for grid-connected micro-renewable energy (electricity and thermal) generation systems is presented.

CHAPTER 6
OPTIMISED INTEGRATION OF GRID-CONNECTED MICRO-RENEWABLE ENERGY GENERATION SYSTEMS

6.1. Overview

In this chapter, a novel technique for the optimised integration of grid-connected micro-renewable energy (electricity and thermal) generation systems is presented. The chapter is split into two stages. In the first stage, a technique is developed to integrate the selected commercially-available micro-renewable electricity and thermal generation systems. In the second stage, the results obtained from applying this technique for current Irish conditions and parameters studies are thoroughly analysed and discussed.

6.2. Introduction

The deployment of micro-renewable energy generation systems for domestic dwellings is of huge importance for current and future dwelling design. In Ireland, newly built dwellings, and dwellings for sale or lease have to obtain the Building Energy Rating (BER). The dwelling which acquires a good BER is very energy efficient. Good insulation, appropriate glazing and airtightness are applied to ensure the dwelling requires minimum heating. The hotwater storage cylinder and pipe works should also be well insulated in order to prevent energy loss and thereby reduce the energy required to generate hotwater. In addition, with the aim of reducing the household electricity

demand and subsequently achieving an energy efficient dwelling, energy-saving electrical appliances should also be employed. After all the above energy-efficient measures have been taken, the utilisation of a micro-renewable energy generation system for supplying electricity, heating and hotwater becomes critically important. This is also one of the most effective ways in improving the BER of a dwelling and helping the dwelling become truly sustainable and energy efficient. The use of renewable energy generation systems can enhance the security of the energy supply of the dwelling, as very little energy will be required from an external source e.g. electricity, natural gas and oil. Therefore the supply of electricity, heating and hotwater remains consistent even if there is a shortage from the conventional energy supply. Furthermore, this should also ease the impact of conventional energy price increase on the householder.

The integration of micro-renewable energy generation systems for a domestic dwelling or a residential building has already been studied as shown in the literature review. Different techniques have been developed and applied to find the most suitable systems from these studies. The optimal system, in general, can be determined in terms of either economic viability or energy efficiency. In this study, an investigation of the economic viability of integrated grid-connected micro-renewable energy generation systems for domestic applications in Ireland has been carried out. The results obtained from economic analysis are very important for the homeowner in deciding:

- if a micro-renewable energy generation system is worthwhile to install.
- if an integrated system has an advanced economic viability over a single system.
- which of the single or the combined system can achieve the most economic benefit.

It is very important for homeowners to know the various types of micro-renewable energy generation system available when intending to install a domestic renewable energy system. However, it is equally or even more important to decide on the optimal system which accomplishes the maximum economic benefit under each case scenario.

This chapter presents a novel technique for the optimised integration of a grid-connected micro-renewable energy generation system consisting of a micro-renewable electricity generation system and/or a micro-renewable thermal generation system. A micro-renewable electricity generation system consists of a single micro wind turbine or a single solar PV system, or a combination of both; a micro-renewable thermal generation system consists of a single ASHP or a single solar thermal system, or a combination of both. The integration technique is deployed for dwellings in Ireland; however it is generally applicable to any location. In this integration technique, LCC analysis is employed to identify the optimal system, while also taking into consideration the technical and economical constraints and guidelines. The sub-technique developed to obtain the predicted hourly electricity values from a micro wind turbine and/or a solar PV system is described in Chapter 4. An annual household electrical load and an average annualised electrical load profile is used to calculate the hourly household electrical loads for a complete year, the detailed calculation procedure is also described in Chapter 4. Another sub-technique, described in Chapter 5, is developed to attain the consumed hourly electricity values from an ASHP and/or a solar thermal system in order to meet all heating and hotwater demand based on realistic hourly household thermal loads. The predicted system performance is realistic and reflects the real life circumstance if a system integration occurs, and the obtained economic results give an accurate implication of an actual installed system. The chapter also demonstrates the

modification in the change of system configuration when realistic assumptions (economic and demand) are made.

6.3. The Integration Technique

The overall integration technique, displayed in a flowchart as shown in Figure 6.1, obtains the optimal configuration of a mono/hybrid micro-renewable electricity and/or a micro-renewable mono/hybrid thermal generation system. In this study, four types of renewable energy generation systems suitable for supplying domestic electricity, heating and hotwater are considered. These systems are micro wind turbines, solar PV systems (formed from sole capacity solar PV modules), ASHPs and solar thermal systems (formed from either flat plate solar thermal collector(s) or evacuated tube solar thermal collector(s)). The integration technique is implemented in MATLAB. The detailed description of the MATLAB model developed and the sample codes have been presented in Appendix E. The integration starts with the selection of a number of micro wind turbines, solar PV modules, ASHPs, a solar thermal flat plate collector and two solar thermal evacuated tube collectors for analysis. The orientation of both the solar PV modules and solar thermal collectors is set to face south as maximum solar radiation is received at this orientation when the solar systems are located in the northern hemisphere. The optimal slope of the solar PV module and the solar thermal collector is determined individually based on the maximum annual power production predicted from three solar PV systems assembled from three different capacities of solar PV modules, or two solar thermal systems assembled from solar flat plate collectors or solar evacuated tube collectors. All solar PV modules and solar thermal collectors are positioned at these optimal slopes respectively. The detailed description of optimal slope determination has been shown in Chapter 4 and Chapter 5. All combinations of

systems are considered and formed from the selected renewable energy technologies. The detailed formation of mono/hybrid micro-renewable electricity generation systems and mono/hybrid micro-renewable thermal generation systems has been described in Chapter 4 and Chapter 5 respectively. A database, stored in MATLAB, is set up to contain all available information in order to carry out the integration and determine the optimal system that satisfies the electricity, heating and hotwater demand for a domestic dwelling. In the database, the selected micro wind turbines and their hourly power outputs, the selected solar PV modules and their hourly power outputs, the selected ASHP, the selected solar flat plate/evacuated tube collectors, the hourly power inputs required to operate a mono or a hybrid micro-renewable thermal generation system for providing the entire heating and hotwater, the hourly power inputs to drive the primary and/or the auxiliary heating system and the electrical immersion in the hotwater storage cylinder, and hourly household electrical loads are all stored. It should be noted that the area of each solar PV module and of each solar thermal collector is also stored in the database. This allows one to restrict the total area permitted for installing solar types of systems if a renewable energy technology regulation is implemented, e.g. in order to qualify for the planning permission exemption in Ireland, the total area of solar PV modules and/or solar thermal collectors cannot be more than 12 m^2. Therefore, if this regulation is applied, a single solar PV system, a single solar thermal system or a combined solar PV system and solar thermal system, will have to be formed within this limit; other systems are not considered for economic analysis. However, this current study has not set the limitation on the total area of the solar PV system or the combined system consisting of a solar PV system. The renewable energy requirement is also applied into this overall integration in order to accomplish the desired percentage of the total electrical load requirement (both household electrical load and the electrical load

required for operating heating and hotwater generation systems) that must be satisfied from the on-site micro-renewable electricity generation system. Any micro-renewable electricity generation system that cannot satisfy the renewable energy requirement is eliminated from the economic analysis. For the systems that do satisfy the renewable energy requirement, the LCC is calculated based on the capital costs of the system(s), the cost of the imported electricity used, the revenue generated from the exported electricity to the grid, the costs of replacement of a micro wind turbine (without mast), solar PV modules, ASHPs and/or solar thermal collectors if the project lifespan is greater than the lifespan of the renewable energy devices themselves, the costs of replacement of inverter, circulating pump and/or solar pump unit, maintenance costs of each individual system and the salvage value. The salvage value is the value left in the device (exclusive of installation cost) if the lifespan of a device is longer than the desired project lifespan. In this integration technique, the major assumption made is that the entire capital cost of the micro-renewable electricity generation system and micro-renewable thermal generation system is funded from a loan. Capital grant options are also built into this integration technique. Once all possible system configurations have been analysed, the system having the lowest LCC is deemed the optimal choice and the system configuration is thus obtained.

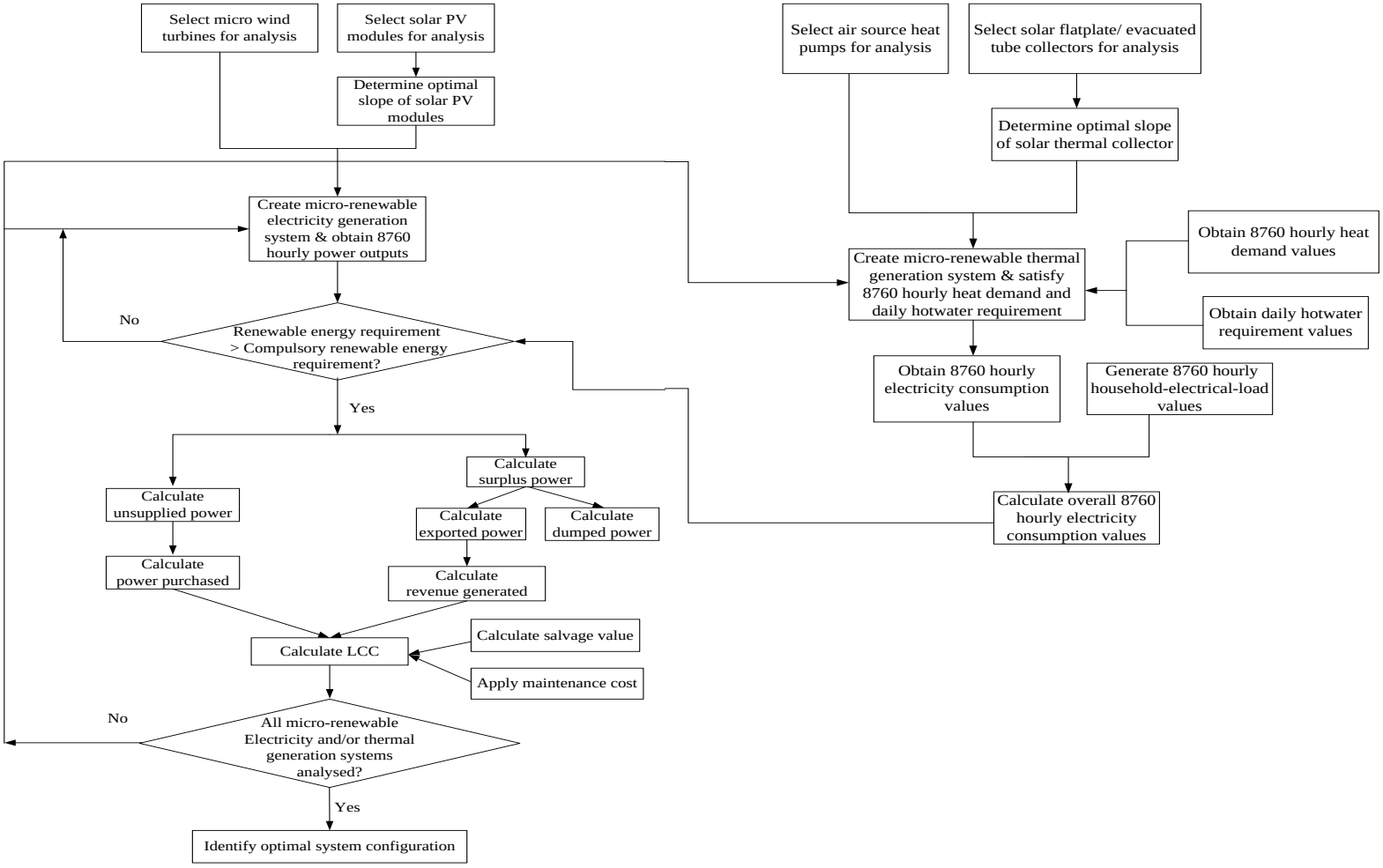

Figure 6.1. Grid-connected micro-renewable electricity and thermal generation integration technique.

6.4. Results and Discussion

The overall integration technique is applied to determine the optimal system that meets the entire electricity, heating and hotwater demand for a domestic dwelling in Ireland. The selected micro-renewable electricity generation technologies are micro wind turbines and solar PV modules, and the selected micro-renewable thermal generation technologies are ASHPs and solar thermal collectors; these selected systems for analysis represent other similar market-available micro wind turbines, solar PV modules, ASHPs and solar thermal collectors. The exemption conditions from planning permission are considered in the initial selection process. The hub height of a micro wind turbine is set at 10 m in this study as the total height including turbine blades cannot exceed 13 m in order to meet the exemption requirement. Micro wind turbines with a capacity of 6 kW generally have a diameter equal to or less than 6 m. The total area of an ASHP is the main constraint of selection; the selected ASHPs are all within this restriction which is less than 2.5 m^2. The solar thermal systems (formed from selected solar thermal collectors) also adhere to the conditions for exemption from planning permission. The maximum surface area of the thermal collectors in a solar thermal system must be less than or equal to 12 m^2 as stated in the exemption conditions. However, solar PV systems (formed from selected solar PV modules) are the only exceptions that are not designed to adhere to the conditions for exemption in this study. The solar PV system is sized based on the most commonly installed capacity range of domestic solar PV system which is less than or equal to 3 kW_p. The selected micro wind turbines are the Ampair 600-230, the Swift 1.5 kW, the Skystream 3.7, the Siliken 3.4, the Evance R9000 and the CF6d; the selected solar PV modules are the Sharp 235 W, the CareyGlass Solar 185 W and the Kyocera 135 W. The selected ASHPs are the Mitsubishi Ecodan W50 (rated at a thermal capacity of 5 kW), the Mitsubishi Ecodan W85 (rated at a thermal

capacity of 9 kW), the Mitsubishi Ecodan W140 (rated at a thermal capacity of 14 kW); the selected solar thermal collectors are the Kingspan flatplate collector, Kingspan evacuated tube collector HP400 and Kingspan evacuated tube collector HP450. Tables 4.6-4.8, Table 5.16 and Table 5.18 give relevant information for the selected micro wind turbines, the selected solar PV modules and the inverters employed, the selected ASHPs, and the solar thermal collectors employed respectively. This indicative information was obtained from either official websites or from personal communications. The system integration is carried out assuming the micro-renewable electricity and/or thermal generation system is installed in the Dublin area, with the following conditions and assumptions:

- An annual average ambient air temperature of 9.9^{o}C.
- An annual solar radiation value of 970 kWh/m^{2}.
- An annual average wind speed of 5.76 m/s.
- An average annual household electrical load of 5,016 kWh.
- An average annual household thermal load of 16,536 kWh.
- The daily hotwater requirement of 199.8 L at 60^{o}C.
- The Weibull k factor is 2.12, autocorrelation factor is 0.929, diurnal pattern strength is 0.156 and hour of peak wind speed is 14:00.
- The installed solar PV system and solar thermal system is south facing.
- The ground reflectance is 0.2.
- The efficiency of a solar-PV-system inverter is taken as 95%.
- An imported electricity price of €0.1928/kWh.
- An exported electricity tariff of €0.09/kWh.
- The maximum rate of electricity export is capped at 6 kW.

- A green loan having a loan rate of 4.5%.
- An annual inflation rate of 2.26%. This was the average annual inflation rate for Ireland for the period January 2001 to December 2010 [178].
- A solar thermal system capital grant of €800 and no capital grant available for other types of technologies.
- A 0% renewable energy requirement.
- The project lifespan is 20 years.

6.4.1. Economic Discussion and Identification of the Optimal System under Current Irish Conditions

The LCC of a micro-renewable electricity generation system and/or a micro-renewable thermal generation system has been calculated with the conditions given in the previous section. The overall system must satisfy electricity, heating and hotwater demand for a domestic dwelling and the system with the lowest LCC is determined as the optimal system over the project lifespan. The optimal system is deemed to consist of an ASHP having a thermal capacity of 14 kW which provides heating and preheats hotwater, an electrical immersion which heats water to the required temperature (60^{o}) and the electricity grid which supplies the electricity. This optimal system accomplished an LCC of €49,131 (this value is increased to €50,231 when making an economic comparison with conventional electricity, heating and hotwater generation systems, to account for the cost increase between the domestic heating distribution systems as explained in Chapter 5) over a 20-year project lifespan.

It should be noted that the economic analysis is carried out based on a best case scenario. The micro-renewable heating generation system is designed to connect with an underfloor heating system. However, an underfloor heating system is rarely installed for

Irish applications as traditional high-temperature radiators are still the dominant heating distribution system where a gas boiler or an oil boiler is employed for domestic heating generation. Therefore the economic outcome presented in this study is generally applicable to newly-built but also to existing dwellings with an underfloor heating system.

The economic viability of the optimal system is determined by comparing it with conventional electricity supply and domestic thermal (heating and hotwater) generation systems. The electricity grid is considered for electricity supply, and an oil or a natural gas boiler system is considered for domestic heating and hotwater supply. For providing the entire electricity, heating and hotwater, the LCC of a conventional combination of the electricity grid and an oil boiler system, and a combination of the electricity grid and a natural gas boiler system is €60,027 and €41,197 respectively for a 20-year project lifespan. Figure 6.2 shows the LCC comparison between the optimal micro-renewable energy generation system and the conventional generation systems. This clearly shows that the optimal system has an economic advantage over the conventional combination system consisting of an oil boiler and the electricity grid. However it has an economic disadvantage when compared to the system consisting of a natural gas boiler and the electricity grid. Electricity generation using a micro-renewable system is still very costly, and has not yet become competitive in comparison with the grid supplied electricity under the conditions stated in the study. The inclusion of any micro-renewable electricity generation system resulted in an increase in the overall LCC over the project lifespan. The hotwater demand and profile imposed particularly for the current study may affect the involvement of the solar thermal system for the overall optimal system selection. The majority of the hotwater demand is for morning and evening hours. However, there is very little or no solar radiation available to generate

hotwater for the demand required for morning hours; therefore, only hotwater demand for evening hours can be fully or partially satisfied from hotwater generated by the solar thermal system. In this case, the solar thermal system operates to its full strength; however it only partially meets the demand. If, in a different case, hotwater is demanded mainly from the afternoon to evening hours, then it is possible for the solar thermal system to meet most of the requirements, which results in the solar thermal system being more effective and enhances its economic viability. In this scenario there will be a better chance that the solar thermal system is chosen as part of the optimal system.

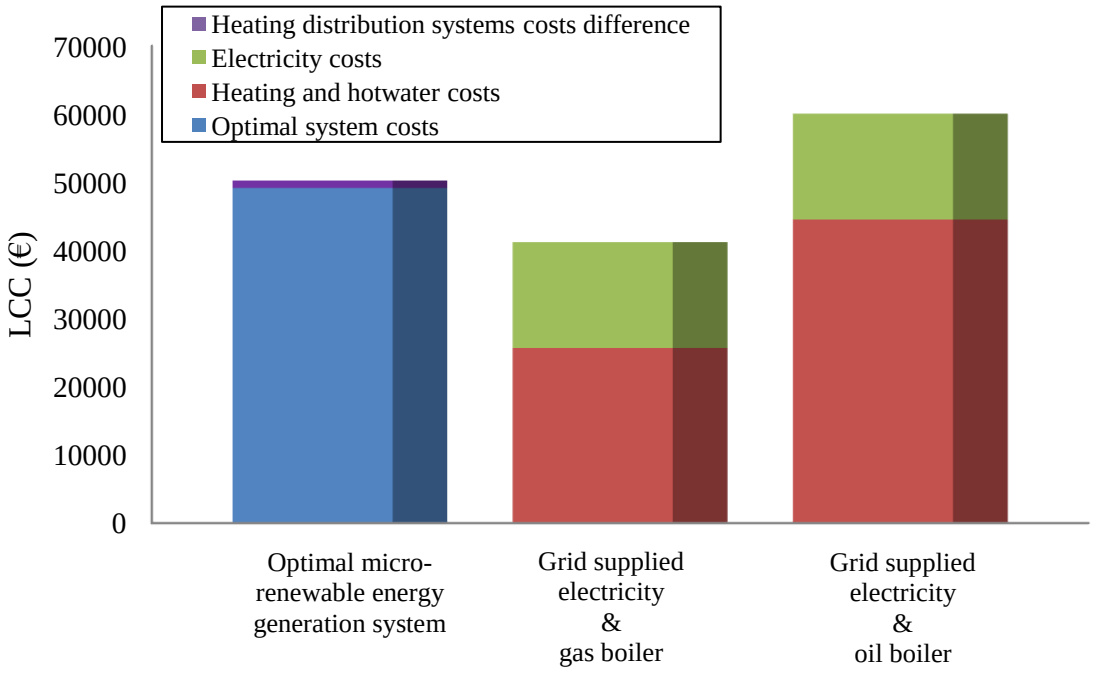

Figure 6.2. LCC comparison between the optimal micro-renewable energy generation system and conventional generation systems.

6.4.2. Effect of Imported Electricity Price on the Optimal System

A change in the imported electricity price can affect the economic evaluation of micro-renewable electricity and thermal generation systems individually and also the determination of the optimal system selection from each of the energy generation systems respectively, as presented in Chapter 4 and Chapter 5. However, due to the fact

that a micro-renewable electricity generation system can only produce electricity, therefore the increased imported electricity price, in this case, can help increase the savings made and improve the economic viability of the mono/hybrid systems available. Conversely, the micro-renewable thermal generation system can only consume electricity, the increased imported electricity price can result in an increased cost required to generate the same amount of heating and hotwater for a domestic dwelling. Consequently, this impairs the economic viability of the mono/hybrid systems available. For the overall integrated system, the electricity generated from a micro-renewable electricity generation system is more likely to be consumed in the location of production since an extra amount of electricity is required for operating the micro-renewable thermal generation system. The cost of the overall integrated system is likely to increase with increasing imported electricity price. A large capacity micro-renewable electricity generation system, with a high capital cost however, has to be installed in order to reduce the amount of grid supplied electricity and subsequently offset the added cost of electricity purchases. In another case as the electricity is supplied from the same capacity system, the increased overall cost is driven by the increased operational cost as the same amount of electricity has to be purchased from electricity grid, however at a higher price.

Figure 6.3 (LCC vs. imported electricity price) shows that the LCC of the optimal system, as expected, increases reasonably as the imported electricity price rises. From the results shown, a mono/hybrid micro-renewable electricity generation system is still not economically competitive when compared with the electricity supplied from electricity grid, even if the imported electricity price rises to €0.30/kWh. Neither a mono nor a hybrid micro-renewable electricity generation system was selected as a part of the integrated optimal system. The large thermal capacity of an ASHP (14 kW) has

been selected as the main heating system for all of the imported electricity prices investigated, and it also functions to preheat hotwater in the hotwater storage cylinder. When the imported electricity prices are relatively low (i.e. not significantly increased from the current price, e.g. €0.22/kWh and €0.24/kWh), there is no solar thermal system selected for the optimal system and the hotwater is heated by an electrical immersion to the desired temperature. However at higher imported electricity prices (€0.26/kWh, €0.28/kWh and €0.30/kWh), the solar thermal systems are selected at the current set up. This indicates that the cost of solar thermal system can be offset by the extra costs required to operate the electrical immersion when the imported electricity prices have significantly increased. It is important to recognise that the increased imported electricity prices can have a significant impact on the economic viability of the micro-renewable energy generation systems; furthermore it will also alter the determination of the components of the optimal system. If the weather conditions (wind speed and/or solar radiation) at a location are superior to the current weather conditions applied, then a micro-renewable electricity generation system is possible to be considered as part of the integrated system.

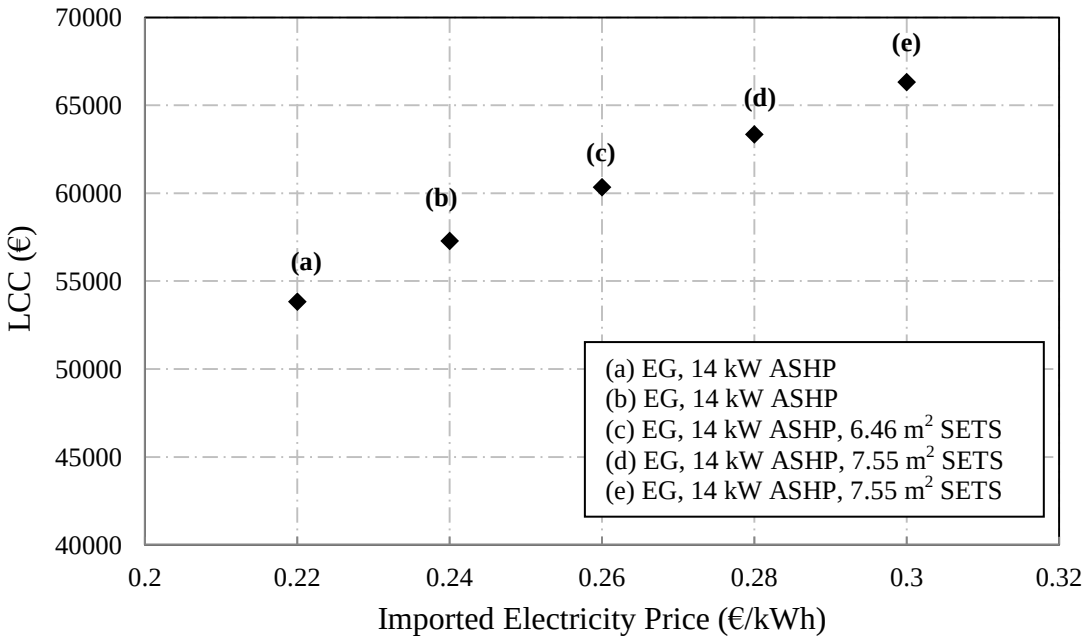

Figure 6.3. LCC of the optimal system versus imported electricity price. Exported electricity tariff is €0.09/kWh and the loan rate is 4.5%. EG= electricity grid, ASHP = air source heat pump and SETS= solar evacuated tube thermal system.

6.4.3. Effect of Exported Electricity Tariff on the Optimal System

The electricity generated from a micro-renewable electricity generation system is either used by the domestic dwelling or exported to the electricity grid. For the overall integrated system, this generated electricity is not only used to meet the consumption from lighting and electrical appliances existing within the dwelling, but also the extra electricity required to operate the ASHP and/or solar thermal system for heating and hotwater generation purpose. The majority of electricity generated is likely to be utilised at the location of production and therefore little is exported to the grid. An increase in exported electricity tariff however will still favour the installation of a micro-renewable electricity generation system. This will possibly even encourage the installation of a large capacity system due to the fact that more electricity can be exported at a higher tariff after the electricity demand is met.

Figure 6.4 (LCC vs. exported electricity tariff) shows that the LCC of the optimal system decreases significantly as the exported electricity tariff rises. There are two significant points that should be noted. First, when the exported electricity tariff reaches €0.23/kWh, the integrated micro-renewable generation system containing a 6 kW micro wind turbine and a 14 kW thermal capacity ASHP becomes truly economically viable compared with a conventional system having electricity supplied from the electricity grid, and heating and hotwater generated from a natural gas boiler system. The LCC (€38,187; this value is increased to €39,287 when takes into account the cost difference between heating distribution systems) of the micro-renewable energy generation system at this exported electricity tariff was lower than the conventional system that achieved the lowest LCC (€41,197) amongst all conventional systems. Second, the micro-renewable electricity generation was introduced as the main electricity supplying system rather than the electricity grid when the exported electricity tariff was €0.18/kWh. The increased revenue generated from exporting electricity helped this micro-renewable electricity generation system overcome the economic deficit between a micro wind turbine and grid supplied electricity, and made it become a more economically viable solution; hence it is included as part of the optimal system. It should also be noted that the wind speed at the location of interest (Dublin) in this study only represents an average wind speed in Ireland as a whole. There are many locations, especially areas on the coast that have a stronger and more consistent wind. The increased exported electricity tariff will certainly help even smaller capacity micro wind turbines, installed at these sites, become economically viable, even though an increased electricity demand has to be accounted for operating a micro-renewable thermal generation system.

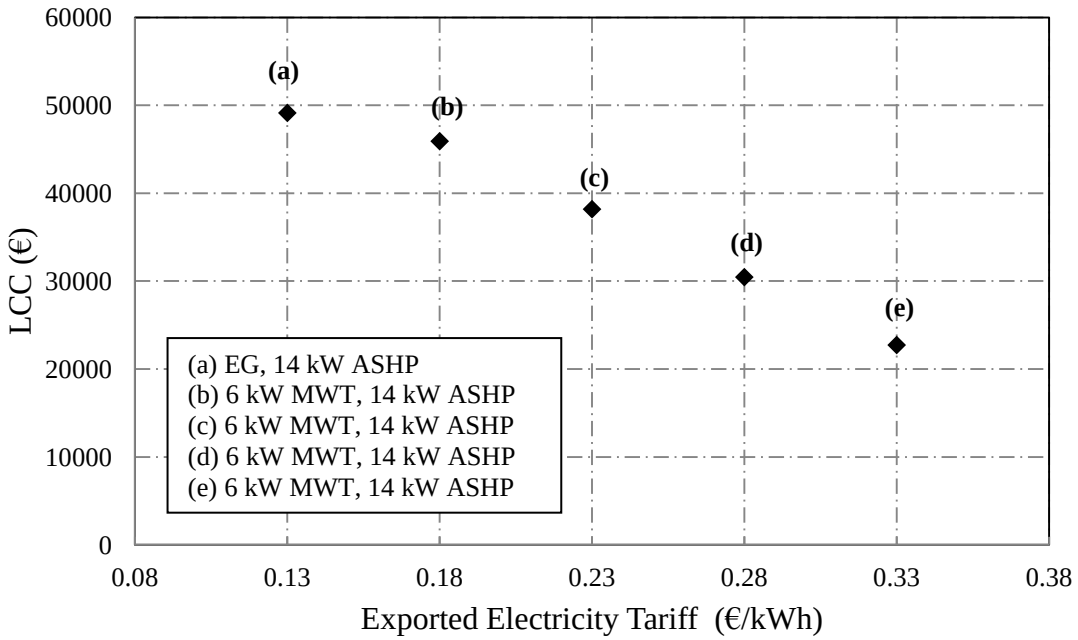

Figure 6.4. LCC versus exported electricity tariff. Imported electricity price is €0.1928/kWh and the loan rate is 4.5%. EG= electricity grid, ASHP = air source heat pump and MWT= micro wind turbine.

6.4.4. Effect of Renewable Energy Requirement on the Optimal System

For a net-zero-energy house identification, the amount of exported electricity has to be greater than or equal to the electricity supplied from the grid. There is no consideration of the electricity generated from a micro-renewable electricity generation system actually meets the amount of on-site electrical load in the dwelling. However, this renewable energy requirement imposes the user specified percentage of electricity demand must be satisfied by the on-site micro-renewable electricity generation system. Furthermore, if a high requirement is set, only the systems that are able to meet a sufficient amount of on-site electricity demand can be included for optimal system selection. There are several benefits which are observed when a large percentage of electricity demand is satisfied from the on-site micro-renewable electricity generation system. From a national point of view, this reduces the energy flows and related losses in transmission system; from a consumer point of view, this increases consumer's sense

of ownership and self-energy supply security, while also encouraging the use of a larger capacity of micro-renewable electricity generation system in order to make the most of local renewable energy available, and eliminating the effect of increasing imported electricity price.

Figure 6.5 (LCC vs. renewable energy requirement) shows that the LCC of the optimal system increases initially, followed by no alteration and then goes to infinity as the renewable energy requirement increases. The electricity supplied from the electricity grid is superior to any of the micro-renewable electricity generation system in terms of economic viability when there is no requirement of renewable energy requirement; a small capacity (2.4 kW) micro wind turbine was introduced to the overall integrated system to supply electricity in order to meet renewable energy requirement of 20%; the largest micro-wind turbine (6 kW) considered in this study was introduced into the overall integrated system when 40% or 60% of the overall electricity demand (electricity for domestic lighting and appliances, and operating the thermal generation systems) had to be met; however no mono/hybrid micro-renewable electricity generation system is capable of supplying a renewable energy requirement of 80%. This clearly shows that, under the current conditions stated, a mono/hybrid micro-renewable electricity generation system with a capacity larger than that considered in the study has to be used on site in order to meet the total or even the majority of the overall electricity demand. However, this can also be achieved from the existing systems in the study. For example, if a planning permission can be granted, micro wind turbines are allowed to be installed with a higher mast. Micro wind turbines, in general, harvest more energy and produce greater power at greater height. Therefore, with the enhanced power generated it is likely that the electricity demand will be met compared to micro wind turbines that are installed at a low height.

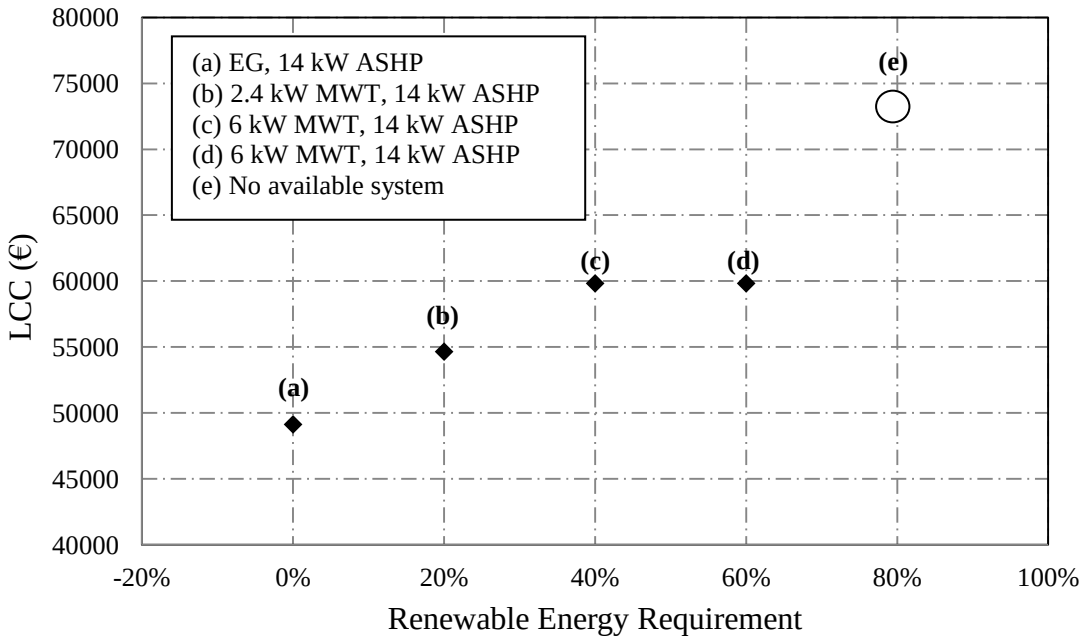

Figure 6.5. LCC versus renewable energy requirement. Imported electricity price is €0.1928/kWh, exported electricity tariff is €0.09/kWh and the loan rate is 4.5%. EG= electricity grid, ASHP = air source heat pump and MWT= micro wind turbine.

6.5. Conclusion

In this chapter, an overall technique is presented for the optimised integration of a grid-connected micro-renewable electricity generation system and a grid-connected micro-renewable thermal generation system in order to satisfy the entire electricity, heating and hotwater demand. Micro wind turbines and solar PV systems were considered in this study for micro-renewable electricity generation systems, the grid was also considered as the main electricity provider or as a backup system; ASHPs and solar thermal systems were considered in this study for micro-renewable thermal generation systems. A primary and an auxiliary electrical heating system, and an electrical immersion were also employed for the generation of space heating and hotwater. Six micro wind turbines, three solar PV modules (used to form the solar PV systems for analysis), three thermal capacity ASHPs, and a flat plate solar collector and two

evacuated tube solar thermal collectors (used to form the solar thermal systems for analysis) which are commercially-available and industry-representative were employed in this study. A database containing all considered micro wind turbines, solar PV modules, ASHPs and solar thermal collectors was established. However, the existing data is not restricted to these considered capacity systems; it can be also expanded to include any other capacity of micro-renewable electricity or thermal generation system for analysis. Applying the developed overall integration technique, the system which has the lowest LCC after the project lifespan is determined as the optimal system. Under the conditions stated in the study based on weather data obtained from Dublin, the optimal system is a system consisting of an ASHP having a thermal capacity of 14kW, and the electricity grid which provides all household electrical load and operates the heating and hotwater generation system. However, the LCC of this optimal system is greater than the LCC obtained from a conventional system whereby the electricity grid supplies the entire electricity demand, and a domestic gas boiler system provides all heating and hotwater. Therefore, the optimal system is deemed not economically viable in this comparison. Nevertheless, this optimal system shows its economic advantage over two other conventional systems: the electricity grid and a domestic oil boiler system, and the electricity grid alone to provide the entire electricity, heating and hotwater for a domestic dwelling. The micro-renewable electricity generation system is not considered as part of the optimal system under the conditions stated. The high capital costs and lack of financial supports make the micro-renewable electricity generation system unable to compete with the electricity grid. However, it should be noted that the weather conditions at many other locations are superior to the condition at the location for where this study was conducted, wind energy in particular. The micro-renewable electricity generation systems are likely to become economically viable if

they are installed at those locations. An ASHP is the only micro-renewable energy generation system contained in the optimal system. The mild weather conditions in Ireland can help an ASHP work efficiently, and become economically viable compared with other traditional heating generation systems, apart from a gas boiler system. ASHPs should be the preferred option in the locations without gas supply. The solar thermal system is, in general, the most commonly installed micro-renewable energy generation system. However, the time periods of hotwater demand for the domestic dwelling in the study, makes it difficult for the solar thermal system to be utilised to its full working capacity; therefore it becomes economically unviable. The hotwater generated from the system is most likely to use for the demand at nights while hotwater required for the mornings has to be met from an electrical immersion. Three parameter studies to assess the effect of imported electricity price, exported electricity tariff and renewable energy requirement have been performed. The LCC of the overall integrated systems increases moderately with an increased imported electricity price. The increased imported electricity price raises the LCC by increasing the cost of purchased electricity from the electricity grid when the household electrical load is not met from the mono/hybrid micro-renewable electricity generation system, as well as increasing the operational cost of running the micro-renewable thermal systems. However it should also be noted that the solar thermal systems gradually become economically viable over time. Conversely, the increased exported electricity tariff encourages the involvement of micro-renewable electricity generation systems. Micro wind turbines, in particular, have been selected to be part of the optimal system when the exported electricity tariff reaches to €0.18/kWh. Furthermore, all micro-renewable electricity generation systems benefit from the increased exported electricity tariffs, and will become economically viable when the electricity grid is taken as the reference point. There is no significant

effect on the micro-renewable thermal generation system, as the electricity generated from any of micro-renewable electricity generation is prioritised of supplying demand on site first and then exported to the electricity grid. The increased renewable energy requirement demands an increased capacity micro-renewable electricity generation system with the intention of meeting a user specified percentage of electricity demand from generation on site. The LCCs of the systems that fulfil the requirement increase along with the growing capacity of the systems. However, the current considered systems cannot meet the requirement if a high renewable energy requirement is enforced.

The decision of installing a micro-renewable electricity generation system and/or a micro-renewable thermal generation system should be made based on the realistic economic viability of these systems for every household. The weather condition at the location of interest, the household electrical load and the household thermal load are different and are all critically important factors for analysis for each case scenario. The renewable energy system market is also dynamic and continuously influenced by the advancements in technologies, the production in scale and the change of Irish government policies towards micro renewable energy technologies.

6.6. Summary

A novel optimised integration technique for grid-connected micro-renewable energy generation systems is presented in this chapter. The developed integration technique for selected micro-renewable electricity and thermal generation systems is described in detail. The results are then analysed and discussed.

CHAPTER 7
CONCLUSION AND RECOMMENDATION

7.1. Conclusion

In recent years, a number of studies have presented various developed techniques of system integration for electricity, heating and hotwater generation for residential and commercial buildings. However, many of the studies looked at either community-scale or apartment blocks rather than any individual domestic dwelling. The type of renewable energy technologies available, the capacity and quantity of the system required for the generation of a large amount of energy differs from the smaller amount of energy required such as for a domestic dwelling. The system combinations were also determined based on an artificial building/housing design; for example, a dwelling with provided U values for walls, attics, windows and doors where space heating is evaluated from the simulated design. Overall electricity demand is obtained based on the capacity of electrical appliances and lighting provided, and the number of hours that they operate. However, these approximations cannot provide accurate consumption data and will affect the system integration determination. In Ireland, the number of smart meters is on the increase; therefore it is possible that the exact consumption data may soon be obtained. However, very few studies so far have presented a purposely-developed technique for a system integration taking into account measured high-resolution electricity and heating load.

The net-zero-energy housing concept has been introduced for a number of years as shown in several studies demonstrated in the literature. In general, the systems satisfy this concept in which the amount of exported electricity is equal to or greater than the amount of imported electricity. This is a valid concept solution for an optimal system determination. However, this is not possible to reveal the percentage of electricity demand is satisfied by the on-site renewable electricity generation system. This concept can be meaningful for each individual householder; however, for a community or a nation this becomes less attractive approach since the issue of power transmission loss has still not been considered effectively. Despite this observation, very few studies have taken this into consideration.

The aim of this research study is to develop a novel technique to optimise the integration of grid-connected renewable energy technologies for a domestic dwelling in order to provide the entire electricity, heating and hotwater requirement. This generally-applicable and robust integration technique was developed to purposely employ high-resolution measured electrical and thermal load data and a user-specified renewable energy requirement. The technique was developed in three stages: a technique for the integration of grid-connected micro-renewable electricity generation systems, a technique for the integration of grid-connected micro-renewable thermal generation systems, and an overall technique for the integration of grid-connected micro-renewable energy generation systems.

The dwelling investigated in this study is assumed to represent a best case scenario, with the following assumptions being made:

- The dwelling is new and features an underfloor heating system so that an ASHP will work at its optimum condition.

- The dwelling is located in a rural region and is surrounded by open fields so that a relatively high wind speed is available for a micro wind turbine.
- The roof(s) of the dwelling are directly south-facing so that a relatively high solar radiation is received by solar PV modules and solar thermal collectors.
- A representative household electrical load and a distinctive household heating load are employed for an average Irish dwelling (a three/four-bedroom dwelling having a floor area of 120 m^2 and with two-four occupants).
- An average hotwater consumption rate is employed for a family of four occupants.

The integration of a grid-connected micro-renewable electricity generation system can be either a mono or a hybrid system and consists of a micro wind turbine and/or a solar PV system. A single micro wind turbine or a single solar PV system forms a mono system; a combination of both forms a hybrid system. This developed generally-applicable integration sub-technique was employed for an Irish application. Therefore, the technical and economical constraints and guidelines under specific conditions in Ireland were considered for the selection and integration process, and economic analysis. The NPV was the factor used to identify the optimal system available from a mono system or a hybrid system from six commercially-available micro wind turbines and/or a solar PV system assembled from three commercially-available solar PV modules. The hourly power outputs of the micro-renewable electricity generation system for one year were accurately and realistically predicted based on statistical calculations performed by applying a minimum weather data, i.e. monthly wind speed values and monthly solar radiation values. The realistic costs associated with each system considered in the study were also obtained. This ensures that the economic analysis carried out is accurate. The high-resolution, i.e. hourly household electrical

loads for one year were also calculated from an average annual household electrical load and an average annualised electrical load profile, and then used as the base load (electricity consumption from existing electrical appliances and lighting devices in a domestic dwelling) in the integration technique. This integration sub-technique is able to accurately predict system performance (either mono or hybrid) and then attains an economic outcome if an actual system was installed. Based on the economic results, the optimal system can be determined and the system configuration can then be obtained. The economic viability of the optimal system or any of the system can also be decided. This would give the householder a clear indication whether a micro-renewable electricity generation system is worthwhile to install, and what the most suitable system is in terms of economic benefit.

The integration of micro-renewable thermal generation system comprises an ASHP and/or a solar thermal system. The micro-renewable thermal generation system, either a mono system or a hybrid system, has to satisfy the entire heating and hotwater requirements for a domestic dwelling. The primary electrical heating system, the auxiliary electrical heating system and/or an electrical immersion can be also employed when necessary in order to achieve the domestic thermal requirement. This developed integration sub-technique considers technical and economic constraints and guidelines under current Irish conditions, and uses LCC to find the optimal system from selected three thermal capacity commercially-available ASHPs and three solar thermal collectors used to form a solar thermal system. The practical hourly heating loads and hourly hotwater demand for one year were obtained. The monthly ambient air temperature values and monthly solar radiation values were applied in order to statistically generate the reasonable hourly ambient air temperature values and hourly solar radiation values for an entire year respectively. Therefore, the energy outputs of the analysed ASHPs

and solar thermal systems can then be realistically predicted, and used to satisfy the obtained hourly heating loads and hotwater demand. The primary and/or auxiliary heating system, and/or an electrical immersion may be used when there is a deficit between the supply and demand. The predicted system performance and the obtained economic results can truly reflect the circumstance in which an actual system is installed in a domestic dwelling. The economic viability of the optimal system, or any mono/hybrid system, is decided based on comparing the LCC of the system with the LCC calculated from the most commonly employed conventional heating and hotwater generation systems whilst meeting the same domestic demand in Ireland. This can give a specific indication whether a micro-renewable thermal generation system is economically viable and/or justified to replace the current existing system available in the domestic dwelling. The result obtained from economic analysis is also used to select the optimal system for each case scenario.

The overall integration of grid-connected micro-renewable electricity generation systems and/or micro-renewable thermal generation systems is then developed and presented in Chapter 6. The four types of micro-renewable energy generation systems require no external fuel supply, besides being connected to the electricity grid. The micro-renewable thermal generation system, assisted by the auxiliary electrical heating system and immersion, is to provide the entire heating and hotwater demand for a domestic dwelling. The micro-renewable electricity generation system, supported by the electricity grid, is to supply electricity for satisfying the domestic electrical load and for running a micro-renewable thermal generation system. This overall integration technique is suitable for applications in all locations; Ireland was chosen to be analysed however. The optimal system is determined based on the least LCC achieved from an accurate economic analysis performed by realistically predicting power and energy

outputs from the selected commercially-available technologies and all system combinations. The economic viability of the micro-renewable energy generation systems was evaluated by comparing it with the economic outcome obtained from a conventional energy supply system available in the domestic dwelling. In this study, the conventional system takes into account the purchase of grid supplied electricity, combined with a heating and hotwater generating system from a domestic gas boiler system, a domestic oil boiler system or a domestic electrical heating system. This study gives an important economic indication for a domestic dwelling that has or is planning to have energy supplied from a micro-renewable energy generation system. Also, it shows whether any system can achieve an economic advantage over the conventional systems employed. The optimal system selected also presents the most economic benefit amongst all of the considered systems.

From the study shown, of all mono/hybrid renewable electricity generation systems, the optimal system is a single micro wind turbine having a capacity of 2.4 kW under current Irish conditions and that also meets the 50% renewable energy requirement; however this system is not economically viable since the calculated NPV is negative. It should be noticed that none of the analysed systems are economically viable even if there is no restriction of renewable energy requirement as all mono/hybrid systems considered can only attain a negative NPV. An assessment of the effect of varying household electrical load, imported electricity price, exported electricity tariff and wind speed was conducted. Firstly, from the assessment of the household electrical load, the NPV of the optimal system varies moderately with increasing household electrical load subjected to satisfy the 50% renewable energy requirement. However, the optimal system cannot achieve economic viability whether the household electrical load is low or high. It is also seen that a system assembled from the same capacity micro wind turbine and the

same capacity of solar PV modules will endure a reduced economic loss over the project lifespan as the household electrical load increases. Secondly, from the assessment of the imported electricity price, the NPV of the optimal system improves considerably as the imported electricity price increases. However, the optimal system is still not economically viable even if the imported electricity price reaches €0.30/kWh. The economic loss will be reduced for a system assembled from the same capacity micro wind turbine and the same capacity solar PV system as the imported electricity increases. Thirdly, from the assessment of exported electricity tariff, the NPV of the optimal system improves significantly with increasing exported electricity tariff. The optimal system which meets the 50% renewable energy requirement, is a micro wind turbine having a capacity of 6 kW when the exported electricity tariff is €0.18/kWh. This optimal system becomes economically viable since the NPV has turned from negative to positive. The effect of increasing exported electricity tariff results in a system assembled from the same capacity micro wind turbine and the same capacity solar PV system experiences further economic gain over the project lifespan. Finally, from the assessment of the wind speed, the optimal system which meets the 50% renewable energy requirement, is a micro wind turbine having a capacity of 2.4 kW and is nearly economically viable when the average wind speed reaches 7 m/s. Furthermore, the optimal system, a micro wind turbine having a capacity of 6 kW, is economically viable when the average wind speed reaches 8 m/s since it has a positive NPV and also meets the renewable energy requirement. A system assembled from the same capacity micro wind turbine and the same capacity solar PV system will endure a modest economic loss or even becomes economically viable at the location having a good annual average wind speed.

From the study shown, of all micro-renewable thermal generation systems, the optimal system is an ASHP having a thermal capacity of 14 kW and no solar thermal system, and assisted by an auxiliary electrical heating system and an electrical immersion. This optimal system satisfies the entire heating and hotwater requirement for a domestic dwelling. This optimal system is economically viable if this system is compared with an oil boiler system or an electrical heating system since its LCC is lower than the LCC of these two conventional systems; this optimal system however is not determined economically viable when compared with a natural gas boiler system since the LCC of this system is greater than the LCC of the natural gas boiler system providing the same amount of heating and hotwater. Two parameter studies were carried out to assess the effect of household heating load and imported electricity price on the optimal system determination. From the assessment of household heating load, the LCC of the optimal system increases moderately with an increasing household heating load. However, it should be noted that this assessment was carried out differently from the assessment of household electrical load. A unique profile is corresponded with each of the household heating load, from low to high, rather than scaling down or up an annual household electrical load and utilising an identical load profile. A system assembled from the same thermal capacity ASHP and the same size of solar thermal system would economically cost more over the project lifespan as the household heating load increases. From the assessment of the imported electricity price, the rising operation cost caused by the increased imported electricity price leads to the LCC of the optimal system increasing moderately. A system assembled from the same capacity ASHP and the same size solar thermal system will have to suffer a larger cost in order to satisfy the same heating and hotwater requirement if the imported electricity price increases.

From the study shown, of the integration of all grid-connected micro-renewable electricity and thermal generation systems, the optimal system is a system in which electricity is supplied from the electricity grid, and heating and hotwater are provided from an ASHP having a thermal capacity of 14 kW with assistance from an auxiliary electrical heating system and an electrical immersion. This optimal system is however not economically viable when it is judged based on a comparison made with a conventional system comprising grid supplied electricity, and heating and hotwater is provided from a natural gas boiler system. However, this optimal system can be declared economically viable if compared with two other conventional systems: grid supplied electricity, heating and hotwater are provided from an electrical heating system; or grid supplied electricity, and heating and hotwater are supplied from an oil boiler system. The effect of the imported electricity price, the exported electricity tariff and the renewable energy requirement were investigated. Based on the results obtained from the imported electricity price study, the LCC of the optimal system increases reasonably as the imported electricity price rises. The component of the optimal system includes an ASHP having a 14 kW thermal capacity, no solar thermal system and without any micro-renewable electricity generation system when the imported electricity price has not increased significantly. However, the solar thermal system is determined as part of the optimal system when the imported electricity price has risen considerably. The optimal system is not economically viable at the current imported electricity price when compared with a conventional system consisting of the grid supplied electricity and a gas boiler system. Furthermore the optimal system could be in an even worse economic circumstance if the imported electricity price has risen significantly, and possibly resulted in becoming not economically viable even if compared with a conventional system containing the grid supplied electricity and an oil

boiler system. The parameter study of the exported electricity tariff shows that the LCC of the optimal system decreases significantly as the exported electricity tariff increases. Even though the current exported electricity tariff offered cannot help the optimal system become economically viable, an increased exported electricity tariff would have significant impact on the economic viability of the systems. The optimal system can genuinely become economically viable even if it is compared with a system comprising the grid supplied electricity and a natural gas boiler system when the exported electricity tariff is €0.23/kWh as the study shown. The result also shows that the optimal system consists of a micro wind turbine having a capacity of 6 kW and an ASHP having a thermal capacity of 14 kW when the exported electricity tariff is €0.18/kWh; this indicates that micro-renewable electricity generation is introduced as the main electricity supply system rather than the electricity grid. Finally, from the study of renewable energy requirement demonstrates that the LCC of the optimal system increases initially, follows by no alteration and then becomes infinity as the renewable energy requirement increases. The optimal system includes a micro wind turbine having a low capacity (2.4 kW) at first. However, a large capacity micro wind turbine is required in order to satisfy the increased renewable energy requirement, and eventually there is no system available for optimal system determination as none of them are able to provide the amount of electricity required for household consumption.

The developed integration technique can perform a very detailed and accurate economic analysis for grid-connected micro-renewable energy generation systems to provide electricity, heating and hotwater for a domestic dwelling. The results obtained provide extremely valuable information for each householder to assess the economic viability of the systems considered; thereafter the optimal system is determined based on the maximum economic benefit achieved.

However, it should be noted that the analyses undertaken in this study are based on a best case scenario. For example, the solar PV modules considered in this study are assumed to be directly south-facing even though the roofs of many Irish dwellings may not be directly south-facing. As such, the PV modules and thermal collectors may not function as efficiently as predicted in this study. As the assumed conditions do not adequately characterise the entire Irish housing stock, careful consideration should be given before drawing any policy-related conclusions from the results presented in this study.

Under the stated conditions and the selected commercially-available systems in the study, most of the systems presented are not economically viable compared with the conventional electricity, heating and hotwater generation systems. The high capital costs and the lack of financial support from the government are the two main reasons which resulted in this economic drawback. The cost of manufacturing micro-renewable energy generation systems has been gradually decreasing, e.g. the cost of solar PV generation per Watt has decreased significantly from early 2000 to the present. The innovation and improvement in technologies, the massive increase in production, alternate materials utilisation etc, resulted in reduced costs for the micro-renewable energy generation systems. Ireland has an extremely good wind conditions, and even if the cost of micro wind turbines do not significantly reduce in the near future, they are still likely to achieve economic viability providing they are installed at a location with a good wind resource. On average Ireland receives as much solar radiation as most parts of Germany where solar PV and solar thermal have been widely employed for domestic applications. There is a potential that solar technologies can be extensively exploited here. The marine climate ensures that Ireland is rarely too cold in seasons in which heating and hotwater are required. An ASHP would be an ideal choice for many domestic

applications for providing heating and hotwater. This has been proven from the results shown as an ASHP is always selected to be a part of the optimal system, and can genuinely become economically viable if it is compared with some of the conventional systems. An offered grant can be the most direct support for any of the micro-renewable energy generation system implementation. However, there is no national grant or deployment programme available towards micro wind turbines and solar PV systems. It is extremely likely to have a very positive reaction from a householder if a grant is offered for micro wind turbines and solar PV systems as demonstrated in the period when the incentive electricity tariff was offered. The number of micro wind turbines and solar PV systems installed had increased considerably; much improved from the period before the incentive electricity tariff had been offered, in particular for micro wind turbines. The added economic benefit of installing a micro-renewable electricity generation system can be considered as one of the most important factors for this increased number of systems installed. The same effect has also been noticed during the period when grants were offered for ASHPs and solar thermal systems under the Greener Homes Scheme. The number of installations had been stimulated which shows the very positive outcome of offering grants for householders. However, there is currently only a single grant available for solar thermal systems in Ireland. The very limited grants available make it very difficult for micro-renewable energy generation systems being used more extensively for domestic application. Grants can be offered in many forms, such as direct capital grants, reinstating the previously-ceased incentive exported electricity tariff, improved generally-applied exported electricity tariff, reduced tax/levy on purchasing the micro-renewable energy generation systems etc. A micro-renewable energy generation system will likely to become a popular choice for electricity, heating and hotwater generation in Ireland in the future since there is an

abundant renewable energy source available and if an appropriate grant programme is offered. The developed integration sub-techniques and overall technique for micro-renewable electricity generation systems, micro-renewable thermal generation systems, or a hybrid of both can certainly help domestic dwellings achieve sustainable living and maximise economic effectiveness.

7.2. Limitations

The locations where micro wind turbine can be installed are restricted as an urban area is generally not practical since there is no open field. The micro wind turbines considered in this study are primarily suitable for installation in locations surrounded by wide open fields where relatively high wind speeds are observed. The wind speed in an urban area is typically lower than locations where wide fields are available. The adverse effect of dwellings on the wind speed can also result in the reduction of power output from micro wind turbines. Up to 28% of the total number of dwellings is possibly located in less compact dwelling regions and could be suitable for micro wind turbine installation in Ireland. Nonetheless, the option of a micro wind turbine for electricity generation should be eliminated for the analysis if the investigated dwelling is not located in a suitable site.

Secondly, the household electrical load profile used in this study was an average annualised electrical load profile. This profile was the only credited profile available for conducting this research study at the time. However, it should be noted that each domestic dwelling has its own unique electrical load profile. This is directly related to the occupants' behaviour, and the electrical appliances available and their usage. This study has demonstrated that various domestic heating loads can have an impact on the LCC analysis of the considered systems; therefore, various household electrical loads

with their unique profiles are also likely to influence the outcome of the economic analysis and, subsequently, affect the selection of the optimal system. However, it is important to recognise that this developed integration technique is generally applicable. The adopted hourly household electrical loads for a year describe the electrical demand in an average Irish dwelling (defined as the total residential energy demand divided by the number of permanently occupied dwellings and approximately represents a three/four-bedroom dwelling having a floor area of 120 m^2 and with two-four occupants) [5], and is used to demonstrate the proposed integration technique. This set of hourly household electrical loads is only applicable to this employed dwelling and does not account for variations in the electrical demand which are very likely to occur from one dwelling to another. The employed hourly household electrical loads do not characterise the electrical demand of the entire Irish housing stock and, in the practical application of the proposed integration technique, an accurately-measured electrical load should be generated and considered for each individual investigated household.

Thirdly, the adopted hourly household heating loads (with a unique heating demand profile) describe the heating demand in a chosen Irish dwelling having a total annual usage, in the form of fossil fuels, that is very close to the energy consumption of an average dwelling (a three/four-bedroom dwelling having a floor area of 120 m^2 and with two-four occupants), and is used to demonstrate the proposed integration technique. This set of hourly household heating loads is only applicable to this employed dwelling and does not account for variations in the heating demand which are very likely to occur from one dwelling to another. The employed hourly household heating loads do not characterise the heating demand of the entire Irish housing stock and, in the practical application of the proposed integration technique, an accurately-measured heating load should be generated and considered for each individual investigated household.

Fourthly, the domestic hotwater demand and profile comes from the EU reference Tapping Cycle Number 3. This was repetitively used for each day of the year; therefore there is no weekday and weekend, and seasonal variance shown. However, this demand and profile is still the most suitable to represent the general domestic scenario since there is very few data available on variety of domestic hotwater loads for Irish applications. Nonetheless, the integration technique is developed to accurately perform economic analysis and then determine the optimal system. The hotwater demand and profile applied into the technique should be, ideally, measured and recorded for the investigated domestic dwelling. The general demand and profile would provide important indicative information for an average domestic dwelling; however, it is not possible to provide a specific figure for an individual case.

Fifthly, the solar thermal system described in this study is used for generating hotwater only. However, the solar thermal system can be also used for space heating generation in some practical cases, especially for locations in a tropical climate. The hotwater generated is more than enough to satisfy the entire hotwater demand, and can also provide the partial heating requirement. Ireland is located in the region of the temperate climate. The hotwater generated from solar thermal systems installed is unlikely to satisfy the entire hotwater demand; hence it is even more difficult to contribute for heating. The majority of solar thermal systems are installed for the sole purpose of supplying domestic hotwater in Ireland. Only in limited number cases that they are installed for the purpose of supplying both heating and hotwater. This study reasonably takes the general approach to which solar thermal system is set up for the hotwater generation alone.

Sixthly, concerning the use of batteries to reduce the amount of exported electricity, the proposed technique is focused on grid-connected systems due to the fact that batteries

are very costly, and both their lifespan and performance is difficult to predict. Also, sizing the capacity of batteries is complex. In particular, if the capacity of the batteries is oversized, the economic analysis results will be negatively impacted due to increases in both their initial and replacement cost.

Seventhly, a carbon tax was not taken into consideration for the up-to-date analysis. There is currently no such tax applied for electricity consumption. A rate of carbon tax is difficult to predict, and it may not be appropriated to assume the same as the current carbon tax rate that is imposed on domestic heating fossil fuels in Ireland. Also, the micro-renewable thermal generation systems are all electricity-driven systems, and the CO_2 emission saved from local consumption of the natural gas or the oil has to be considered to offset the CO_2 emission caused if the electricity is supplied by the electricity grid. Thus, the cost saving made on utilising the micro-renewable thermal generation system is not possible to perform since the carbon tax for electricity generation is unknown. However, this will be one of the important factors to be considered in future analyses if a carbon tax is imposed on electricity generation in Ireland.

Finally, the personal discount rate is defined as the rate at which an individual trades current for future currency [337]. The determination of the personal discount rate is a provocative subject with important implications for many aspects of economic behaviour and public policy [337]. The personal discount rate used for an investment project varies with the time delay of the reward or penalty and also varies with income and other personal characteristics. One approach to determine the rate for an investment project is to consider the cost of capital which has to be recovered by the investor to warrant the investment [338]. The opportunity cost of capital [339] or the weighted average cost of capital [340] are commonly employed as the discount rate for an

investment project. A different approach is to choose the rate of return on an investment project as the discount rate. For a domestic household, due to uncertainties such as the investment period, availability of capital, income and non-economic factors, the expected rate of return can vary significantly [338]. Another approach to choosing the discount rate for an investment project is the relevant going market interest rates faced by the individual (whether a borrower or a lender) [339]. The methodology of employing the real interest rate as the discount rate is adopted in this study. This methodology is supported by several previous studies [21, 34, 35, 37, 38, 43, 97, 268, 341-352]. For example, Hong et al. conducted a study to develop a framework for the implementation of building-scale new renewable energy systems (solar photovoltaic, solar thermal, geothermal, and wind energy systems). The discount rate was calculated from the nominal interest rate and inflation rate, and was used to estimate the LCC in this study [342]. Marszal et al. conducted a study to investigate the LCC of different renewable energy supply options for a net zero energy building in Denmark. The real interest rate was used as the discount rate to calculate the LCC in the study [21]. Ringwood et al. conducted a study to estimate the economics of renewable microgeneration of electricity from wind and solar energy sources, and the annual percentage rate (interest rate offered by the loan issuer) was used as the discount rate to calculate the discounted payback period [97]. Janjai et al. conducted a study to investigate the potential application of concentrating solar power systems for producing electricity in Thailand and the debt interest rate was used as the discount rate to calculate the levelised cost [352]. Alphen et al. conducted a study to quantify and evaluate the potential of solar and wind resources in the Maldives for electricity applications, and the real interest rate was used to discount all future cash flows and thereafter to calculate the NPV [348]. As explained previously however, this

methodology of adopting the real interest rate is only one of several possible approaches which have been proposed for determining the discount rate.

The discount rate adopted in this study could be considered low due to the fact that the nominal interest rate of the selected green loan is also rather low (4.5%) and represents a best case scenario. However, in general, the personal loan rate from Irish banks is typically higher than the value used in the current study, e.g. Bank of Ireland offers a personal loan rate of 11.5% [353]. If the current rate from Bank of Ireland is applied, the real interest rate (discount rate) would be increased to a value of 9.03%. The discount rate used to perform economic analyses can vary considerably. For example, the discount rate specified by the Irish Department of Communication, Energy and Natural Resource ranges from 5% to 8% for various energy generation and/or supply projects [32]. The European Wind Energy Association generally utilises a discount rate of 7.5% for wind power generation [354]; however a rate of 10% is used by the International Renewable Energy Agency as wind power generation projects are considered to have a relatively high risk [355]. Additionally, a discount rate of between 6% and 8% is used for residential solar PV systems by the same agency [356]. The United States Department of Energy however employs a low discount rate of 3% for projects related to energy conservation, renewable energy resources and water conservation [357]. The SEAI normally utilises a discount rate of 8% when performing economic analyses of renewable energy generation systems for Irish applications [358]. If this rate is adopted for the current analysis, the optimal micro-renewable energy generation system is deemed to consist of an ASHP having a thermal capacity of 9 kW which supplies heating and preheats hotwater, an electrical immersion is employed to heat water to the required temperature (60^{o}), and grid-supplied electricity. This optimal system achieved an LCC of €34,355 (this value is increased to €35,455 when making an

economic comparison with conventional electricity, heating and hotwater generation systems, to account for the cost increase between the domestic heating distribution systems) over a 20-year project lifespan. It is worth noting that the specification of the higher discount rate has an effect upon the optimal system configuration. A 9 kW ASHP is obtained as the optimal system rather than the 14 kW ASHP due to the fact that the operational cost becomes less when it is discounted at a higher value. However, the higher discount rate used does not alter the determination of the system economic viability in this case. The optimal system is not economically viable when compared with a conventional energy supply system consisting of grid-supplied electricity and a gas boiler system; this system combination achieved an LCC of €26,357. Conversely, the optimal system remains economically viable when compared with the conventional system consisting of grid-supplied electricity and an oil boiler system which obtained an LCC of €38,456. Rather than assuming a discount rate, it should be selected (calculated) based on each individual household situation. Although the current study provides valuable information in the case where a low discount rate is adopted, the results should be carefully considered before making any policy-related conclusions. Clearly, this issue should be considered as a potential avenue for future research in this area.

7.3. Recommendation for Future Research

The investigation of domestic household electrical load may be carried out in order to find the effect of various profiles on the economic analysis. A number of measured hourly electrical load data had been made available from research performed through smart metering trial by CER. Two possible avenues can be explored for future research. Firstly, the hourly electrical loads are statistically the same in magnitude however having varies electrical load profiles; these loads can be applied into the study and used

as the based electrical load. The obtained economic analysis results and thus determined optimal system should give an indication if variation in electrical load profile would make any impact and the significance of the impact. Secondly, a more realistic approach can be taken to perform the parameter study. Each selected household electrical load has a different magnitude (from low to high) and its unique load profile. In general, a decrease or an increase in the overall household electrical load is more likely to be caused by reducing or extending the distribution of the hourly household electrical load rather than scaling the hourly load down or up.

This can be also expanded to the use of various domestic hotwater loads if an investigation of the effect is required. The domestic hotwater load is entirely based on each householder's consumption habit. The domestic hotwater load used in this study is for a typical family in which it is assumed the occupants have day-time work. The load may vary significantly if the occupants spend large time in the dwelling; the hotwater usage could be increased in total quantity, and also be more distributed and less peaked. The season variance could also affect the hotwater usage. The domestic hotwater load is possible to have an impact on the optimal system determination from an economic analysis performed. For example, the solar thermal system is used more effectively if the majority of hotwater is consumed in the afternoon or evening; the electrical immersion is turn on less frequently as most hotwater consumed is likely to be generated from the solar thermal system. In contrast to this, if the hotwater is consumed mostly in the morning, the solar thermal system can hardly provide any useful hotwater for the occupants' usage. The electrical immersion has to turn on regularly in order to satisfy the hotwater demand. Another example, the water supply (cold water) is preheated by an ASHP once it is on. This is likely to happen in the seasons which heating is required; therefore less energy is required from an electrical immersion to

heat the hotwater to the desired temperature. However, during the period of no heating demand, the solar thermal system with help from an electrical immersion is used to bring the hotwater temperature to the required standard. Therefore, the real hotwater consumption load is desirable if available. This is possible to achieve an even more realistic result than the current employed domestic hotwater load in the study.

GSHPs or WSHPs can be investigated and integrated into the considered systems in the study. Like ASHP, these two heat pumps are electricity-driven devices, therefore the electricity generated from micro wind turbines and/or solar PV systems assisted by the electricity grid can operate these heating and hotwater generation systems, and no solid or liquid fuel is required e.g. gas, oil, biomass. A GSHP or a WSHP can be used to replace an ASHP considered in the study to be the main heating supply system. For a GSHP, the configuration of the pipes that absorb heat from the soil has to be decided, either horizontal or vertical. In order to accurately predict the energy output from a GSHP, several main factors have to be decided in advance, such as:

- the size of the land available and the depth planned for laying down the pipes for a horizontal system
- the depth of borehole, and an open loop or a closed loop for a vertical system
- the efficiency of the heat pump unit
- the heating distribution system employed in the domestic dwelling

For a WSHP, there are also factors that have to be verified at the initial process such as the availability of the water source, and the temperature of the water source and its variance over the year. These two heat pump systems should be eliminated if the heat source is not available e.g. there is not enough land to install a horizontal loop pipe for a GSHP system. The methods of integrating a heat pump system and a solar thermal system are presented in numerous ways, in particular for the combination of a GSHP

and a solar thermal system. The most traditional way is to have a GSHP or a WSHP to generate heating and also preheat water, and the solar thermal system is used to heat the hotwater alone. Another ways is to have a GSHP or a WSHP generate heating and hotwater, and the solar thermal system assists the heat pump for both heating and hotwater generation. There are other newer ways implemented such as the solar heat collected is used to recharge the soil during the summer months with the purpose of GSHP can absorb more heat during heating seasons, thus increasing the heat pump efficiency. Therefore the method of integration should be also determined. In order to carry out the most accurate economic analysis, the detailed cost of the heat pump systems should be provided in the integration technique. The hourly power inputs of any considered system should be added into the data base. The installation cost of a GSHP is significantly higher than an ASHP because of the extra cost involved such as drilling, purchasing, and laying pipes. However, a GSHP generally has a higher COP and a lower operational cost than an ASHP since the variation of soil temperature is small during the year, unlike the ambient air temperature which fluctuates considerably during the year. There is a possibility that a GSHP or a WSHP to be more cost effective under an individual scenario. The use of a GSHP or a WSHP can be a valid recommended future study; however the heat transfer between soil and fluid flowing in the pipe, and the heat transfer in the heat exchanger between the heat pump and the domestic heating distribution system should be completely understood and applied into the study.

BIBLIOGRAPHY

1. Martin Howley, et al., Energy in Ireland 1990 - 2011. 2012.

2. Ireland's Greenhouse Gas Emission Projections 2012 -2030. 2013.

3. Delivering A Sustainable Energy Future For Ireland, M.a.N.R. Department of Communications, Editor. 2007.

4. Allen, S.R., G.P. Hammond, and M.C. McManus, Prospects for and barriers to domestic micro-generation: A United Kingdom perspective. Applied Energy, 2008. 85(6): p. 528-544.

5. Dennehy, E. and M. Howley, Energy in the Residential Sector. 2013, Sustainable Energy Authority of Ireland.

6. McCarthy, M., ESBN NC6 Stats. 2011, Sustainable Energy Authority Ireland.

7. Planning and development regulations 2007, H.a.L.G. Department of Environment, Editor. 2007.

8. Li, Z., F. Boyle, and A. Reynolds, Domestic application of micro wind turbines in Ireland: Investigation of their economic viability. Renewable Energy, 2012. 41(0): p. 64-74.

9. Li, Z., F. Boyle, and A. Reynolds, Domestic application of solar PV systems in Ireland: The reality of their economic viability. Energy, 2011. 36(10): p. 5865-5876.

10. Connect a Micro-Generator, E.S.B. (ESB), Editor. 2009, Electricity Supply Board

11. Athienitis, A.K.a.M.S., Thermal analysis and design of passive solar buildings. 2002: James & James (Science Publishers) Ltd.

12. Passive solar heating project analysis. 2004, RETScreen International.

13. Connolly, D., et al., A review of computer tools for analysing the integration of renewable energy into various energy systems. Applied Energy, 2010. 87(4): p. 1059-1082.

14. Athienitis, A.K. and M. Santamouris, Thermal analysis and design of passive solar buildings. 2002: James & James (Science Publishers) Ltd.

15. Yu, Z., et al., Experiment and prediction of hybrid solar air heating system applied on a solar demonstration building. Energy and Buildings, 2014. 78(0): p. 59-65.

16. Elkinton, M.R., J.G. McGowan, and J.F. Manwell, Wind power systems for zero net energy housing in the United States. Renewable Energy, 2009. 34(5): p. 1270-1278.

17. Wang, L., J. Gwilliam, and P. Jones, Case study of zero energy house design in UK. Energy and Buildings, 2009. 41(11): p. 1215-1222.

18. Marszal, A.J. and P. Heiselberg, Life cycle cost analysis of a multi-storey residential Net Zero Energy Building in Denmark. Energy, 2011. 36(9): p. 5600-5609.

19. Carrilho da Graça, G., A. Augusto, and M.M. Lerer, Solar powered net zero energy houses for southern Europe: Feasibility study. Solar Energy, 2012. 86(1): p. 634-646.

20. Milan, C., C. Bojesen, and M.P. Nielsen, A cost optimization model for 100% renewable residential energy supply systems. Energy, 2012. 48(1): p. 118-127.

21. Marszal, A.J., et al., On-site or off-site renewable energy supply options? Life cycle cost analysis of a Net Zero Energy Building in Denmark. Renewable Energy, 2012. 44(0): p. 154-165.

22. Kapsalaki, M., V. Leal, and M. Santamouris, A methodology for economic efficient design of Net Zero Energy Buildings. Energy and Buildings, 2012. 55(0): p. 765-778.

23. Goodbody, C., et al., Regional integration of renewable energy systems in Ireland – The role of hybrid energy systems for small communities. International Journal of Electrical Power & Energy Systems, 2013. 44(1): p. 713-720.

24. Thygesen, R. and B. Karlsson, Economic and energy analysis of three solar assisted heat pump systems in near zero energy buildings. Energy and Buildings, 2013. 66(0): p. 77-87.

25. Sinha, S. and S.S. Chandel, Review of software tools for hybrid renewable energy systems. Renewable and Sustainable Energy Reviews, 2014. 32(0): p. 192-205.

26. Lee, K.-H., et al., Preliminary determination of optimal size for renewable energy resources in buildings using RETScreen. Energy, 2012. 47(1): p. 83-96.

27. Hagos, D.A., A. Gebremedhin, and B. Zethraeus, Towards a flexible energy system – A case study for Inland Norway. Applied Energy, 2014. 130(0): p. 41-50.

28. Ouellette, A., et al., Achieving emissions reduction through oil sands cogeneration in Alberta's deregulated electricity market. Energy Policy, 2014. 71(0): p. 13-21.

29. Sáfián, F., Modelling the Hungarian energy system – The first step towards sustainable energy planning. Energy, 2014. 69(0): p. 58-66.

30. Sen, R. and S.C. Bhattacharyya, Off-grid electricity generation with renewable energy technologies in India: An application of HOMER. Renewable Energy, 2014. 62(0): p. 388-398.

31. Prasetyaningsari, I., A. Setiawan, and A.A. Setiawan, Design Optimization of Solar Powered Aeration System for Fish Pond in Sleman Regency, Yogyakarta by HOMER Software. Energy Procedia, 2013. 32(0): p. 90-98.

32. Adaramola, M.S., Viability of grid-connected solar PV energy system in Jos, Nigeria. International Journal of Electrical Power & Energy Systems, 2014. 61(0): p. 64-69.

33. Al-Karaghouli, A. and L.L. Kazmerski, Optimization and life-cycle cost of health clinic PV system for a rural area in southern Iraq using HOMER software. Solar Energy, 2010. 84(4): p. 710-714.

34. Fazelpour, F., N. Soltani, and M.A. Rosen, Feasibility of satisfying electrical energy needs with hybrid systems for a medium-size hotel on Kish Island, Iran. Energy, 2014. 73(0): p. 856-865.

35. Kim, H., et al., Optimal green energy management in Jeju, South Korea – On-grid and off-grid electrification. Renewable Energy, 2014. 69(0): p. 123-133.

36. Shafiullah, G.M., et al., Prospects of renewable energy – a feasibility study in the Australian context. Renewable Energy, 2012. 39(1): p. 183-197.

37. Demiroren, A. and U. Yilmaz, Analysis of change in electric energy cost with using renewable energy sources in Gökceada, Turkey: An island example. Renewable and Sustainable Energy Reviews, 2010. 14(1): p. 323-333.

38. Fantidis, J.G., et al., Cost of PV electricity – Case study of Greece. Solar Energy, 2013. 91(0): p. 120-130.

39. Silva, S.B., M.M. Severino, and M.A.G. de Oliveira, A stand-alone hybrid photovoltaic, fuel cell and battery system: A case study of Tocantins, Brazil. Renewable Energy, 2013. 57(0): p. 384-389.

40. Abdilahi, A.M., et al., Feasibility study of renewable energy-based microgrid system in Somaliland′s urban centers. Renewable and Sustainable Energy Reviews, 2014. 40(0): p. 1048-1059.

41. Kusakana, K., Techno-economic analysis of off-grid hydrokinetic-based hybrid energy systems for onshore/remote area in South Africa. Energy, 2014. 68(0): p. 947-957.

42. Castellanos, J.G., et al., Modelling an off-grid integrated renewable energy system for rural electrification in India using photovoltaics and anaerobic digestion. Renewable Energy, 2015. 74(0): p. 390-398.

43. Hafez, O. and K. Bhattacharya, Optimal planning and design of a renewable energy based supply system for microgrids. Renewable Energy, 2012. 45(0): p. 7-15.

44. Asrari, A., A. Ghasemi, and M.H. Javidi, Economic evaluation of hybrid renewable energy systems for rural electrification in Iran—A case study. Renewable and Sustainable Energy Reviews, 2012. 16(5): p. 3123-3130.

45. Adaramola, M.S., S.S. Paul, and O.M. Oyewola, Assessment of decentralized hybrid PV solar-diesel power system for applications in Northern part of Nigeria. Energy for Sustainable Development, 2014. 19(0): p. 72-82.

46. Dalton, G.J., D.A. Lockington, and T.E. Baldock, Feasibility analysis of stand-alone renewable energy supply options for a large hotel. Renewable Energy, 2008. 33(7): p. 1475-1490.

47. Gupta, A., et al., A conceptual framework to support solar PV simulation using an open-BIM data exchange standard. Automation in Construction, 2014. 37(0): p. 166-181.

48. Rajkumar, R.K., et al., Techno-economical optimization of hybrid pv/wind/battery system using Neuro-Fuzzy. Energy, 2011. 36(8): p. 5148-5153.

49. Rahman, M.M., et al., Hybrid application of biogas and solar resources to fulfill household energy needs: A potentially viable option in rural areas of developing countries. Renewable Energy, 2014. 68(0): p. 35-45.

50. Chargui, R. and H. Sammouda, Modeling of a residential house coupled with a dual source heat pump using TRNSYS software. Energy Conversion and Management, 2014. 81(0): p. 384-399.

51. Hobbi, A. and K. Siddiqui, Optimal design of a forced circulation solar water heating system for a residential unit in cold climate using TRNSYS. Solar Energy, 2009. 83(5): p. 700-714.

52. Kalogirou, S.A., Use of TRNSYS for modelling and simulation of a hybrid pv–thermal solar system for Cyprus. Renewable Energy, 2001. 23(2): p. 247-260.

53. Li, H., L. Sun, and Y. Zhang, Performance investigation of a combined solar thermal heat pump heating system. Applied Thermal Engineering, 2014. 71(1): p. 460-468.

54. Soussi, M., M. Balghouthi, and A. Guizani, Energy performance analysis of a solar-cooled building in Tunisia: Passive strategies impact and improvement techniques. Energy and Buildings, 2013. 67(0): p. 374-386.

55. Ampatzi, E. and I. Knight, Modelling the effect of realistic domestic energy demand profiles and internal gains on the predicted performance of solar thermal systems. Energy and Buildings, 2012. 55(0): p. 285-298.

56. Baniyounes, A.M., M.G. Rasul, and M.M.K. Khan, Assessment of solar assisted air conditioning in Central Queensland's subtropical climate, Australia. Renewable Energy, 2013. 50(0): p. 334-341.

57. Abdelhady, S., D. Borello, and E. Tortora, Design of a small scale stand-alone solar thermal co-generation plant for an isolated region in Egypt. Energy Conversion and Management, 2014. 88(0): p. 872-882.

58. Ferrara, M., et al., A simulation-based optimization method for cost-optimal analysis of nearly Zero Energy Buildings. Energy and Buildings, 2014. 84(0): p. 442-457.

59. Pärisch, P., et al., Short-term experiments with borehole heat exchangers and model validation in TRNSYS. Renewable Energy, 2015. 74(0): p. 471-477.

60. Ruschenburg, J., T. Ćutić, and S. Herkel, Validation of a black-box heat pump simulation model by means of field test results from five installations. Energy and Buildings, 2014. 84(0): p. 506-515.

61. Pärisch, P., et al., Investigations and model validation of a ground-coupled heat pump for the combination with solar collectors. Applied Thermal Engineering, 2014. 62(2): p. 375-381.

62. Kalogirou, S.A. and C. Papamarcou, Modelling of a thermosyphon solar water heating system and simple model validation. Renewable Energy, 2000. 21(3–4): p. 471-493.

63. Ayompe, L.M., et al., Validated TRNSYS model for forced circulation solar water heating systems with flat plate and heat pipe evacuated tube collectors. Applied Thermal Engineering, 2011. 31(8–9): p. 1536-1542.

64. Ruiz, E. and P.J. Martínez, Analysis of an open-air swimming pool solar heating system by using an experimentally validated TRNSYS model. Solar Energy, 2010. 84(1): p. 116-123.

65. Hazami, M., et al., Long-term performances prediction of an evacuated tube solar water heating system used for single-family households under typical Nord-African climate (Tunisia). Solar Energy, 2013. 94(0): p. 283-298.

66. Kamel, R.S. and A.S. Fung, Modeling, simulation and feasibility analysis of residential BIPV/T+ASHP system in cold climate—Canada. Energy and Buildings, 2014. 82(0): p. 758-770.

67. Qu, M., H. Yin, and D.H. Archer, A solar thermal cooling and heating system for a building: Experimental and model based performance analysis and design. Solar Energy, 2010. 84(2): p. 166-182.

68. Wang, W., Z. Tian, and Y. Ding, Investigation on the influencing factors of energy consumption and thermal comfort for a passive solar house with water thermal storage wall. Energy and Buildings, 2013. 64(0): p. 218-223.

69. Kalogirou, S.A., Artificial neural networks in renewable energy systems applications: a review. Renewable and Sustainable Energy Reviews, 2001. 5(4): p. 373-401.

70. Azadeh, A., R. Babazadeh, and S.M. Asadzadeh, Optimum estimation and forecasting of renewable energy consumption by artificial neural networks. Renewable and Sustainable Energy Reviews, 2013. 27(0): p. 605-612.

71. Velik, R. and P. Nicolay, Grid-price-dependent energy management in microgrids using a modified simulated annealing triple-optimizer. Applied Energy, 2014. 130(0): p. 384-395.

72. Garlík, B. and M. Křivan, Renewable energy unit commitment, with different acceptance of balanced power, solved by simulated annealing. Energy and Buildings, 2013. 67(0): p. 392-402.

73. Baños, R., et al., Optimization methods applied to renewable and sustainable energy: A review. Renewable and Sustainable Energy Reviews, 2011. 15(4): p. 1753-1766.

74. Pezzini, P., O. Gomis-Bellmunt, and A. Sudrià-Andreu, Optimization techniques to improve energy efficiency in power systems. Renewable and Sustainable Energy Reviews, 2011. 15(4): p. 2028-2041.

75. Novoa, C. and T. Jin, Reliability centered planning for distributed generation considering wind power volatility. Electric Power Systems Research, 2011. 81(8): p. 1654-1661.

76. Rahmani, R., et al., Hybrid technique of ant colony and particle swarm optimization for short term wind energy forecasting. Journal of Wind Engineering and Industrial Aerodynamics, 2013. 123, Part A(0): p. 163-170.

77. Sanchez, V.M., et al., Techno-economical optimization based on swarm intelligence algorithm for a stand-alone wind-photovoltaic-hydrogen power system at south-east region of Mexico. International Journal of Hydrogen Energy, 2014. 39(29): p. 16646-16655.

78. Mohandes, M.A., Modeling global solar radiation using Particle Swarm Optimization (PSO). Solar Energy, 2012. 86(11): p. 3137-3145.

79. Hakimi, S.M. and S.M. Moghaddas-Tafreshi, Optimal sizing of a stand-alone hybrid power system via particle swarm optimization for Kahnouj area in south-east of Iran. Renewable Energy, 2009. 34(7): p. 1855-1862.

80. Rezaei Mirghaed, M. and R. Roshandel, Site specific optimization of wind turbines energy cost: Iterative approach. Energy Conversion and Management, 2013. 73(0): p. 167-175.

81. Khatib, T., A. Mohamed, and K. Sopian, Optimization of a PV/wind micro-grid for rural housing electrification using a hybrid iterative/genetic algorithm: Case study of Kuala Terengganu, Malaysia. Energy and Buildings, 2012. 47(0): p. 321-331.

82. Aparicio Ruiz, P., et al., An integrated optimisation method for residential building design: A case study in Spain. Energy and Buildings, 2014. 80(0): p. 158-168.

83. Kaabeche, A., M. Belhamel, and R. Ibtiouen, Techno-economic valuation and optimization of integrated photovoltaic/wind energy conversion system. Solar Energy, 2011. 85(10): p. 2407-2420.

84. Petersen, S. and S. Svendsen, Method for component-based economical optimisation for use in design of new low-energy buildings. Renewable Energy, 2012. 38(1): p. 173-180.

85. Kaabeche, A. and R. Ibtiouen, Techno-economic optimization of hybrid photovoltaic/wind/diesel/battery generation in a stand-alone power system. Solar Energy, 2014. 103(0): p. 171-182.

86. Nfah, E.M., Evaluation of optimal photovoltaic hybrid systems for remote villages in Far North Cameroon. Renewable Energy, 2013. 51(0): p. 482-488.

87. Böhringer, C. and T.F. Rutherford, Integrated assessment of energy policies: Decomposing top-down and bottom-up. Journal of Economic Dynamics and Control, 2009. 33(9): p. 1648-1661.

88. Giannantoni, C., et al., Multicriteria approach for the improvement of energy systems design. Energy, 2005. 30(10): p. 1989-2016.

89. Prasad, A.R. and E. Natarajan, Optimization of integrated photovoltaic–wind power generation systems with battery storage. Energy, 2006. 31(12): p. 1943-1954.

90. Zhou, W., et al., Current status of research on optimum sizing of stand-alone hybrid solar–wind power generation systems. Applied Energy, 2010. 87(2): p. 380-389.

91. Clancy, M. and J. Scheer, Energy Forecasts for Ireland to 2020. 2011, Sustainable Energy Authority Ireland.

92. Dihrab, S.S. and K. Sopian, Electricity generation of hybrid PV/wind systems in Iraq. Renewable Energy, 2010. 35(6): p. 1303-1307.

93. Yang, H., Z. Wei, and L. Chengzhi, Optimal design and techno-economic analysis of a hybrid solar–wind power generation system. Applied Energy, 2009. 86(2): p. 163-169.

94. Hoicka, C.E. and I.H. Rowlands, Solar and wind resource complementarity: Advancing options for renewable electricity integration in Ontario, Canada. Renewable Energy, 2011. 36(1): p. 97-107.

95. Essalaimeh, S., A. Al-Salaymeh, and Y. Abdullat, Electrical production for domestic and industrial applications using hybrid PV-wind system. Energy Conversion and Management, 2013. 65(0): p. 736-743.

96. Arribas, L., et al., PV–wind hybrid system performance: A new approach and a case study. Renewable Energy, 2010. 35(1): p. 128-137.

97. Kelleher, J. and J.V. Ringwood, A computational tool for evaluating the economics of solar and wind microgeneration of electricity. Energy, 2009. 34(4): p. 401-409.

98. Howley, M., et al., Energy in Ireland 1990 – 2011. November 2012.

99. Small wind turbines: The unsung heroes of the wind industry. Refocus, 2002. 3(2): p. 30-36.

100. Şahin, A.D., Progress and recent trends in wind energy. Progress in Energy and Combustion Science, 2004. 30(5): p. 501-543.

101. How wind power works. 2012 [cited 2014 04 02]; Available from: http://science.howstuffworks.com/environmental/green-science/wind-power1.htm.

102. Lenzen, M. and J. Munksgaard, Energy and CO2 life-cycle analyses of wind turbines—review and applications. Renewable Energy, 2002. 26(3): p. 339-362.

103. Micro wind turbines for domestic applications. 2007 [cited 2014 02 08]; Available from: http://www.tsunamigreen.com/FrontPagePanel?page=1.

104. Wind Over Ireland. 2012, The Irish Meteorological Service Online.

105. Roaf, S., M. Fuentes, and S. Thomas-Rees, Ecohouse. 3rd Edition ed. 2007: Routledge.

106. A horizontal axis wind turbine. 2013 [cited 2014 05 06]; Available from: http://www.microgreening.com/micro-generation/wind-turbines.php.

107. A vertical axis wind turbine. 2013 [cited 2014 04 23]; Available from: http://www.solar.excluss.com/contact-excluss-solar.html.

108. Peacock, A.D., et al., Micro wind turbines in the UK domestic sector. Energy and Buildings, 2008. 40(7): p. 1324-1333.

109. Sunderland, K.M., G. Mills, and M.F. Conlon, Estimating the wind resource in an urban area: A case study of micro-wind generation potential in Dublin, Ireland. Journal of Wind Engineering and Industrial Aerodynamics, 2013. 118(0): p. 44-53.

110. Seguro, J.V. and T.W. Lambert, Modern estimation of the parameters of the Weibull wind speed distribution for wind energy analysis. Journal of Wind Engineering and Industrial Aerodynamics, 2000. 85(1): p. 75-84.

111. Li, Z., A. Reynolds, and F. Boyle, Domestic integration of micro-renewable electricity generation in Ireland – The current status and economic reality. Renewable Energy, 2014. 64(0): p. 244-254.

112. Markvart, T., Solar Electricity. 2nd Edition ed. 2000: John Wiley and Sons.

113. Boyle, G., Renewable Energy Power for a Sustainable Future. 2nd Edition ed. 2004: Oxford University Press.

114. Lacour, A., Performance and Policy Evaluation of Solar Energy Technologies for Domestic Application in Ireland, in School of Civil and Building Services 2011, Dublin Institute of Technology: Dublin.

115. McNicholl, A. and J.O. Lewis, Green Design: Sustainable Building for Ireland. 1996: Stationery Office.

116. HOMER, How HOMER Calculates the Radiation Incident on the PV Array. 2013, HOMER.

117. Trinuruk, P., C. Sorapipatana, and D. Chenvidhya, Estimating operating cell temperature of BIPV modules in Thailand. Renewable Energy, 2009. 34(11): p. 2515-2523.

118. Alonso García, M.C. and J.L. Balenzategui, Estimation of photovoltaic module yearly temperature and performance based on Nominal Operation Cell Temperature calculations. Renewable Energy, 2004. 29(12): p. 1997-2010.

119. Wohlgemuth, J.H. and S.J. Ransome, Performance of BP Solar tandem junction amorphous silicon modules in Photovoltaic Specialists Conference. 2002, Conference Record of the Twenty-Ninth IEEE.

120. Photovoltaic system performance monitoring – Guidelines for measurement, data exchange and analysis, International Electrotechnical Commission: Geneva, Switzerland.

121. Ayompe, L.M., et al., Measured performance of a 1.72 kW rooftop grid connected photovoltaic system in Ireland. Energy Conversion and Management, 2011. 52(2): p. 816-825.

122. Nagelkerke, N.J.D., A Note on a General Definition of the Coefficient of Determination. Biometrika, 1991. 78(3): p. 691-692.

123. Gueymard, C., Prediction and Performance Assessment of Mean Hourly Global Radiation. Solar Energy, 2000. 68(3): p. 285-303.

124. Orsini, A., et al., Cloud cover classification through simultaneous ground-based measurements of solar and infrared radiation. Atmospheric Research, 2002. 61(4): p. 251-275.

125. Fuentes, M., et al., Application and validation of algebraic methods to predict the behaviour of crystalline silicon PV modules in Mediterranean climates. Solar Energy, 2007. 81(11): p. 1396-1408.

126. Kaldellis, J.K., et al., Experimental validation of autonomous PV-based water pumping system optimum sizing. Renewable Energy, 2009. 34(4): p. 1106-1113.

127. Ma, T., H. Yang, and L. Lu, Solar photovoltaic system modeling and performance prediction. Renewable and Sustainable Energy Reviews, 2014. 36(0): p. 304-315.

128. Molina, M.G. and E.J. Espejo, Modeling and simulation of grid-connected photovoltaic energy conversion systems. International Journal of Hydrogen Energy, 2014. 39(16): p. 8702-8707.

129. Zogou, O. and H. Stapountzis, Experimental validation of an improved concept of building integrated photovoltaic panels. Renewable Energy, 2011. 36(12): p. 3488-3498.

130. Zhou, W., H. Yang, and Z. Fang, A novel model for photovoltaic array performance prediction. Applied Energy, 2007. 84(12): p. 1187-1198.

131. Sarhaddi, F., et al., An improved thermal and electrical model for a solar photovoltaic thermal (PV/T) air collector. Applied Energy, 2010. 87(7): p. 2328-2339.

132. Hernández-Moro, J. and J.M. Martínez-Duart, Analytical model for solar PV and CSP electricity costs: Present LCOE values and their future evolution. Renewable and Sustainable Energy Reviews, 2013. 20(0): p. 119-132.

133. Amori, K.E. and H.M. Taqi Al-Najjar, Analysis of thermal and electrical performance of a hybrid (PV/T) air based solar collector for Iraq. Applied Energy, 2012. 98(0): p. 384-395.

134. Tadj, M., K. Benmouiza, and A. Cheknane, An innovative method based on satellite image analysis to check fault in a PV system lead–acid battery. Simulation Modelling Practice and Theory, 2014. 47(0): p. 236-247.

135. da Silva, R.M. and J.L.M. Fernandes, Hybrid photovoltaic/thermal (PV/T) solar systems simulation with Simulink/Matlab. Solar Energy, 2010. 84(12): p. 1985-1996.

136. Tonui, J.K. and Y. Tripanagnostopoulos, Performance improvement of PV/T solar collectors with natural air flow operation. Solar Energy, 2008. 82(1): p. 1-12.

137. Di Vincenzo, M.C. and D. Infield, Detailed PV array model for non-uniform irradiance and its validation against experimental data. Solar Energy, 2013. 97(0): p. 314-331.

138. Liu, Y., et al., A comparative study of the maximum power point tracking methods for PV systems. Energy Conversion and Management, 2014. 85(0): p. 809-816.

139. Jung, T.H., et al., Output characteristics of PV module considering partially reverse biased conditions. Solar Energy, 2013. 92(0): p. 214-220.

140. Saber, E.M., et al., PV (photovoltaics) performance evaluation and simulation-based energy yield prediction for tropical buildings. Energy, 2014. 71(0): p. 588-595.

141. Casares, F.J., et al., Mathematical approach to the characterization of daily energy balance in autonomous photovoltaic solar systems. Energy, 2014. 72(0): p. 393-404.

142. Amori, K.E. and M.A. Abd-AlRaheem, Field study of various air based photovoltaic/thermal hybrid solar collectors. Renewable Energy, 2014. 63(0): p. 402-414.

143. Su, Y., et al., Real-time prediction models for output power and efficiency of grid-connected solar photovoltaic systems. Applied Energy, 2012. 93(0): p. 319-326.

144. Gupta, B.L., M. Bhatnagar, and J. Mathur, Optimum sizing of PV panel, battery capacity and insulation thickness for a photovoltaic operated domestic refrigerator. Sustainable Energy Technologies and Assessments, 2014. 7(0): p. 55-67.

145. Lo Brano, V., A. Orioli, and G. Ciulla, On the experimental validation of an improved five-parameter model for silicon photovoltaic modules. Solar Energy Materials and Solar Cells, 2012. 105(0): p. 27-39.

146. Ji, J., et al., Experimental comparison of two PV direct-coupled solar water heating systems with the traditional system. Applied Energy, 2014. 136(0): p. 110-118.

147. Mohanty, P., et al., MATLAB based modeling to study the performance of different MPPT techniques used for solar PV system under various operating conditions. Renewable and Sustainable Energy Reviews, 2014. 38(0): p. 581-593.

148. Mazumdar, B.M., M. Saquib, and A.K. Das, An empirical model for ramp analysis of utility-scale solar PV power. Solar Energy, 2014. 107(0): p. 44-49.

149. Dyreson, A.R., et al., Modeling solar irradiance smoothing for large PV power plants using a 45-sensor network and the Wavelet Variability Model. Solar Energy, 2014. 110(0): p. 482-495.

150. Ashhab, M.d.S.S., H. Kaylani, and A. Abdallah, PV solar system feasibility study. Energy Conversion and Management, 2013. 65(0): p. 777-782.

151. Pavlović, T., et al., Possibility of electricity generation using PV solar plants in Serbia. Renewable and Sustainable Energy Reviews, 2013. 20(0): p. 201-218.

152. Tyagi, V.V., et al., Progress in solar PV technology: Research and achievement. Renewable and Sustainable Energy Reviews, 2013. 20(0): p. 443-461.

153. Kaplani, E. and S. Kaplanis, A stochastic simulation model for reliable PV system sizing providing for solar radiation fluctuations. Applied Energy, 2012. 97(0): p. 970-981.

154. Hocaoglu, F.O., O.N. Gerek, and M. Kurban, The effect of model generated solar radiation data usage in hybrid (wind–PV) sizing studies. Energy Conversion and Management, 2009. 50(12): p. 2956-2963.

155. Ismail, M.S., M. Moghavvemi, and T.M.I. Mahlia, Characterization of PV panel and global optimization of its model parameters using genetic algorithm. Energy Conversion and Management, 2013. 73(0): p. 10-25.

156. Kaushika, N.D., N.K. Gautam, and K. Kaushik, Simulation model for sizing of stand-alone solar PV system with interconnected array. Solar Energy Materials and Solar Cells, 2005. 85(4): p. 499-519.

157. Shah, R., et al., A review of key power system stability challenges for large-scale PV integration. Renewable and Sustainable Energy Reviews, 2015. 41(0): p. 1423-1436.

158. Kharb, R.K., et al., Modeling of solar PV module and maximum power point tracking using ANFIS. Renewable and Sustainable Energy Reviews, 2014. 33(0): p. 602-612.

159. Zahedi, A., Maximizing solar PV energy penetration using energy storage technology. Renewable and Sustainable Energy Reviews, 2011. 15(1): p. 866-870.

160. Zahedi, A., Development of an economical model to determine an appropriate feed-in tariff for grid-connected solar PV electricity in all states of Australia. Renewable and Sustainable Energy Reviews, 2009. 13(4): p. 871-878.

161. Hoppmann, J., et al., The economic viability of battery storage for residential solar photovoltaic systems – A review and a simulation model. Renewable and Sustainable Energy Reviews, 2014. 39(0): p. 1101-1118.

162. White, L.V., B. Lloyd, and S.J. Wakes, Are Feed-in Tariffs suitable for promoting solar PV in New Zealand cities? Energy Policy, 2013. 60(0): p. 167-178.

163. Saloux, E., A. Teyssedou, and M. Sorin, Analysis of photovoltaic (PV) and photovoltaic/thermal (PV/T) systems using the exergy method. Energy and Buildings, 2013. 67(0): p. 275-285.

164. Urmee, T. and D. Harries, The solar home PV program in Fiji – A successful RESCO approach? Renewable Energy, 2012. 48(0): p. 499-506.

165. Buker, M.S., B. Mempouo, and S.B. Riffat, Performance evaluation and techno-economic analysis of a novel building integrated PV/T roof collector: An experimental validation. Energy and Buildings, 2014. 76(0): p. 164-175.

166. Shum, K.L. and C. Watanabe, An innovation management approach for renewable energy deployment—the case of solar photovoltaic (PV) technology. Energy Policy, 2009. 37(9): p. 3535-3544.

167. Bakhshi, R., J. Sadeh, and H.-R. Mosaddegh, Optimal economic designing of grid-connected photovoltaic systems with multiple inverters using linear and nonlinear module models based on Genetic Algorithm. Renewable Energy, 2014. 72(0): p. 386-394.

168. Dubey, S. and G.N. Tiwari, Analysis of PV/T flat plate water collectors connected in series. Solar Energy, 2009. 83(9): p. 1485-1498.

169. Gang, P., et al., Annual analysis of heat pipe PV/T systems for domestic hot water and electricity production. Energy Conversion and Management, 2012. 56(0): p. 8-21.

170. Geisemeyer, I., et al., Prediction of silicon PV module temperature for hot spots and worst case partial shading situations using spatially resolved lock-in thermography. Solar Energy Materials and Solar Cells, 2014. 120, Part A(0): p. 259-269.

171. Tossa, A.K., et al., A new approach to estimate the performance and energy productivity of photovoltaic modules in real operating conditions. Solar Energy, 2014. 110(0): p. 543-560.

172. Castañeda, M., et al., Sizing optimization, dynamic modeling and energy management strategies of a stand-alone PV/hydrogen/battery-based hybrid system. International Journal of Hydrogen Energy, 2013. 38(10): p. 3830-3845.

173. Zhang, Q., et al., Integration of PV power into future low-carbon smart electricity systems with EV and HP in Kansai Area, Japan. Renewable Energy, 2012. 44(0): p. 99-108.

174. Liu, G., et al., Techno-economic simulation and optimization of residential grid-connected PV system for the Queensland climate. Renewable Energy, 2012. 45(0): p. 146-155.

175. Khatib, H., Economic Evaluation of Projects in the Electricity Supply Industry. 2003: The Institution of Engineering and Technology.

176. McAllister, E.W., Pipeline Rules of Thumb Handbook. Seventh Edition ed. A Manual of Quick, Accurate Solutions to Everyday Pipeline Engineering Problems. 2009: Elsevier.

177. Eschenbach, T.G., Engineering Economy - Applying Theory to Practice 3rd Edition ed: Oxford University Press.

178. Inflation rate. 2012, European Central Bank.

179. Swift rooftop wind energy system (Swift)--- frequently asked questions. 2007, Cascade renewable energy.

180. Small three-bladed horizontal axis wind turbine --- Skystream. 2012, Archi expo.

181. The price list and technical data of siliken 3.4 and siliken 4.1 micro wind turbines. 2011, Siliken wind energy.

182. Ibrahim, A., et al., Recent advances in flat plate photovoltaic/thermal (PV/T) solar collectors. Renewable and Sustainable Energy Reviews, 2011. 15(1): p. 352-365.

183. C&F6d wind turbine specification,performance and price data. 2011, C&F green energy.

184. Mondol, J.D., Y.G. Yohanis, and B. Norton, The impact of array inclination and orientation on the performance of a grid-connected photovoltaic system. Renewable Energy, 2007. 32(1): p. 118-140.

185. Best Practice Guide Photovoltaics (PV), Sustainable Energy Authority of Ireland.

186. Energy price statistics. 2012, European Commision.

187. Feed-in tariffs scheme. 2012, Energy saving trust UK.

188. Rourke, F.O., F. Boyle, and A. Reynolds, Renewable energy resources and technologies applicable to Ireland. Renewable and Sustainable Energy Reviews, 2009. 13(8): p. 1975-1984.

189. Module pricing. 2012, NPD Solarbuzz.

190. Howley, M. and D.B.Ó. Gallachóir, Understanding Electricity & Gas Prices in Ireland. September 2008.

191. Howley, M., et al., Electricity & Gas Prices in Ireland. June 2012.

192. Slimani, L. and T. Bouktir, Application of Differential Evolution Algorithm to Optimal Power Flow with High Wind Energy Penetration, in ACTA ELECTROTEHNICA. 2012, Mediamira Science.

193. The Smart Metering Gas Customer Behaviour Trials, in 2010 and 2011. 2013, Commission for Energy Regulation (CER).

194. Crichton, N. (1999) Tukey Multiple Comparison Test.

195. Home, Y., Active solar thermal system, Department of Climate Change and Energy Efficiency, Australia

196. Oughton, D. and S. Hodkinson, Faber & Kell's Heating and Air Conditioning of Buildings. 2012: Routledge.

197. Chong, K.K. and C.W. Wong, General formula for on-axis sun-tracking system and its application in improving tracking accuracy of solar collector. Solar Energy, 2009. 83(3): p. 298-305.

198. Kalogirou, S.A., Solar thermal collectors and applications. Progress in Energy and Combustion Science, 2004. 30(3): p. 231-295.

199. Hossain, M.S., et al., Review on solar water heater collector and thermal energy performance of circulating pipe. Renewable and Sustainable Energy Reviews, 2011. 15(8): p. 3801-3812.

200. Dehghan, A.A. and A. Barzegar, Thermal performance behavior of a domestic hot water solar storage tank during consumption operation. Energy Conversion and Management, 2011. 52(1): p. 468-476.

201. Shukla, R., et al., Recent advances in the solar water heating systems: A review. Renewable and Sustainable Energy Reviews, 2013. 19(0): p. 173-190.

202. Hourly weather data generator. 2011, Transient System Simulation Tool.

203. Solar Collector With Capacitance Effects & Controls To Maintain A Desired Outlet Temperature. 2011, Transient System Simulation Tool.

204. Nielsen, J.E., A typical efficiency curve of a solar thermal collector. 2006, European solar thermal industry federation.

205. F’ Equations As a Function of Fav. 2011, Transient System Simulation Tool.

206. Duffie, J.A. and W.A. Beckman, Solar Engineering of Thermal Processes. 3rd Edition ed. 2006: John Wiley & Sons.

207. Evacuated Tube Solar Collector With Controls To Maintain A Desired Outlet Temperature. 2011, Transient System Simulation Tool.

208. HEAT PIPE VACUUM TUBE SOLAR COLLECTOR, in THERMOMAX HP400. 2012, Kingspan

209. Ayompe, L.M., et al., Comparative field performance study of flat plate and heat pipe evacuated tube collectors (ETCs) for domestic water heating systems in a temperate climate. Energy, 2011. 36(5): p. 3370-3378.

210. Carbonell, D., J. Cadafalch, and R. Consul, Dynamic modelling of flat plate solar collectors. Analysis and validation under thermosyphon conditions. Solar Energy, 2013. 89(0): p. 100-112.

211. Cadafalch, J., A detailed numerical model for flat-plate solar thermal devices. Solar Energy, 2009. 83(12): p. 2157-2164.

212. Bhattarai, S., et al., Simulation and model validation of sheet and tube type photovoltaic thermal solar system and conventional solar collecting system in transient states. Solar Energy Materials and Solar Cells, 2012. 103(0): p. 184-193.

213. Belessiotis, V., E. Mathioulakis, and E. Papanicolaou, Theoretical formulation and experimental validation of the input–output modeling approach for large solar thermal systems. Solar Energy, 2010. 84(2): p. 245-255.

214. Brideau, S.A. and M.R. Collins, Development and validation of a hybrid PV/Thermal air based collector model with impinging jets. Solar Energy, 2014. 102(0): p. 234-246.

215. Rad, F.M., A.S. Fung, and W.H. Leong, Feasibility of combined solar thermal and ground source heat pump systems in cold climate, Canada. Energy and Buildings, 2013. 61(0): p. 224-232.

216. Torres Lobera, D. and S. Valkealahti, Dynamic thermal model of solar PV systems under varying climatic conditions. Solar Energy, 2013. 93(0): p. 183-194.

217. Pasamontes, M., et al., Hybrid modeling of a solar-thermal heating facility. Solar Energy, 2013. 97(0): p. 577-590.

218. Yaïci, W. and E. Entchev, Performance prediction of a solar thermal energy system using artificial neural networks. Applied Thermal Engineering, (0).

219. Dwivedi, V.K. and G.N. Tiwari, Experimental validation of thermal model of a double slope active solar still under natural circulation mode. Desalination, 2010. 250(1): p. 49-55.

220. Chow, T.-T., et al., Selection between single-phase and two-phase evacuated-tube solar water heaters in different climate zones of China. Solar Energy, 2013. 98, Part C(0): p. 265-274.

221. Liang, R., et al., Performance analysis of a new-design filled-type solar collector with double U-tubes. Energy and Buildings, 2013. 57(0): p. 220-226.

222. Badar, A.W., R. Buchholz, and F. Ziegler, Experimental and theoretical evaluation of the overall heat loss coefficient of vacuum tubes of a solar collector. Solar Energy, 2011. 85(7): p. 1447-1456.

223. Osório, T. and M.J. Carvalho, Testing of solar thermal collectors under transient conditions. Solar Energy, 2014. 104(0): p. 71-81.

224. Rodríguez-Hidalgo, M.C., et al., Flat plate thermal solar collector efficiency: Transient behavior under working conditions. Part I: Model description and experimental validation. Applied Thermal Engineering, 2011. 31(14–15): p. 2394-2404.

225. Stanciu, C. and D. Stanciu, Optimum tilt angle for flat plate collectors all over the World – A declination dependence formula and comparisons of three solar radiation models. Energy Conversion and Management, 2014. 81(0): p. 133-143.

226. Khamis Mansour, M., Thermal analysis of novel minichannel-based solar flat-plate collector. Energy, 2013. 60(0): p. 333-343.

227. Villar, N.M., et al., Numerical 3-D heat flux simulations on flat plate solar collectors. Solar Energy, 2009. 83(7): p. 1086-1092.

228. Tang, R., et al., Experimental and modeling studies on thermosiphon domestic solar water heaters with flat-plate collectors at clear nights. Energy Conversion and Management, 2010. 51(12): p. 2548-2556.

229. Wei, L., et al., A study on a flat-plate type of solar heat collector with an integrated heat pipe. Solar Energy, 2013. 97(0): p. 19-25.

230. Abu Bakar, M.N., et al., Design concept and mathematical model of a bi-fluid photovoltaic/thermal (PV/T) solar collector. Renewable Energy, 2014. 67(0): p. 153-164.

231. Sohel, M.I., et al., A dynamic model for air-based photovoltaic thermal systems working under real operating conditions. Applied Energy, 2014. 132(0): p. 216-225.

232. Nithyanandam, K. and R. Pitchumani, Cost and performance analysis of concentrating solar power systems with integrated latent thermal energy storage. Energy, 2014. 64(0): p. 793-810.

233. Chaabane, M., et al., Performance evaluation of concentrating solar photovoltaic and photovoltaic/thermal systems. Solar Energy, 2013. 98, Part C(0): p. 315-321.

234. Andersen, E. and S. Furbo, Theoretical variations of the thermal performance of different solar collectors and solar combi systems as function of the varying yearly weather conditions in Denmark. Solar Energy, 2009. 83(4): p. 552-565.

235. Allouhi, A., et al., Modeling of a thermal adsorber powered by solar energy for refrigeration applications. Energy, 2014. 75(0): p. 589-596.

236. Yu, Q., et al., Modeling and dynamic simulation of the collector and receiver system of 1 MWe DAHAN solar thermal power tower plant. Renewable Energy, 2012. 43(0): p. 18-29.

237. Fong, J. and Z. Alwan, Modelling to predict future energy performance of solar thermal cooling systems for building applications in the North East of England. Applied Thermal Engineering, 2013. 57(1–2): p. 81-89.

238. Chen, Y., K. Galal, and A.K. Athienitis, Modeling, design and thermal performance of a BIPV/T system thermally coupled with a ventilated concrete slab in a low energy solar house: Part 2, ventilated concrete slab. Solar Energy, 2010. 84(11): p. 1908-1919.

239. Atia, D.M., et al., Optimal sizing of a solar water heating system based on a genetic algorithm for an aquaculture system. Mathematical and Computer Modelling, 2012. 55(3–4): p. 1436-1449.

240. Huang, B.-J., et al., Maximum-power-point tracking control of solar heating system. Solar Energy, 2012. 86(11): p. 3278-3287.

241. Rodríguez-Hidalgo, M.C., et al., Domestic hot water consumption vs. solar thermal energy storage: The optimum size of the storage tank. Applied Energy, 2012. 97(0): p. 897-906.

242. Sharma, N. and G. Diaz, Performance model of a novel evacuated-tube solar collector based on minichannels. Solar Energy, 2011. 85(5): p. 881-890.

243. Kumar, S., A. Dubey, and G.N. Tiwari, A solar still augmented with an evacuated tube collector in forced mode. Desalination, 2014. 347(0): p. 15-24.

244. Liang, R., et al., Theoretical and experimental investigation of the filled-type evacuated tube solar collector with U tube. Solar Energy, 2011. 85(9): p. 1735-1744.

245. Singh, R.V., et al., Performance of a solar still integrated with evacuated tube collector in natural mode. Desalination, 2013. 318(0): p. 25-33.

246. Kıyan, M., et al., Modelling and simulation of a hybrid solar heating system for greenhouse applications using Matlab/Simulink. Energy Conversion and Management, 2013. 72(0): p. 147-155.

247. Nikolić, N. and N. Lukić, A mathematical model for determining the optimal reflector position of a double exposure flat-plate solar collector. Renewable Energy, 2013. 51(0): p. 292-301.

248. Baritto, M. and J. Bracamonte, A dimensionless model for the outlet temperature of a nonisothermal flat plate solar collector for air heating. Solar Energy, 2012. 86(1): p. 647-653.

249. Eismann, R. and H.-M. Prasser, Correction for the absorber edge effect in analytical models of flat plate solar collectors. Solar Energy, 2013. 95(0): p. 181-191.

250. Subiantoro, A. and K.T. Ooi, Analytical models for the computation and optimization of single and double glazing flat plate solar collectors with normal and small air gap spacing. Applied Energy, 2013. 104(0): p. 392-399.

251. Boutebila, H., A theoretical model of a free flow solution over an inclined long flat plate solar still. Desalination, 2009. 249(3): p. 1249-1258.

252. Roberts, D.E. and A. Forbes, An analytical expression for the instantaneous efficiency of a flat plate solar water heater and the influence of absorber plate absorptance and emittance. Solar Energy, 2012. 86(5): p. 1416-1427.

253. Khoukhi, M. and S. Maruyama, Theoretical approach of a flat-plate solar collector taking into account the absorption and emission within glass cover layer. Solar Energy, 2006. 80(7): p. 787-794.

254. Maia, C.B., A.G. Ferreira, and S.M. Hanriot, Evaluation of a tracking flat-plate solar collector in Brazil. Applied Thermal Engineering, 2014. 73(1): p. 951-960.

255. Kostić, L.T. and Z.T. Pavlović, Optimal position of flat plate reflectors of solar thermal collector. Energy and Buildings, 2012. 45(0): p. 161-168.

256. Badescu, V., Optimum fin geometry in flat plate solar collector systems. Energy Conversion and Management, 2006. 47(15–16): p. 2397-2413.

257. Dagdougui, H., et al., Thermal analysis and performance optimization of a solar water heater flat plate collector: Application to Tétouan (Morocco). Renewable and Sustainable Energy Reviews, 2011. 15(1): p. 630-638.

258. Elminir, H.K., et al., Optimum solar flat-plate collector slope: Case study for Helwan, Egypt. Energy Conversion and Management, 2006. 47(5): p. 624-637.

259. Gertzos, K.P., S.E. Pnevmatikakis, and Y.G. Caouris, Experimental and numerical study of heat transfer phenomena, inside a flat-plate integrated

collector storage solar water heater (ICSSWH), with indirect heat withdrawal. Energy Conversion and Management, 2008. 49(11): p. 3104-3115.

260. Hepbasli, A. and Y. Kalinci, A review of heat pump water heating systems. Renewable and Sustainable Energy Reviews, 2009. 13(6–7): p. 1211-1229.

261. The principle of the heat pump. 2013 [cited 2014 05 14]; Available from: http://www.evergreenventuresltd.co.uk/heat-pumps/.

262. Heat pumps performance and efficiency. 2010 [cited 2014 04 15]; Available from: www.engineeringtoolbox.com.

263. Hong, T., et al., An economic and environmental assessment for selecting the optimum new renewable energy system for educational facility. Renewable and Sustainable Energy Reviews, 2014. 29(0): p. 286-300.

264. Comakli, K., et al., Determination of optimum working conditions R22 and R404A refrigerant mixtures in heat-pumps using Taguchi method. Applied Energy, 2009. 86(11): p. 2451-2458.

265. (2010) What You Should Know about Refrigerants When Purchasing or Repairing a Residential A/C System or Heat Pump

266. Bolaji, B.O., Performance investigation of ozone-friendly R404A and R507 refrigerants as alternatives to R22 in a window air-conditioner. Energy and Buildings, 2011. 43(11): p. 3139-3143.

267. Domestic Ground Source Heat Pumps: Design and installation of closed-loop systems. 2007, Energy Saving Trust.

268. Fleck, B. and M. Huot, Comparative life-cycle assessment of a small wind turbine for residential off-grid use. Renewable Energy, 2009. 34(12): p. 2688-2696.

269. Ground source heat pump. 2012 [cited 2014 05 10]; Available from: http://americandreamgeothermal.com/types-of-geothermal-ground-loops/.

270. Water source heat pump. 2013 [cited 2014 05 14]; Available from: http://www.thegreenage.co.uk/tech/water-source-heat-pumps/.

271. Hewitt, N.J., et al., Advanced air source heat pumps for UK and European domestic buildings. Applied Thermal Engineering, 2011. 31(17–18): p. 3713-3719.

272. Air source heat pump. 2012 [cited 2014 05 08]; Available from: http://www.bse.ie/pages/mechanical/mitsubishi-electric-ecodan.php.

273. Xu, G., X. Zhang, and S. Deng, A simulation study on the operating performance of a solar–air source heat pump water heater. Applied Thermal Engineering, 2006. 26(11–12): p. 1257-1265.

274. 03/01975 Study on a direct-expansion solar-assisted heat pump water heating system: Kuang, Y. H. et al. International Journal of Energy Research, 2003, 27, (5), 531–548. Fuel and Energy Abstracts, 2003. 44(5): p. 329.

275. Li, Y.W., et al., Experimental performance analysis on a direct-expansion solar-assisted heat pump water heater. Applied Thermal Engineering, 2007. 27(17–18): p. 2858-2868.

276. Huang, B.J., J.P. Lee, and J.P. Chyng, Heat-pipe enhanced solar-assisted heat pump water heater. Solar Energy, 2005. 78(3): p. 375-381.

277. TYPE 941:AIR TO WATER HEAT PUMP. 2011, Transient System Simulation Tool.

278. Correction factors for capacity and power of a heat pump. 2011, Transient System Simulation Tool.

279. Browne, S., Case study of an air-source heat pump for a domestic application, Z. Li, Editor. 2012, Mitsubishi Electric.

280. Barker, R., 2011 Annual Weather Summary, in 2011. 2012, Royston (Iceni) Weather Station. UK.

281. Song, M., S. Deng, and L. Xia, A semi-empirical modeling study on the defrosting performance for an air source heat pump unit with local drainage of melted frost from its three-circuit outdoor coil. Applied Energy, 2014. 136(0): p. 537-547.

282. Ibrahim, O., et al., Air source heat pump water heater: Dynamic modeling, optimal energy management and mini-tubes condensers. Energy, 2014. 64(0): p. 1102-1116.

283. Neves, D. and C.A. Silva, Modeling the impact of integrating solar thermal systems and heat pumps for domestic hot water in electric systems – The case study of Corvo Island. Renewable Energy, 2014. 72(0): p. 113-124.

284. Koury, R.N.N., et al., Dynamic model and experimental study of an air–water heat pump for residential use. International Journal of Refrigeration, 2013. 36(3): p. 674-688.

285. Panaras, G., E. Mathioulakis, and V. Belessiotis, Investigation of the performance of a combined solar thermal heat pump hot water system. Solar Energy, 2013. 93(0): p. 169-182.

286. Liu, Z., G. Tang, and F. Zhao, Dynamic simulation of air-source heat pump during hot-gas defrost. Applied Thermal Engineering, 2003. 23(6): p. 675-685.

287. Touchie, M.F. and K.D. Pressnail, Testing and simulation of a low-temperature air-source heat pump operating in a thermal buffer zone. Energy and Buildings, 2014. 75(0): p. 149-159.

288. Hakkaki-Fard, A., Z. Aidoun, and M. Ouzzane, Applying refrigerant mixtures with thermal glide in cold climate air-source heat pumps. Applied Thermal Engineering, 2014. 62(2): p. 714-722.

289. Li, X., et al., Energy saving potential of low temperature hot water system based on air source absorption heat pump. Applied Thermal Engineering, 2012. 48(0): p. 317-324.

290. Guo, J.J., et al., Experimental research and operation optimization of an air-source heat pump water heater. Applied Energy, 2011. 88(11): p. 4128-4138.

291. Yao, Y., et al., A study on the performance of the airside heat exchanger under frosting in an air source heat pump water heater/chiller unit. International Journal of Heat and Mass Transfer, 2004. 47(17–18): p. 3745-3756.

292. Qu, M., et al., A study of the reverse cycle defrosting performance on a multi-circuit outdoor coil unit in an air source heat pump – Part II: Modeling analysis. Applied Energy, 2012. 91(1): p. 274-280.

293. Jang, J.Y., et al., Continuous heating of an air-source heat pump during defrosting and improvement of energy efficiency. Applied Energy, 2013. 110(0): p. 9-16.

294. Byrne, P., J. Miriel, and Y. Lenat, Experimental study of an air-source heat pump for simultaneous heating and cooling – Part 1: Basic concepts and performance verification. Applied Energy, 2011. 88(5): p. 1841-1847.

295. Zhu, L., et al., Performance analysis of a novel dual-nozzle ejector enhanced cycle for solar assisted air-source heat pump systems. Renewable Energy, 2014. 63(0): p. 735-740.

296. Byrne, P., J. Miriel, and Y. Lenat, Experimental study of an air-source heat pump for simultaneous heating and cooling – Part 2: Dynamic behaviour and two-phase thermosiphon defrosting technique. Applied Energy, 2011. 88(9): p. 3072-3078.

297. Touchie, M.F. and K.D. Pressnail, Evaluating a proposed retrofit measure for a multi-unit residential building which uses an air-source heat pump operating in an enclosed balcony space. Energy and Buildings, 2014. 85(0): p. 107-114.

298. Kelly, N.J., P.G. Tuohy, and A.D. Hawkes, Performance assessment of tariff-based air source heat pump load shifting in a UK detached dwelling featuring phase change-enhanced buffering. Applied Thermal Engineering, 2014. 71(2): p. 809-820.

299. Wang, W., et al., Characteristics of an air source heat pump with novel photoelectric sensors during periodic frost–defrost cycles. Applied Thermal Engineering, 2013. 50(1): p. 177-186.

300. Lohani, S.P. and D. Schmidt, Comparison of energy and exergy analysis of fossil plant, ground and air source heat pump building heating system. Renewable Energy, 2010. 35(6): p. 1275-1282.

301. Li, H. and H. Yang, Study on performance of solar assisted air source heat pump systems for hot water production in Hong Kong. Applied Energy, 2010. 87(9): p. 2818-2825.

302. Gong, G., et al., Research on frost formation in air source heat pump at cold-moist conditions in central-south China. Applied Energy, 2013. 102(0): p. 571-581.

303. Di Perna, C., et al., Experimental assessment and dynamic analysis of a hybrid generator composed of an air source heat pump coupled with a condensing gas boiler in a residential building. Applied Thermal Engineering, (0).

304. Karagiorgas, M., et al., Solar assisted heat pump on air collectors: A simulation tool. Solar Energy, 2010. 84(1): p. 66-78.

305. Wu, W., et al., Techno-economic analysis of air source absorption heat pump: Improving economy from a design perspective. Energy and Buildings, 2014. 81(0): p. 200-210.

306. Li, L.T., et al., Investigation of defrosting water retention on the surface of evaporator impacting the performance of air source heat pump during periodic frosting–defrosting cycles. Applied Energy, 2014. 135(0): p. 98-107.

307. Long, Z., et al., A novel defrosting method using heat energy dissipated by the compressor of an air source heat pump. Applied Energy, 2014. 133(0): p. 101-111.

308. Wang, Z., et al., Experimental analysis on a novel frost-free air-source heat pump water heater system. Applied Thermal Engineering, 2014. 70(1): p. 808-816.

309. Song, M., et al., An experimental study on the negative effects of downwards flow of the melted frost over a multi-circuit outdoor coil in an air source heat pump during reverse cycle defrosting. Applied Energy, (0).

310. Li, R., R. Ooka, and M. Shukuya, Theoretical analysis on ground source heat pump and air source heat pump systems by the concepts of cool and warm exergy. Energy and Buildings, 2014. 75(0): p. 447-455.

311. Wang, W., et al., Performances of air source heat pump system for a kind of mal-defrost phenomenon appearing in moderate climate conditions. Applied Energy, 2013. 112(0): p. 1138-1145.

312. Wu, W., et al., A new heating system based on coupled air source absorption heat pump for cold regions: Energy saving analysis. Energy Conversion and Management, 2013. 76(0): p. 811-817.

313. Song, M., et al., An experimental study on the effects of downwards flowing of melted frost over a vertical multi-circuit outdoor coil in an air source heat pump on defrosting performance during reverse cycle defrosting. Applied Thermal Engineering, 2014. 67(1–2): p. 258-265.

314. Jiang, Y., et al., Experimental study on concentration change of spray solution used for a novel non-frosting air source heat pump system. Energy and Buildings, 2014. 68, Part B(0): p. 707-712.

315. Wang, R., et al., An air source heat pump with an advanced cycle for heating buildings in Beijing. Energy Conversion and Management, 2011. 52(2): p. 1493-1500.

316. Dong, J., et al., An experimental study on defrosting heat supplies and energy consumptions during a reverse cycle defrost operation for an air source heat pump. Applied Thermal Engineering, 2012. 37(0): p. 380-387.

317. Qu, M., et al., An experimental investigation on reverse-cycle defrosting performance for an air source heat pump using an electronic expansion valve. Applied Energy, 2012. 97(0): p. 327-333.

318. Byun, J.-S., J. Lee, and C.-D. Jeon, Frost retardation of an air-source heat pump by the hot gas bypass method. International Journal of Refrigeration, 2008. 31(2): p. 328-334.

319. Liu, X., S.-K. Lau, and H. Li, Optimization and analysis of a multi-functional heat pump system with air source and gray water source in heating mode. Energy and Buildings, 2014. 69(0): p. 1-13.

320. Hewitt, N. and M.J. Huang, Defrost cycle performance for a circular shape evaporator air source heat pump. International Journal of Refrigeration, 2008. 31(3): p. 444-452.

321. Guoyuan, M., C. Qinhu, and J. Yi, Experimental investigation of air-source heat pump for cold regions. International Journal of Refrigeration, 2003. 26(1): p. 12-18.

322. Heo, J., et al., Comparison of the heating performance of air-source heat pumps using various types of refrigerant injection. International Journal of Refrigeration, 2011. 34(2): p. 444-453.

323. Zhang, J., R.Z. Wang, and J.Y. Wu, System optimization and experimental research on air source heat pump water heater. Applied Thermal Engineering, 2007. 27(5–6): p. 1029-1035.

324. Anderson, I.D.R., et al., Building and Renovating Schools: Design, Construction Management, Cost Control 4th Edition ed. 2004: RSMeans.

325. Means, R.S., Green Building: Project Planning and Cost Estimating. 3rd Edition ed. 2011: John Wiley & Sons.

326. Fuller, S.K. and S.R. Peterson, Life-Cycle Costing Manual for the Federal Energy Management Programme, U.S.D.o. Commerce, Editor. 1995, Technology administration.

327. Browne, S., Data obtained from a monitered case study. 2012, Mitsubishi Electric Heat Pump.

328. Private Households in Permanent Housing Units by Type of Central Heating, Aggregate Town or Rural Area, Period in which Built, Province County or City and CensusYear. 2011, Central Statistics Office.

329. Air source heat pump service manual. 2008, Mitsubishi Electric.

330. Domestic heating price list. 2012, Mitsubishi Electric.

331. Albion Aerocyl unvented copper hotwater cylinders for heat pump and solar unit, Kingspan.

332. Kingspan solar flat plate, Kingspan solar.

333. Thermomax HP400, Kingspan solar.

334. Kane, S.O., Price of a solar flatplate system. 2012, Green-house Renewable Energy Centre.

335. Kane, S.O., Price of a solar evacuated tube collector system. 2012, Green-house Renewable Energy Centre.

336. Nolan, A., Price of domestic conventional heating and hotwater generation systems. 2013, Varming Consulting Engineers.

337. Warner, J.T. and S. Pleeter, The Personal Discount Rate: Evidence from Military Downsizing Programs. The American Economic Review, 2001. 91(1): p. 33-53.

338. Short, W., D.J. Packey, and T. Holt, A Manual for the Economic Evaluation of Energy Efficiency and Renewable Energy Technologies 1995, National Renewable Energy Laboratory.

339. Liebermann, Y. and M. Ungar, Efficiency of consumer intertemporal choice under life cycle cost conditions. Journal of Economic Psychology, 2002. 23(6): p. 729-748.

340. Talavera, D.L., et al., Grid parity and self-consumption with photovoltaic systems under the present regulatory framework in Spain: The case of the University of Jaén Campus. Renewable and Sustainable Energy Reviews, 2014. 33(0): p. 752-771.

341. Ouyang, X. and B. Lin, Levelized cost of electricity (LCOE) of renewable energies and required subsidies in China. Energy Policy, 2014. 70(0): p. 64-73.

342. Hong, T., C. Koo, and T. Kwak, Framework for the implementation of a new renewable energy system in an educational facility. Applied Energy, 2013. 103(0): p. 539-551.

343. Elsafty, A. and A.J. Al-Daini, Economical comparison between a solar-powered vapour absorption air-conditioning system and a vapour compression system in the Middle East. Renewable Energy, 2002. 25(4): p. 569-583.

344. Montuori, L., et al., Integration of renewable energy in microgrids coordinated with demand response resources: Economic evaluation of a biomass gasification plant by Homer Simulator. Applied Energy, 2014. 132(0): p. 15-22.

345. Jakob, M., Marginal costs and co-benefits of energy efficiency investments: The case of the Swiss residential sector. Energy Policy, 2006. 34(2): p. 172-187.

346. Rohani, G. and M. Nour, Techno-economical analysis of stand-alone hybrid renewable power system for Ras Musherib in United Arab Emirates. Energy, 2014. 64(0): p. 828-841.

347. Dalton, G.J., D.A. Lockington, and T.E. Baldock, Case study feasibility analysis of renewable energy supply options for small to medium-sized tourist accommodations. Renewable Energy, 2009. 34(4): p. 1134-1144.

348. van Alphen, K., W.G.J.H.M. van Sark, and M.P. Hekkert, Renewable energy technologies in the Maldives—determining the potential. Renewable and Sustainable Energy Reviews, 2007. 11(8): p. 1650-1674.

349. Ozyogurtcu, G., M. Mobedi, and B. Ozerdem, Techno-economic evaluation of a ventilation system assisted with exhaust air heat recovery, electrical heater and solar energy. Energy and Buildings, 2014. 72(0): p. 17-23.

350. Jaber, S. and S. Ajib, Optimum design of Trombe wall system in mediterranean region. Solar Energy, 2011. 85(9): p. 1891-1898.

351. Ucar, A. and M. Inalli, Thermal and economic comparisons of solar heating systems with seasonal storage used in building heating. Renewable Energy, 2008. 33(12): p. 2532-2539.

352. Janjai, S., J. Laksanaboonsong, and T. Seesaard, Potential application of concentrating solar power systems for the generation of electricity in Thailand. Applied Energy, 2011. 88(12): p. 4960-4967.

353. Personal loans at Bank of Ireland. 2014, Bank of Ireland.

354. Krohn, S., P.-E. Morthorst, and S. Awerbuch, The Economics of Wind Energy. 2009.

355. RENEWABLE ENERGY TECHNOLOGIES:COST ANALYSIS SERIES Wind Power 2012, International Renewable Energy Agency.

356. RENEWABLE ENERGY TECHNOLOGIES: COST ANALYSIS SERIES Solar Photovoltaics. 2012, International Renewable Energy Agency.

357. Fuller, S.K. and S.R. Peterson, Life Cycle Cost Manual for the Federal Energy Management Programme. 1996, Building and Fire Research Laboratory.

358. Renewable Energy Resources in Ireland for 2010 and 2020 – A Methodology. 2004, Sustainable Energy Authority of Ireland

359. Manwell, J.F., J.G. McGowan, and A.L. Rogers, Wind Energy Explained: Theory, Design and Application. 2010: John Wiley & Sons.

360. Koçak, K., Practical ways of evaluating wind speed persistence. Energy, 2008. 33(1): p. 65-70.

361. Carapellucci, R. and L. Giordano, The effect of diurnal profile and seasonal wind regime on sizing grid-connected and off-grid wind power plants. Applied Energy, 2013. 107(0): p. 364-376.

362. Masseran, N., A.M. Razali, and K. Ibrahim, An analysis of wind power density derived from several wind speed density functions: The regional assessment on wind power in Malaysia. Renewable and Sustainable Energy Reviews, 2012. 16(8): p. 6476-6487.

363. Mathew, S., K.P. Pandey, and A. Kumar.V, Analysis of wind regimes for energy estimation. Renewable Energy, 2002. 25(3): p. 381-399.

364. Ucar, A. and F. Balo, Assessment of wind power potential for turbine installation in coastal areas of Turkey. Renewable and Sustainable Energy Reviews, 2010. 14(7): p. 1901-1912.

365. Saleh, H., A. Abou El-Azm Aly, and S. Abdel-Hady, Assessment of different methods used to estimate Weibull distribution parameters for wind speed in Zafarana wind farm, Suez Gulf, Egypt. Energy, 2012. 44(1): p. 710-719.

366. Graham, V.A., K.G.T. Hollands, and T.E. Unny, A time series model for Kt with application to global synthetic weather generation. Solar Energy, 1988. 40(2): p. 83-92.

367. Blake, I.F., An Introduction to Applied Probability. 1979: John Wiley & Sons.

368. Hollands, K.G.T. and R.G. Huget, A probability density function for the clearness index, with applications. Solar Energy, 1983. 30(3): p. 195-209.

369. Knight, K.M., S.A. Klein, and J.A. Duffie, A methodology for the synthesis of hourly weather data. Solar Energy, 1991. 46(2): p. 109-120.

370. Bendt, P., M. Collares-Pereira, and A. Rabl, The frequency distribution of daily insolation values. Solar Energy, 1981. 27(1): p. 1-5.

371. Graham, V.A. and K.G.T. Hollands, A method to generate synthetic hourly solar radiation globally. Solar Energy, 1990. 44(6): p. 333-341.

372. Erbs, D.G., S.A. Klein, and J.A. Duffie, Estimation of the diffuse radiation fraction for hourly, daily and monthly-average global radiation. Solar Energy, 1982. 28(4): p. 293-302.

373. Knight, K.M., Development and validation of a weather data generation model, in Department of Mechanical Engineering. 1988, University of Wisconsin-Madison.

374. Liu, B.Y.H. and R.C. Jordan, The interrelationship and characteristic distribution of direct, diffuse and total solar radiation. Solar Energy, 1960. 4(3): p. 1-19.

375. Box, G.E.P., G.M. Jenkins, and G.C. Reinsel, Time Series Analysis: Forecasting and Control (Wiley Series in Probability and Statistics). 2008: Wiley.

376. Graham, V.A., Stochastic synthesis of the solar atmospheric transmittance. 1985: University of Waterloo.

APPENDIX A
GENERATION OF HOURLY WIND SPEED VALUES

Realistic hourly wind speed values for a year can be generated by performing statistical calculations based on 12 monthly-average-wind-speed values, one for each month, and four statistical parameters: Weibull k factor, autocorrelation factor, diurnal pattern strength and hour of peak wind speed [359]. The monthly-average-wind-speed values must be supplied. The hourly wind speed values for a year are generated in five steps:

Step 1. Generate a sequence of autocorrelated numbers.

Step 2. Generate a desired average diurnal wind speed profile and then scale it to fit for each month.

Step 3. Perform a probability transformation on the sequence of numbers generated in Step 2 to make it conform to the same normal distribution as Step 1.

Step 4. Add the sequence of numbers generated in Step 3 to the sequence of numbers generated in Step 1.

Step 5. Perform a probability transformation on the sequence of numbers generated in Step 4 to make it conform to a desired Weibull distribution.

In Step 1, a first-order autoregressive model is used to generate a sequence of autocorrelated numbers, one for each time step into which the year duration is discretised. A single hour is used as the time step in this study. The formula to generate the sequence is shown in Equation A.1.

$$z_t = a * z_{t-1} + f(t) \tag{A.1}$$

where z_t is the hour t value , z_{t-1} is the value for the previous hour t-1 and the initial z_{t-1} is chosen as zero, f(t) is a random number drawn from a normal distribution having a mean of 0 and a standard deviation of 1, and a is the autoregressive parameter which is equal to the one-hour autocorrelation factor as shown in Equation A.2.

$$a = r_1 \tag{A.2}$$

The autocorrelation factor r_1 is the autocorrelation between any two time values in a sequence separated by a lag of one time unit. This autocorrelation factor typically has a value in the range of 0.80-0.95, and reflects how strongly the wind speed in one hour tends to depend on the wind speed in the previous hour. Historical measured hourly wind speed data is used to calculate this factor using Equation A.3 [360]. In this study, year 2010 hourly wind speed data is employed.

$$r_1 = \frac{\sum_{i=1}^{n-1} (z_i - \bar{z}) * (z_{i+1} - \bar{z})}{\sum_{i-1}^{n} (z_i - \bar{z})^2} \tag{A.3}$$

where z_i is the hour i value, z_{i+1} is the value for the subsequent hour i+1, $\bar{z}$ is the yearly-average value and n is the number of hours in a year.

From Step 1, a series of numbers for a year is generated. These numbers conform to a normal distribution with a mean of 0 and a standard deviation of 1.

In Step 2, a desired average diurnal wind speed profile is generated using Equation A.4 [361].

$$U_i = \bar{U}\left\{1+\delta\cos\left[\left(\frac{2*\pi}{24}\right)*(i-\phi)\right]\right\} \text{ for i=1, 2, … 24} \quad \text{(A.4)}$$

where U_i is the average wind speed in hour i, $\bar{U}$ is the yearly-average wind speed, and i is the hour in a day. δ is the diurnal pattern strength which reflects how strongly the wind speed tends to depend on the time of the day. It is a number in the range of 0 and 1, and typically has a value of between 0 and 0.4. ϕ is the hour of peak windspeed which represents the hour of the day that tends to be windiest on average. The δ and ϕ are calculated and determined from measured hourly wind speed data for Dublin in 2010.

This generated diurnal wind speed profile is used repeatedly for all days in a year. However, due to the fact that the average wind speed varies each month, the average diurnal wind speed profile is then scaled to fit for the average of each month; within each month the diurnal pattern is repeatedly for each day.

In Step 3, a probability transformation, a statistical procedure by which one modifies a set of numbers to conform to a desired probability distribution function, is performed. The sequence of values generated in Step 2 is transformed to conform to the same normal distribution used in Step 1. In order to perform this probability transformation, the cumulative distribution function of the original set of data (values in Step 2) is produced. The percentile value of each original data point is calculated from this produced cumulative distribution function. Finally, the percentile value is employed in the desired cumulative distribution function (in this case, it is a normal distribution function with a mean of 0 and a standard deviation of 1) to obtain the corresponding transformed value.

In Step 4, a sequence, conforms to a normal distribution and also shows the desired degree of autocorrelation, is created. This resulting sequence is achieved by adding the sequence generated in Step 1 to the sequence generated in Step 3.

The final step, Step 5, is to perform another probability transformation on the sequence generated in Step 4 to make it conform to a desired Weibull distribution. The Weibull distribution is a two-parameter function that is commonly used to represent a good-fit to a wind speed frequency. The probability density function [362] and cumulative distribution function [363] of a Weibull distribution are expressed in the Equation A.5 and Equation A.6 respectively:

$$f(v) = \frac{k}{c} * \left(\frac{v_i}{c}\right)^{k-1} * \exp\left[-\left(\frac{v_i}{c}\right)^{k}\right] \tag{A.5}$$

$$F(v) = 1 - \exp\left[-\left(\frac{v_i}{c}\right)^{k}\right] \tag{A.6}$$

where v_i is the wind speed at time step i, k is the Weibull k factor (shape) which reflects the breadth of a distribution of wind speeds in the Weibull distribution, and c is the Weibull scale parameter. The relationship between the Weibull k factor and the Weibull scale parameter [364] is given by Equation A.7.

$$c = \frac{\bar{v}}{\Gamma\left(\frac{1}{k} + 1\right)} \tag{A.7}$$

where $\bar{v}$ is the annual average wind speed value and Γ is the gamma function.

In order to construct the Weibull cumulative distribution function, the determination of Weibull k factor is essential. The maximum likelihood method is used to calculate this factor in this study using Equation A.8 [365]:

$$k = \left(\frac{\sum_{i=1}^{n} (v_i)^k * \ln(v_i)}{\sum_{i=1}^{n} (v_i)^k} - \frac{\sum_{i=1}^{n} \ln(v_i)}{n} \right)^{-1} \quad \text{(A.8)}$$

where v_i is the wind speed in time step i, and n is the number of non-zero wind speed data points. Because it is an implicit equation, it is solved in an iterative manner. The initial guess for k is 2 [364]. Once the Weibull k factor is obtained, the Weibull scale parameter can be solved explicitly using Equation A.7. The probability transformation can then be performed on the sequence of numbers generated in Step 4 (a normal distribution function) to a desired Weibull distribution function which is created based on an annual average wind speed, and calculated Weibull k factor and Weibull scale parameter. The procedures used to calculate the transformed values are very similar to Step 3; the only difference is that a desired Weibull distribution function is employed rather than a normal distribution function.

APPENDIX B
GENERATION OF HOURLY SOLAR RADIATION VALUES FOR A SOLAR PV SYSTEM

The generation of hourly solar radiation values on a horizontal surface are based on the stochastic mathematical models developed from Graham theory. These models are used to generate synthetic data from the solar simulation program itself, without having to perform the costly and time-consuming reading of solar irradiation data nor to provide for it [366]. These mathematical models are capable of generating solar irradiation information for almost any location globally. The hourly solar radiation values on a tilted surface are then evaluated from the predicted hourly solar radiation values on a horizontal surface using HDKR model (the Hay, Davis, Klucher, Reindl). The hourly solar radiation values on a tilted solar PV module for a year are generated from five steps:

Step 1. Convert 12 monthly-average daily solar radiation values into 12 monthly clearness index values, one for each month.

Step 2. Generate daily clearness index values for a year from converted monthly clearness index values.

Step 3. Generate hourly clearness index values for a year from predicted daily clearness index values.

Step 4. Convert predicted hourly clearness index values into hourly solar radiation values on a horizontal surface.

Step 5. Generate hourly solar radiation values on a tilted surface from predicted hourly solar radiation values on a horizontal surface.

In Step 1, solar radiation is often converted into a dimensionless form named as clearness index which is defined as the ratio of the total solar radiation on a horizontal surface at a specific time to the extraterrestrial global solar radiation on a horizontal surface at the same time. The clearness index indicates the fraction of the solar radiation striking the top of the atmosphere that can make it through and strike the earth's surface. The hourly, daily and monthly clearness index is expressed as k_{hr}, k_d and k_m respectively. The daily index, k_d, is not the same as the average of the hourly clearness indices of the day. The average of the daily clearness indices of the month is not identical to the monthly clearness index, however the difference is small and the quantities can generally be used interchangeably. If the monthly-average daily solar radiation on a horizontal surface of the earth for a given latitude is known, the monthly clearness index can be calculated from Equation B.1.

$$k_m = \frac{H_{ave}}{H_{o,ave}} \tag{B.1}$$

where k_m is the monthly clearness index, H_{ave} is the monthly-average daily solar radiation on a horizontal surface which is the value provided for the study and $H_{o,ave}$ is the monthly-average daily extraterrestrial solar radiation on a horizontal surface and is calculated from Equation B.2.

$$H_{o,ave} = \frac{\sum_{n=1}^{N} H_o}{N} \tag{B.2}$$

where H_o is the monthly-average daily extraterrestrial solar radiation on a horizontal surface and calculated using Equation B.3 for latitudes in the range of -60° to +60° [206], and N is the number of days in the month:

$$\begin{aligned} H_o &= \frac{24*3600*G_{sc}}{\pi}*\left(1+0.033*\cos\frac{360*n}{365}\right) \\ &*\left(\cos\phi*\cos\delta*\sin\omega_s+\frac{\pi*\omega_s}{180}*\sin\phi*\sin\delta\right) \\ I_o &= \frac{12*3600*G_{sc}}{\pi}*\left(1+0.033*\cos\frac{360*n}{365}\right) \\ &*\left(\cos\phi*\cos\delta*(\sin\omega_2-\sin\omega_1)+\frac{\pi*(\omega_2-\omega_1)}{180}*\sin\phi*\sin\delta\right) \end{aligned} \tag{B.3}$$

where G_{sc} is the solar constant and has a value of 1,367 W/m^2, n is the day of the year and in this case this is the mean day of the month as shown in Table B.1. ϕ is the latitude which is the angular location north or south of the equator, north positive; -90°< ϕ <+90°. δ, calculated using Equation B.4, is the declination which is the angular position of the sun at solar noon with respect to the plane of equator, north positive; -23.45°≤ δ≤ 23.45° [206]. ω_s is the sunset hour angle and can be calculated using Equation B.5.

$$\delta = 23.45*\sin\left(360*\frac{284+n}{365}\right) \tag{B.4}$$

$$\cos\omega_s = -\frac{\sin\phi*\sin\delta}{\cos\phi*\cos\delta} = -\tan\phi\tan\delta \tag{B.5}$$

The monthly-average daily extraterrestrial radiation H_o can be estimated using Equation B.6 if the latitudes are not in the range as previously stated, i.e. -60°< ϕ <+60° [206]:

$$H_o = \frac{24*3600*G_{sc}}{\pi} *(1.00110 + 0.034221*\cos B + 0.001280*\sin B + 0.000719*\cos 2B + 0.000077*\sin 2B) *\left(\cos\phi*\cos\delta*\sin\omega_s + \frac{\pi*\omega_s}{180}*\sin\phi*\sin\delta\right) \quad \text{(B.6)}$$

where $B = (n-1)*\frac{360}{365}$

Month	Day of Month	n
January	17	17
February	31+16	47
March	29+16	75
April	90+15	105
May	120+15	135
June	151+11	162
July	181+17	198
August	212+16	228
September	243+15	258
October	273+15	288
November	304+14	318
December	334+10	344

Table B.1. Average days for months and values of n by month [206].

In Step 2, the stochastic mathematic models for generating synthetic k_d values are not constructed with the domain of k_d, but instead use an intermediate Gaussian variable that is obtained by performing a probability transformation between the distribution of k_d and the Gaussian domain [366]. The k_d series are non-stationary and non-Gaussian, these characters can be corrected by transforming k_d into a new Gaussian random variable χ with statistics that are invariant which have the same mean and variance for

all months. The f_j represents the unknown monthly transformation function that maps k_d into a Gaussian variable χ as shown in Equation B.7 [366].

$$f_j[k_d] = \chi \tag{B.7}$$

The Gaussian distribution of χ has a mean of zero and a variance of one. Both the distribution of k_d and χ can be specified. The transformation must ensure that their respective marginal probabilities are unaltered. $g[\chi]$ is the Gaussian probability density function for χ. $P[k_d, \bar{k}_d]$ is the probability density function for k_d and $\bar{k}_d$ is the monthly-average daily clearness index which is equal to k_m. u is the cumulative probability of χ and v is the cumulative probability of k_d given in Equation B.8 and Equation B.9 respectively.

$$u = \int_{-\infty}^{\chi} g(t)dt = \frac{1}{\sqrt{2*\pi}} * \int_{-\infty}^{\chi} e^{\frac{t^2}{2}} dt = \frac{1}{2} * \left[1 + \mathrm{erf}\left(\frac{\chi}{\sqrt{2}}\right)\right] \tag{B.8}$$

where erf is the error function.

$$v = \int_{k_{dl}}^{k_d} P[k_d^*, \bar{k}_d]dk_d^* = F[k_d, \bar{k}_d] \tag{B.9}$$

where $P[k_d^*, \bar{k}_d]$ is the probability that an event has its k_d in the narrow interval $k_d^* \leq k_d \leq k_d^* + dk_d^*$. The obtained k_m, based on provided monthly-average daily values, are required to specify the cumulative probability function $F[k_d, \bar{k}_d]$. Random variables that are transformed by their distribution function always yield a transformed variable that is uniformly distributed on (0,1) [367]. Therefore, both u and v should be uniformly distributed on the (0,1) interval. u and v must be equal since u and v have the same distribution function and the sought transformation requires that the cumulative

probabilities be maintained. Hence the integral transformations can give the desired function f_j by rearranging Equation B.10.

$$\frac{1}{2}*\left[1+\operatorname{erf}\left(\frac{\chi}{\sqrt{2}}\right)\right]=\int_{k_{dl}}^{k_d} P\left[k_d^*,\bar{k}_d\right]dk_d^*=F\left[k_d,\bar{k}_d\right] \tag{B.10}$$

Hence

$$\chi=\sqrt{2}*\operatorname{erf}^{-1}\ \ 2*F*\left[k_d,\bar{k}_d\right]-1\ \ =f_j\ \ k_d \tag{B.11}$$

The generalised cumulative probability function $F[k_d,\ \bar{k}_d]$ can be obtained by using the historic record to evaluate it, or mathematical expressions for the probability function as shown in Equation B.12 [368]:

$$F\left[k_d,\bar{k}_d\right]=\int_0^{k_d} P\left[k_d,\bar{k}_d\right]dk_d \tag{B.12}$$

The theoretical expression for $P[k_d,\ \bar{k}_d]$ is expressed in Equation B.13 and Equation B.14 when assuming a random solar radiation sequence [368].

$0\le k_d<k_{dl}$

$$P\left[k_d,\bar{k}_d\right]=0 \tag{B.13}$$

$K_{dl}\le k_d\le k_{du}$

$$P\left[k_d,\bar{k}_d\right]=\frac{\nu*\exp(\nu*k_d)}{\exp(\nu*k_{du})-\exp(\nu*k_{dl})} \tag{B.14}$$

In these equations, k_{dl} and k_{du} are the lower and upper bound of the range for k_d respectively. K_{dl} has always been set equal to 0.05 [368] and k_{du} is a monotonically increasing function of $\bar{k}_d$ and is calculated using Equation B.15 [369]. ν is also a function of $\bar{k}_d$; a unique solution of ν can be found by iterating this transcendental Equation B.16 [370].

$$k_{du} = 0.6313 + 0.267 * \bar{k}_d - 11.9 * (\bar{k}_d - 0.75)^8 \quad \text{(B.15)}$$

$$\bar{k}_d = \frac{(\nu * k_{du} - 1) * \exp(\nu * k_{du}) - (\nu * k_{dl} - 1) * \exp(k_{dl})}{\nu * (\exp(\nu * k_{du}) - \exp(\nu * k_{dl}))} \quad \text{(B.16)}$$

The $F[k_d, \bar{k}_d]$ function corresponding to the $P[k_d, \bar{k}_d]$ function is then expressed as shown in Equation B.17 [369].

$$F\left[k_d, \bar{k}_d\right] = \frac{\exp(\nu * k_d) - \exp(\nu * k_{dl})}{\exp(\nu * k_{du}) - \exp(\nu * k_{dl})} \quad \text{(B.17)}$$

The stochastic mathematical model for the annual series of $\chi(n)$ is constructed using the universal first-order autoregressive model of the form as follows [366]:

$$\chi(n) = \phi_1 * \chi(n-1) + w(n) \quad \text{(B.18)}$$

where $\chi(n)$ is the value of χ on day n, n and n-1 are day numbers; n-1 represents a day previous to day n, ϕ_1 is the first-order autoregressive parameter, w(n) is the value on day n of a random number drawn from a set of uncorrelated Gaussian numbers having a mean of zero and a variance of σ_w^2; the noise variance σ_w^2 is managed by ϕ_1 in relation to $\sigma_w^2 = 1 - \phi_1^2$. Thus, the χ series can be produced once ϕ_1 is known (fixed). The estimations of ϕ_1 vary with location from 0.253±0.02 to 0.348±0.02; the average value of 0.29 is appropriate to be used for the generalised model for $\chi(n)$ since such a small adjustment is highly unlikely to be of any significance for engineering simulation work [366].

For each k_d to be generated, an uncorrelated number is randomly produced from a generator (usually uniform) based on a parent distribution knowing the mean and the

variance. The output from this generator is then transformed from this parent distribution to a Gaussian distribution with a mean of zero and a variance of σ_w^2. Random values drawn from this set represents the value of w(n) in Equation B.18. The first value of χ, required to begin the process of generating the series of $\chi(n)$, is generated at random from the governing Gaussian distribution for χ. Once a set of Gaussian variable $\chi(n)$ has been produced, the $k_d(n)$ set can be obtained by performing an inverse probability transformation through Equation B.11 (rearranged to express k_d as a function of χ).

In Step 3, from previous description of generation of daily clearness index k_d, it is known that the probability of daily events change on a monthly basis. There is also strong evidence that the probability of a specific hourly clearness index k_h value depends on the clearness index k_d for the day which is occurred [369]. A time series mathematical model for the k_t sequence which is flexible in nature and also incorporates the varying nature of its probability features is developed by Graham and used in this study. The generated k_d form is used as input in this generation of hourly clearness index k_h. The variation in k_h events is containing two components: a trend (or mean) component and a random component as follows [371]:

$$k_h = k_{hm} + \alpha \tag{B.19}$$

where k_{hm} is the mean hourly clearness index if the presence of radiation attenuators were uniformly distributed over the day and α is the effect of unpredictable perturbations in the radiation attenuators, mainly caused by varying cloud cover; the random component will be small if it is a clear day with little or no clouds, however this component will be significant if it is a cloudy day. The k_{hm} component consists of two

sub-components which are the beam trend component and the diffuse trend component, and is obtained by evaluating both. A simple exponential equation is used to represent the beam trend component that is a function of air mass as shown in Equation B.20:

$$k_{hbm} = a_0 + a_1 * \exp(-\kappa * m) \tag{B.20}$$

where m is the air mass taken at the centre of the hour; the air mass is defined by the solar zenith angle (θ_z) and can be worked out from $\theta_z = \sec^{-1} m$ [206], and a_0, a_1 and κ are functions of the daily clearness index k_d. The diffuse trend component has a strong dependence on the beam trend component and is also a similar function of k_{hbm}. Therefore, the overall k_{hm} should be of a form as follows:

$$k_{hm}(t) = \lambda + \varepsilon * \exp(-\kappa * m) \tag{B.21}$$

where the parameters λ, ε and κ are unique functions of the clearness index k_d for the day considered and demonstrated in the following empirical expression:

$$\lambda(k_d) = k_d - b_0 * k_d^3 * (1 - k_d) \tag{B.22}$$

$$\varepsilon(k_d) = b_1 * (1 - k_d) \tag{B.23}$$

$$\kappa(k_d) = b_2 * (1 - k_d) / k_d \tag{B.24}$$

where b_0, b_1, and b_2 are constants and have a value of -1.167, 0.979 and 1.141 respectively.

The random component can be obtained from a first-order regression model which $\alpha(t)$, expressed in Equation B.25, is related to the value in the immediately preceding hour ($\alpha(t-1)$) plus a random value drawn from an uncorrelated random set.

$$\alpha(t) = \phi * \alpha(t-1) + \upsilon(t) \quad \text{(B.25)}$$

where ϕ is the coefficient and is equal to the autocorrelation coefficient r estimated between values separated by one hour. This autocorrelation coefficient r reflects the effect of past values of α on the current value; an estimate of non-zero of r implies that past values do have influence on current values, otherwise a zero estimate suggests the opposite. The r value is depended on the k_d value and calculated using Equation B.26.

$$r = c_1 + c_2 * k_d(1 - k_d) \quad \text{(B.26)}$$

where c_1 and c_2 are constants, and have a value of 0.35 and 1.1 respectively. However, in order to simplify the calculation but still give an accurate result, a constant value of 0.54 is generally utilised for r.

The generation of daily sets α requires a definition of its probability distribution. This is fixed by the distribution of υ, the set of uncorrelated random values used to generate α. The Gaussian distribution is generally used to represent the random variable υ in the stochastic model. However the frequency distribution of υ is non-Gaussian, as a result the frequency distribution of α is also non-Gaussian, Therefore it is necessary to employ a model for α's distribution function. The probability model used to present frequency distribution of α is expressed in Equation B.27. The frequency of α is identical to the frequency of the corresponding k_h. Thus, this frequency distribution varies depending on the daily clearness index, the standard deviation σ_α also changes with k_d as shown in Equation B.33. The k_d random variable is bounded between an upper limit k_{hu} and a lower limit k_{hl}.

$$P(\alpha : k_d) = P(k_h : k_d) = \frac{\Gamma(p+q) * u^{p-1} * (1-u)^{q-1}}{\Gamma(p) * \Gamma(q) * (k_{hu} - k_{hl})} \quad \text{(B.27)}$$

where $\Gamma(.)$ is the gamma function, p and q are parameters and can be calculated in Equation B.28 and Equation B.29, u is a random variable within the range of between 0 and 1, and can be calculated in Equation B.30.

where

$$p = \frac{\bar{u}^2 * (k_{hu} - k_{hl})}{\sigma_u^2} - \bar{u} \quad \text{(B.28)}$$

$$q = \frac{p * (1 - \bar{u})}{\bar{u}} \quad \text{(B.29)}$$

$$u = \frac{p}{(p+q)} \quad \text{(B.30)}$$

where $\bar{u}$ and σ_u are the mean and the standard deviation of u, and they are calculated in Equation B.31 and Equation B. 32 respectively.

$$\bar{u} = \frac{k_{hm} - k_{hl}}{k_{hu} - k_{hl}} \quad \text{(B.31)}$$

$$\sigma_u = \frac{\sigma_\alpha}{k_{hu} - k_{hm}} \quad \text{(B.32)}$$

where

$$\sigma_\alpha = 0.16 * \sin\left(\frac{\pi * k_d}{0.90}\right) \quad \text{(B.33)}$$

The accuracy of the frequency distribution is determined by the estimates of k_{hl} and k_{hu} values. The suitable values of k_{hl} and k_{hu} can be obtained using Equations B.34 and B.35 respectively.

$$k_{hl} = \max(0, k_{hm} - 4 * \sigma_{\alpha}) \tag{B.34}$$

$$k_{hu} = \min(0.9, k_{hm} + 4 * \sigma_{\alpha}) \tag{B.35}$$

Since the frequency distribution of α is not Gaussian, therefore simply select the random variable υ from a non-Gaussian distribution is not sufficient. The mathematics required to manipulate non-Gaussian variables is much more complex than with Gaussian ones. Thus, α values are directly obtained rather than finding individual υ values. A probability transformation has to be carried out in order to transform the non-Gaussian random variables α to the Gaussian random variables β with a mean of zero and a variance of one. This procedure is the same as the probability transformation performed for generating daily clearness index. The relationship between α and β is shown in Equation B.36.

$$\beta = \sqrt{2} * \text{erf}^{-1}\ 2 * F(\alpha : k_d) - 1 \tag{B.36}$$

where $F[\alpha:k_d]$ is the cumulative probability of α which is calculated by integrating Equation B.27. Since β is Gaussian, the serial relationship between hourly events can be obtained from its random set as shown in Equation B.37.

$$\beta(t) = \phi * \beta(t-1) + b(t) \tag{B.37}$$

where b(t) is selected from uncorrelated set of Gaussian random numbers having a mean of zero and a variance of $1-\phi^2$. The autocorrelated β random variable is transformed into the non-Gaussian distribution for α, and a corresponding α value can then be obtained from this β value. Thus sets of α(t) values are generated with the correct

frequency distribution and hourly serial relationship. The value of ϕ is the same as that used for α which is a reasonable approximation of 0.54.

In Step 4, the evaluation of the total solar radiation on a tilted surface is generally of interest. The predicted hourly clearness index has to be converted to the hourly total solar radiation on a horizontal surface. The Equation B.38 is used to perform this conversion.

$$k_h = \frac{I}{I_o} \tag{B.38}$$

Where I is the total solar radiation on a horizontal surface for an hour period, I_o is the extraterrestrial radiation on a horizontal surface for an hour period, and is calculated in Equation B.39. ω_1 and ω_2 are hour angles which are used to define an hour (where ω_2 is the larger).

$$I_o = \frac{12*3600*G_{sc}}{\pi}*\left(1+0.033*\cos\frac{360*n}{365}\right) *\left(\cos\phi*\cos\delta*(\sin\omega_2-\sin\omega_1)+\frac{\pi*(\omega_2-\omega_1)}{180}*\sin\phi*\sin\delta\right) \tag{B.39}$$

In Step 5, the HDKR model is used to calculate the total solar radiation fall on a tilted solar PV module. Three components, beam, diffuse and ground-reflected solar radiation, are estimated individually. Once these three components have been calculated, the sum of them is the total solar radiation on a tilted solar PV module.

The diffuse solar radiation on a horizontal surface is calculated from the hourly diffuse fraction correlation. The diffuse fraction, I_d/I (the ratio of the hourly diffuse solar radiation on a horizontal surface to the hourly global solar radiation on a horizontal surface), of the hourly total solar radiation is strongly correlated with k_h. The correlation is presented in Table B.2 [372], where I_d is the diffuse solar radiation on a horizontal

surface. The beam solar radiation on a horizontal surface, I_b, is then calculated by subtracting the diffuse solar radiation on a horizontal surface from total solar radiation on a horizontal surface.

For $k_h \leq 0.22$
$I_d / I = 1.0 - 0.09 * k_h$
For $0.22 < k_h \leq 0.80$
$I_d / I = 0.9511 - 0.1604 * k_h + 4.388 * k_h^2 - 16.638 * k_h^3 + 12.366 * k_h^4$
For $k_h > 0.80$
$I_d / I = 0.165$

Table B.2. The correlation between the diffuse fraction, I_d/I and the hourly clearness index, k_h.

The contribution of diffuse solar radiation on a tilted surface can be calculated using Equation B.40.

$$I_{dt} = I_d * \left[0.5 * (1 - A_i) * (1 + \cos\beta) * \left\{ 1 + f * \sin^3\left(\frac{\beta}{2}\right) \right\} + A_i * R_b \right] \qquad (B.40)$$

where I_{dt} is the diffuse solar radiation on a tilted surface, A_i is the anisotropy index and calculated from Equation B.41, β is the slope of the surface relative to the horizontal, f is the modulating factor and is calculated from Equation B.42, and R_b is the ratio of beam solar radiation on a tilted surface to beam solar radiation on a horizontal surface, and is calculated using Equation B.43.

$$A_i = \frac{I_b}{I_o} \qquad (B.41)$$

$$f = \sqrt{\frac{I_b}{I}} \tag{B.42}$$

$$R_b = \frac{\cos\theta}{\cos\theta_z} \tag{B.43}$$

where θ is the angle of incidence of beam solar radiation on surface, is calculated from Equation B.44.

$$\cos\theta = \cos\theta_z * \cos\beta + \sin\theta_z * \cos(\gamma_s - \gamma) * \sin\beta \tag{B.44}$$

where β is the slope of the surface which is defined as the angle between the surface and the horizontal; the slope is measured as a positive value when the surface is tilted in the direction of the azimuth specification, γ_s is the solar azimuth angle and is calculated in Equation B.45, and γ is the azimuth angle of surface which is the angle between the projection of the normal to the surface into the horizontal plane and the local meridian; the signs utilised for γ_s and γ are identical which are zero if facing the equator, positive if facing west and negative if facing east. θ_z is the solar zenith angle and is calculated from Equation B.46. The slope, solar azimuth angle, surface azimuth angle and solar zenith angle for a tilted surface are demonstrated in Figure B.1.

$$\sin\gamma_s = \frac{\cos\delta * \sin\omega}{\sin\theta_z} \tag{B.45}$$

$$\cos\theta_z = \sin\delta * \sin\phi + \cos\phi * \cos\delta * \cos\omega \tag{B.46}$$

where δ is the solar declination angle, ϕ is the latitude and ω is the angular displacement of the sun east or west of the local meridian due to rotation of the earth on its axis at 15^o per hour; morning negative, afternoon positive.

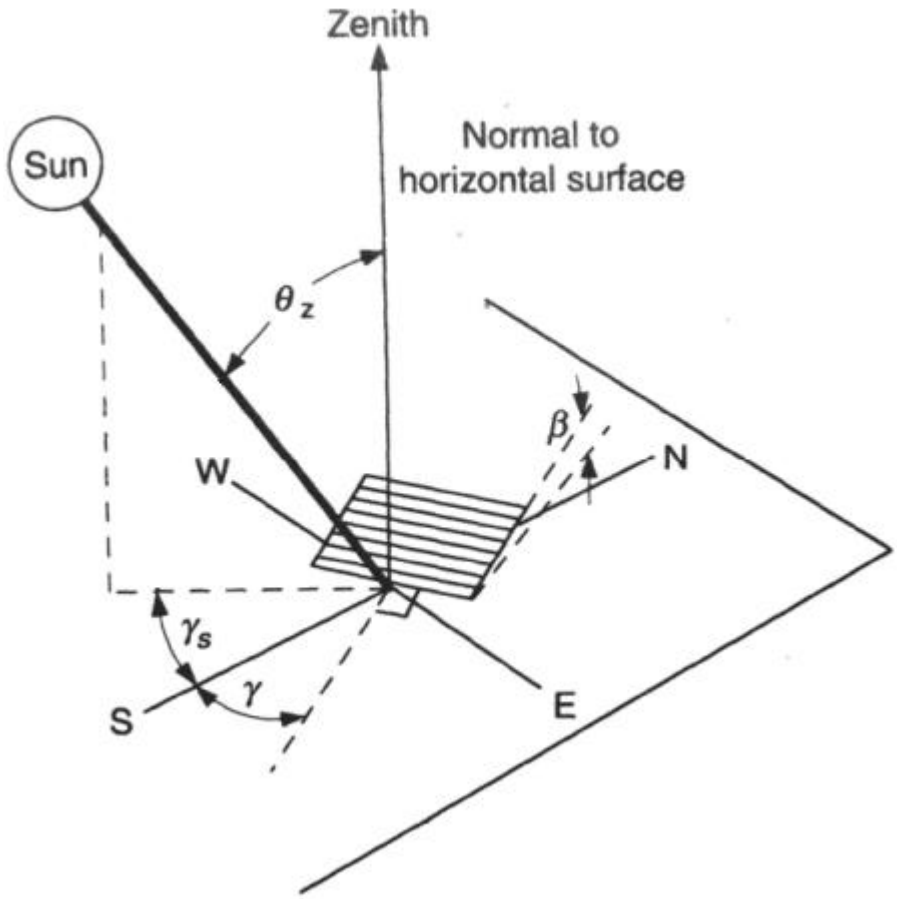

Figure B.1. The slope (β), solar azimuth angle (γ_s), surface azimuth angle (γ) and solar zenith angle (θ_z) for a tilted surface.

The contribution of beam solar radiation on a tilted surface can be calculated using Equation B.47.

$$I_{bt} = (I_b + I_d * A_i) * R_b \qquad \text{(B.47)}$$

where I_{bt} is the beam solar radiation on a tilted surface, I_b is the beam solar radiation on a horizontal surface, I_d is the diffuse solar radiation on a horizontal surface.

The contribution of ground-reflected solar radiation can be calculated using Equation B.48 and by assuming the ground as an isotropic reflector.

$$I_{gr} = I * \frac{1}{2} * \rho_{gr} * (1 - \cos\beta) \quad \text{(B.48)}$$

where ρ_{gr} is the ground reflectance.

APPENDIX C
GENERATION OF HOURLY SOLAR RADIATION VALUES FOR A SOLAR THERMAL SYSTEM

The generation of hourly solar radiation values on a horizontal surface are based on the mathematical models developed from Degelman and Graham (with a slight modification) theory. These mathematical models have been used extensively to predict solar irradiation values for many locations worldwide. The hourly solar radiation values on a tilted surface are then evaluated from the predicted hourly solar radiation values on a horizontal surface using Reindl model. The generation of hourly solar radiation values on a tilted solar thermal collector consists of four main steps. They are:

Step 1. Convert monthly-average daily solar radiation values into monthly clearness index values.

Step 2. Generate daily clearness index values for a year from converted monthly clearness index values.

Step 3. Generate hourly clearness index values for a year from predicted daily clearness index values.

Step 4. Generate hourly beam, diffuse and ground-reflect solar radiation values on a tilted surface from predicted total hourly solar radiation values on a horizontal surface.

In Step 1, monthly solar radiation values are converted into a dimensionless form called clearness index. The detailed description of this conversion is given in Appendix B. Equation C.1 is used to calculate the monthly clearness index:

$$k_m = \frac{H_{ave}}{H_{o,ave}} \tag{C.1}$$

where k_m is the monthly-average clearness index, H_{ave} is the monthly-average daily solar radiation value on a horizontal surface which is required for the study, $H_{o,ave}$ is the monthly-average daily extraterrestrial solar radiation on a horizontal surface and is calculated from Equation C.2.

$$H_{o,ave} = \frac{\sum_{n=1}^{N} H_o}{N} \tag{C.2}$$

where H_o is the daily extraterrestrial solar radiation on a horizontal surface and is calculated from Equation C.3, and N is the number of days in the month:

$$H_o = \frac{24*3600*G_{sc}}{\pi}*\left(1+0.033*\cos\frac{360*n}{365}\right) *\left(\cos\phi*\cos\delta*\sin\omega_s+\frac{\pi*\omega_s}{180}*\sin\phi\sin\delta\right) \tag{C.3}$$

where G_{sc} is the solar constant, n is the day of the year, ϕ is the latitude, δ is the solar declination angle and is calculated in Equation C.4, and ω_s is the sunset hour angle which is calculated in Equation C.5.

$$\delta = 23.45^o * \sin\left[360^o * \frac{284+n}{365}\right] \tag{C.4}$$

$$\cos\omega_s = -\tan\phi*\tan\delta \tag{C.5}$$

In Step 2, the monthly clearness index is used to establish the cumulative distribution function (long-term monthly distribution). The cumulative distribution function is generated using Equation C.6. The generation procedure is given in details in Appendix B.

$$F\left[k_d, \bar{k}_d\right] = \frac{\exp(\nu * k_d) - \exp(\nu * k_{dl})}{\exp(\nu * k_{du}) - \exp(\nu * k_{dl})} \quad (C.6)$$

where k_d is daily clearness index, $\bar{k}_d$ is the average of the daily clearness indices of the month which is equal to k_m, and k_{dl} and k_{du} are the lower and upper bound of the range for k_d.

The N k_d for a month has to be selected from this cumulative distribution to represent the long-term conditions, where N is the number of days in the month (28, 30 or 31). The cumulative distribution is related to the cumulative fraction of occurrence, F. The cumulative fraction of occurrence specifies the fraction of time the k_d variable is less than a specified value of k_d. If it is a 31-day month, the value of k_d corresponding to F equal to 1/31, which means that for 1/31 of the time, i.e. one day in a 31-day month, will a k_d value less than a particular value occur. However, one out of 31 days must be less than this value of k_d [373]. The range from 0 to this value of k_d is not specified; however a logical way to pick a value is to get the value of k_d at the average of the F-value and the previous one, e.g. the second k_d value obtained is corresponding to F-value equal to 3/62 since this F-value is the average of the value (2/31) and the previous value (1/31) [373].

The obtained N k_d values for a month is placed in an order which the k_d values should occur. However, this order should not be neither in an ascending or a descending order nor should be in a random order [369]. The lag-one autocorrelation of the annual series

of daily total solar radiation is generally between 0.15 and 0.35 which is an indication of weak positive correlation and shows no systematic dependence on location or climate type [369]. A fixed order is developed based on the autocorrelation capitalised at different locations. The orders of k_d values depend on the k_m value and show a correct lag-one daily k_d autocorrelation. For a 31-day month, the numbers 1 to 31 are assigned to the 31 values obtained from the cumulative distribution; 1 represents the smallest k_d value and 31 represents the largest value. The numbers 1 to 31 are then placed in an order such that when the k_d values corresponding to the N numbers are placed in that order, the approximate lag-one autocorrelation is reproduced. The sequences of ordering daily clearness index values are shown in Table C.1.

$k_m \leq 0.45$	24, 28, 11, 19, 18, 3, 2, 4, 9, 20, 14, 23, 8, 16, 21, 26, 15, 10, 22, 17, 5, 1, 6, 29, 12, 7, 31, 30, 27, 13, 25
$0.45< k_m < 0.55$	24, 27, 11, 19, 18, 3, 2, 4, 9, 20, 14, 23, 8, 16, 21, 7, 22, 10, 28, 6, 5, 1, 26, 29, 12, 17, 31, 30, 15, 13, 25
$k_m \geq 0.55$	24, 27, 11, 4, 18, 3, 2, 19, 9, 25, 14, 23, 8, 16, 21, 26, 22, 10, 15, 17, 5, 1, 6, 29, 12, 7, 31, 20, 28, 13, 30

Table C.1. Sequences of ordering daily clearness index values [369].

The same sequence of the numbers 1 to 31 is always utilised for ordering the daily k_d values, however, the beginning point with the sequence is determined randomly at the start of the generation process. For months of other than 31 days, only the numbers of days (e.g. 28 or 30) are obtained from the 31-day cumulative distribution. The number (e.g. number 31 in a 30-day month) is simply skipped in the sequence. Even though this does have a slight impact on the daily autocorrelation, it is small and considered less important than maintaining the long-term distribution.

In Step 3, if the daily clearness index value of k_d is known, the long term mean value of clearness index for each hour, k_{hm}, can be estimated from Equation C.7:

$$k_{hm} = \frac{H}{H_o} * \frac{I}{H} * \frac{H_o}{I_o} \approx k_d * r_t * \frac{H_o}{I_o} \tag{C.7}$$

where r_t is ratio of hourly global solar radiation on a horizontal surface to daily global solar radiation on a horizontal surface [374], and is calculated using Equation C.8.

$$r_t = (a + b * \cos\omega) * \frac{I_o}{H_o} \tag{C.8}$$

where

$$\begin{aligned} a &= 0.409 + 0.5016 * \sin(\omega_s - 60) \\ b &= 0.6609 + 0.4767 * \sin(\omega_s - 60) \end{aligned} \tag{C.9}$$

where ω is the hour angle, ω_s is the sunset hour angle, I_o is the hourly global extraterrestrial solar radiation on a horizontal surface, and is calculated in Equation C.10. H_o is the daily extraterrestrial global solar radiation on a horizontal surface, and is calculated in Equation C.11.

$$\begin{aligned} I_o = {} & \frac{12 * 3600}{\pi} * G_{sc} * \left(1 + 0.033 * \cos\frac{360n}{365}\right) * \\ & \left[\cos\phi\cos\delta(\sin\omega_2 - \sin\omega_1) + \frac{\pi * (\omega_2 - \omega_1)}{180} * \sin\phi\sin\delta\right] \end{aligned} \tag{C.10}$$

$$\begin{aligned} H_o = {} & \frac{24 * 3600}{\pi} * G_{sc} * \left(1 + 0.033 * \cos\frac{360n}{365}\right) \\ & * \left[\cos\phi\cos\delta\sin\omega_s + \frac{\pi * \omega}{180} * \sin\phi\sin\delta\right] \end{aligned} \tag{C.11}$$

where G_{sc} is the solar constant, ϕ is the latitude, δ is the declination, and n is the day of the year. The description of each term in details is given in Appendix B.

The k_h values are transferred from the cumulative distribution function to a normal distribution variable, χ, with a mean of 0 and a variance of 1. This transferred variable can then be represented by a first-order autoregressive model [375], as shown in Equation C.12.

$$\chi_t = \phi_1 * \chi_{t-1} + \phi_2 * \chi_{t-2} + ... + \phi_N * \chi_{N-1} + \varepsilon_t \quad \text{(C.12)}$$

For a first-order autoregressive model, N is equal to 1 and ϕ_1 is the lag-one autocorrelation. In this case, this parameter was estimated by performing a large number of calculations using Equation C.13 [376], and found to be a weak function of k_d. However this parameter is not statistically different from the mean value of 0.54. This value is also used to represent the lag-one autocorrelation of the deviations of k_h from k_{hm}.

$$\phi_1 = \frac{\sum_{\text{days}} \sum_{i=2}^{N-1} (y_i - \bar{y}) * (y_{i+1} - \bar{y})}{\sum_{\text{days}} \sum_{i=2}^{N-1} (y_i - \bar{y})} \quad \text{(C.13)}$$

where N is the number of hourly k_h values in a day. The first and the last hour for which solar radiation recorded each day were discarded, as the radiation amounts are always small and inaccurate. In order to generate the k_h values, a χ value for each hour is obtained by randomly selecting a value for ε_t from a Gaussian (normal) distribution with a mean of 0 and a variance of $1-\phi_1^2$, and then applying this selected ε_t value into a first-order lag correlation as shown in Equation C.14.

$$\chi_t = \phi_1 * \chi_{t-1} + \varepsilon_t \quad \text{(C.14)}$$

The χ is transferred to a non-Gaussian k_h by equating the normal cumulative distribution function of χ to the non-Gaussian distribution function of k_h. The equation for a normal cumulative distribution with a mean of 0 and a variance of 1 is as follows:

$$\begin{aligned} F_{normal} &= \frac{1}{\sqrt{2*\pi}} * \int_{-\infty}^{\chi} \exp\left(-\frac{1}{2} * t^2\right) dt \\ &= \frac{1}{2} * \left[1 + \text{erf}\left(\frac{\chi}{\sqrt{2}}\right)\right] \end{aligned} \tag{C.15}$$

where erf(z) is the error function which is given in Equation C.16.

$$\text{erf}(z) = \frac{2}{\pi} * \int_0^z e^{-t^2} dt \tag{C.16}$$

Both the mean and the shape of the cumulative distribution of k_h values are dependent on the hour of the day and the k_d value. Therefore the functional dependence can be approximated by a single curve. The cumulative distribution function of the k_h is represented in Equation C.17.

$$F_{k_h} = \frac{1}{1 + \exp(-1.585 * h)} \tag{C.17}$$

where

$$h = (k_h - k_{hm}) / (\sigma_{k_h}) \tag{C.18}$$

where k_{hm} is estimated from Equation C.6 and σ_{k_h} is calculated from Equation C.19 [376].

$$\sigma_{k_h} = 0.1557 * \sin\left(\frac{\pi * k_d}{0.933}\right) \tag{C.19}$$

k_h can be solved using Equation C.20 by equating the cumulative distribution functions.

$$k_h = k_{hm} - \frac{\sigma_{k_h}}{1.585} * \ln\left[\frac{1}{\frac{1}{2} * \left\{1 + \text{erf}\left(\frac{\chi}{\sqrt{2}}\right)\right\}} - 1\right] \quad \text{(C.20)}$$

The k_h's sequence is not continuous; therefore a new χ's series has to be generated for each day (the last hour χ on the previous day should not be used as the χ_{t-1} for the first hour of the next day). Zero, mean value of χ, is utilised for the initial value of χ_{t-1}.

The daily total of the summed hourly solar radiation values is not necessarily equal to the initially generated daily solar radiation value. To correct this, a correction factor, a ratio of the generated daily solar radiation value to the sum of all generated hourly solar radiation values for the day, is employed. Each k_h value is then multiplying by this correction factor, therefore ensure that the total hourly solar radiation values for the day is the same as the daily solar radiation value generated from the monthly value. This correction does not have any significant effect on the diurnal variation, and also makes sure that the long-term daily statistic is maintained.

In Step 4, for most of the cases, the total solar radiation fall on a tilted solar thermal collector surface is of interest. This is obtained by calculating and summing the beam, diffuse and ground-reflected solar radiation components. The Reindl model is used to calculate these components in this Appendix. The procedure employed to calculate the contribution of beam solar radiation on a tilted surface, shown in Equation C.21, is the only difference between this model and the HDKR model presented in Appendix B:

$$I_{bt} = I_b * R_b \quad \text{(C.21)}$$

where I_{bt} is the beam solar radiation on a tilted surface, I_b is the beam solar radiation on a horizontal surface, and R_b is the ratio of beam solar radiation on a tilted surface to beam solar radiation on a horizontal surface and is calculated in Equation C.22.

$$R_b = \frac{\cos\theta}{\cos\theta_z} \tag{C.22}$$

where θ is the angle of incidence of beam solar radiation on surface, and is calculated from Equation C.23.

$$\cos\theta = \cos\theta_z * \cos\beta + \sin\theta_z * \cos(\gamma_s - \gamma) * \sin\beta \tag{C.23}$$

where θ_z is the solar zenith angle and is calculated from Equation C.24, β is the slope of the surface, γ_s is the solar azimuth angle and is calculated in Equation C.25, and γ is the azimuth angle of the surface.

$$\cos\theta_z = \sin\delta * \sin\phi + \cos\phi * \cos\delta * \cos\omega \tag{C.24}$$

$$\sin\gamma_s = \frac{\cos\delta * \sin\omega}{\sin\theta_z} \tag{C.25}$$

where δ is the solar declination angle, ϕ is the latitude and ω is the mean hour angle of time step.

The correlation employed to calculate the hourly diffuse solar radiation on a horizontal surface is identical to that described in Appendix B. The contribution of diffuse solar radiation and ground-reflected solar radiation on a tilted surface are the same as described in Appendix B which can be calculated using Equations C.26 and C.27 respectively.

$$I_{dt} = I_d * \left[0.5*(1-A_i)*(1+\cos\beta)*\left\{1+f*\sin^3\left(\frac{\beta}{2}\right)\right\} + A_i * R_b \right] \quad \text{(C.26)}$$

where I_{dt} is the diffuse solar radiation on a tilted surface, I_d is the diffuse solar radiation on a horizontal surface, A_i is the anisotropy index and f is the modulating factor.

$$I_{gr} = I*\frac{1}{2}*\rho_{gr}*(1-\cos\beta) \quad \text{(C.27)}$$

where ρ_{gr} is the ground reflectance.

APPENDIX D
GENERATION OF HOURLY AMBIENT AIR TEMPERATURE VALUES

The hourly ambient air temperature values for a year can be reasonably and statistically generated using Delgelman's theory. The calculations performed are based on provided 12 monthly-average daily ambient air temperature values, one for each month, and two predetermined sequences for ordering daily-average and daily-maximum ambient air temperature values. The hourly ambient air temperature values for a year are generated from seven steps:

Step 1. Calculate daily standard deviation about the monthly-average daily ambient air temperature.

Step 2. Calculate monthly-average daily-maximum ambient air temperature values.

Step 3. Calculate daily-maximum standard deviation about the monthly-average daily-maximum ambient air temperature.

Step 4. Generate daily-average ambient temperature values.

Step 5. Generate daily-maximum ambient air temperature values.

Step 6. Generate daily-minimum ambient air temperature values.

Step 7. Generate hourly ambient air temperature values.

In Step 1, the daily standard deviation, δ_d, about the monthly-average daily ambient air temperature is calculated in Equation D.1 [373]:

$$\delta_d = 9.273 - 0.07952 * T_m + 0.0097111 * \delta_{yr} \quad \text{(D.1)}$$

where T_m is the monthly-average daily ambient air temperature and δ_{yr} is the standard deviation of the monthly-average daily temperature about the yearly-average monthly temperature.

In Step 2, the monthly-average daily-maximum ambient air temperature values, $T_{m,max}$, are calculated from the monthly-average daily ambient air temperature values and the monthly clearness index values, as shown in Equation D.2.

$$T_{m,max} = T_m + \frac{1}{2} * A \quad \text{(D.2)}$$

where A is the peak-to-peak amplitude of the monthly-average diurnal variation of the ambient temperature, and is calculated from Equation D.3.

$$A = 25.8 * k_m - 5.21 \quad \text{(D.3)}$$

where k_m is the monthly clearness index which is the ratio of monthly-average daily solar radiation on a horizontal surface to the monthly-average daily extraterrestrial radiation.

In Step 3, the standard deviation of the daily-maximum temperature ($\delta_{d,max}$) about the monthly-average daily-maximum temperature is calculated from the daily standard deviation, as shown in Equation D.4.

$$\delta_{d,max}(i) = \frac{\delta_d(i) - C_1(i)}{C_2(i)} \quad \text{(D.4)}$$

where i indicates the month, and C_1 and C_2 are determined from Table D.1.

Month	C_1	C_2
January	0.8033	0.7900
February	1.8151	0.6899
March	2.9018	0.5823
April	2.397	0.6053
May	0.6159	0.7343
June	0.3275	0.7920
July	1.2187	0.9717
August	1.4222	1.0269
September	0.2053	0.8326
October	3.0621	0.5167
November	3.0242	0.5811
December	5.0849	0.3777

Table D.1. Coefficients used to estimate the standard deviation of the maximum daily ambient temperature from the standard deviation of the average daily ambient temperature [373].

In Step 4, the daily-average ambient air temperature values (for each month) are obtained from a normal cumulative, and then ordered by a fixed sequence to replicate the daily correlation. The knowledge of both the mean and the standard deviation is required to uniquely specify this normal distribution. The mean is the monthly-average daily ambient air temperature and the daily standard deviation is calculated in Equation D.1.

The generation of the daily-average temperature values for a month consists of two steps:

A) Obtain N daily-average ambient air temperature (T_d) values from the cumulative distribution in a manner such that the N values will recreate the distribution. N is the number of days in a month (31, 30 or 28). The cumulative distribution is related to the cumulative fraction of occurrence, F. The cumulative fraction of occurrence can specify the fraction of time that the T_d variable is less than a specified T_d value. As an example, assuming a 31-day month, there is only one value of T_d corresponding to F equal to 1/31, which indicates that for 1/31 of the time will T_d less than a particular value occur. However, 1 out of 31 days must be less than this value of T_d. The range from 0 to this value of T_d is not specified; however a logical way to choose a value is to take the value of T_d at the average of the F value and the previous one, e.g. the T_d value for a day is obtained corresponding to F value equal to 1/62 as this F value is the average of the F value (1/31) and previous F value (0), as shown in an exaggerated Figure D.1.

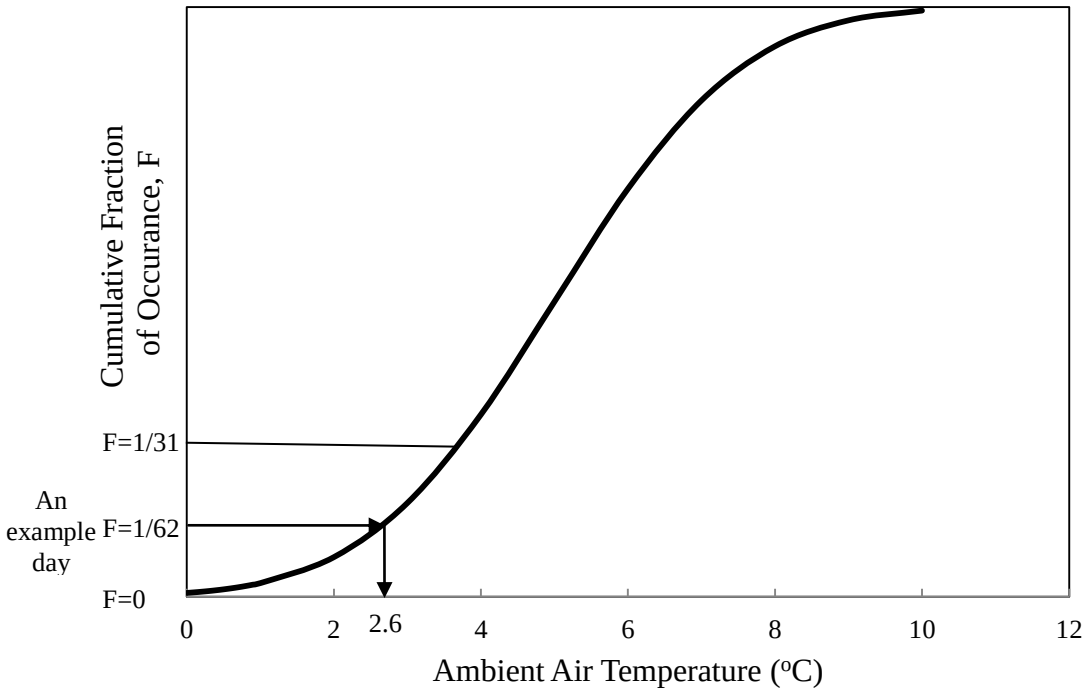

Figure D.1. A demonstration of obtaining a T_d value from an exaggerated cumulative distribution diagram.

Like the example shown, one and only one T_d value will occur between the T_d value associated with F=1/31 and F=2/31; hence the T_d value corresponding to F=3/62 can be found. 31 daily-average ambient air temperature values can be generated in this manner. The same method can be easily applied to a 30-day or a 28-day month.

B) Ordering these N daily-average ambient air temperature values in order to produce a correct daily autocorrelation. Again, the order is determined from a fixed sequence, However, this sequence used to order the daily-average ambient air temperature values is a distinctly different sequence from the one used to order the k_d values. The sequence starting position is determined at the beginning of the generation process and remains the same for all of the sequences.

In Step 5, the daily-maximum ambient air temperature values can be also generated in a similar approach as the generation of daily-average ambient temperature values. The cumulative distribution of the maximum temperature is also assumed to be normal; the mean and the standard deviation are calculated from Equation D.2 and D.4 respectively. However a different sequence is used to order these daily-maximum ambient temperature values; this sequence employed presents a significant correlation between the daily-average and daily-maximum ambient temperature values. The sequences for ordering daily-average ambient air temperature values and daily-maximum ambient air temperature values are shown in Table D.2.

T_m	20, 29, 13, 26, 31, 30, 21, 12, 14, 11, 2, 1, 3, 15, 25, 9, 5, 7, 6, 4, 19, 8, 10, 23, 22, 27, 16, 18, 28, 17, 24
$T_{m,max}$	24, 29, 14, 21, 31, 30, 23, 5, 12, 11, 2, 1, 7, 16, 25, 10, 8, 3, 4, 9, 18, 6, 13, 26, 20, 22, 15, 17, 27, 19, 28

Table D.2. Sequences for ordering daily average ambient temperature and daily maximum ambient temperature values [371].

In Step 6, the daily-minimum ambient air temperature values are calculated by assuming the daily-average values are equal to the median which is the average of the daily-maximum and daily-minimum ambient temperature values.

In Step 7, the hourly ambient air temperature values are generated by performing a cosine interpolation between the daily-maximum and daily-minimum ambient air temperature values. This produces a continuous series of hourly ambient air temperature values and also gives a smooth transition between adjacent days.

The minimum hourly ambient temperature is assumed to be the value for the hour in which sun rises; the maximum hourly ambient temperature is assumed to be the value at 3pm. All of the daily-average and the daily-maximum ambient temperature values have

to be generated one day in advance, therefore the next day's minimum ambient temperature value is available for the interpolation between the maximum ambient temperature of one day and the minimum temperature of the following day. Equation D.5 is used to calculate the hourly ambient temperature, T_{hr}:

$$T_{hr} = T_{ave} + B * \cos(\frac{\pi * \Delta}{R}) \qquad (D.5)$$

where T_{ave} is the median ambient temperature for the particular portion of the day as shown in Table D.3. B is the amplitude for the particular portion of the day which is one half of the difference between the appropriate maximum and minimum temperatures. This amplitude is negative during the sunrise-to-3pm period. Δ is the number of hours goes into the time period and R is the number of hours in the appropriate time period.

From sunrise of the day (the minimum ambient temperature of the day) to 3pm of the day (the maximum ambient temperature of the day)	T_{ave} is equivalent to the daily-average ambient temperature.
From 3pm of the day (the maximum ambient temperature of the day) to sunrise of the next day (the minimum ambient temperature of the next day)	T_{ave} is the average of the maximum ambient temperature of the day and the minimum ambient temperature of the following day.

Table D.3. Variation of T_{ave} used for calculating hourly ambient temperature values.

APPENDIX E

OPTIMISED INTEGRATION CODE DEVELOPED IN MATLAB

The optimised integration of a micro-renewable energy generation system is performed using a custom-written MATLAB code. The custom-written model is purposely developed and a database containing the selected micro wind turbines and their hourly power outputs, the selected solar PV modules and their hourly power outputs, the selected ASHP, the selected solar flat plate/evacuated tube collectors, the hourly power inputs required to operate a mono/hybrid micro-renewable thermal generation system for providing the entire heating and hotwater, the hourly power inputs to drive the primary and/or the auxiliary heating system and the electrical immersion in the hotwater storage cylinder, hourly household electrical loads, and complete costs (installation, operation, replacement and maintenance) associated with these energy generation systems are all stored in the model. The mono or hybrid micro-renewable electricity generation system combination, single or combined micro-renewable thermal generation system, and the combination of both are first realistically formed. The formed systems that can satisfy the imposed constraints and guideline are subsequently considered in the economic analysis, whilst the rest are discarded. A comprehensive economic analysis over the project lifespan is then performed and the system that performs best economically is deemed as the optimum system which allows the system configuration to be determined. The optimised integration Matlab code was written in three phases and consists of an overall code and two separate types of sub-codes.

The overall code, as shown in Figure E.1-E.3, contains the information including the capacity and physical sizes of all selected micro-renewable energy generation systems, the costs of these systems and other associated components, the individual lifespan of these systems and the user-specified project period, the constraints and guidelines enforced, and the economic parameters required to perform the economic analysis. This overall code is developed to compare all sub-optimal systems, and determine the overall optimal system and then illustrate the system configuration. Each sub-optimal system is determined from the sub-code developed for a mono/hybrid micro-renewable electricity generation system consisting of a selected micro wind turbine and a solar PV system assembled from a solo capacity solar PV module, combined with all mono/hybrid micro-renewable thermal generation systems.

```
function [optimalresult, SCT_optimal,
 SCN_optimal,ASHPC_optimal,SMN_optimal,WTN_optimal,COMB_optimal] =
bestLCC(SS1,SS2,SS3,WW1,WW2,WW3, WW4, WW5, WW6,S1,S2,S3,W1,W2,W3, W4, W5, W6,EL)

global i
global rp
global in1 IN1 in2 IN2 in3 IN3  ivr wivr
global SMP1 WTP1 SMP2 WTP2 SMP3 WTP3 WTP4 WTP5 WTP6
global ip ep iep
global rir  mcS
global TCS MCS TAREA AS1 AS2 AS3
global ICPKW1 ICPKW2 ICPKW3
global iy pl
global cgw cgspv cgASHP cgst
global mcW1 mcW2 mcW3
global sl1 sl2 sl3 wl1 wl2 wl3 wl4 wl5 wl6
global win1 win2 win3 win4 win5 win6 WIN1 WIN2 WIN3 WIN4 WIN5 WIN6
global  cpr  spsr  SF1  SE1  ASHP11  ASHP12  ASHP13  HWC1  MCSFS  MCSTS  MCASHP1  MCASHP2
MCASHP3 IniICSFS ICPFP IniICSES ICPEP ASHPP1 ASHPP2 ASHPP3 pocp HWCP posps


 rp=0;                  % Renewable energy requirement
 TCS=3;                 % Total Capacity of a solar PV system (kW)
MCS=0.5;                % Minimum Capacity of Solar system (kW)
TAREA=100;              % Total area of a solar energy generation system
AS1=1.0;                % Area of Kyocera 135W solar PV module
AS2=1.28;               % Area of CareyGlass 185W solar PV module
AS3=1.63;               % Area of Sharp 235W solar PV module
 in1=1.32;               % Sunny boy-1200 inverter
IN1=1150;               % Price of a sunny boy-1200 inverter
in2=2.70;               % Sunny boy-2500 inverter
IN2=1700;               % Price of a sunny boy-2500 inverter
in3=3.2;                % Sunny boy-3000 inverter
IN3=1900;               % Price of a sunny boy-3000 inverter
 win1=1.2;              % Windy boy-1200 inverter
WIN1=1100;              % Windy boy-1200 inverter price
win2=1.7;
WIN2=1400;
win3=2.5;
WIN3=1800;
win4=3.8;
WIN4=2250;
win5=5;
WIN5=3200;
win6=6;
WIN6=3250;
ivr=15;                 % The year of inverter replacement
wivr=15;                % The year of wind turbine inverter replacement
cpr=15;                 % Circulating pump replacement
spsr=15;                % Solar pump station replacement
ip=0.1928;              % Imported electricity price
ep=0.09;                % Exported electricity price
iep=0.09;               % Incentive exported price if it is applicable, otherwise it is the same as the
exported  price
rir= 0.0219;            % Real interest rate
iy=0;                   % Incentive years
sl1=25;                 % 135kW Solar PV module lifespan
sl2=25;                  % 185kW Solar PV module lifespan
sl3=25;                 % 235kW Solar PV module lifespan

wl1=15;                 % wind turbine lifespan 1
wl2=20;                 % wind turbine lifespan 2
wl3=20;                 % wind turbine lifespan 3
wl4=20;                 % wind turbine lifespan 4
wl5=20;                 % wind turbine lifespan 5
wl6=25;                 % wind turbine lifespan 6
SF1=25;                 % Solar flatplate collector lifespan
SE1=25;                 % Solar evacuated tube collector lifespan
ASHP11=20;              % Air Source Heat Pump 5kW lifespan 1
ASHP12=20;              % Air Source Heat Pump 9kW lifespan 2
ASHP13=20;              % Air Source Heat Pump 14 kW lifespan 3
HWC1=25;                % Hotwater Cylinder lifespan
pl=20;                  % Project lifespan
mcS=50;                 % Maintenance cost for a Solar PV system
```

Figure E.1. The Matlab code developed to perform the overall optimised integration.

```
mcW1=100;          % Maintenance cost for a wind turbine having a capacity less than 2kW
mcW2=180;          % Maintenance cost for a wind turbine having a capacity between 2kW and 4 kW
inclusive
mcW3=280;          % Maintenance cost for a wind turbine having a capacity greater than 4 kW
MCSFS=50;           % Maintenance cost for a solar flatplate collector system
MCSTS=50;           % Maintenance cost for a solar evacuated tube collector system
MCASHP1=230;       % Maintenance cost for 5kW Air Source Heat Pump
MCASHP2=230;       % Maintenance cost for 5kW Air Source Heat Pump
MCASHP3=230;       % Maintenance cost for 5kW Air Source Heat Pump
cgw=0;             % Capital grant for a wind turbine
cgspv=0;           % Capital grant for a solar PV system
cgASHP=0;          % Capital grant for an air source heat pump
cgst=800;          % Capital grant for a solar thermal system
SMP1= 400;         % Price for a 135W solar PV module
WTP1= 4800;        % Price for an Ampair 600-230 wind turbine
SMP2= 500;         % Price for a 185W solar PV module
WTP2= 7000;        % Price for a Swift 1.5kW wind turbine
SMP3=650;          % Price for a 235W solar PV module
WTP3=14000;        % Price for a skystream 3.7 wind turbine
WTP4=25000;        % Price for a siliken 3.4 wind turbine
WTP5=35000;        % Price for an Evance R9000 wind turbine
WTP6=45000;        % Price for a CF6d wind turbine
 ICPKW1=2550;      % Installation cost per kW for a solar PV system assembled from 135W PV solar
module
ICPKW2=2050;       % Installation cost per kW for a solar PV system assembled from 185W PV solar
module
ICPKW3=1400;       % Installation cost per kW for a solar PV system assembled from 235W PV solar
module
IniICSFS = 2750;   % Initial cost for an installed solar flatplate collector system
ICPFP = 580;       % Installation cost for a flatplate collector per 2m^2
IniICSES = 2700;   % Initial cost for an installed solar evacuated tube collector system
ICPEP = 500;       % Installation cost for an evacuated tube collector per 10 tubes
ASHPP1= 8100;      % Installed cost of an air source heat pump having a capacity of 5kW
ASHPP2 = 9500;     % Installed cost of an air source heat pump having a capacity of 9kW
ASHPP3=12200;      % Installed cost of an air source heat pump having a capacity of 14kW
pocp=180;          % Price of a circulating pump
posps=430;         % Price of a solar pump station
```

```
HWCP=950;              % Price of an hotwater cylinder

for i=1:18

[minLCC{1}, minSMN{1}, minWTN{1}, minCOMB{1}, minSCT{1}, minSCN{1}, minASHPC{1}] =
combineS1W1(S1,SS1,W1,WW1,EL)
[minLCC{2}, minSMN{2} minWTN{2}, minCOMB{2}, minSCT{2}, minSCN{2}, minASHPC{2}] =
combineS1W2(S1,SS1,W2,WW2,EL)
[minLCC{3}, minSMN{3}, minWTN{3}, minCOMB{3}, minSCT{3}, minSCN{3}, minASHPC{3}] =
combineS1W3(S1,SS1,W3,WW3,EL)
[minLCC{4}, minSMN{4}, minWTN{4}, minCOMB{4}, minSCT{4}, minSCN{4}, minASHPC{4}] =
combineS1W4(S1,SS1,W4,WW4,EL)
[minLCC{5}, minSMN{5}, minWTN{5}, minCOMB{5}, minSCT{5}, minSCN{5}, minASHPC{5}] =
combineS1W5(S1,SS1,W5,WW5,EL)
[minLCC{6}, minSMN{6}, minWTN{6}, minCOMB{6}, minSCT{6}, minSCN{6}, minASHPC{6}] =
combineS1W6(S1,SS1,W6,WW6,EL)
[minLCC{7}, minSMN{7}, minWTN{7}, minCOMB{7}, minSCT{7}, minSCN{7}, minASHPC{7}] =
combineS2W1(S2,SS2,W1,WW1,EL)
[minLCC{8}, minSMN{8}, minWTN{8}, minCOMB{8}, minSCT{8}, minSCN{8}, minASHPC{8}] =
combineS2W2(S2,SS2,W2,WW2,EL)
[minLCC{9}, minSMN{9}, minWTN{9}, minCOMB{9}, minSCT{9}, minSCN{9}, minASHPC{9}] =
combineS2W3(S2,SS2,W3,WW3,EL)
[minLCC{10}, minSMN{10}, minWTN{10}, minCOMB{10}, minSCT{10}, minSCN{10},
minASHPC{10}] = combineS2W4(S2,SS2,W4,WW4,EL)
[minLCC{11}, minSMN{11}, minWTN{11}, minCOMB{11}, minSCT{11}, minSCN{11},
minASHPC{11}] = combineS2W5(S2,SS2,W5,WW5,EL)
[minLCC{12}, minSMN{12}, minWTN{12}, minCOMB{12}, minSCT{12}, minSCN{12},
minASHPC{12}] = combineS2W6(S2,SS2,W6,WW6,EL)
[minLCC{13}, minSMN{13}, minWTN{13}, minCOMB{13}, minSCT{13}, minSCN{13},
minASHPC{13}] = combineS3W1(S3,SS3,W1,WW1,EL)
[minLCC{14}, minSMN{14}, minWTN{14}, minCOMB{14}, minSCT{14}, minSCN{14},
minASHPC{14}] = combineS3W2(S3,SS3,W2,WW2,EL)
[minLCC{15}, minSMN{15}, minWTN{15}, minCOMB{15}, minSCT{15}, minSCN{15},
minASHPC{15}] = combineS3W3(S3,SS3,W3,WW3,EL)
[minLCC{16}, minSMN{16}, minWTN{16}, minCOMB{16}, minSCT{16}, minSCN{16},
minASHPC{16}] = combineS3W4(S3,SS3,W4,WW4,EL)
```

Figure E.2. The Matlab code developed to perform the overall optimised integration.

```
[minLCC{17}, minSMN{17}, minWTN{17}, minCOMB{17}, minSCT{17}, minSCN{17},
minASHPC{17}] = combineS3W5(S3,SS3,W5,WW5,EL)
[minLCC{18}, minSMN{18}, minWTN{18}, minCOMB{18}, minSCT{18}, minSCN{18},
minASHPC{18}] = combineS3W6(S3,SS3,W6,WW6,EL)


        [optimalresult,idx]=min(cell2mat(minLCC))

        SCT_optimal=minSCT{idx}

        SCN_optimal=minSCN{idx}

        ASHPC_optimal=minASHPC{idx}

        SMN_optimal=minSMN{idx}

        WTN_optimal=minWTN{idx}

        COMB_optimal=minCOMB{idx}

end
end
```

Figure E.3. The Matlab code developed to perform the overall optimised integration.

Of the two separate types of sub-codes, one type is designed for the integration of micro-renewable electricity generation systems, as shown in Figure E.4-E.9, whilst the other is designed for the integration of micro-renewable thermal generation systems as shown in Figure E.10-E.11. Due to the interacting effect, as the domestic heating generation system, either an ASHP or a primary electrical heating system, is used to provide entire heating, but also employed to preheat water in the hotwater storage cylinder. All systems (either a mono or a hybrid thermal generation system) have to be individually simulated, and hourly power inputs required to operate the system for providing the entire heating and hotwater are then obtained. The detailed costs required for these heating and hotwater generation are also calculated. All of this useable information is fed into the sub-code which has been developed for the integration of micro-renewable electricity generation systems. The overall hourly electricity consumption for a domestic dwelling is obtained by adding the hourly household electrical loads with the hourly power inputs required for the thermal generation systems. The mono or hybrid micro-renewable electricity systems are formed from a selected micro wind turbine and/or a solar PV system assembled from a selected solo capacity solar PV module(s); the capacity of the solar PV system is dependent on the number of solar PV modules utilised. The formed system is then assessed in order to verify that if it can satisfy the enforced constraints and guidelines i.e. renewable energy requirement. The economic analysis is carried out for the satisfied systems. If the calculated economic outcome of a system combination is better than the previous system combination, this combined system is then deemed as the temporary optimum system. However, if the calculated economic result is worse than the previous one, the system is then discarded. The sub-optimal system is then determined once all systems

(one kind of system combination consisting of a selected micro wind turbine and/or a selected solar PV module) have been analysed and compared.

```
function [minLCC, minSMN, minWTN, minCOMB, minSCT, minSCN,
minASHPC]=combineS1W1(S1,SS1,W1,WW1,EL)

global Goodresult
global i
global S2 SS2 S3 SS3 W2 WW2 W3 WW3 W4 WW4 W5 WW5 W6 WW6
global rp
global in1 IN1 in2 IN2 in3 IN3 ivr wivr
global SMP1 SMP2 SMP3 WTP1 WTP2 WTP3 WTP4 WTP5 WTP6
global ip ep iep
global rir mcS mcW irwl
global TCS MCS TAREA AS1 AS2 AS3
global ICPKW1 ICPKW2 ICPKW3
global iy pl
global cgw cgspv cgASHP cgst
global mcW1 mcW2 mcW3
global sl1 sl2 sl3 wl1 wl2 wl3 wl4 wl5 wl6
global win1 win2 win3 win4 win5 win6 WIN1 WIN2 WIN3 WIN4 WIN5 WIN6
global cpr SF1 SE1 ASHP11 ASHP12 ASHP13 HWC1 MCSFS MCSTS MCASHP1 MCASHP2
MCASHP3 IniICSFS ICPFP IniICSES ICPEP ASHPP1 ASHPP2 ASHPP3 pocp HWCP posps spsr
%S1 hourly power outputs from a solar PV module
%SS1 capacity of a solar PV module
%W1 hourly power outputs from a wind turbine
%WW1 capacity of a wind turbine
%EL hourly electrical load

leastLCC=100000000;

for ii=1:68
        [AreaSC(1),ICTS{1},ELTS{1}, MCTS{1}, RCTS{1},SCTS{1}, SCT{1}, SCN{1},
ASHPC{1}] = combineSFS2ASHP1();
        [AreaSC(2),ICTS{2},ELTS{2}, MCTS{2}, RCTS{2},SCTS{2}, SCT{2}, SCN{2},
ASHPC{2}] = combineSFS4ASHP1();
        [AreaSC(3),ICTS{3},ELTS{3}, MCTS{3}, RCTS{3},SCTS{3}, SCT{3}, SCN{3},
ASHPC{3}] = combineSFS6ASHP1();
        [AreaSC(4),ICTS{4},ELTS{4}, MCTS{4}, RCTS{4},SCTS{4}, SCT{4}, SCN{4},
ASHPC{4}] = combineSFS8ASHP1();
        [AreaSC(5),ICTS{5},ELTS{5}, MCTS{5}, RCTS{5},SCTS{5}, SCT{5}, SCN{5},
ASHPC{5}] = combineSFS10ASHP1();
        [AreaSC(6),ICTS{6},ELTS{6}, MCTS{6}, RCTS{6},SCTS{6}, SCT{6}, SCN{6},
ASHPC{6}] = combineSFS12ASHP1();
        [AreaSC(7),ICTS{7},ELTS{7}, MCTS{7}, RCTS{7},SCTS{7}, SCT{7}, SCN{7},
ASHPC{7}] = combineSFS2ASHP2();
        [AreaSC(8),ICTS{8},ELTS{8}, MCTS{8}, RCTS{8},SCTS{8}, SCT{8}, SCN{8},
ASHPC{8}] = combineSFS4ASHP2();
        [AreaSC(9),ICTS{9},ELTS{9}, MCTS{9}, RCTS{9},SCTS{9}, SCT{9}, SCN{9},
ASHPC{9}] = combineSFS6ASHP2();
        [AreaSC(10),ICTS{10},ELTS{10}, MCTS{10}, RCTS{10},SCTS{10}, SCT{10}, SCN{10},
ASHPC{10}] = combineSFS8ASHP2();
        [AreaSC(11),ICTS{11},ELTS{11}, MCTS{11}, RCTS{11},SCTS{11}, SCT{11}, SCN{11},
ASHPC{11}] = combineSFS10ASHP2();
        [AreaSC(12),ICTS{12},ELTS{12}, MCTS{12}, RCTS{12},SCTS{12}, SCT{12}, SCN{12},
ASHPC{12}] = combineSFS12ASHP2();
        [AreaSC(13),ICTS{13},ELTS{13}, MCTS{13}, RCTS{13},SCTS{13}, SCT{13}, SCN{13},
ASHPC{13}] = combineSFS2ASHP3();
        [AreaSC(14),ICTS{14},ELTS{14}, MCTS{14}, RCTS{14},SCTS{14}, SCT{14}, SCN{14},
ASHPC{14}] = combineSFS4ASHP3();
        [AreaSC(15),ICTS{15},ELTS{15}, MCTS{15}, RCTS{15},SCTS{15}, SCT{15}, SCN{15},
ASHPC{15}] = combineSFS6ASHP3();
        [AreaSC(16),ICTS{16},ELTS{16}, MCTS{16}, RCTS{16},SCTS{16}, SCT{16}, SCN{16},
ASHPC{16}] = combineSFS8ASHP3();
        [AreaSC(17),ICTS{17},ELTS{17}, MCTS{17}, RCTS{17},SCTS{17}, SCT{17}, SCN{17},
ASHPC{17}] = combineSFS10ASHP3();
        [AreaSC(18),ICTS{18},ELTS{18}, MCTS{18}, RCTS{18},SCTS{18}, SCT{18}, SCN{18},
ASHPC{18}] = combineSFS12ASHP3();
        [AreaSC(19),ICTS{19},ELTS{19}, MCTS{19}, RCTS{19},SCTS{19}, SCT{19}, SCN{19},
ASHPC{19}] = combineSTS2ASHP1();
        [AreaSC(20),ICTS{20},ELTS{20}, MCTS{20}, RCTS{20},SCTS{20}, SCT{20}, SCN{20},
ASHPC{20}] = combineSTS3ASHP1();
        [AreaSC(21),ICTS{21},ELTS{21}, MCTS{21}, RCTS{21},SCTS{21}, SCT{21}, SCN{21},
ASHPC{21}] = combineSTS4ASHP1();
        [AreaSC(22),ICTS{22},ELTS{22}, MCTS{22}, RCTS{22},SCTS{22}, SCT{22}, SCN{22},
ASHPC{22}] = combineSTS5ASHP1();
        [AreaSC(23),ICTS{23},ELTS{23}, MCTS{23}, RCTS{23},SCTS{23}, SCT{23}, SCN{23},
ASHPC{23}] = combineSTS6ASHP1();
        [AreaSC(24),ICTS{24},ELTS{24}, MCTS{24}, RCTS{24},SCTS{24}, SCT{24}, SCN{24},
ASHPC{24}] = combineSTS7ASHP1();
        [AreaSC(25),ICTS{25},ELTS{25}, MCTS{25}, RCTS{25},SCTS{25}, SCT{25}, SCN{25},
ASHPC{25}] = combineSTS8ASHP1();
```

Figure E.4. The Matlab code developed to perform the integration of micro-renewable electricity generation systems

```
[AreaSC(26),ICTS{26},ELTS{26}, MCTS{26}, RCTS{26},SCTS{26}, SCT{26}, SCN{26},
ASHPC{26}] = combineSTS9ASHP1();
[AreaSC(27),ICTS{27},ELTS{27}, MCTS{27}, RCTS{27},SCTS{27}, SCT{27}, SCN{27},
ASHPC{27}] = combineSTS10ASHP1();
[AreaSC(28),ICTS{28},ELTS{28}, MCTS{28}, RCTS{28},SCTS{28}, SCT{28}, SCN{28},
ASHPC{28}] = combineSTS11ASHP1();
[AreaSC(29),ICTS{29},ELTS{29}, MCTS{29}, RCTS{29},SCTS{29}, SCT{29}, SCN{29},
ASHPC{29}] = combineSTS2ASHP2();
[AreaSC(30),ICTS{30},ELTS{30}, MCTS{30}, RCTS{30},SCTS{30}, SCT{30}, SCN{30},
ASHPC{30}] = combineSTS3ASHP2();
[AreaSC(31),ICTS{31},ELTS{31}, MCTS{31}, RCTS{31},SCTS{31}, SCT{31}, SCN{31},
ASHPC{31}] = combineSTS4ASHP2();
[AreaSC(32),ICTS{32},ELTS{32}, MCTS{32}, RCTS{32},SCTS{32}, SCT{32}, SCN{32},
ASHPC{32}] = combineSTS5ASHP2();
[AreaSC(33),ICTS{33},ELTS{33}, MCTS{33}, RCTS{33},SCTS{33}, SCT{33}, SCN{33},
ASHPC{33}] = combineSTS6ASHP2();
[AreaSC(34),ICTS{34},ELTS{34}, MCTS{34}, RCTS{34},SCTS{34}, SCT{34}, SCN{34},
ASHPC{34}] = combineSTS7ASHP2();
[AreaSC(35),ICTS{35},ELTS{35}, MCTS{35}, RCTS{35},SCTS{35}, SCT{35}, SCN{35},
ASHPC{35}] = combineSTS8ASHP2();
[AreaSC(36),ICTS{36},ELTS{36}, MCTS{36}, RCTS{36},SCTS{36}, SCT{36}, SCN{36},
ASHPC{36}] = combineSTS9ASHP2();
[AreaSC(37),ICTS{37},ELTS{37}, MCTS{37}, RCTS{37},SCTS{37}, SCT{37}, SCN{37},
ASHPC{37}] = combineSTS10ASHP2();
[AreaSC(38),ICTS{38},ELTS{38}, MCTS{38}, RCTS{38},SCTS{38}, SCT{38}, SCN{38},
ASHPC{38}] = combineSTS11ASHP2();
[AreaSC(39),ICTS{39},ELTS{39}, MCTS{39}, RCTS{39},SCTS{39}, SCT{39}, SCN{39},
ASHPC{39}] = combineSTS2ASHP3();
[AreaSC(40),ICTS{40},ELTS{40}, MCTS{40}, RCTS{40},SCTS{40}, SCT{40}, SCN{40},
ASHPC{40}] = combineSTS3ASHP3();
[AreaSC(41),ICTS{41},ELTS{41}, MCTS{41}, RCTS{41},SCTS{41}, SCT{41}, SCN{41},
ASHPC{41}] = combineSTS4ASHP3();
[AreaSC(42),ICTS{42},ELTS{42}, MCTS{42}, RCTS{42},SCTS{42}, SCT{42}, SCN{42},
ASHPC{42}] = combineSTS5ASHP3();
[AreaSC(43),ICTS{43},ELTS{43}, MCTS{43}, RCTS{43},SCTS{43}, SCT{43}, SCN{43},
ASHPC{43}] = combineSTS6ASHP3();
[AreaSC(44),ICTS{44},ELTS{44}, MCTS{44}, RCTS{44},SCTS{44}, SCT{44}, SCN{44},
ASHPC{44}] = combineSTS7ASHP3();
[AreaSC(45),ICTS{45},ELTS{45}, MCTS{45}, RCTS{45},SCTS{45}, SCT{45}, SCN{45},
ASHPC{45}] = combineSTS8ASHP3();
```

```
[AreaSC(46),ICTS{46},ELTS{46}, MCTS{46}, RCTS{46},SCTS{46}, SCT{46}, SCN{46},
ASHPC{46}] = combineSTS9ASHP3();
[AreaSC(47),ICTS{47},ELTS{47}, MCTS{47}, RCTS{47},SCTS{47}, SCT{47}, SCN{47},
ASHPC{47}] = combineSTS10ASHP3();
[AreaSC(48),ICTS{48},ELTS{48}, MCTS{48}, RCTS{48},SCTS{48}, SCT{48}, SCN{48},
ASHPC{48}] = combineSTS11ASHP3();
[AreaSC(49),ICTS{49},ELTS{49}, MCTS{49}, RCTS{49},SCTS{49}, SCT{49}, SCN{49},
ASHPC{49}] = combineSFS2Elec();
[AreaSC(50),ICTS{50},ELTS{50}, MCTS{50}, RCTS{50},SCTS{50}, SCT{50}, SCN{50},
ASHPC{50}] = combineSFS4Elec();
[AreaSC(51),ICTS{51},ELTS{51}, MCTS{51}, RCTS{51},SCTS{51}, SCT{51}, SCN{51},
ASHPC{51}] = combineSFS6Elec();
[AreaSC(52),ICTS{52},ELTS{52}, MCTS{52}, RCTS{52},SCTS{52}, SCT{52}, SCN{52},
ASHPC{52}] = combineSFS8Elec();
[AreaSC(53),ICTS{53},ELTS{53}, MCTS{53}, RCTS{53},SCTS{53}, SCT{53}, SCN{53},
ASHPC{53}] = combineSFS10Elec();
[AreaSC(54),ICTS{54},ELTS{54}, MCTS{54}, RCTS{54},SCTS{54}, SCT{54}, SCN{54},
ASHPC{54}] = combineSFS12Elec();
[AreaSC(55),ICTS{55},ELTS{55}, MCTS{55}, RCTS{55},SCTS{55}, SCT{55}, SCN{55},
ASHPC{55}] = combineSTS2Elec();
[AreaSC(56),ICTS{56},ELTS{56}, MCTS{56}, RCTS{56},SCTS{56}, SCT{56}, SCN{56},
ASHPC{56}] = combineSTS3Elec();
[AreaSC(57),ICTS{57},ELTS{57}, MCTS{57}, RCTS{57},SCTS{57}, SCT{57}, SCN{57},
ASHPC{57}] = combineSTS4Elec();
[AreaSC(58),ICTS{58},ELTS{58}, MCTS{58}, RCTS{58},SCTS{58}, SCT{58}, SCN{58},
ASHPC{58}] = combineSTS5Elec();
[AreaSC(59),ICTS{59},ELTS{59}, MCTS{59}, RCTS{59},SCTS{59}, SCT{59}, SCN{59},
ASHPC{59}] = combineSTS6Elec();
[AreaSC(60),ICTS{60},ELTS{60}, MCTS{60}, RCTS{60},SCTS{60}, SCT{60}, SCN{60},
ASHPC{60}] = combineSTS7Elec();
[AreaSC(61),ICTS{61},ELTS{61}, MCTS{61}, RCTS{61},SCTS{61}, SCT{61}, SCN{61},
ASHPC{61}] = combineSTS8Elec();
[AreaSC(62),ICTS{62},ELTS{62}, MCTS{62}, RCTS{62},SCTS{62}, SCT{62}, SCN{62},
ASHPC{62}] = combineSTS9Elec();
[AreaSC(63),ICTS{63},ELTS{63}, MCTS{63}, RCTS{63},SCTS{63}, SCT{63}, SCN{63},
ASHPC{63}] = combineSTS10Elec();
[AreaSC(64),ICTS{64},ELTS{64}, MCTS{64}, RCTS{64},SCTS{64}, SCT{64}, SCN{64},
ASHPC{64}] = combineSTS11Elec();
[AreaSC(65),ICTS{65},ELTS{65}, MCTS{65}, RCTS{65},SCTS{65}, SCT{65}, SCN{65},
ASHPC{65}] = combineElecASHP1();
```

Figure E.5. The Matlab code developed to perform the integration of micro-renewable electricity generation systems.

```
        [AreaSC(66),ICTS{66},ELTS{66}, MCTS{66}, RCTS{66},SCTS{66}, SCT{66}, SCN{66},
ASHPC{66}] = combineElecASHP2();
        [AreaSC(67),ICTS{67},ELTS{67}, MCTS{67}, RCTS{67},SCTS{67}, SCT{67}, SCN{67},
ASHPC{67}] = combineElecASHP3();
        [AreaSC(68),ICTS{68},ELTS{68}, MCTS{68}, RCTS{68},SCTS{68}, SCT{68}, SCN{68},
ASHPC{68}] = combineElecElec();

    result1=0;
    n1=floor(MCS/SS1+1);
    n11=0;
while  SS1*n1+WW1*n11<=WW1*n11+TCS
    TEL= EL +  ELTS{ii}; % TEL is the Total electrical load
    m=sum(TEL((find(S1*n1+W1*n11-TEL>=0)))); % fully satisfy electrical load
    n=sum(S1(find(S1*n1+W1*n11-TEL<0))*n1+W1(find(S1*n1+W1*n11-TEL<0))*n11);  %partially
satisfy electrical load
 if     ((m+n)/sum(TEL))>rp %if renewable energy technology can supply enough electricity as required
by the owner
      H= S1*n1+W1*n11-TEL;
      H(H>=6)=6;
      mm=sum(H([find(H>=0)])); % sum of surplus electricity generated in a particular hour
      nn=sum(TEL([find(H<0)])-S1([find(H<0)])*n1-W1([find(H<0)])*n11);    % electricity imported
from the grid when energy can not meet the load
      v=nn*ip; %paid electricity from the grid
      if mm<3000    % the limited amount of electricity that has been offered with incentive electricity
price
      u=mm*iep;    %profit made by exporting electircity at the condition of the amount is less than the
value stated above
      else u= 3000*iep+(mm-3000)*ep; %profit made by exporting electircity at the condition of the
amount is greater than the value stated above
      end
      w=mm*ep;
      cf1=v-u+mcS+MCTS{ii};  % cash flow for the first 5 years
      cf2=v-w+mcS+MCTS{ii};    % cash flow for the rest of the lifespan
      if SS1*n1<=in1 % if the total module has less capacity than inverter 1,then using inverter 1
        POI=IN1;    %price of an inverter
      elseif SS1*n1<=in2
        POI=IN2;
      else
        POI=IN3;
      end
```

```
      IC=SS1*n1*ICPKW1;       %Installation Cost Per KW
      ca=WTP1*n11+SMP1*n1+IC+POI;    %capital cost
      if iy==0
        l=0;
      else k=1:iy;
        l=cf1./(1+rir).^k; % discounted cash flow for the first 5 years
      end
      j=iy+1:pl;        % project lifespan
      ll=cf2./(1+rir).^j; % discounted cash flow for the rest of lifespan
      noi=floor(pl/ivr-0.00001); %number of replaced inverter
      if noi==0;
        qq=0;
      else
      ine=1:noi;
      q=POI./(1+rir).^(ivr*ine);    %discounted inverter replacement
      qq=sum(q);                % discounted total replaced inverter cost
      end
      nors=floor(pl/sl1-0.00001); % nors is number of replaced solar PV panel
      if nors==0;
        rcs=0;                % rcs is replacement cost solar
      else
        sne=1:nors;
        ircs=SMP1*n1./(1+rir).^(sl1*sne); % ircs is individual replacement cost solar
        rcs=sum(ircs);
      end
      if pl>sl1
      svl=SMP1*n1*(1-(pl-sl1*nors)/sl1); %vl=value left, sl=solar lifespan
      else svl=SMP1*n1*((sl1-pl)/sl1);
      end
      if pl>ivr
      ivl=POI*(1-(pl-ivr*noi)/ivr);%inverter value left
      else ivl=POI*((ivr-pl)/ivr);
      end
      vl=svl+ivl;
      sal=vl/(1+rir)^pl;      % salvage value
      result1(n1)=sum(l)+sum(ll)+ca+ICTS{ii}+qq+rcs-sal+RCTS{ii}-SCTS{ii}-cgspv; %LCC  for  all
cases
      result1(result1==0)=1000000;
 end
      n1=1+n1;
```

Figure E.6. The Matlab code developed to perform the integration of micro-renewable electricity generation systems.

```
        if n1*AS1+AreaSC(ii)>TAREA
            result1=10000000;
        end
end
        result2=0;
        n2=floor(MCS/SS1+1);
        n22=1;
while  SS1*n2+WW1*n22<=WW1*n22+TCS
    TEL= EL+ ELTS{ii};
    m=sum(TEL((find(S1*n2+W1*n22-TEL>=0)))); % fully satisfy electrical load
    n=sum(S1(find(S1*n2+W1*n22-TEL<0))*n2+W1(find(S1*n2+W1*n22-TEL<0))*n22);  %partially
satisfy electrical load
 if     ((m+n)/sum(TEL))>rp %if renewable energy technology can supply enough electricity as required
by the owner
        H= S1*n2+W1*n22-TEL;
        H(H>=6)=6;
        mm=sum(H([find(H>=0)])); % sum of surplus electricity generated in a particular hour
        nn=sum(TEL([find(H<0)])-S1([find(H<0)])*n2-W1([find(H<0)])*n22);    % saving made when
energy can not meet the load
        v=nn*ip; %savings made
        if mm<3000    % the limited amount of electricity that has been offered with incentive electricity
price
        u=mm*iep;    %profit made by exporting electircity at the condition of the amount is less than the
value stated above
        else u= 3000*iep+(mm-3000)*ep; %profit made by exporting electricity at the condition of the
amount is greater than the value stated above
        end
        w=mm*ep;
        if  WW1<2
            mcW=mcW1;
        elseif WW1<=4
            mcW=mcW2;
        else
            mcW=mcW3;
        end
        cf1=v-u+mcS+mcW+MCTS{ii};  % cash flow for the first 5 years
        cf2=v-w+mcS+mcW+MCTS{ii};     % cash flow for the rest of the lifespan
        if SS1*n2<=in1 % if the total module has less capacity than inverter 1,then using inverter 1
            POI=IN1;    %price of an inverter
        elseif SS1*n2<=in2
            POI=IN2;
        else
            POI=IN3;
        end
        IC=SS1*n2*ICPKW1;        %Installation Cost Per KW
        ca= WTP1*n22+SMP1*n2+IC+POI;    %capital cost
        if iy==0
            l=0;
        else k=1:iy;
            l=cf1./(1+rir).^k; % discounted cash flow for the first 5 years
        end
        j=iy+1:pl;         % project lifespan
        ll=cf2./(1+rir).^j;  % discounted cash flow for the rest of lifespan
        noi=floor(pl/ivr-0.00001); %number of replaced inverter
        if noi==0;
            qq=0;
        else
        ine=1:noi;
        q=POI./(1+rir).^(ivr*ine);    %discounted inverter replacement
        qq=sum(q);                  % discounted total replaced inverter cost
        end
        nors=floor(pl/sl1-0.00001); % nors is number of replaced solar PV panel
        if nors==0;
            rcs=0;                  % rcs is replacement cost solar
        else
          sne=1:nors;
          ircs=SMP1*n2./(1+rir).^(sl1*sne); % ircs is individual replacement cost solar
          rcs=sum(ircs);
        end
         if pl>sl1
        svl=SMP1*n2*(1-(pl-sl1*nors)/sl1); %vl=value left, sl=solar lifespan
        else svl=SMP1*n2*((sl1-pl)/sl1);
        end
        if pl>ivr
        ivl=POI*(1-(pl-ivr*noi)/ivr);%inverter value left
        else ivl=POI*((ivr-pl)/ivr);
        end
        vl=svl+ivl;
        sal=vl/(1+rir)^pl;      % solar salvage value
        if WW1<=win1
```

Figure E.7. The Matlab code developed to perform the integration of micro-renewable electricity generation systems.

```
            POWI=WIN1;
        elseif WW1<=win2
            POWI=WIN2;
        elseif WW1<=win3
            POWI=WIN3;
        elseif WW1<=win4
            POWI=WIN4;
        elseif WW1<=win5
            POWI=WIN5;
        else
            POWI=WIN6;
        end
        nowi=floor(pl/wivr-0.00001); %number of replaced wind turbine inverter
        if nowi==0;
            oo=0;
        else
        inwe=1:nowi;
        p=POWI./(1+rir).^(ivr*inwe);    %discounted wind turbine inverter replacement
        oo=sum(p);                  % discounted total replaced wind turbine inverter cost
        end
         norw=floor(pl/wl1-0.00001); % norw is number of replaced wind turbine
        if norw==0;
            rcw=0;                  % rcs is replacement cost wind
        else
            wne=1:norw;
            ircw=WTP1*0.5./(1+rir).^(wl1*wne); % ircw is individual replacement cost wind
            rcw=sum(ircw);
        end
        if pl>wl1
        wtvl=WTP1*0.5*(1-(pl-wl1*norw)/wl1); %vl=value left, sl=solar lifespan
        else wtvl=WTP1*((wl1-pl)/wl1);
        end
        if pl>wivr
        wivl=POWI*(1-(pl-wivr*nowi)/wivr);%wind turbine inverter value left
        else wivl=POWI*((wivr-pl)/wivr);
        end
        wvl=wtvl+wivl;
        wal=wvl/(1+rir)^pl;    % wind salvage value
        result2(n2)=sum(l)+sum(ll)+ca+ICTS{ii}+qq+oo+rcs+rcw-sal-wal+RCTS{ii}-SCTS{ii}-cgw-
cgspv; %LCC for all cases
```

```
        result2(result2==0)=1000000;
    end
        n2=1+n2;

        if n2*AS1+AreaSC(ii)>TAREA
            result2=10000000;
        end
end
        TEL= EL+ ELTS{ii};
        nn=sum(TEL);   % sum of electricity used for a year
        v=nn*ip+MCTS{ii}; %savings made
        r=1:pl;
        ll=v./(1+rir).^r;  % discounted cash flow for the rest of lifespan
        result3=sum(ll)+ICTS{ii}+RCTS{ii}-SCTS{ii}; %LCC for all cases
        if rp>0
            result3=10000000;
        end
        [goodresult1, minn1]=min(result1);
        goodresult1(goodresult1==0)=1000000;
        [goodresult2, minn2]=min(result2);
        goodresult2(goodresult2==0)=1000000;
        goodresult3=result3;
        betterresult=([goodresult1 goodresult2 goodresult3]);
        LCC=min(betterresult);
       new_min = LCC
        if (new_min < leastLCC)
        leastLCC = new_min
        SCT_best=SCT{ii} (find(leastLCC==LCC))
        SCN_best=SCN{ii} (find(leastLCC==LCC))
        ASHPC_best=ASHPC{ii} (find(leastLCC==LCC))
        if leastLCC==goodresult2
        SMN=minn2
        WTN='Yes'
        COMB='135W Solar PV module and 0.6 kW micro wind turbine'
        elseif leastLCC==goodresult1
        SMN=minn1
        WTN='No'
        COMB='135W Solar PV module and 0.6 kW micro wind turbine'

        else
```

Figure E.8. The Matlab code developed to perform the integration of micro-renewable electricity generation systems.

```
            SMN='No';
            WTN='No';
            COMB= 'Electricity from grid';
        end
        end
end
minLCC=leastLCC
minSCT =SCT_best
minSCN=SCN_best
minASHPC=ASHPC_best
minSMN=SMN
minWTN=WTN
minCOMB=COMB
end
```

Figure E.9. The Matlab code developed to perform the integration of micro-renewable electricity generation systems.

```
function [AreaSC, ICTS,ELTS, MCTS, RCTS,SCTS, SCT, SCN, ASHPC] = combineSFS2ASHP1()%SFS is the
Solar Flatplate System and ASHP is the Air Source Heat Pump
global cpr SFl ASHPl1 ASHPl2 ASHPl3 HWCl MCSFS MCSTS MCASHP1 MCASHP2 MCASHP3 IniICSFS
ICPFP IniICSES ICPEP ASHPP1 ASHPP2 ASHPP3 pocp HWCP posps spsr
global Goodresult
global i
global rp
global in1 IN1 in2 IN2 in3 IN3  ivr wivr
global SMP1 WTP1 SMP2 WTP2 SMP3 WTP3 WTP4 WTP5 WTP6
global ip ep iep
global rir mcS mcW
global TCS MCS
global ICPKW1 ICPKW2 ICPKW3
global iy pl
global cgw cgspv cgASHP cgst
global mcW1 mcW2 mcW3
global sl1 sl2 sl3 wl1 wl2 wl3 wl4 wl5 wl6
global win1 win2 win3 win4 win5 win6 WIN1 WIN2 WIN3 WIN4 WIN5 WIN6

    AreaSC= 1.93;
    ELTS=[Hourly power inputs for this system combination];%ELTS is the Electrical Load for Thermal
System
    ICTS = ASHPP1+IniICSFS+ICPFP*1-cgASHP-cgst;
    MCTS = MCSFS+ MCASHP1; %MCSFS is the Maintenance Cost for Solar Flatplate System and MCASHP
is the Maintenance Cost for Air Source Heat Pump
    nocp=floor(pl/cpr-0.00001); %number of replaced circulating pump, cpr is circulating pump replacement
    if nocp==0;
      rccp=0;
    else
    cpe=1:nocp;
    irccp=pocp./(1+rir).^(cpr*cpe);    %discounted circulating pump replacement
    rccp=sum(irccp);                % discounted total replaced circulating pump cost
    end
    nsps=floor(pl/spsr-0.00001);% number of replaced solar pump station
    if nsps==0;
      rcsps=0;
    else
    spse=1:nsps;
    ircsps=posps./(1+rir).^(spsr*spse);    %discounted solar pump station replacement
    rcsps=sum(ircsps);                % discounted total replaced solar pump station cost
    end
    norhp=floor(pl/ASHPl1-0.00001); % norhp is number of replaced heat pump
    if norhp==0;
      rchp=0;                % rcs is replacement cost heat pump
    else
      hpne=1:norhp;
      irchp=(ASHPP1-HWCP)./(1+rir).^(ASHPl1*hpne); % irchp is individual replacement cost heat pump
      rchp=sum(irchp);
    end
    norst=floor(pl/SFl-0.00001); % norst is number of replaced solar thermal
    if norst==0;
      rcst=0;                % rcs is replacement cost solar thermal
    else
      stne=1:norst;
      ircst=ICPFP*1./(1+rir).^(SFl*stne); % ircst is individual replacement cost solar thermal
      rcst=sum(ircst);
    end
    norhc=floor(pl/HWCl-0.00001); % norhc is number of replaced hotwater cylinder
    if norhc==0;
      rchc=0;                % rchc is replacement cost hotwater cylinder
    else
      hcne=1:norhc;
      irchc=HWCP*1./(1+rir).^(HWCl*hcne); % irchc is individual replacement cost hotwater cylinder
      rchc=sum(irchc);
    end
    RCTS= rccp+rchp+rcst+rchc+rcsps;
    if pl>ASHPl1
    ASHPvl=(ASHPP1-HWCP)*(1-(pl-ASHPl1*norhp)/ASHPl1); %vl=value left,
    else ASHPvl=ASHPP1*((ASHPl1-pl)/ASHPl1);
    end
    if pl>SFl
    SFvl=ICPFP*1*(1-(pl-SFl*norst)/SFl); %vl=value left,
    else SFvl=ICPFP*1*((SFl-pl)/SFl);
    end
```

Figure E.10. The Matlab code developed to perform the integration of micro-renewable thermal generation systems.

```
 if pl>HWCl
HWCvl=HWCP*1*(1-(pl-HWCl*norhc)/HWCl); %vl=value left,
else HWCvl=HWCP*1*((HWCl-pl)/HWCl);
end
if pl>cpr % circulating pump replacement
cpvl=pocp*(1-(pl-cpr*nocp)/cpr);%circulating pump value left
else cpvl=pocp*((cpr-pl)/cpr); % pocp is the price of circulating pump
end
if pl>spsr % circulating pump replacement
spsvl=posps*(1-(pl-spsr*nsps)/spsr);%circulating pump value left
else spsvl=posps*((spsr-pl)/spsr); % pocp is the price of circulating pump
end


SCTSvl= ASHPvl+SFvl+HWCvl+cpvl+spsvl;
SCTS= SCTSvl/(1+rir)^pl;
SCT={'Flatplate'};%Solar Collector Type
SCN={'1,1.93m2'}; %solar collector Number
ASHPC={'5kW'}; %Air Source Heat Pump Capacity
end
```

Figure E.11. The Matlab code developed to perform the integration of micro-renewable thermal generation systems.